The Influence of Gravity on Fluid-Structure Impact

Hussein Jebrail Zekri

School of Mathematics, UEA

Norwich, NR7 4TJ, England.

A thesis submitted to the University of East Anglia for the degree of *Doctor of Philosophy*

May 2016

Acknowledgements

First and foremost I want to express my gratitude to my supervisors Prof. Alexander A. Korobkin and Dr. Mark J. Cooker for their patience, respect, kindness, and motivation. I am extremely grateful to their always available advice, valuable encouragements, and discussions on analysis of my Ph.D.

My Ph.D work was funded by a Kurdistan Regional Government scholarship, I am very thankful for the opportunity provided. I am also grateful to School of Mathematics in UEA and its people for every thing they provided for me in completing my Ph.D.

I would like to thank my family for their every day love and support. Specially my beloved parents (Bahiya and Jebrail) who taught me how to love, thank you mother, thank you father.

Mina, my love, thank you for your support, encourage, and patience during the every stages of this Ph.D. Without your love, sacrifice, and tolerance, I could not have completed this thesis. You and Kiyan were the source of spirit for me in every step during my Ph.D.

Lastly, I would like to thank my friends who offered me advice and support.

Abstract

Fluid-structure interaction is a well-known and complicated problem. Its formulation requires simplifications in modelling, and usually the presence of gravity is one aspect which is neglected, especially in violent impact. In this thesis we account for the influence of gravity on two physically different but mathematically similar two-dimensional flows. First (in Chapters 2–4), sloshing impact of a standing wave on the lid of a rigid tank, and second (in Chapter 5), impact of a rigid blunt body entering water which is initially at rest.

Chapter 1 presents the motivation, literature, aim and structure of the thesis. In Chapter 2, gravity is neglected and model equations are solved analytically, in particular the linearised hydrodynamic problem with and without the lid using the Wagner approximation, time and coordinate stretching, and displacement potential. Chapter 3, introduces gravity into the formulation and the model is solved semi-analytically to determine its influence on the width of the wetted region and on the pressure distribution on the lid during impact. We numerically find the effect of gravity on the moving contact points, hydrodynamic pressure, and surface elevation in Chapter 4. Chapter 5 studies the influence of gravity on the impact of a blunt body entering vertically with a constant speed into an initially flat water. All problems are formulated and solved within the Wagner model.

In both problems we found visible effects of gravity on the positions of moving contact points after the early stage of impact. Gravity shortens the size of the wetted region. Consequently, the velocities of the contact points are decreased by gravity. The effect of gravity on the surface elevation is shown for both problems. Negative hydrodynamic pressures and forces are found during the

sloshing impact stage when gravity is neglected. Numerically, it was found that gravity decreases the hydrodynamic pressure on the lid of the tank. Similarly the hydrodynamic pressure is found to be decreased by gravity in the water-entry problem. Also in the water-entry problem it is shown that gravity increases both the thickness and the mass flux into the spray jets. Also the total energy (potential and kinetic) of the system, and the work done by the body on the fluid are decreased by gravity.

Contents

Chapter 1

Introduction

1.1 Physical motivation

"Worse things still happen at sea" is the title of an article in The Guardian newspaper from Saturday, 10th of January 2015, see (George 2015). The author provided information about the recent losses of ships and fatalities; tragic numbers of accidents and losses are reported. The majority of the accidents have been caused in severe sea weather conditions experienced by the ship structures. Liquefied Natural Gas (LNG) carriers are also a part of these incidents. On 26th of January 2016, LNG Journal Newsletter, published an article (LNG-Journal 2016) stating that ExxonMobil, one of the largest liquefied natural gas trader seller, expects that demand for natural gas and LNG will increase by 50 percent by 2040. Transporting natural gas via pipeline is the safest way. Pipelines are more economical for short distances where feasible, but due to geopolitical reasons and conflicts this option is not always available. However, for long distance routes, ocean-going LNG carriers are more competitive, since overall costs are less affected by distance. Therefore, there has been a significant rise in LNG transportation. For the history of the gas transportation see (Graczyk 2008) and (Woodward & Pitbaldo 2010).

Today, we have two main containment systems which are most widely operating for transporting LNG. The Moss type, (Woodward & Pitbaldo 2010), with a containment system of spherical design, and the Membrane type with containment system of rectangular design. The size of the LNG carriers has increased significantly compared to the classical LNG carriers (from 138 000 m^3 to 240 000 m^3) during the past several decades. These tanks nowadays are very complex structures with insulation to keep the natural gas below its liquefaction temperature of approximately -163°C. LNG is pressurized by a factor of 600 of its gaseous state by cooling. For more details about the structure and operating of

LNG carriers see (Godderidge 2009), (Woodward & Pitbaldo 2010) and references therein.

Because of the LNG boils-off of approximately 0.1% to 0.2% per day on laden journeys, the LNG tanks are never completely filled. Therefore, one of the concerns with LNG carriers is the sloshing of LNG inside the tank. Sloshing is the dynamic movement of a liquid with a free surface inside a tank which can consequently apply loads on the tank structure. Violent liquid sloshing is of concern for cargo tank designers due to the problems of safety in extreme loadings which could destabilize the ship motion or cause structural damage to the tank, see (Abramson, Bass, Faltinsen & Olsen 1976). For the sloshing incidents in LNG carriers and its risks see (Vanem, Antão, Østvik & de Comas 2008), (Hine 2008) and (Woodward & Pitbaldo 2010).

Due to various demands on natural gas supply, LNG carriers should operate at any filling level. Different filling levels lead to different kinds of sloshing impacts inside the LNG tank. For partial or low filling levels (10–60%), there could be surface waves moving from one side of the tank to the other and reflecting at boundaries. As the height of the filling level increases the sloshing motion of liquid becomes that of standing-wave type, which is considered in this study, with LNG moving up and down impacting the top of the tank, or rising along the tank's walls and impacting the top corners where the wall and the ceiling meet.

In two papers, (Longuet-Higgins 2001) and (Longuet-Higgins & Dommermuth 2001), it was shown that for steep standing waves, even in deep water, the collapse of a cavity in the wave trough can build up very high local vertical accelerations of the fluid, initiating a strong vertical jet. In one example they found that the acceleration exceeds $100g$. Also (Bredmose, Brocchini, Peregrine & Thais 2003), both experimentally and numerically, studied the motion of standing waves generated by vertically accelerating a tank containing water with an external force. They observed impacts of both sharp and flat-topped wave crests with the lid.

It is shown both by numerical and experimental studies that sloshing pressure magnitude is larger for low filling levels than for high filling levels, see (Abramson et al. 1976) and (Kim, Shin, Bai et al. 2002). In all previously mentioned kinds of impacts, there is a possibility of gas (or mixture of vapour and gas) to be trapped by the liquid free surface at the instant of impact. Consequently the liquid may become mixed with gas, which in these cases, influences gas compressibility significantly affecting the impact loads on the tank's surfaces, see (Rognebakke & Faltinsen 2005) and (Malenica, Korobkin, Scolan, Gueret, Delafosse, Gazzola, Mravak, Chen & Zalar 2006).

There is confidence in the Moss type design, because they are less susceptible

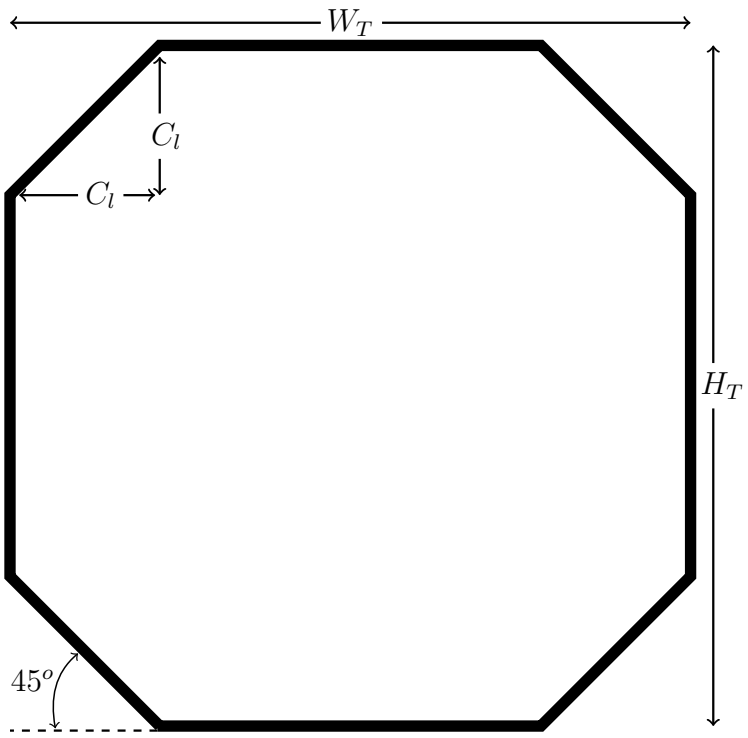

Figure 1.1: Dimensions for an LNG tank in membrane carrier, (Woodward & Pitbaldo 2010). The height of the tank $H_T = 30.58$m, the width $W_T = 30$m and the cut edge (chamfer) $C_l = 6.60$m.

to sloshing and there is no restriction on the filling level compared to membrane type design. Nevertheless, nowadays the membrane type design is more popular. The membrane type is preferred because of the relatively larger weight, less efficient use of space within the ship, and higher construction cost for the Moss type design. Almost 60% of the working LNG carriers in the world are membrane type design, and 80% of the world's LNG carriers under construction are of membrane type design. Therefore we will focus our attention on a rectangular tank configuration, because our concern is with the impact occurring at the lid's centre where the solid boundary is plane. We neglect the cut on the corners of the real membrane tank. The cut corners are there, see Figure 1.1, to reduce the sloshing load on the tank's corners which are assumed to be the most vulnerable parts of the tank to sloshing impact.

1.2 Aim of this thesis

Sloshing is one of the most important phenomena of LNG flow inside a tank during transportation, as it may lead to violent impact on the tank's surface, and it may affect the stability of the motion of the whole ship. From a mathematical point of view, problems of sloshing impacts are formulated similar to the problem

of water entry. The water-entry problems describe the flows caused by a body impacting on a free surface of liquid which is initially at rest. In both problems, high hydrodynamic loads are detected. The loads acting over the wetted region of a structure are of main concern in design. The aim of this thesis is to model and investigate the influence of gravity on these impact loads. We investigate this influence for both sloshing of liquid inside LNG tanks with high filling level, and water-entry impact of a rigid body with constant speed. It is well-known that during the early stage of liquid impact, when the liquid acceleration is much greater than gravitational acceleration, gravity is negligible. The acceleration of the liquid by impacts can be estimated as $\frac{u_0}{T_0}$, where u_0 is the impact velocity (usually of order of few meters per seconds) and T_0 is a duration of the impact loads (usually few milliseconds). Then $\frac{u_0}{T_0} = O(100g)$, where g is gravitational acceleration, and gravity can be safely neglected during the impact stage. In this work, we consider impacts with either small impact velocity u_0 due to restricted free-surface motion or relatively large T_0, when the liquid acceleration is comparable with the acceleration due to gravity. During sloshing in LNG tanks, at high filling, the liquid surface may approach the tank ceiling at a certain speed u_0, then the wetted area of the ceiling increases with relatively high hydrodynamic pressure acting on it. This is the impact stage. The gravity is neglected at the beginning of this stage but becomes important later on when the rate of the wetted (contact) area expansion decreases due to the gravity-driven flow in the main part of the tank. Finally the wetted area stops expanding and starts shrinking (exit stage).

This exit stage is dominated by gravity with downward acting hydrodynamic force on the lid. The same scenario happens when a totally submerged body is made to exit from water, as described by (Greenhow & Moyo 1997). This stage is even more complicated than the impact stage, due to the complexity of the liquid's free-surface behaviour during this stage, such us the speed of contraction of the wetted region. Therefore, it is of crucial importance to understand the influence of gravity even before this stage is reached.

Due to the complex nature of the LNG sloshing it is impossible to include all physical and chemical parameters in an analytical, numerical or even experimental investigation. Therefore some simplifications, depending on the structure of the flow, have to be considered for modelling such a phenomenon. This is done by ignoring some parameters which give minor contribution to the flow. For example with Froude scaling law, (Lee, Kim, Kwon, Kim, Lee et al. 2005), using computational fluid dynamics (CFD) studied the influences of LNG viscosity, LNG-gas density ratio, and ullage pressure on the sloshing pressure during impact. They found these influences insignificant.

In this thesis, we employ some simplifications to model sloshing of LNG and its impacts on the tank ceiling. Based on the following non-dimensional numbers, the Reynolds number $\mathrm{Re} = \frac{\rho_0 \mathrm{u}_0 \mathrm{H}_0}{\mu_0}$ (the ratio of inertia and viscous forces), the Weber number $\mathrm{We} = \frac{\rho_0 \mathrm{u}_0^2 \mathrm{H}_0}{\gamma_0}$ (the ratio of inertia flow to surface tension forces) and the Mach number $\mathrm{Ma} = \frac{\mathrm{u}_0}{c_0}$ (the ratio of the velocity to the speed of sound in the fluid) indicate the importance of viscosity, surface tension and compressibility effects compared with the LNG inertia. Here ρ_0 is the density, μ_0 is the viscosity of LNG, u_0 is the characteristic velocity of the flow, H_0 is the characteristic length, γ_0 is the surface tension of LNG and c_0 is the sound of speed in LNG. The measurement of the above-mentioned properties depend on the temperature of LNG and the pressure applied on it. At the temperature of -163°C, when LNG has pressurized by a factor of (1:600), it has $\rho_0 \approx 4.7\times10^2$ kgm^{-3}, $\mu_0 \approx 1.14\times10^{-4}$ kgm^{-1}s^{-1}, $\gamma_0 \approx 1.4 \times 10^{-2}$Nm^{-1}, and $C_0 \approx 1.32 \times 10^3$ ms^{-1}, (Godderidge 2009).

In this study we are interested in the influence of gravity on impact loads during sloshing inside LNG tanks. For example in a membrane LNG tank with height $\mathrm{H}_0 \approx 30$ m, wave length $\lambda_0 \approx 30$ m , wave amplitude $\mathrm{a}_0 \approx 1$ m and $g \approx 9.8$ ms^{-2}, the sloshing impact velocity of LNG will be $\mathrm{u}_0 \approx 3$ ms^{-1}. Therefore, the non-dimensional numbers are $\mathrm{Re} \approx 10^8 \gg 1$, $\mathrm{We} \approx 10^7 \gg 1$ and $\mathrm{Ma} \approx 10^{-3} \ll 1$. Depending on these numbers the effects of viscosity, surface tension and compressibility are neglected in impact loads during sloshing inside LNG tank.

It is worth mentioning that the speed of sound in LNG is approximated by the speed of sound in methane liquid (LNG consists of 87-90% of methane). The presence of other components, 8-9% ethane and 0.5-1% nitrogen, and 0.5% of the other component gases include propane, butane and isobutane, may significantly decrease the speed of sound in LNG. However even with a speed of sound ten times smaller than the speed of sound in methane liquid and an the flow speed of 40 ms^{-1}, the Mach number is still less than $\frac{1}{3}$ and compressibility effects still can be neglected. In addition, LNG boiling and possibility of mixing LNG with vapour also may significantly reduce the sound speed in LNG. LNG modelled as an incompressible fluid in this study.

In the water-entry problem, the above-mentioned simplifications can be applied as well. Water has density $\rho_w \approx 10^3$ kgm^{-3}, viscosity $\mu_\mathrm{w} \approx 10^{-3}$ kgm^{-1}s^{-1}, with $\gamma_w \approx 7.5 \times 10^{-4}$Nm^{-1} as the water-air interface surface tension, and the sound of speed in water is $c_\mathrm{w} \approx 1.4 \times 10^3$ ms^{-1}. With a body entering water with width $H_\mathrm{w} = 10$ m and constant velocity $\mathrm{u}_\mathrm{w} = 1$ ms^{-1}, the following non-dimensional numbers are approximately, $\mathrm{Re} \approx 10^7 \gg 1$, $\mathrm{We} \approx 10^7 \gg 1$ and $\mathrm{Ma} \approx 10^{-3} \ll 1$. Therefore, in such water-entry problems, the effects of viscosity, surface tension, and compressibility are also negligible.

1.3 Literature Review

Many theoretical and experimental results on fluid-structure interaction have been discussed and published. This is due to its complicated nature and its many applications in real-life problems, starting from very small droplet impact, (Howison, Ockendon, Oliver, Purvis & Smith 2005) up to large breaking sea-wave impact onto a permeable barrier, (Cooker 2001) and (Cooker 2013). The most important pioneering work was done by (von Karman 1929) and (Wagner 1932), on the water-entry of solid bodies. First, (von Karman 1929) developed an asymptotic theory for water-entry problems with linearised boundary conditions on the free surface and body. Later, (Wagner 1932) calculated the rise of the displaced water along the sides of the body, (called splash-up), during the impact motion, for a wedge with a small deadrise angle (the angle between the tangent to the profile and the equilibrium free surface). Modelling water-entry and sloshing problems achieved more attention and improvement because of the simplicity provided by Wagner's model to solve such problems.

Several research programmes that investigated sloshing in LNG carriers are reviewed in (Abramson et al. 1976), with liquid response for different tank geometries and fill levels. Also in their work they discussed the scaling of model data to full data by using the Buckingham Pi theorem with choosing impact pressure as the dependent variable. (Korobkin 1982) introduced the so-called displacement potential to convert the time variable into a parameter by removing the time derivative in the kinematic boundary condition on the liquid's free surface. For more general two-dimensional body shapes, (Cointe & Armand 1987) and (Howison, Ockendon & Wilson 1991), developed some asymptotic results for blunt bodies. These authors used the method of matched asymptotic expansion by introducing the idea of decomposing the wetted region into three regions, namely, outer flow region, inner flow region (or jet root region) and jet region, which will be discussed in detail through this study. (Howison et al. 1991), extended some mathematical results when the tangent to the boundary of the impacting body makes a small angle to the undisturbed water surface.

Further work on wave impact has been done by (Korobkin 1998). He introduced the displacement potential and reduced the impact problem to a system of ordinary differential equations. Also (Korobkin & Khabakhpasheva 2006), (Scolan & Korobkin 2001), (Korobkin & Scolan 2006), (Iafrati & Korobkin 2004), (Cooker & Peregrine 1995), (Cooker 1996) and (Oliver 2002) contributed to understanding and modelling of wave impact. (Cooker & Peregrine 1990) and (Cooker & Peregrine 1995) developed a model of the pressure impulse (the time-integral of the pressure) caused by a wave impacting on a vertical wall.

The elasticity of the body's surface in the sloshing and water-entry problem is not taken into account in this study. Solid bodies are assumed to be rigid. The danger of extremely high pressure impacts depends on the structural response. Therefore the sloshing impact loads have to be coupled with the local elastic response of the structure for better understanding of this phenomena. For recent progress in hydro-elastic models of liquid impact see (Rognebakke & Faltinsen 2005), (Korobkin & Khabakhpasheva 2006), (Malenica et al. 2006), (Ten, Malenica & Korobkin 2011), (Reinhard, Korobkin & Cooker 2013) and references therein.

This thesis studies the sloshing impacts inside an LNG tank and water-entry problem in two-dimensional (2D) formulation with a symmetric impact for both problems. In these kind of impact, the size of the wetted region is unknown in advance and is bounded by two time-dependent points (moving contact points). Due to the symmetry of the flow considered in this study we are required to find the position of only one moving contact point. In 2D impact problems, research has been done also for asymmetric impacts, were the wetted region is defined by two non-symmetric moving contact points, for example see (Reinhard 2013). In three-dimensional (3D) problems, the wetted region is bounded by a time-dependent 2D curve (moving contact line) which is unknown in advance. So far there is no general method to solve 3D impact problems. In special cases of elliptic and almost axisymmetric contact regions, (Korobkin & Scolan 2006) studied the impact of a blunt body onto a liquid in 3D within the Wagner model. They found the moving contact line by the method of asymptotic analysis.

Due to sudden change in the liquid's flow, the problem of sloshing is very complicated even after neglecting the effects of viscosity, surface tension, compressibility and gravity. So far to the author's knowledge no analytical study has been done on the exit stage for sloshing impact of liquid inside a tank. A configuration similar to that during the exit stage, when the contact region is shrinking, can be found in (Benjamin 1968), who studied a gravity current from a box filled with liquid with initially closed ends and one vertical end opened later. Then the liquid starts to flow out from the box under the action of gravity. Ignoring the effects of surface tension and viscosity, Benjamin found that the velocity of the point on the lid, where the liquid separates from the lid, is the same as the velocity of the liquid at the open end of the box, in case when the depth of the downstream is the half of the height of the box.

Experimentally, (Scolan, Remy & Thibault 2006) studied impact of a 3D standing waves on a horizontal plate elevated above the water surface. A plate with width 0.8 m, thickness 0.02 m and 1.5 m long, is fixed rigidly at a distance 0.05-0.11 m from the equilibrium free surface of water with depth 1m. They made

a comparison between the wave profiles with and without the horizontal plate and showed that the presence of the plate significantly disturbs the wave kinematics. Also they found that the duration of the impact stage is slightly shorter than the duration of the exit stage. The force during both stages was studied. It was found that the force peaks are of almost the same magnitude, but with opposite signs of course.

1.4 Structure of thesis

The structure of the thesis is as follows:

Chapter 1 includes the introduction of this thesis which starts by giving the physical motivation of this study and a review of the technical literature, the aim of the thesis, an overview to the literature of fluid-structure interaction, and ending by presenting the structure of this thesis.

The following three chapters are related to the 2D sloshing impacts of liquid inside an LNG tank.

Chapter 2 describes the sloshing impact problem and gives its formulation for a highly filled rectangular LNG tank. We study the impact of the liquid on the lid of the tank as follows. First, we remove the lid and solve analytically the linearised hydrodynamic problem. Then we introduce the lid to the problem and find semi-analytically the correction to the solution which accounts for the lid. This is done by formulating the linearised problem in terms of the velocity potential using the Wagner condition, (Wagner 1932). We identify a small parameter at high filling level. Then, by using stretched variables, we reformulate the problem in terms of the displacement potential, (Korobkin 1982). However, when we introduce the lid to the problem, we do not include gravity into the linearised formulation in this chapter. At the leading order, the size of the wetted region, the hydrodynamic force and the pressure distribution along the wetted region, in non-dimensional variables, are obtained. At the end of Chapter, the energy distribution of the system is investigated.

Chapter 3 studies the influence of gravity on the size of the wetted region. This influence is determined semi-analytically by two different methods, and the results are compared one with another. Also in Chapter 3, we determine the correction to the surface elevation and compare the surface elevations with and without the lid. The last section of this Chapter studies the correction due to gravity on the pressure distribution on the lid of the container during the impact.

Chapter 4 presents the numerical part of this thesis. Keeping gravity in the formulation, we remove the lid of the tank and apply a distribution of pressure along the wetted region with the condition that this pressure should keep the

wetted region at the top boundary of the tank and does not allow the liquid to exceed this elevation. The problem is formulated in terms of the coefficients for the pressure distribution and surface elevation, after we discretise both in space and time. We arrive at a system of algebraic equations at each time step. It is shown that the system is ill-conditioned. Therefore a regularization of the system is performed to stabilize the numerical solution. The surface elevation and pressure distribution, including gravity, are investigated.

Chapter 5 deals with a topic different from LNG sloshing impact, but related to it: the 2D water-entry problem. We consider the normal impact of a symmetric rigid body with constant velocity onto the lower half-plane of liquid with initially flat free surface. We give a description to this problem and write its formulation. We find the correction due to gravity to the size of the wetted region. Then we find the surface elevation, the hydrodynamic pressure distribution and the hydrodynamic force, with corrections due to gravity in each of them. We make a comparison for each to show the difference between gravity-free and with-gravity flows for all the mentioned physical properties. Also in Chapter 5 in the presence of gravity, we evaluate the total energy (kinetic and potential) distribution, taking into account the jets. It is well-known that the energy is not conserved in the Wagner model. The thickness of the spray jets, given by (Wilson 1989) and (Howison et al. 1991), is used to calculate the mass and energy fluxes into the jets when gravity is taken into account.

Finally, in Chapter 6 we draw conclusions together and make suggestion for future work following on from that presented in Chapters 2-5.

Chapter 2

Linearised sloshing-slamming problem

In this chapter, we formulate and study the sloshing-slamming problem in a rectangular container with rigid walls. The container is stationary. The liquid flow in the container and subsequent impact by the liquid onto the lid of the container are caused by initial deflection of the liquid's free-surface from its equilibrium level. The gap between the container's lid and the equilibrium level of the liquid is small compared with the dimensions of the container. The sloshing is considered in high-filling condition. The liquid flow before impact is governed by gravity. If the duration of the impact stage, when the wetted area of the lid is increasing starting from a single point, is small compared with the gravity time scale, the gravity can be approximately neglected in calculations of the size of the wetted area and the impact pressure distribution along the lid. This gravity-free approximation of liquid impact is studied in the present chapter.

In section 2.1, we give a description of the problem and discuss some possible evolutions of the surface elevation. In section 2.2, we carry out the formulation, non-dimensionalisation and linearization of the problem. We consider the problem with and without the rigid plate (lid) and we use asymptotic analysis to formulate the Mixed boundary-value Problem (MBVP) when the rigid lid is present. Next we semi-analytically find results for the sloshing impact in section 2.3, in the leading order. Finally, in section 2.4 we investigate the evolutions of the kinetic and potential energies of the liquid in the tank during the impact, under the assumption of the total energy conservation.

2.1 Description of the Problem

In this study we consider a highly-filled rectangular tank containing an inviscid, incompressible fluid in two-dimensional motion. The rectangular cross-section of the tank has height H and length $2L$ and lies in the upper half plane ($y \geq 0$) centered at the origin. Also $y = 0$ is the bottom and $y = H$ is the rigid lid of the tank, $y = H - h$ is the still water level, and $x = \pm L$ are the rigid side walls of the tank. (Woodward & Pitbaldo 2010) presented with illustrations and diagrams all the details of the LNG tanks and storages' structure and design.

The fluid is initially at rest, $t = 0$ is the instant when the fluid starts to move due to gravity. The initial shape of the free-surface is sketched in Figure 2.1 and is described by the equation $y = \mathrm{f}(x)$, where x is the horizontal coordinate and y is the vertical coordinate. In non-dimensional variables (designated with tilde ˜) the initial free-surface shape is given by the equation $\tilde{y} = \tilde{\mathrm{f}}(\tilde{x})$, where

$$\tilde{\mathrm{f}}(\tilde{x}) = 1 - \epsilon + \epsilon \sum_{n=1}^{\infty} \bar{f}_n \cos(k_n \tilde{x}), \tag{2.1}$$

where the constants $\bar{f}_n$ and k_n will be introduced later in section 2.2.3 and ˜stands for non-dimensional coefficients. The coefficient ϵ is small, as we are concerned with high fill levels.

Initially there is no contact between the rigid lid and the liquid and the free-surface is the upper boundary of the liquid domain. The fluid starts to flow, from rest, at $t = 0$. Gravity forces the fluid to fill in the depression shown in the middle of Figure 2.1. After a short period of time the fluid hits the rigid lid from below, as shown in Figure 2.2, impact occurs at time $t = t_n, n = 3, 4, 5, 6$, where t_n represents the different time of several events for each $n = 1, 2, \ldots, 8$, and if $n > m$, then $t_n > t_m$. At $t = t_3$ the free-surface hits the plate from below and creates an interval of wetted contact with the plate. The wetted interval lengthens until $t = t_6$ and later shrinks. The fluid then separates from the plate at $t = t_7$. During this work the period of impact with expanding wetted interval will be called the *impact stage* and the period of shrinking until it separates will be called the *exit stage*. The former stage is of our interest in this study.

As shown Figures 2.1 and 2.2, both the shape and the flow are symmetric in such a way that no air cushion is assumed to exist between the rigid lid and the fluid during the time of contact. The air cavity in highly filled tanks is discussed experimentally and numerically in (Rognebakke & Faltinsen 2005) and (Ten et al. 2011).

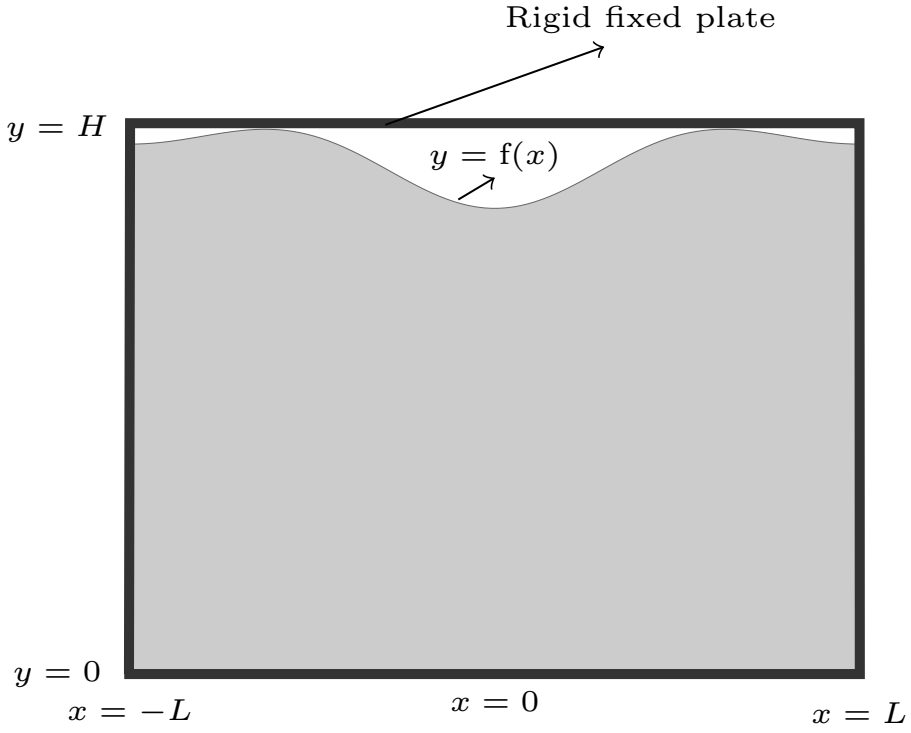

Figure 2.1: Vertical cross-section of the tank. Sketch of the initial shape of the free-surface.

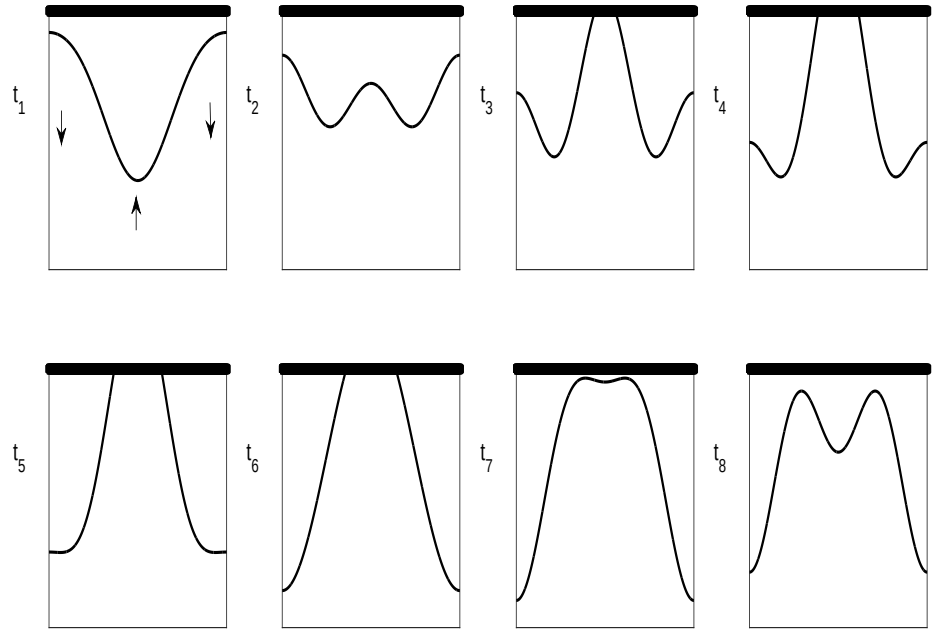

Figure 2.2: Evolution of the free-surface during approach to first impact at the centre of the tank, and the subsequent wetting and drying of the rigid lid plate.

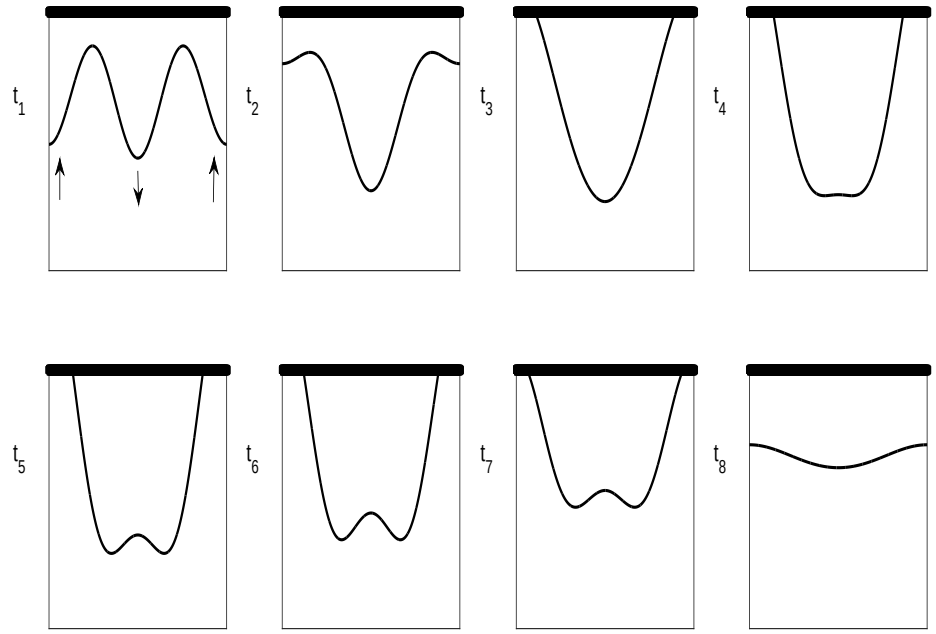

Figure 2.3: Evolution of the free-surface during approach to impact at the top corners of the tank, and the subsequent wetting and drying of the rigid lid plate.

Two other different impacts, which are assumed to follow the first one but in different situations, are shown in Figures 2.3–2.4, where the evolution of the second contact and the third contact, respectively, which occur one after another with the initial free-surface given by equation (2.1) is demonstrated. The two later contacts are different from the earlier one in that they hit the rigid lid in two different points simultaneously. The middle sloshing is when the fluid comes to hit the rigid lid along the walls of the tank and in the last sloshing, the fluid hits the rigid lid from the centre in two contact points with air trapped between them.

2.2 Mathematical formulation

In this section the problem is formulated and non-dimensionalized, first, without a rigid lid, then the rigid lid is introduced. For the former case the problem is linearised and solved analytically. As to the latter case, the problem is asymptotically analysed by using a stretched variable to help reduce the problem to a MBVP, in terms of a complex velocity potential and a displacement potential. The problem is solved semi-analytically (semi-numerically).

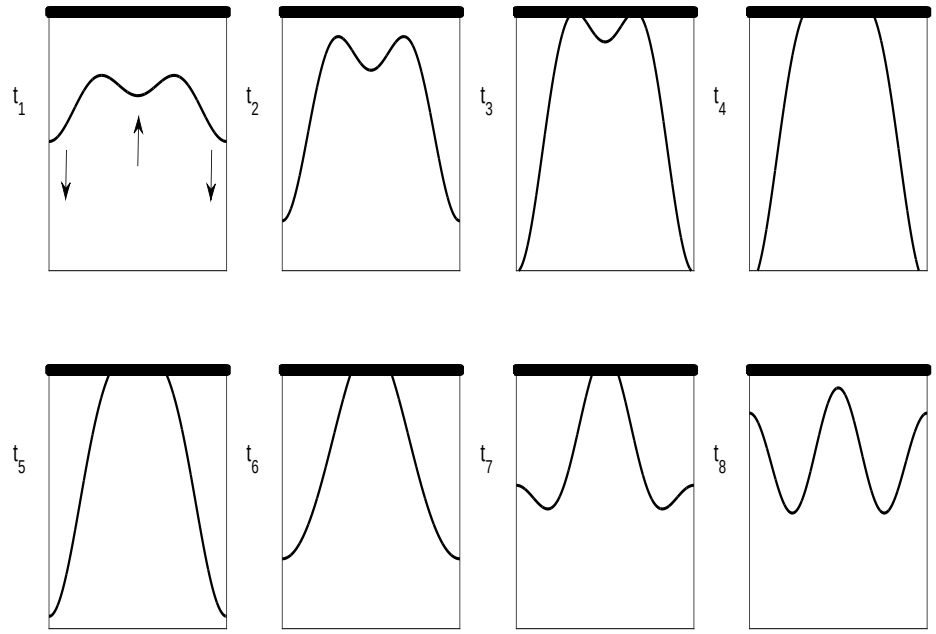

Figure 2.4: Free-surface evolution before, during and after the third impact between the fluid and the rigid lid.

2.2.1 Governing Equations

The fluid is initially at rest and considered to be inviscid and incompressible. If the fluid starts from rest, then by Kelvin's theorem the fluid flow is subsequently irrotational, and therefore the fluid velocity, $\mathbf{u}$, can be described by the velocity potential $\phi(x, y, t)$, that is

$$\mathbf{u} = \frac{\partial \phi}{\partial x}\mathbf{i} + \frac{\partial \phi}{\partial y}\mathbf{k},$$

where $\mathbf{i}$ and $\mathbf{k}$ are unit vectors pointing in the directions x-increasing and y-increasing. The incompressibility of the fluid implies that the velocity potential, $\phi(x, y, t)$, satisfies Laplace's equation in the flow domain:

$$\frac{\partial^2 \phi}{\partial x^2} + \frac{\partial^2 \phi}{\partial y^2} = 0.$$

The boundary conditions are imposed on the walls of the tank $|x| = L$, $y = 0, y = H$ and on the free-surfaces. After wetting from the centre, there will be two free-surfaces, between the walls and the contact region, see Figure 2.6. The presence of the rigid fixed plate which does not allow the fluid to go above $y = H$ in the interval $-L < x < L$ is modelled by an external air pressure $p(x, t)$ acting on the fluid boundary in the contact region, where the plate is wetted. The free-surface

elevation is described by

$$y = H - h + \eta(x,t), \tag{2.2}$$

where $y = H$ is the position of the lid and h is the distance between the static liquid surface, in its equilibrium state, and the rigid lid, as shown in Figure 2.5. Throughout this work we choose $h = 0.05H$, so the fluid level in the tank is 95% of the tank's height which is highly filled. The surface elevation (relative to its horizontal equilibrium level) is denoted by $\eta(x,t)$. The initial position of the free-surface is given by

$$\mathrm{f}(x) = H - h + h\sum_{n=1}^{\infty} \bar{f}_n \cos\left(\frac{k_n}{H}x\right), \tag{2.3}$$

where $\bar{f}_n$ and k_n are defined in equations (2.41) and (2.43), respectively. As presented in the following formulation in terms of the velocity potential that governs the liquid flow inside the tank

$$\frac{\partial^2\phi}{\partial x^2} + \frac{\partial^2\phi}{\partial x^2} = 0 \qquad |x| < L, 0 < y < H - h + \eta, \tag{2.4}$$

$$\frac{\partial\phi}{\partial x} = 0 \qquad x = \pm L, 0 < y < H - h + \eta, \tag{2.5}$$

$$\frac{\partial\phi}{\partial y} = 0 \qquad |x| < L, y = 0, \tag{2.6}$$

$$\frac{\partial\phi}{\partial y} = 0 \qquad |x| \le x_c, y = H, \tag{2.7}$$

$$\frac{\partial\phi}{\partial y} - \frac{\partial\phi}{\partial x}\frac{\partial\eta}{\partial x} = \frac{\partial\eta}{\partial t} \qquad x_c < |x| < L, y = H - h + \eta, \tag{2.8}$$

$$\frac{\partial\phi}{\partial t} + \frac{1}{2}\left[\left(\frac{\partial\phi}{\partial x}\right)^2 + \left(\frac{\partial\phi}{\partial y}\right)^2\right] + gy + C = \frac{-1}{\rho}p \quad |x| < L, 0 < y < H - h + \eta, \tag{2.9}$$

with initial data

$$\phi(x,y,0) = 0, \tag{2.10}$$

$$\eta(x,0) = \mathrm{f}(x). \tag{2.11}$$

Where ρ and g are the constant fluid density and the gravitational acceleration, respectively, and $\mathrm{f}(x)$ is given by equation (2.3). We consider the initial condition (2.10) from a mathematical point of view which is formal to start with it, however physically this situation is difficult to be considered. On $y = H$, the points $x = \mp x_c$ are the end points of the wetted interval, up to the turnover points.

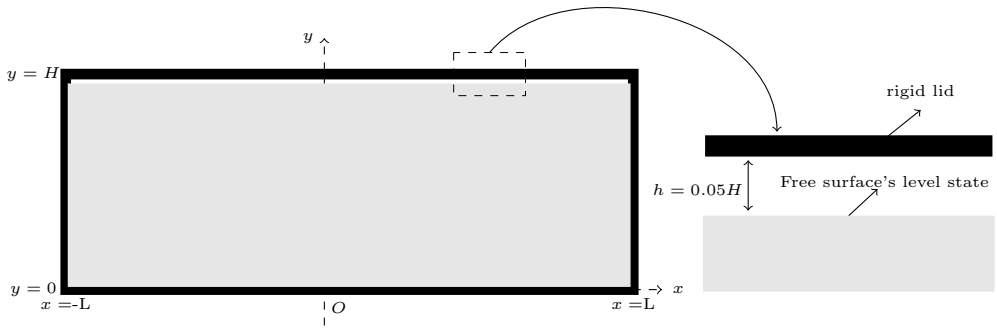

Figure 2.5: Container description with the free-surface at its equilibrium static level state.

We neglect the very thin jets beyond the turnover points shown in Figure 2.6. The length of the wetted interval is $2x_c(t)$ as shown in Figure 2.6. The function $x_c(t)$ is unknown and should be determined as part of the solution. p is the pressure on the upper boundary of the liquid domain, which is a combination of the atmospheric pressure p_{atm} on the free-surface and unknown pressure $\hat{p}$ in the wetted interval of the rigid lid. Also in equation (2.9) C is a constant and its value is defined to be

$$C = g(h - H) - \rho^{-1} p_{atm}. \tag{2.12}$$

This value of C ensures that $p = p_{atm}$ on the static liquid surface when the liquid is at rest. The atmospheric pressure (ullage pressure) p_{atm} is constant throughout the fluid motion because the fluid's total area and tank's total area are constants. Therefore, having this and the symmetric impact which starts from a point (the centre of the rigid lid) the liquid does not compress the gas between the free-surface and the fixed rigid lid during the interaction.

On the free-surface, $y = H - h + \eta$, Bernoulli′s equation (2.9) can be written as the following boundary relation, (as we do not know $\hat{p}$ on plate or ϕ or η on the free-surface)

$$\frac{-1}{\rho}\hat{p} = \frac{\partial \phi}{\partial t} + \frac{1}{2}\left[\left(\frac{\partial \phi}{\partial x}\right)^2 + \left(\frac{\partial \phi}{\partial y}\right)^2\right] + g\eta. \tag{2.13}$$

Before the impact on the free-surface $\hat{p} = 0$ and also after interaction on the two free-surfaces between the walls and the contact region. On the other hand $\hat{p} > 0$ and $\eta = h$ along the wetted part of the rigid lid which is created after the interaction starts.

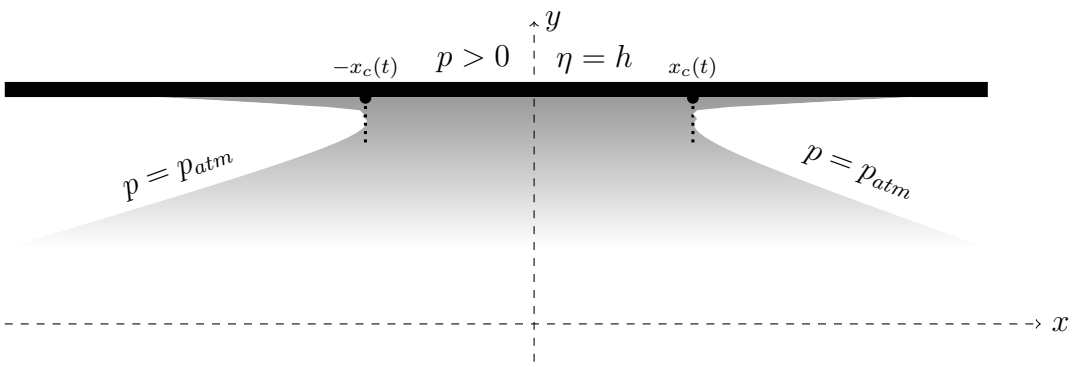

Figure 2.6: Fluid in contact with the rigid lid. The liquid domain shaded in gray and the gas occupies the white zones.

2.2.2 Non-dimensional variables

First we consider the tank to be without a rigid lid, so that the pressure on the free-surface is only the atmospheric pressure p_{atm} and $\hat{p} = 0$ in equation (2.13). We replace both the velocity potential $\phi(x, y, t)$ and the surface elevation $\eta(x, t)$ by $\phi_n(x, y, t)$ and $\eta_n(x, t)$ as new velocity potential and surface elevation to be used in this stage, respectively. The velocity potential $\phi_n(x, y, t)$ satisfies Laplace's equation in the flow domain. For the conditions on the boundaries we still have the same conditions as before with the exception of the one on the rigid lid $y = H$. Since there is no rigid lid so there will be no boundary condition on $y = H$ as we have in equation (2.7) and the surface position $y = H - h + \eta_n$ is considered to be free for all t. The mathematical formulation of the problem in two-dimensional fluid flow with respect to the velocity potential $\phi_n(x, y, t)$ and the surface elevation $\eta_n(x, t)$ in the symmetric fluid flow region takes the form

$$\frac{\partial^2 \phi_n}{\partial x^2} + \frac{\partial^2 \phi_n}{\partial y^2} = 0 \qquad |x| < L, 0 < y < H - h + \eta_n, \tag{2.14}$$

$$\frac{\partial \phi_n}{\partial x} = 0 \qquad x = \pm L, 0 < y < H - h + \eta_n, \tag{2.15}$$

$$\frac{\partial \phi_n}{\partial y} = 0 \qquad |x| < L, y = 0, \tag{2.16}$$

$$\frac{\partial \phi_n}{\partial y} - \frac{\partial \phi_n}{\partial x}\frac{\partial \eta_n}{\partial x} = \frac{\partial \eta_n}{\partial t} \qquad |x| < L, y = H - h + \eta_n, \tag{2.17}$$

$$\frac{\partial \phi_n}{\partial t} + \frac{1}{2}\left[\left(\frac{\partial \phi_n}{\partial x}\right)^2 + \left(\frac{\partial \phi_n}{\partial y}\right)^2\right] = -g\eta_n \quad |x| < L, y = H - h + \eta_n, \tag{2.18}$$

with initial data

$$\phi_n(x, y, 0) = 0, \tag{2.19}$$

$$\eta_n(x, 0) = \mathrm{f}(x). \tag{2.20}$$

We start to non-dimensionalize the problem (2.14)–(2.20) by introducing the non-dimensional variables

$$\begin{aligned} x &= H\tilde{x}, & y &= H\tilde{y}, \qquad t = T_{sc}\tilde{t}, \\ \phi_n &= \phi_{sc}\tilde{\phi}_n, & \eta_n &= h\tilde{\eta}_n. \end{aligned} \tag{2.21}$$

In non-dimensional variables (2.21), the kinematic boundary condition (2.17) requires

$$T_{sc} = \frac{h\ H}{\phi_{sc}}, \tag{2.22}$$

and the dynamic boundary condition (2.17) in non-dimensional variables (2.21) together with equation (2.22), give the two scales, velocity potential scale, ϕ_{sc}, and time scale, T_{sc}, respectively, to be

$$\phi_{sc} = h\sqrt{Hg}, \qquad T_{sc} = \sqrt{\frac{H}{g}}. \tag{2.23}$$

The above scales (2.21)–(2.23) introduce two non-dimensional parameters

$$\epsilon = \frac{h}{H}, \qquad \lambda = \frac{L}{H}. \tag{2.24}$$

The ratio of gas depth to the liquid depth is the parameter ϵ and it is very small. We will find that it represents the non-linearity of the problem. The parameter λ is of order unity and represents the tank's height and width ratio. The new formulation of the problem (2.14)–(2.20) in non-dimensional variables (with the tilde's dropped) takes the form

$$\frac{\partial^2\phi_n}{\partial x^2} + \frac{\partial^2\phi_n}{\partial y^2} = 0 \qquad |x| < \lambda, 0 < y < 1 - \epsilon + \epsilon\eta_n, \tag{2.25}$$

$$\frac{\partial\phi_n}{\partial x} = 0 \qquad x = \pm\lambda, 0 < y < 1 - \epsilon + \epsilon\eta_n, \tag{2.26}$$

$$\frac{\partial\phi_n}{\partial y} = 0 \qquad |x| < \lambda, y = 0, \tag{2.27}$$

$$\epsilon\frac{\partial\phi_n}{\partial x}\frac{\partial\eta_n}{\partial x} + \frac{\partial\eta_n}{\partial t} = \frac{\partial\phi_n}{\partial y} \qquad |x| < \lambda, y = 1 - \epsilon + \epsilon\eta_n, \tag{2.28}$$

$$\frac{\partial\phi_n}{\partial t} + \frac{\epsilon}{2}\left[\left(\frac{\partial\phi_n}{\partial x}\right)^2 + \left(\frac{\partial\phi_n}{\partial y}\right)^2\right] = -\eta_n \qquad |x| < \lambda, y = 1 - \epsilon + \epsilon\eta_n, \tag{2.29}$$

with the initial data

$$\phi_n(x, y, 0) = 0, \tag{2.30}$$

$$\eta_n(x, 0) = \mathrm{f}(x), \tag{2.31}$$

where we must choose $\mathrm{f}(x) < 1$.

After linearization the presence of ϵ in the kinematic boundary condition (2.28) and dynamic boundary condition (2.29), suggest that we express $\phi_n(x, y, t)$ and $\eta_n(x, t)$ in terms of regular series expansions with respect to ϵ:

$$\phi_n = \phi_{n0} + \epsilon\phi_{n1} + O(\epsilon^2),$$
$$\eta_n = \eta_{n0} + \epsilon\eta_{n1} + O(\epsilon^2).$$

The non-dimensional problem (2.25)–(2.31) at the leading order takes the form

$$\frac{\partial^2\phi_{n0}}{\partial x^2} + \frac{\partial^2\phi_{n0}}{\partial y^2} = 0 \qquad |x| < \lambda, 0 < y < 1, \tag{2.32}$$
$$\frac{\partial\phi_{n0}}{\partial x} = 0 \qquad x = \pm\lambda, 0 < y < 1, \tag{2.33}$$
$$\frac{\partial\phi_{n0}}{\partial y} = 0 \qquad |x| < \lambda, y = 0, \tag{2.34}$$
$$\frac{\partial\phi_{n0}}{\partial y} = \frac{\partial\eta_{n0}}{\partial t} \qquad |x| < \lambda, y = 1, \tag{2.35}$$
$$\frac{\partial\phi_{n0}}{\partial t} = -\eta_{n0} \qquad |x| < \lambda, y = 1, \tag{2.36}$$

with initial data

$$\phi_{n0}(x, y, 0) = 0, \tag{2.37}$$
$$\eta_{n0}(x, 0) = \mathrm{f}(x). \tag{2.38}$$

2.2.3 The leading-order solution without a rigid lid

The boundary-value problem (2.32)–(2.38) can be solved by using separation of variables and Fourier series techniques for $\phi_{n0}(x, y, t)$ and $\eta_{n0}(x, t)$, these give

$$\phi_{n0}(x, y, t) = \sum_{n=1}^{\infty} f_n \cosh(k_n y)\cos(k_n x)\sin(w_n t), \tag{2.39}$$

and

$$\eta_{n0}(x, t) = \sum_{n=1}^{\infty} \bar{f}_n \cos(k_n x)\cos(w_n t), \tag{2.40}$$

for $n = 1, 2, \ldots$, where f_n and $\bar{f}_n$ are constants such that,

$$\bar{f}_n = -\frac{2}{\lambda} f_n \omega_n \cosh(k_n), \tag{2.41}$$

and the frequency dispersion relation

$$\omega_n = \sqrt{k_n \tanh(k_n)}, \tag{2.42}$$

with the wave number

$$k_n = \frac{n\pi}{\lambda}. \tag{2.43}$$

The initial shape of the free-surface is given by equation (2.3). We can design the shape with the aim to reproduce particular impact situations by choosing $\bar{f}_n = 0$ for $n = 3, 4, ...$ and some non-zero values for $\bar{f}_1$ and $\bar{f}_2$ which are enough to obtain required initial shapes, as shown in Figure 2.7. Each of the shapes in Figure 2.7 as we see gives a different initial shape depending on the values of $\bar{f}_1$ and $\bar{f}_2$. It is noticed that the values of $\bar{f}_1$ near -0.5891 and $\bar{f}_2$ near -0.3724 result in shapes almost similar to those shown in Figure 2.1, which are our desired initial free-surface shape.

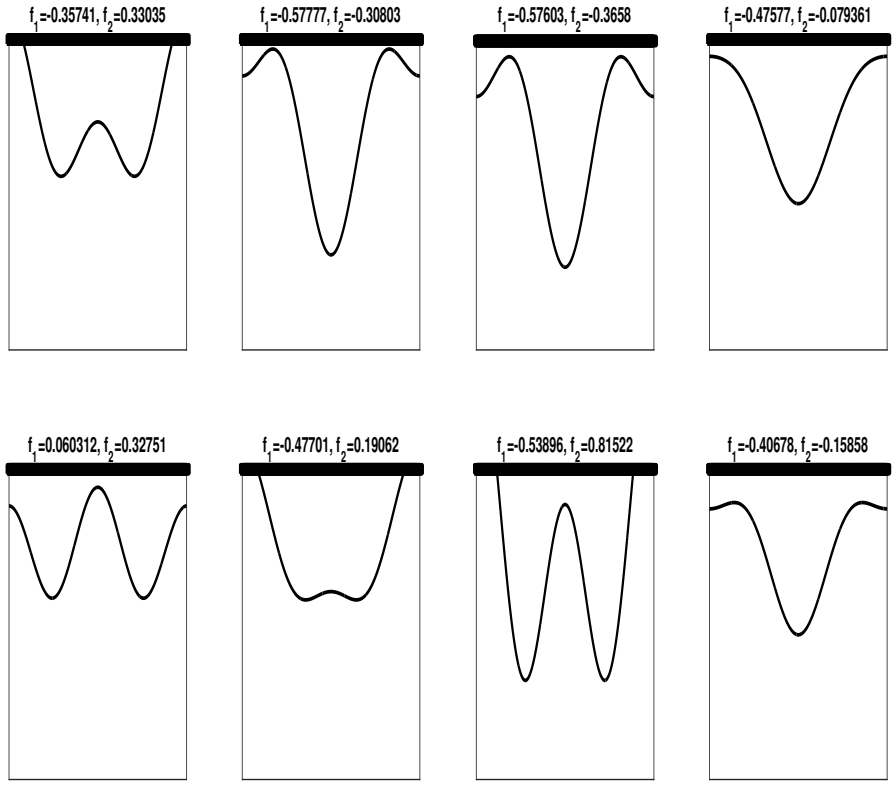

Figure 2.7: Examples of initial free-surface elevations, the values of $\bar{f}_1$ and $\bar{f}_2$ are shown above each plot.

A contour plot of the non-dimensional free-surface $\eta_{n0}(x, t)$ in the leading order

for t varying from $t = 0$ to $t = 2.5$, is shown in Figure 2.8. Only the free-surface elevation is plotted and the plot is vertically exaggerated between $y = 0.85$ and $y = 1.05$. The red contour line is when the elevation of the free-surface is at its peak and this occurs at the centre. The blue contour line is when the free-surface has its minimum height.

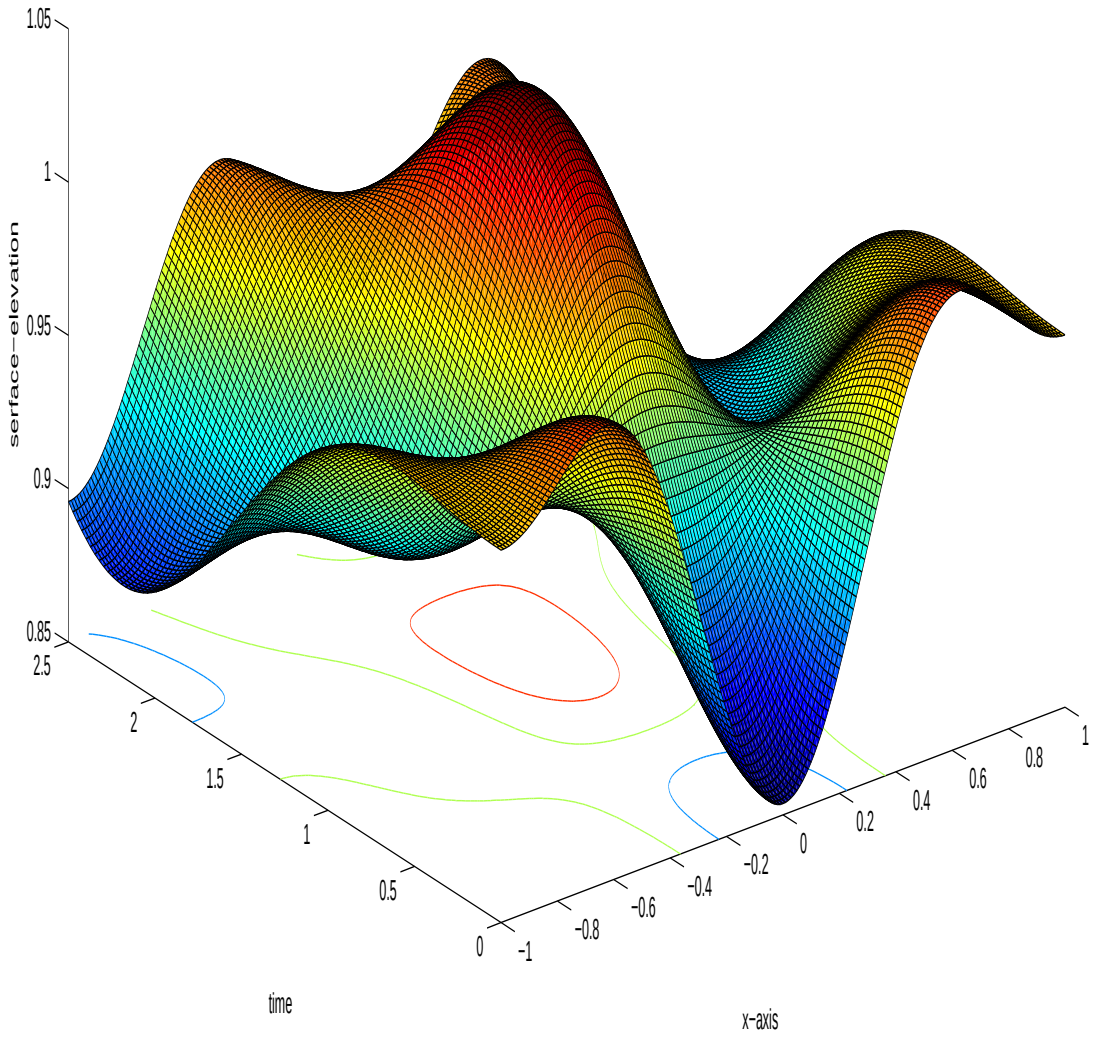

Figure 2.8: The leading-order free-surface elevation $\eta_{n0}(x, t)$.

2.2.4 The flow in the presence of a rigid lid

Let the non-dimensional time t_* be the instant when the fluid free-surface hits the centre of the rigid lid. After the start of the interaction between the fluid flow and the rigid lid, i.e. for $t \geq t_*$, the unknown function $x_c(t)$ is introduced into our problem which gives the half-length of the wetted part of the rigid lid at time t. The function $x_c(t)$ represents the right moving point (turnover point) of the free-surface where it turns over and very thin jets are formed at the periphery of the wetted interval. After wetting starts, $\hat{p} > 0$ in $|x| \leq x_c, y = 1$. We return to the velocity potential $\phi(x, y, t)$, which governs the fluid flow in our problem and we write the formulation of the problem (2.4)–(2.11) in non-dimensional variables. We use the same non-dimensional variables, scales and parameters as in the problem (2.14)–(2.20), noting that the pressure $\hat{p}(x, t)$ and $x_c(t)$ now appear in this formulation. We use

$$\hat{p} = \rho g h \tilde{p}, \qquad x_c(t) = H\tilde{x}_c(t), \tag{2.44}$$

to non-dimensionalise the pressure $\hat{p}(x, t)$ and $x_c(t)$. The problem (2.4)–(2.11) in non-dimensional variables (without tilde) is

$$\frac{\partial^2\phi}{\partial x^2} + \frac{\partial^2\phi}{\partial y^2} = 0 \qquad |x| < \lambda, 0 < y < 1 - \epsilon + \epsilon\eta, \tag{2.45}$$

$$\frac{\partial\phi}{\partial x} = 0 \qquad x = \pm\lambda, 0 < y < 1 - \epsilon + \epsilon\eta, \tag{2.46}$$

$$\frac{\partial\phi}{\partial y} = 0 \qquad |x| < \lambda, y = 0, \tag{2.47}$$

$$\frac{\partial\phi}{\partial y} = 0 \qquad |x| \leq x_c, y = 1, \tag{2.48}$$

$$\epsilon\frac{\partial\phi}{\partial x}\frac{\partial\eta}{\partial x} + \frac{\partial\eta}{\partial t} = \frac{\partial\phi}{\partial y} \qquad x_c < |x| < \lambda, y = 1 - \epsilon + \epsilon\eta, \tag{2.49}$$

$$\frac{\partial\phi}{\partial t} + \frac{\epsilon}{2}\left[\left(\frac{\partial\phi}{\partial x}\right)^2 + \left(\frac{\partial\phi}{\partial y}\right)^2\right] + \eta = -p \quad |x| \leq x_c, y = 1, \tag{2.50}$$

$$\frac{\partial\phi}{\partial t} + \frac{\epsilon}{2}\left[\left(\frac{\partial\phi}{\partial x}\right)^2 + \left(\frac{\partial\phi}{\partial y}\right)^2\right] + \eta = 0 \qquad x_c < |x| < \lambda, y = 1 - \epsilon + \epsilon\eta, \tag{2.51}$$

where $y = 1$ refers to the wetted zone on the lid where $\eta = 1$. The Wagner condition (Wagner 1932) suggests that by neglecting the jets due to their tiny width (Howison et al. 1991), the surface elevation at its turnover points $x = \pm x_c$ is at the position of the lid, this provides

$$\eta(\pm x_c, t) = 1. \tag{2.52}$$

The above formulation is supplemented with initial data

$$\phi(x, y, 0) = 0, \tag{2.53}$$

$$\eta(x, 0) = \mathrm{f}(x). \tag{2.54}$$

The parameter ϵ is small, $\epsilon \ll 1$, in this formulation, so we linearise the kinematic boundary condition (2.49) and the dynamic boundary conditions (2.50)–(2.51). Linearisation also involves posing the free-surface boundary conditions on $y = 1$. The length of the wetted interval $-x_c(t) < x < x_c(t)$, is $2x_c(t)$, which is of order $O(1)$ as $\epsilon \longrightarrow 0$, and so we write it in terms of an asymptotic expansion, as follows

$$x_c(t) = x_{c0}(t) + \epsilon x_{c1}(t) + O(\epsilon^2), \tag{2.55}$$

with the asymptotic expansions of the velocity potential, surface elevation and pressure in the wetted interval, respectively,

$$\phi(x, y, t) = \phi_0(x, y, t) + \epsilon\phi_1(x, y, t) + O(\epsilon^2), \tag{2.56}$$

$$\eta(x, t) = \eta_0(x, t) + \epsilon\eta_1(x, t) + O(\epsilon^2), \tag{2.57}$$

$$p(x, t) = p_0(x, t) + \epsilon p_1(x, t) + O(\epsilon^2). \tag{2.58}$$

In the leading order, the velocity potential $\phi_0(x, y, t)$ satisfies the following equations

$$\frac{\partial^2\phi_0}{\partial x^2} + \frac{\partial^2\phi_0}{\partial y^2} = 0 \qquad |x| < \lambda, 0 < y < 1, \tag{2.59}$$

$$\frac{\partial\phi_0}{\partial x} = 0 \qquad x = \pm\lambda, 0 < y < 1, \tag{2.60}$$

$$\frac{\partial\phi_0}{\partial y} = 0 \qquad |x| < \lambda, y = 0, \tag{2.61}$$

$$\frac{\partial\phi_0}{\partial y} = 0 \qquad |x| \leq x_{c0}, y = 1, \tag{2.62}$$

$$\frac{\partial\phi_0}{\partial y} = \frac{\partial\eta_0}{\partial t} \qquad x_{c0} < |x| < \lambda, y = 1, \tag{2.63}$$

$$\frac{\partial\phi_0}{\partial t} + \eta_0 = -p_0 \qquad |x| \leq x_{c0}, y = 1, \tag{2.64}$$

$$\frac{\partial\phi_0}{\partial t} + \eta_0 = 0 \qquad x_{c0} < |x| < \lambda, y = 1, \tag{2.65}$$

$$\eta_0 = 1 \qquad \text{at} \qquad x = \pm x_c, \tag{2.66}$$

with initial data

$$\phi_0(x, y, 0) = 0, \tag{2.67}$$

$$\eta_0(x, 0) = \mathrm{f}(x). \tag{2.68}$$

For $t < t_*$ the velocity potential $\phi_0(x, y, t)$ and the surface elevation $\eta_0(x, t)$ of the flow are given by $\phi_{n0}(x, y, t)$ and $\eta_{n0}(x, t)$, respectively, which were evaluated in the previous section. For $t > t_*$, the velocity potential $\phi_0(x, y, t)$ can be decomposed as $\phi_{n0}(x, y, t)$ which is the velocity potential of the flow without the rigid lid and a correction term $\phi_{c0}(x, y, t)$. The same could be done with the surface elevation $\eta_0(x, t)$ decomposed into $\eta_{n0}(x, t)$ which is the surface elevation of the flow without a rigid lid and the correction term $\eta_{c0}(x, t)$. Hence

$$\phi_0 = \phi_{n0} + \phi_{c0}, \tag{2.69}$$

$$\eta_0 = \eta_{n0} + \eta_{c0}. \tag{2.70}$$

The formulation of the problem at leading order with respect to the correction functions $\phi_{c0}(x, y, t)$ and $\eta_{c0}(x, t)$ and the pressure $p_0(x, t)$ in the wetted region reads

$$\frac{\partial^2 \phi_{c0}}{\partial x^2} + \frac{\partial^2 \phi_{c0}}{\partial y^2} = 0 \qquad |x| < \lambda, 0 < y < 1, \tag{2.71}$$

$$\frac{\partial \phi_{c0}}{\partial x} = 0 \qquad |x| = \lambda, 0 < y < 1, \tag{2.72}$$

$$\frac{\partial \phi_{c0}}{\partial y} = 0 \qquad |x| < \lambda, y = 0, \tag{2.73}$$

$$\frac{\partial \phi_{c0}}{\partial y} = -\frac{\partial \eta_{n0}}{\partial t} \qquad |x| \leq x_{c0}, y = 1, \tag{2.74}$$

$$\frac{\partial \phi_{c0}}{\partial t} + \eta_{c0} = -p_0 \qquad |x| \leq x_{c0}, y = 1, \tag{2.75}$$

$$\frac{\partial^2 \phi_{c0}}{\partial t^2} + \frac{\partial \phi_{c0}}{\partial y} = 0 \qquad x_{c0} < |x| < \lambda, y = 1, \tag{2.76}$$

$$\eta_{c0} + \eta_{n0} = 1 \qquad \text{at} \qquad x = \pm x_c, \tag{2.77}$$

with initial data

$$\phi_{c0}(x, y, t_*) = 0, \tag{2.78}$$

$$\eta_{c0}(x, t_*) = 0. \tag{2.79}$$

In this formulation the velocity potential $\phi_{n0}(x, y, t)$ and the surface elevation $\eta_{n0}(x, t)$ are known functions while the velocity potential $\phi_{c0}(x, y, t)$, the surface elevation $\eta_{c0}(x, t)$, the pressure $p_o(x, t)$ and the function $x_{c0}(t)$ are to be determined. The MBVB (2.71)–(2.79) can be solved if $x_{c0}(t)$ is known. An equation or a condition should be added to the formulation (2.71)–(2.79), to determine the size of the wetted region $(-x_{c0}, x_{c0})$.

At $t = t_*$ the flow hits the rigid lid in a single point, which gives the initial condition

$$x_{c0}(t_*) = 0, \tag{2.80}$$

which will be crucial as an initial condition in finding the unknown function $x_{c0}(t)$ later. However, the problem (2.71)–(2.80) is still difficult to be solved and we approach the solution asymptotically in the next section.

2.2.5 Asymptotic analyses of the flow during the early stage

We consider the asymptotics of the flow when t is close to t_* for the boundary-value problem (2.71)–(2.80) in a small time interval by introducing stretched variables. Locally close to the contact point, the shape of the free-surface elevation, without the rigid lid, at $t = t_*$ is $y = 1 - \epsilon + \epsilon\eta_n(x, t_*)$. Since the flow is symmetric and the free-surface has its maximum elevation at $x = 0$, we write its Taylor series expansion about $x = 0$ as

$$\eta_n(x, t_*) = 1 + x\frac{\partial \eta_n}{\partial x}(0, t_*) + \frac{x^2}{2}\frac{\partial^2 \eta_n}{\partial x^2}(0, t_*) + ..., \tag{2.81}$$

but from symmetry we have

$$\frac{\partial \eta_n}{\partial x}(0, t_*) = 0,$$

and close to the contact point we have

$$\frac{\partial^2 \eta_n}{\partial x^2}(0, t_*) = O(1).$$

Therefore from equation (2.81) the free-surface elevation shape close to the contact point at the time instant of impact is approximately a parabola, which moves up against the rigid lid, and which has the form

$$y \simeq 1 - \frac{1}{2R}x^2 + \mathrm{h}(t), \tag{2.82}$$

where $\mathrm{h}(t) = V_0(t - t_*)$, V_0 is assumed to be the constant impact velocity and $R > 0$ is the parabola's radius of curvature at $x = 0$. Actually the shape of the free-surface elevation $\eta_n(x, t_*)$ may be more complicated, but during the very short initial stage before impact the shape of the free-surface elevation $\eta_n(x, t_*)$ can be approximated by a parabola.

Following the pioneering work of (von Karman 1929), from equation (2.82), can be approximated to give

$$x_k \simeq \sqrt{2RV_0(t-t_*)}, \tag{2.83}$$

where $x = x_k$ is assumed to be the approximated moving contact point for $t > t_*$. The small speed of the approximated parabola comparing to the speed of the jets gives us this motivation to introduce the following parameter δ. In this stage when t is close to t_*, we introduce the parameter δ, where $\delta \ll 1$, to describe a suitable time variable when time is close to t_*. The flow is driven by gravity, and this small parameter indicates the small duration of impact. Depending on equations (2.82)–(2.83) we introduce the following stretched variables

$$\begin{aligned} t &= t_* + \delta\ \tau, \\ x &= \delta^{1/2}\ \xi, \\ y &= 1 + \delta^{1/2}\ \zeta. \end{aligned} \tag{2.84}$$

The time is stretched by the formal parameter δ close to the instant of impact at $t = t_*$. The horizontal x variable is stretched by $\delta^{1/2}$, using the approximated Karman's assumption (2.83). To retain the balance in Laplace's equation the vertical y variable is stretched by $\delta^{1/2}$. In this problem the leading-order velocity potential correction $\phi_{c0}(x, y, t)$ is $O(1)$. This gives the leading-order variable for the velocity potential correction $\phi_{c0}(x, y, t)$, the surface elevation $\eta_{n0}(x, t)$ and the surface elevation correction $\eta_{c0}(x, t)$ in terms of the new stretched variables, using equation (2.74) , respectively, as

$$\begin{aligned} \phi_{c0}(x, y, t) &= \delta^{1/2}\ \Phi(\xi, \zeta, \tau, \delta), \\ \eta_{n0}(x, t) &= 1 + \delta\ \tilde{\eta}_n(\xi, \tau, \delta), \\ \eta_{c0}(x, t) &= \delta\ \tilde{\eta}_c(\xi, \tau, \delta). \end{aligned} \tag{2.85}$$

Now, we reformulate the problem (2.71)–(2.80) in terms of new dependent and independent variables (with dropping tildes). In this short period of time, $\delta \ll 1$, to analyse the motion of the fluid we scale the two dimensions of the shape, vertically and horizontally. It is shown from relations given in (2.84) that the variables x and y are replaced by the equally stretched variables, ξ and ζ, respectively. Here $\zeta = 0$ represents the rigid lid $y = H$ in dimensional variable. Laplace's equation (2.71) in new variables is

$$\frac{\partial^2 \Phi}{\partial \xi^2} + \frac{\partial^2 \Phi}{\partial \zeta^2} = 0 \qquad\qquad -\infty < \xi < \infty, -\infty < \zeta < 0. \tag{2.86}$$

We do not consider equations (2.72)–(2.73), (2.75) and (2.79) during this short period. The contact points $x = \pm x_{c0}$ in the leading order have been replaced by $\xi = \pm\xi_c(\tau)$. The kinematic boundary condition (2.74) on the contact region gives

$$\frac{\partial \Phi}{\partial \zeta} = -\frac{\partial \eta_n}{\partial \tau} \qquad |\xi| \leq \xi_c, \zeta = 0. \tag{2.87}$$

The Wagner condition (2.77) reads

$$\eta_c + \eta_n = 0 \qquad \text{at} \qquad \xi = \pm \xi_c. \tag{2.88}$$

At time t_* we have $\tau = 0$, therefore the initial conditions (2.78) and (2.80) are rewritten

$$\Phi(\xi, \zeta, 0) = 0, \tag{2.89}$$

$$\xi_c(0) = 0. \tag{2.90}$$

The combined dynamic and kinematic free-surface boundary condition (2.76) in terms of τ and ζ on the two regions between the contact region and the far field takes the form

$$\frac{1}{\delta^{\frac{3}{2}}} \frac{\partial^2 \Phi}{\partial \tau^2} + \frac{\partial \Phi}{\partial \zeta} = 0 \qquad |\xi| > \xi_c, \zeta = 0,$$

multiplying both sides by $\delta^{\frac{3}{2}}$ we have

$$\frac{\partial^2 \Phi}{\partial \tau^2} + \delta^{\frac{3}{2}} \frac{\partial \Phi}{\partial \zeta} = 0 \qquad |\xi| > \xi_c, \zeta = 0. \tag{2.91}$$

This means that $\frac{\partial^2 \Phi}{\partial \tau^2}$ is of order $O(\delta^{\frac{3}{2}})$, hence the second term on the right-hand side can be neglected in the limit as $\delta \longrightarrow 0$:

$$\frac{\partial^2 \Phi}{\partial \tau^2} = O(\delta^{\frac{3}{2}}) \qquad |\xi| > \xi_c, \zeta = 0,$$

then we integrate twice with respect to τ and apply the initial condition (2.89) to obtain

$$\Phi(\xi, 0, \tau) = 0 \qquad |\xi| > \xi_c, \zeta = 0. \tag{2.92}$$

The condition (2.92) refers to the fact that the influence of gravity, g, is negligible in this short period of impact when the fluid flow is highly accelerated. Keeping δ in equation (2.91) represents the effects of gravity on the impact, and this will be studied in details in Chapter 3.

To control the flow in this short period we need to introduce the so-called far-field condition for this stage

$$\Phi(\xi, \zeta, \tau) \longrightarrow 0 \qquad \text{as} \qquad \xi^2 + \zeta^2 \longrightarrow \infty. \tag{2.93}$$

2.2.6 Mixed boundary-value problem in terms of complex velocity potential

The kinematic boundary condition (2.87) is the Neumann boundary condition on the wetted part, and the dynamic boundary condition (2.92) is the Dirichlet boundary condition on the free-surface.

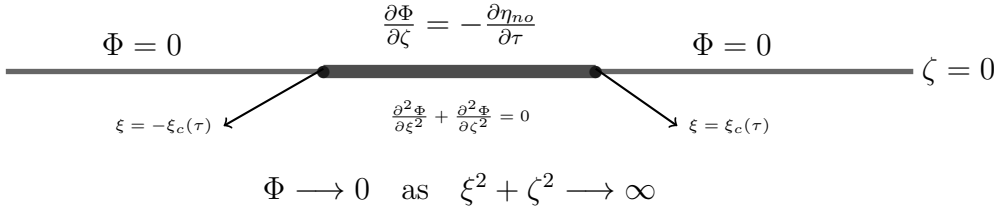

Figure 2.9: The MBVP at the leading order. Bold line in the middle is the wetted region surrounded by two thinner lines that represent the free-surface.

Therefore the resulting problem (2.86)–(2.93) is a MBVP which is summarized in Figure 2.9. The problem does not contain any derivative with respect to time for the unknown functions, and the time variable τ can be considered as a parameter in this problem.

We start by formulating the problem (2.86)–(2.93) in terms of the complex velocity potential, see (Carrier, Krook & Pearson 2005)

$$\mathrm{w}(z,\tau) = \Phi(\xi,\zeta,\tau) + i\Psi(\xi,\zeta,\tau),$$

with the complex variable $z = \xi + i\zeta$, where the imaginary part $\Psi(\xi,\zeta,\tau)$ is the stream function. The analytic function $\mathrm{w}(z,\tau)$ tends to zero as $\xi^2 + \zeta^2 \longrightarrow \infty$. The real and imaginary parts of the analytic function $\mathrm{w}(z,\tau)$ satisfy the Cauchy-Riemann equations

$$\frac{\partial \Phi}{\partial \xi} = \frac{\partial \Psi}{\partial \zeta}, \qquad \frac{\partial \Phi}{\partial \zeta} = -\frac{\partial \Psi}{\partial \xi}. \tag{2.94}$$

By using (2.94) boundary condition (2.87) can be written in terms of the stream function

$$\frac{\partial \Psi}{\partial \xi}(\xi,\zeta,\tau) = \frac{\partial \eta_n}{\partial \tau}(\xi,\tau) \qquad |\xi| < \xi_c, \zeta = 0. \tag{2.95}$$

We integrate both sides of equation (2.95) with respect to ξ from 0 to ξ to obtain

$$\Psi(\xi,0,\tau) = \int_0^{\xi} \frac{\partial \eta_n}{\partial \tau}(\xi^*,\tau)d\xi^* + c_1, \tag{2.96}$$

where c_1 is a constant of integration. The fluid flow is symmetric inside the tank, hence

$$\frac{\partial \Phi}{\partial \xi}(0, \zeta, \tau) = 0 \qquad \zeta < 0, \tag{2.97}$$

and, by using the Cauchy-Riemann conditions (2.94), we obtain

$$\frac{\partial \Psi}{\partial \zeta}(0, \zeta, \tau) = 0 \qquad\qquad \zeta < 0.$$

Integrating the latter equation with respect to ζ yields

$$\Psi(0, \zeta, \tau) = c_2 \qquad\qquad \zeta < 0,$$

where c_2 is a constant. It can be concluded that $c_2 = 0$, since the imaginary part $\Psi(\xi, \zeta, \tau)$ of the analytic function $\mathrm{w}(z, \tau)$ is defined in such a way that it vanishes as $\xi^2 + \zeta^2 \longrightarrow \infty$. Therefore

$$\Psi(0, \zeta, \tau) = 0 \qquad\qquad \zeta < 0,$$

consequently,

$$\Psi(0, 0, \tau) = 0,$$

and in equation (2.96) we conclude that

$$c_1 = 0.$$

The rewritten kinematic boundary condition (2.96) reads

$$\Psi(\xi, 0, \tau) = \int_0^{\xi} \frac{\partial \eta_n}{\partial \tau}(\xi^*, \tau) d\xi^*. \tag{2.98}$$

Now, we seek an analytic function $\mathrm{w}(z, \tau)$ such that

$$\mathrm{Re}\left[\mathrm{w}(\xi - i0, \tau)\right] = 0 \qquad\qquad |\xi| > \xi_c, \tag{2.99}$$

$$\mathrm{Im}[\mathrm{w}(\xi - i0, \tau)] = \int_0^{\xi} \frac{\partial \eta_n}{\partial \tau}(\xi^*, \tau) \mathrm{d}\xi^* \qquad |\xi| < \xi_c, \tag{2.100}$$

$$\mathrm{w}(z, \tau) \longrightarrow 0 \qquad \text{as} \qquad |z| \longrightarrow \infty. \tag{2.101}$$

The problem (2.99)–(2.101) is a MBVP. It can be reduced to the Dirichlet boundary-value problem. We introduce a new function $W(z, \tau)$ as a product of the charac-

teristic function $\sqrt{z^2-\xi_c^2}$ and the analytic function $\mathrm{w}(z,\tau)$,

$$W(z,\tau)=\sqrt{z^2-\xi_c^2}\ \mathrm{w}(z,\tau).$$

The function $\mathrm{W}(z,\tau)$ is the product of two functions that are analytic in the lower half-plane except at $z=\pm\xi_c$, so it is also analytic. The boundary conditions (2.99)–(2.100) provide

$$\mathrm{Re}\left[\mathrm{W}(\xi,0,\tau)\right]=\sqrt{\xi^2-\xi_c^2}\Phi(\xi,0,\tau)=0 \qquad \xi>\xi_c, \tag{2.102}$$

$$\mathrm{Re}\left[\mathrm{W}(\xi,0,\tau)\right]=-\sqrt{\xi^2-\xi_c^2}\Phi(\xi,0,\tau)=0 \quad \xi<-\xi_c, \tag{2.103}$$

$$\begin{aligned}\mathrm{Re}\left[\mathrm{W}(\xi,0,\tau)\right]&=\sqrt{\xi_c^2-\xi^2}\ \Psi(\xi,0,\tau)\\ &=\sqrt{\xi_c^2-\xi^2}\int_0^{\xi}\frac{\partial\eta_n}{\partial\tau}(\xi^*,\tau)\mathrm{d}\xi^* \quad |\xi|<\xi_c.\end{aligned} \tag{2.104}$$

The analytic function $W(z,\tau)$ which satisfies the boundary conditions (2.102)–(2.104) is given by (see (Gakhov & Sneddon 1966) and (Carrier et al. 2005))

$$W(z,\tau)=\frac{i}{\pi}\int_{-\xi_c}^{\xi_c}\frac{\sqrt{\xi_c^2-\xi^{*2}}}{\xi^*-z}\mathrm{v}(\xi^*,\tau)\mathrm{d}\xi^*+ic_0+ic_1z+...,$$

where c_n for $n=0,1,2,...$ are real constants and

$$\mathrm{v}(\xi^*,\tau)=\int_0^{\xi^*}\frac{\partial\eta_n}{\partial\tau}(\hat{\xi},\tau)\mathrm{d}\hat{\xi}.$$

Now, the analytic function $\mathrm{w}(z,\tau)$ can be written as

$$\mathrm{w}(z,\tau)=i\frac{1}{\pi\sqrt{z^2-\xi_c^2}}\int_{-\xi_c}^{\xi_c}\frac{\sqrt{\xi_c^2-\xi^{*2}}}{\xi^*-z}\mathrm{v}(\xi^*,\tau)\mathrm{d}\xi^*+i\frac{c_0}{\sqrt{z^2-\xi_c^2}}+i\frac{c_1z}{\sqrt{z^2-\xi_c^2}}+...,$$

from the far-field condition (2.101) we deduce that $c_n=0$ for $n=1,2,...$ while c_0 could be non-zero. As $\zeta\longrightarrow^{-}0$ and $|\xi|<\xi_c(\tau)$, the Plemelj formula gives

$$\Phi+i\Psi=i\mathrm{v}(\xi,\tau)-\frac{1}{\pi\sqrt{\xi_c^2-\xi^2}}\int_{-\xi_c}^{\xi_c}\frac{\sqrt{\xi_c^2-\xi^{*2}}}{\xi^*-\xi}\mathrm{v}(\xi^*,\tau)\mathrm{d}\xi^*-\frac{c_0}{\sqrt{\xi_c^2-\xi^2}}.$$

The stream function $\Psi(\xi,0,\tau)$ takes the form

$$\Psi(\xi,0,\tau)=\mathrm{v}(\xi,\tau),$$

and the potential $\Phi(\xi,0,\tau)$ along the rigid lid is given in terms of a Cauchy principal-value integral

$$\Phi(\xi,0,\tau)=\frac{-1}{\pi\sqrt{\xi_c^2-\xi^2}}\left[\int_{-\xi_c}^{\xi_c}\frac{\sqrt{\xi_c^2-\xi^{*2}}}{\xi^*-\xi}\mathrm{v}(\xi^*,\tau)\mathrm{d}\xi^*+\pi c_0\right]. \tag{2.105}$$

The velocity potential is zero for $|\xi|>\xi_c, \zeta=0$, (2.92) and has square root behaviour, $\phi\sim\sqrt{\xi_c-\xi}$ for $|\xi|<\xi_c, \zeta=0$. Therefore from continuity of the velocity potential we assume

$$\Phi(\xi_c,0,\tau)=0. \tag{2.106}$$

Applying the condition (2.106) on equation (2.105) at $\xi=\xi_c$, with some manipulation we find

$$c_0=\frac{-1}{\pi}\int_{-\xi_c}^{\xi_c}\sqrt{\frac{\xi_c+\xi^*}{\xi_c-\xi^*}}\mathrm{v}(\xi^*,\tau)\mathrm{d}\xi^*. \tag{2.107}$$

Having the constant c_0, (2.107) the potential (2.105) can be rewritten as follow

$$\Phi(\xi,0,\tau)=\sqrt{\xi_c^2-\xi^2}\sum_{n=1}^{\infty}\bar{f}_n\sin(\omega_n\tau)\int_{-\xi_c}^{\xi_c}\frac{\sin(k_n\xi^*)}{(\xi^*-\xi)\sqrt{\xi_c^2-\xi^{*2}}}\mathrm{d}\xi^*, \tag{2.108}$$

by change of variables, using $\xi^*=\xi_c\xi_*$, equation (2.108) then reads

$$\Phi(\xi,0,\tau)=\sqrt{\xi_c^2-\xi^2}\sum_{n=1}^{\infty}\bar{f}_n\sin(\omega_n\tau)\int_{-1}^{1}\frac{\sin(k_n\xi_c\xi_*)}{(\xi_c\xi_*-\xi)\sqrt{1-\xi_*^2}}\mathrm{d}\xi_*. \tag{2.109}$$

The resulting equation (2.109) contains a Cauchy principal-value integral, and it seems very complicated to give an analytic solution without determining the unknown function ξ_c. To make it more convenient to solve, we do not continue with equation (2.109) until later. Instead in the next section, we use the displacement potential technique introduced by (Korobkin 1982) to find the function ξ_c. Using displacement potential will convert the time-dependent problem to a time-independent problem. Much work has been done using this technique, noticeably by (Howison et al. 1991), (Oliver 2002) and (Reinhard et al. 2013). We will later return to equation (2.109) to find the velocity potential, the hydrodynamic pressure and the hydrodynamic force acting on the wetted region of the rigid lid during impact. In a boundary problem with unknown moving limits on the boundaries, it is crucial to determine these limits. In the next section we aim to find these boundaries by introducing the velocity potential into the problem.

2.2.7 Mixed boundary-value problem in terms of a displacement potential

We formulate the problem (2.86)–(2.93) in terms of a displacement potential, $\Phi^*(\xi,\zeta,\tau)$, as suggested by (Korobkin 1982). This is defined as the integral of the velocity potential $\Phi(\xi,\zeta,\tau)$ with respect to time, as follows

$$\Phi^*(\xi,\zeta,\tau)=\int_0^\tau \Phi(\xi,\zeta,\tilde{\tau})\mathrm{d}\tilde{\tau}. \tag{2.110}$$

The function $\frac{\partial\Phi^*}{\partial\zeta}$ describes the vertical displacement of a fluid particle while $\frac{\partial\Phi^*}{\partial\xi}$ describes the horizontal displacement of a fluid particle. The purpose behind this is to remove the time derivative from the formulation and deal with time as a parameter instead of variable. Doing this will enable us to find a formula for the unknown function $\xi_c(t)$ which gives the length of the moving boundary. It is straightforward to apply the displacement potential (2.110) in equations (2.86) and (2.92), which, after transformation, become

$$\frac{\partial^2\Phi^*}{\partial\xi^2}+\frac{\partial^2\Phi^*}{\partial\zeta^2}=0 \qquad -\infty<\xi<\infty,-\infty<\zeta<0, \tag{2.111}$$

$$\Phi^*=0 \qquad |\xi|>\xi_c,\zeta=0. \tag{2.112}$$

We introduce the function $\omega^*(\xi)$, when $\tau=\omega^*(\xi)$ is the time where $\xi_c(\tau)=\xi$. At the time $\tau=\omega^*(\xi)$ the Wagner condition (2.88) requires that the surface elevation is at the position of the rigid lid, mathematically we obtain

$$\eta_n(\xi,\omega^*(\xi))+\eta_c(\xi,\omega^*(\xi))=0. \tag{2.113}$$

Also the kinematic boundary condition (2.63), on the free-surface, $|\xi|>\xi_c,\zeta=0$,

$$\begin{aligned}\frac{\partial\Phi^*}{\partial\zeta}(\xi,0,\tau)&=\int_0^\tau\frac{\partial\Phi}{\partial\zeta}\mathrm{d}\tilde{\tau}\\&=\eta_c(\xi,\tau).\end{aligned} \tag{2.114}$$

To derive the body boundary condition in the wetted area in terms of the displacement potential, we integrate the derivative $\frac{\partial\Phi}{\partial\zeta}(\xi,0,\tau)$ with respect to time from 0 to τ, where $|\xi|<\xi_c$,

$$\frac{\partial\Phi^*}{\partial\zeta}(\xi,0,\tau)\ =\int_0^{\omega^*(\xi)}\frac{\partial\Phi}{\partial\zeta}\mathrm{d}\tilde{\tau}+\int_{\omega^*(\xi)}^\tau\frac{\partial\Phi}{\partial\zeta}\mathrm{d}\tilde{\tau}, \tag{2.115}$$

and use the boundary condition (2.87), the Wagner condition (2.113), the kinematic boundary condition (2.114) for $0<\omega^*(\xi)<\tau$, and the initial condition (2.79), from (2.115), we arrive at

$$\frac{\partial \Phi^*}{\partial \zeta}(\xi,0,\tau) = \eta_c(\xi,\omega^*(\xi)) - \eta_c(\xi,0) - \eta_n(\xi,\tau) + \eta_n(\xi,\omega^*(\xi))$$
$$= -\eta_n(\xi,\tau) \qquad |\xi| < \xi_c, \tag{2.116}$$

The far-field condition (2.93) is straightforward

$$\Phi^* \longrightarrow 0 \qquad as \qquad \xi^2 + \zeta^2 \longrightarrow \infty. \tag{2.117}$$

The new formulation (2.111)–(2.117) together with the initial conditions

$$\Phi^*(\xi,\zeta,0) = 0, \tag{2.118}$$
$$\xi_c(0) = 0, \tag{2.119}$$

are rewritten in terms of the complex displacement potential $\mathrm{w}^*(z,\tau)$ as follows. The complex displacement

$$\frac{\mathrm{dw}^*}{\mathrm{d}z}(z,\tau) = \frac{\partial \Phi^*}{\partial \xi} - i\frac{\partial \Phi^*}{\partial \zeta} \qquad z = \xi + i\zeta, \tag{2.120}$$

is analytic in $\zeta < 0$, decays at infinity, and satisfies the boundary conditions, on the boundary $\zeta = 0^-$:

$$\mathrm{Re}\left[\frac{\mathrm{dw}^*}{\mathrm{d}z}(x - i0,\tau)\right] = \frac{\partial \Phi^*}{\partial \xi}(\xi,0,\tau)$$
$$= 0 \qquad |\xi| > \xi_c, \tag{2.121}$$
$$\mathrm{Im}\left[\frac{\mathrm{dw}^*}{\mathrm{dz}}(x - i0)\right] = -\frac{\partial \Phi^*}{\partial \zeta}(\xi,0)$$
$$= \eta_n(\xi,\tau) \qquad |\xi| < \xi_c. \tag{2.122}$$

Now we introduce the characteristic function $\sqrt{z^2 - \xi_c^2}$ and reformulate the boundary problem (2.121)–(2.122) in terms of a new analytic function $W^*(z,\tau)$ defined by

$$W^*(z,\tau) = \sqrt{z^2 - \xi_c^2}\ \frac{\mathrm{dw}^*}{\mathrm{dz}}, \tag{2.123}$$

to obtain

$$\mathrm{Re}\,[W^*(x - i0)] = 0 \qquad |\xi| > \xi_c, \tag{2.124}$$
$$\mathrm{Re}\,[W^*(x - i0)] = \eta_n\ \sqrt{\xi_c^2 - \xi^2} \qquad |\xi| < \xi_c. \tag{2.125}$$

The solution of the problem (2.124)–(2.125) is given by the (see (Gakhov & Sneddon 1966) and (Carrier et al. 2005))

$$W^*(z,\tau) = \frac{i}{\pi}\int_{-\xi_c}^{\xi_c} \frac{\eta_n \sqrt{\xi_c^2 - \xi^{*2}}}{\xi^* - z}\ \mathrm{d}\xi^* + ic_0 + ic_1 z + ..., \tag{2.126}$$

where c_n for $n = 0, 1, ...$ are real constants. For all $\tau > 0$

$$W^*(z, \tau) \longrightarrow 0 \quad \text{as} \quad z \longrightarrow \infty,$$

which implies c_0, c_1, etc. are zero. From equation (2.123) we find

$$\frac{\mathrm{d}w^*}{\mathrm{d}z} = \frac{i}{\pi\sqrt{z^2 - \xi_c^2}} \int_{-\xi_c}^{\xi_c} \frac{\eta_n(\xi^*, \tau)\sqrt{\xi_c^2 - \xi^{*2}}}{\xi^* - z}\, \mathrm{d}\xi^*. \tag{2.127}$$

On the wetted part of the boundary, where $\zeta \longrightarrow 0^-$ on $|\xi| < \xi_c$, equations (2.120) and (2.127), and the Plemelj formula for the boundary value of the Cauchy-type integral in (2.127), provide the real and imaginary parts of the complex displacement:

$$\frac{\partial \Phi^*}{\partial \xi} = \frac{1}{\pi\sqrt{\xi_c^2 - \xi^2}} \fint_{-\xi_c}^{\xi_c} \frac{\eta_n(\xi^*, \tau)\sqrt{\xi_c^2 - \xi^{*2}}}{\xi^* - \xi}\, \mathrm{d}\xi^*, \tag{2.128}$$

$$\frac{\partial \Phi^*}{\partial \zeta} = -\eta_n(\xi, \tau). \tag{2.129}$$

Equation (2.128) contains a Cauchy principal-value integral preceded by a factor with a square root singularity at the contact points $\xi = \pm\xi_c$. The Wagner condition implies that the displacements are finite. Then $\frac{\partial \Phi^*}{\partial \xi}$ in (2.128) should be finite at $\xi = \pm\xi_c$ which is possible only if the integral in (2.128) is zero. This gives

$$\int_{-\xi_c}^{\xi_c} \frac{(\xi_c + \xi^*)\eta_n}{\sqrt{\xi_c^2 - \xi^{*2}}}\, \mathrm{d}\xi^* = 0. \tag{2.130}$$

The function $\eta_n(\xi^*, \tau)$ in the integrand of (2.128) is an even function of ξ^*. Then (2.130) reads

$$\int_{-\xi_c}^{\xi_c} \frac{\eta_n(\xi^*, \tau)}{\sqrt{\xi_c^2 - \xi^{*2}}}\, \mathrm{d}\xi^* = 0. \tag{2.131}$$

Substituting $\eta_n(\xi^*, \tau)$ from equation (2.40) in this equation, we find

$$\sum_{n=1}^{\infty} \bar{f}_n \cos(\omega_n \tau) \int_{-\xi_c}^{\xi_c} \frac{\cos(k_n \xi^*)}{\sqrt{\xi_c^2 - \xi^{*2}}}\, \mathrm{d}\xi^* = 0. \tag{2.132}$$

For the integrals in (2.132) we use a change of variables $\xi^* = \xi_c \cos(\theta)$. Hence equation (2.132) provides

$$\sum_{n=1}^{\infty} \bar{f}_n \cos(\omega_n \tau) \int_0^{\pi} \cos\left(k_n \cos(\xi_c \theta)\right)\, \mathrm{d}\theta = 0. \tag{2.133}$$

As mentioned in section (2.2.2), the values of $\bar{f}_n$ for $n \geq 3$ are assumed to be zero, however $\bar{f}_1$ and $\bar{f}_2$ are given and non-zero. From (Abramowitz & Stegun 1972), page 360, equation (9.1.18) or (9.1.20), equation (2.133) takes the form

$$\bar{f}_1 \cos(\omega_1 \tau) J_0(k_1 \xi_c(\tau)) + \bar{f}_2 \cos(\omega_2 \tau) J_0\left(k_2 \xi_c(\tau)\right) = 0, \tag{2.134}$$

where the functions $J_0(k_n \xi_c)$ are the zeroth order Bessel functions of the first kind. Equation (2.134) should be solved with respect to $\xi_c(\tau)$ for $\tau > 0$. We use numerical techniques to find the function $\xi_c(\tau)$ in the next section.

2.3 Problem solution in absence of gravity

The two well-known pioneering approaches to impact given by (von Karman 1929) and (Wagner 1932) to find estimates for the size of the wetted region. According to the von Karman approach the moving contact point is the intersection of the free-surface elevation compared with out the lid and the lid, Figure 2.10. The Wagner approach, Figure 2.11, provides more accurate position of the moving point as shown in the Figure 2.12, where the moving point appointed by Wagner (asterisk) is found to be more close to the real moving point than by von Karman (bullet). Wagner assumed the turn over point (the root of the jet) to be the moving point due to the small vertical distance it has with the lid (narrow width of the jet) which is negligible at the leading order.

In free-boundary problem finding the moving contact or turnover points is essential to enable us to go further and discuss the loads on the lid. In the next section we will determine the wetted interval $2\xi_c$ semi-analytically.

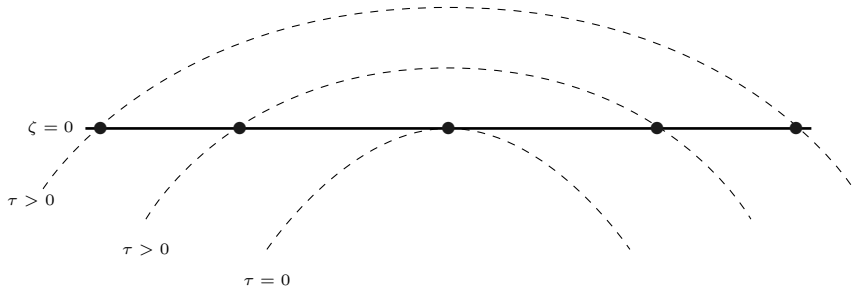

Figure 2.10: Each bullet is a moving contact point, $\xi = \xi_c$, by Karman's assumption.

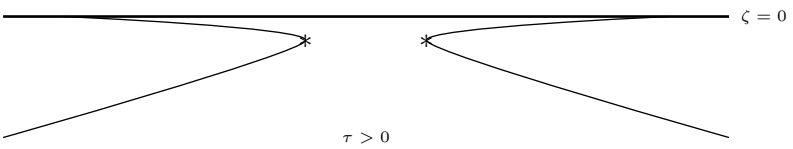

Figure 2.11: Asterisk is a moving turnover point, $\xi = \xi_c$, by Wagner's assumption. The thickness of the jets has been exaggerated, they are very thin compared with the radius of curvature of the surface elevation R.

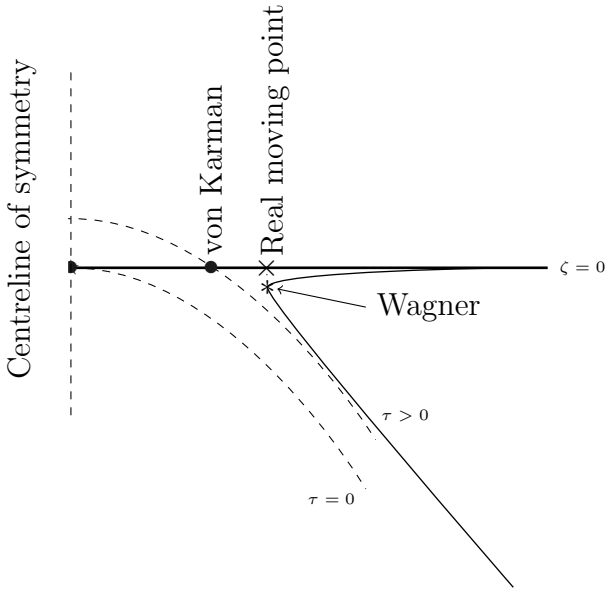

Figure 2.12: Difference in determining the position of the moving point $\xi = \xi_c$, following the assumptions given by Karamn (bullets) and Wagner (asterisk). The position of the turnover point is expected to lie between the approximated location from the models. The real moving contact point is allocated by a multiplication symbol.

2.3.1 Moving point $\xi_c(\tau)$ with no gravity

The aim of this section is to calculate the function $\xi_c(\tau)$ from (2.134). Differentiating equation (2.134) with respect to time implies

$$\dot{\xi}_c(\tau) = \frac{G_1\left(\tau, \xi_c(\tau)\right)}{G_2(\tau, \xi_c(\tau))}, \tag{2.135}$$

where in this work an over dot notation always stand for the time derivative. We have

$$G_1(\tau, \xi_c(\tau)) = -\left[\omega_1 \bar{f}_1 \sin(\omega_1\tau) J_0(k_1\xi_c(\tau)) + \omega_2 \bar{f}_2 \sin(\omega_2\tau) J_0(k_2\xi_c(\tau))\right],$$

and

$$G_2(\tau, \xi_c(\tau)) = k_1 \bar{f}_1 \cos(\omega_1\tau) J_1(k_1\xi_c(\tau)) + k_2 \bar{f}_2 \cos(\omega_2\tau) J_1(k_2\xi_c(\tau)),$$

where the functions $J_1(k_n\xi_c(\tau))$ are the Bessel functions of the first kind and are obtained from the relation

$$J_1(x) = -\frac{\mathrm{d}}{\mathrm{d}x}J_0(x). \tag{2.136}$$

Equation (2.135) and the initial condition (2.119) define an initial-value problem. We use the fourth-order Runge-Kutta method to solve this problem numerically in Matlab.

We expect that $\dot{\xi}_c \geq 0$ for $0 < \tau \leq t^*$, where $\tau = 0$ is the time when the fluid starts to hit the rigid lid. After this time we have the impact stage when the wetted interval grows. However, at $\tau = t^*$, at the end time of the impact stage, $\dot{\xi}_c(t^*) = 0$, or the beginning of the exit stage when the wetted interval starts to shrink, and later leaves the rigid lid.

If we substitute the initial condition (2.119) into equation (2.135), and use the fact that the Bessel functions $J_1(k_n\xi_c)$ for $n = 1, 2$ are zero there, we then obtain a singular value at $\tau = 0$. To avoid the singularity we use condition (2.119) asymptotically:

$$\xi_c(\tau) \longrightarrow 0 \qquad \text{as} \qquad \tau \longrightarrow 0. \tag{2.137}$$

Since we expect that the wetted interval will widen rapidly at the beginning, starting from $\xi_c = 0$.

We display the numerical results in Figure 2.13 in non-dimensional variables. It is shown that at the same time the function $\xi_c(\tau)$ in the case of the condition of (Wagner 1932) is significantly larger than that predicted by (von Karman 1929) approach. We did the calculation for the problem (2.135) and (2.119) by setting $\bar{f}_1 = -0.5891$, $\bar{f}_2 = -0.3724$, $k_1 = \pi$, $k_2 = 2\pi$, $\omega_1 = 1.7691$ and $\omega_2 = 2.5066$. The calculation started at time of $t_* = 1.0561$, the first contact between the fluid and the rigid lid, and contact stopped at $t^* = 1.5312$ (the end-time of the impact stage). We cannot determine the function $\xi_c(\tau)$ for $\tau > t^*$ (exit stage) using Wagner's condition. However, for the von Karman assumption, the wetted interval for both stages is shown in Figure 2.14. In this figure the maximum value of its extension, $\xi_c(\tau) = 0.2119$, occurs at $\tau = 0.6008$ which is only a 0.687% of the length pictured due to Wagner's assumption. The impact period in Wagner's model is shorter than what we have in the von Karman's assumption extension period only by a small percentage difference of 0.04%. We have no information about the exit period when the wetted region starts to shrink and eventually leaves the lid.

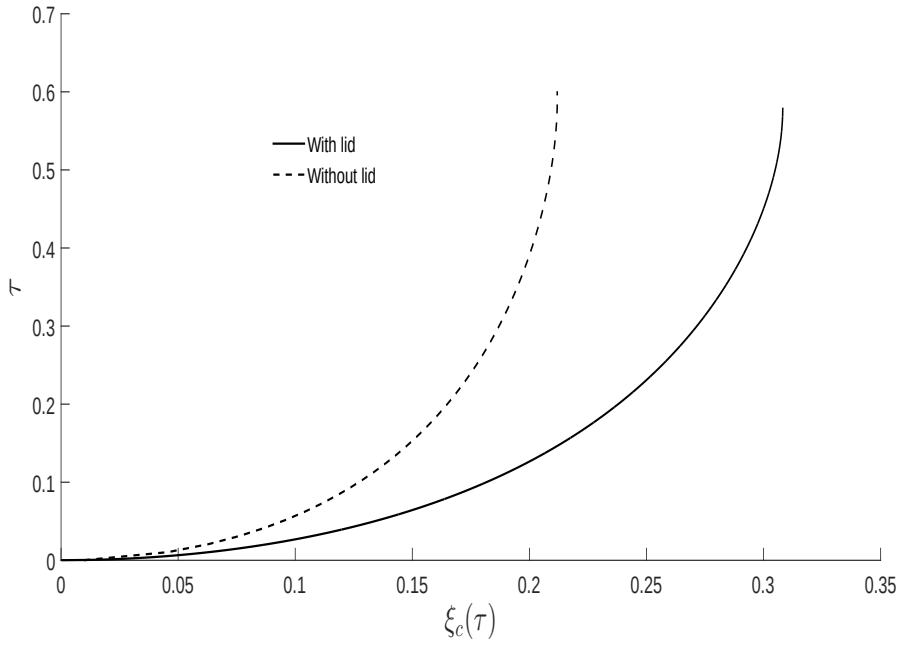

Figure 2.13: Extent of the wetted interval, dashed curve [inner curve] is due to von Karman, and the solid curve [outer curve] is due to Wagner.

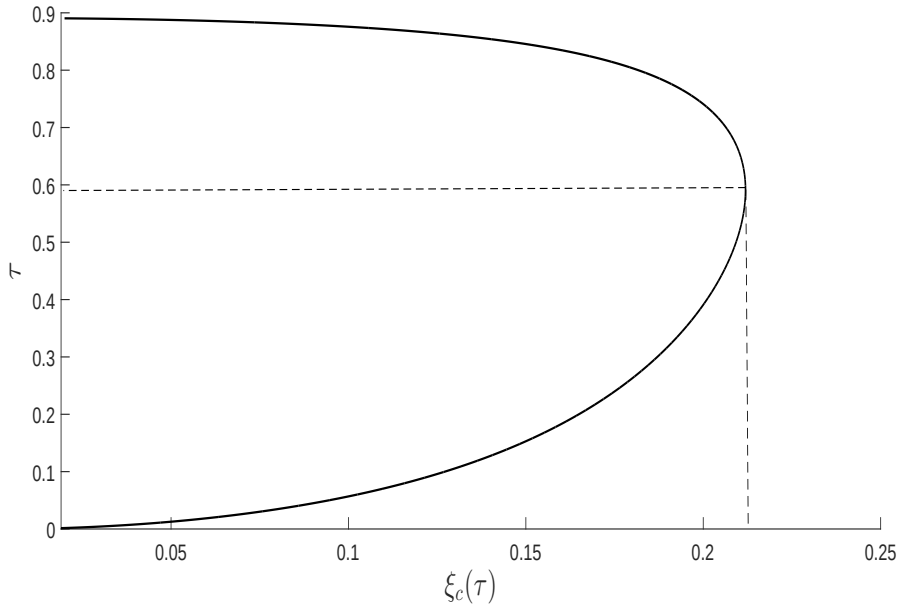

Figure 2.14: Time evolution of the wetted interval, $\xi_c(\tau)$ showing rapid widening towards maximum width, following by shrinking back to separation of the liquid from the lid.

2.3.2 leading-order force

In this section the leading-order force f(τ) of the liquid acting on the plate will be calculated semi-numerically. We first calculate the force on the wetted part of the rigid lid by integrating the pressure distribution over the wetted interval $(-\xi_c, \xi_c)$. Applying the stretched variables (2.84) on the equation (2.75) and using the fact that, on $-\xi_c < \xi < \xi_c$, the sum of the surface elevation with no lid and its correction when the lid is introduced to the problem is a constant:

$$\eta_c(\xi, \tau) + \eta_n(\xi, \tau) = 0 \tag{2.138}$$

we find

$$p(\xi, \tau) = \delta^{3/2}\ \eta_n(\xi, \tau) - \frac{\partial \Phi}{\partial \tau}(\xi, 0, \tau). \tag{2.139}$$

We integrate the first term of (2.139) over $\xi : -\xi_c < \xi < \xi_c$, to obtain the hydrostatic force $F_S(\tau)$, and integrate the last term to obtain the hydrodynamic force $F_D(\tau)$. The hydrostatic force in equation (2.139) plays a small role, while the major contribution comes from the hydrodynamic force. Calculating the hydrostatic force is straightforward. To calculate the hydrodynamic force, we integrate the last term of equation (2.139) over the wetted part of the rigid lid, and we find that

$$F_D(\tau) = -\int_{-\xi_c(\tau)}^{\xi_c(\tau)} \frac{\partial \Phi}{\partial \tau}(\xi, 0, \tau) \mathrm{d}\xi. \tag{2.140}$$

By using Leibniz's rule of integration, the differentiation sign under the integral in equation (2.140) can be converted as follows

$$F_D(\tau) = -\frac{\mathrm{d}}{\mathrm{d}\tau} \int_{-\xi_c}^{\xi_c} \Phi(\xi, 0, \tau) \mathrm{d}\xi - \frac{\mathrm{d}(\xi_c)}{\mathrm{d}\tau} \Phi(\xi_c, 0, \tau) + \frac{\mathrm{d}(-\xi_c)}{\mathrm{d}\tau} \Phi(-\xi_c, 0, \tau), \tag{2.141}$$

from equation (2.92) and the continuity of the velocity potential, the last two terms in equation (2.141) vanish at the contact points, $\xi = \pm\xi_c(\tau)$. Substituting the expression (2.109) into equation (2.141) implies

$$F_D(\tau) = -\frac{\mathrm{d}}{\mathrm{d}\tau} \sum_{n=1}^{\infty} \bar{f}_n \sin(\omega_n \tau) \int_{-\xi_c}^{\xi_c} \sqrt{\xi_c^2 - \xi^2} \int_{-1}^{1} \frac{\sin(k_n \xi_c \xi_*)}{(\xi_c \xi_* - \xi)\sqrt{1 - \xi_*^2}} \mathrm{d}\xi_* \mathrm{d}\xi. \tag{2.142}$$

Some analytic manipulations on equation (2.142) lead to

$$F_D(\tau) = -\pi \frac{\mathrm{d}}{\mathrm{d}\tau} \sum_{n=1}^{\infty} \bar{f}_n \xi_c(\tau) \sin(\omega_n \tau) \int_0^{\pi} \sin(k_n \xi_c \cos(\xi)) \cos(\xi) \mathrm{d}\xi, \tag{2.143}$$

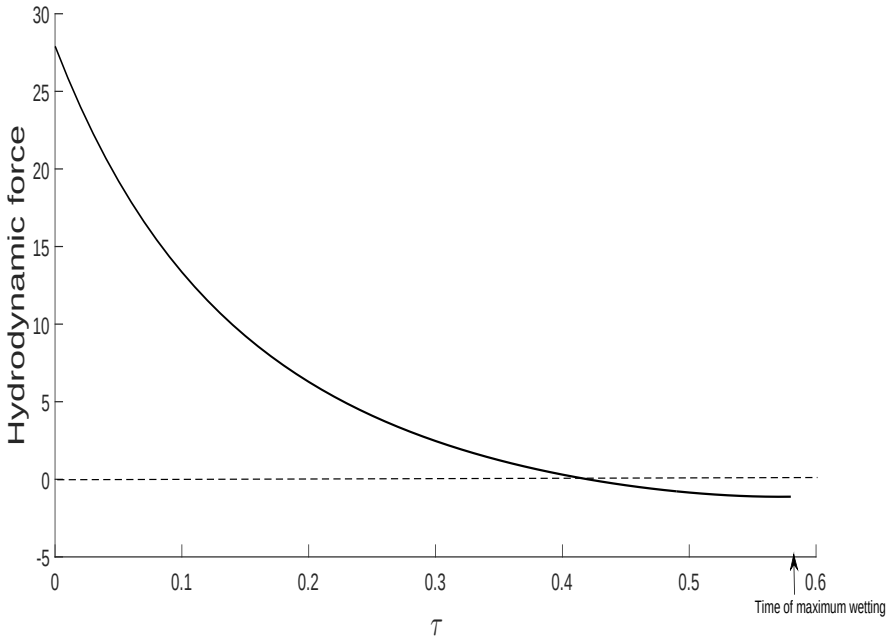

Figure 2.15: The non-dimensional leading-order hydrodynamic force on the plate during the impact stage. A positive force means that the liquid is pushing upward on the lid.

and the integral in equation (2.143) can be represented in terms of Bessel function of the first kind $\pi J_1(k_n\xi_c)$ for $n = 1, 2$, (Gradshteyn & Ryzhik 2014) p. 421.

Now we differentiate with respect to time (2.143). We take into account only the values in the summation for $n = 1, 2$ as we mentioned in the previous section. We use the following relation

$$\frac{\mathrm{d}}{\mathrm{d}x}J_n(x) = \frac{1}{2}[J_{n-1}(x) - J_{n+1}(x)], \tag{2.144}$$

to differentiate the Bessel functions of the first kind. Now the hydrodynamic force in equation (2.143) takes the form

$$\begin{aligned} F_D(\tau) = -\pi^2\xi_c\dot{\xi}_c \Bigg[& \frac{\bar{f}_1\omega_1^2}{k_1\dot{\xi}_c}\cos(\omega_1\tau)J_1(k_1\xi_c) + \frac{\bar{f}_2\omega_2^2}{k_2\dot{\xi}_c}\cos(\omega_2\tau)J_1(k_2\xi_c) \\ & + \frac{1}{2}\bar{f}_1\omega_1\sin(\omega_1\tau)\{J_0(k_1\xi_c) - J_2(k_1\xi_c)\} \\ & + \frac{1}{2}\bar{f}_2\omega_2\sin(\omega_2\tau)\{J_0(k_2\xi_c) - J_2(k_2\xi_c)\} \\ & + \frac{\bar{f}_1\omega_1}{\xi_c k_1}\sin(\omega_1\tau)J_1(k_1\xi_c) + \frac{\bar{f}_2\omega_2}{\xi_c k_2}\sin(\omega_2\tau)J_1(k_2\xi_c)\Bigg], \end{aligned} \tag{2.145}$$

where $\dot{\xi}_c(\tau)$ is given by equation (2.135). The numerical results of the leading-order hydrodynamic force on the contact interval of the rigid lid during the impact

stage are shown in Figure 2.15. The time $\tau = 0$ corresponds to the instant of impact $t = t_*$. The maximum force occurs at the very beginning of the impact stage, then it decreases quickly and at $\tau = 0.4101$, a negative force begins acting on the rigid lid. A negative hydrodynamic force on the plate means that the plate is pulled down by the fluid, and this occurs while the fluid is still moving along the plate and expanding during the impact stage. Figure 2.15 shows the hydrodynamic force during the impact stage. Figure shows that 27% of the impact stage time, force is negative. Consequently we will have negative pressure which will be discussed later on.

The hydrostatic pressure is straightforward to calculate from the first term on the right-hand side of equation (2.139). To calculate the hydrodynamic pressure at this stage in the outer region on the wetted part from equation (2.139), one needs the time-derivative of the velocity potential given by equation (2.109), which would be very complicated to determine. Therefore we start to find the hydrodynamic pressure on the wetted part directly by introducing the acceleration potential $\frac{\partial \Phi}{\partial \tau}(\xi, \zeta, \tau)$.

2.3.3 Mixed boundary-value problem in terms of acceleration potential

To obtain the pressure distribution $p(\xi, \tau)$ on the plate, we formulate the problem (2.86)–(2.93) in terms of an acceleration potential $\frac{\partial \Phi}{\partial \tau}(\xi, \zeta, \tau)$, which is the time-derivative of the velocity potential $\Phi(\xi, \zeta, \tau)$. Differentiating equations (2.86)–(2.93) with respect to time leads to a new MBVP as follows:

$$\frac{\partial^2 \Phi_\tau}{\partial \xi^2} + \frac{\partial^2 \Phi_\tau}{\partial \zeta^2} = 0 \qquad -\infty < \xi < \infty, -\infty < \zeta < \infty, \tag{2.146}$$

$$\frac{\partial \Phi}{\partial \tau} = 0 \qquad |\xi| > \xi_c, \zeta = 0, \tag{2.147}$$

$$\frac{\partial^2 \Phi}{\partial \zeta \partial \tau} = -\frac{\partial^2 \eta_n}{\partial \tau^2} \qquad |\xi| < \xi_c, \zeta = 0, \tag{2.148}$$

$$\frac{\partial \Phi}{\partial \tau} \longrightarrow 0 \qquad as \qquad \xi^2 + \zeta^2 \longrightarrow \infty. \tag{2.149}$$

As we did in sections 2.2.6 and 2.2.7, we write the complex acceleration potential in terms of the acceleration potential $\frac{\partial \Phi}{\partial \tau}(\xi, \zeta, \tau)$ and an acceleration stream function $\frac{\partial \Psi}{\partial \tau}(\xi, \zeta, \tau)$, as follows:

$$\mathrm{w}(z, \tau) = \frac{\partial \Phi}{\partial \tau} + i \frac{\partial \Psi}{\partial \tau}, \tag{2.150}$$

where $z = \xi + i\zeta$ is the complex variable and

$$\frac{\partial \Psi}{\partial \tau} \longrightarrow 0 \quad as \quad \xi^2 + \zeta^2 \longrightarrow \infty. \tag{2.151}$$

Differentiating equation (2.150) gives

$$\begin{aligned}\frac{\mathrm{dw}(z,\tau)}{\mathrm{d}z} &= \frac{\partial^2\Phi}{\partial\xi\partial\tau} + i\frac{\partial^2\Psi}{\partial\xi\partial\tau} \\ &= \frac{1}{i}\frac{\partial^2\Phi}{\partial\zeta\partial\tau} + \frac{\partial^2\Psi}{\partial\zeta\partial\tau}.\end{aligned} \tag{2.152}$$

Equation (2.152) leads to the Cauchy-Riemann equations

$$\frac{\partial^2\Phi}{\partial\xi\partial\tau} = \frac{\partial^2\Psi}{\partial\zeta\partial\tau} \qquad \frac{\partial^2\Phi}{\partial\zeta\partial\tau} = -\frac{\partial^2\Psi}{\partial\xi\partial\tau}. \tag{2.153}$$

Now from (2.153) the body condition (2.148) can be written as

$$\frac{\partial^2\Psi}{\partial\xi\partial\tau} = \frac{\partial^2\eta_n}{\partial\tau^2} \qquad |\xi| < \xi_c,\ \zeta = 0. \tag{2.154}$$

Integrating equation (2.154) with respect to ξ reads

$$\frac{\partial\Psi}{\partial\tau} = \int_0^\xi \frac{\partial^2\eta_n}{\partial\tau^2}\mathrm{d}\xi^* + c_1 \qquad |\xi| < \xi_c, \quad \zeta = 0, \tag{2.155}$$

where c_1 is a constant of integration which can be determined by the symmetric condition (2.97) at $\xi = 0$, that is

$$\frac{\partial\Phi}{\partial\xi}(0,\zeta,\tau) = 0 \qquad\qquad \zeta < 0.$$

The second Cauchy-Riemann relation (2.153) gives

$$\frac{\partial^2\Psi}{\partial\zeta\partial\tau}(0,\zeta,\tau) = 0 \qquad\qquad \zeta < 0,$$

and integrating with respect to ζ yields

$$\frac{\partial\Psi}{\partial\tau}(0,\zeta,\tau) = c_2 \qquad\qquad \zeta < 0,$$

from condition (2.151) we see that $c_2 = 0$ and therefore

$$\frac{\partial\Psi}{\partial\tau}(0,\zeta,\tau) = 0 \qquad\qquad \zeta < 0,$$

and hence we conclude that $c_1 = 0$ in (2.155) which now reads

$$\frac{\partial\Psi}{\partial\tau} = \int_0^\xi \frac{\partial^2\eta_n}{\partial\tau^2}\mathrm{d}\xi^* \qquad |\xi| < \xi_c,\ \zeta = 0. \tag{2.156}$$

The MBVP (2.146)–(2.149) in terms of complex potential reduces to the following Dirichlet boundary-value problem

$$\mathrm{Re}[w(\xi - i0)] = 0 \qquad |\xi| > \xi_c, \zeta = 0, \tag{2.157}$$

$$\mathrm{Im}[w(\xi - i0)] = \int_0^{\xi} \frac{\partial^2 \eta_n}{\partial \tau^2} \mathrm{d}\xi^* \qquad |\xi| < \xi_c, \zeta = 0, \tag{2.158}$$

$$w \longrightarrow 0 \quad as \qquad \xi^2 + \zeta^2 \longrightarrow \infty. \tag{2.159}$$

For the problem (2.157)–(2.159) we find a general solution by introducing a function $W(z,\tau)$ as the product of the characteristic function $\sqrt{z^2 - \xi_c^2}$ and the analytic function $w(z,\tau)$ as follows

$$W(z,\tau) = \sqrt{z^2 - \xi_c^2} w(z,\tau).$$

Now, the problem (2.157)–(2.159) on $\zeta = 0$ can be rewritten as

$$\mathrm{Re}\Big[\pm \sqrt{\xi^2 - \xi_c^2} \left(\frac{\partial \Phi}{\partial \tau} - i \frac{\partial \Psi}{\partial \tau} \right) \Big] = \pm \sqrt{z^2 - \xi_c^2} \, \frac{\partial \Phi}{\partial \tau} = 0 \quad |\xi| > \xi_c, \tag{2.160}$$

$$\begin{aligned} \mathrm{Re}\Big[- i \sqrt{\xi_c^2 - \xi^2} \left(\frac{\partial \Phi}{\partial \tau} - i \frac{\partial \Psi}{\partial \tau} \right) \Big] &= \sqrt{\xi_c^2 - \xi^2} \, \frac{\partial \Psi}{\partial \tau} \\ &= \sqrt{\xi_c^2 - \xi^2} \int_0^{\xi} \frac{\partial^2 \eta_n}{\partial \tau^2} \mathrm{d}\xi^*, \ |\xi| < \xi_c. \end{aligned} \tag{2.161}$$

This has the general solution (see (Gakhov & Sneddon 1966) and (Carrier et al. 2005))

$$W(z,\tau) = \frac{i}{\pi} \int_{-\xi_c}^{\xi_c} \frac{\sqrt{\xi_c^2 - \xi^{*2}}}{\xi^* - z} \int_0^{\xi^*} \frac{\partial^2 \eta_n}{\partial \tau^2} \mathrm{d}\xi_* \mathrm{d}\xi^* + i c_o + i c_1 z + ...,$$

where c_n for $n = 0, 1, ...$ are constants. The analytic function $w(z,\tau)$ takes the form

$$\begin{aligned} \mathrm{w}(z,\tau) = \frac{i}{\pi \sqrt{z^2 - \xi_c^2}} \int_{-\xi_c}^{\xi_c} \frac{\sqrt{\xi_c^2 - \xi^{*2}}}{\xi^* - z} \int_0^{\xi^*} \frac{\partial^2 \eta_n}{\partial \tau^2} \mathrm{d}\xi_* \mathrm{d}\xi^* \\ + \frac{i c_0}{\sqrt{z^2 - \xi_c^2}} + \frac{i c_1 z}{\sqrt{z^2 - \xi_c^2}} + ..., \end{aligned}$$

where $c_i, i = 1, 2, \ldots,$ should be zero due to condition (2.159), except c_0. By the Plemelj formula, as $\zeta \to 0$ and $|\xi| < \xi_c$, we obtain

$$\begin{aligned} \frac{\partial \Phi}{\partial \tau} + i \frac{\partial \Psi}{\partial \tau} = \frac{-1}{i} \int_0^{\xi} \frac{\partial^2 \eta_n}{\partial \tau^2} \mathrm{d}\xi^* \\ - \frac{1}{\sqrt{\xi_c^2 - \xi^2}} \left[\frac{1}{\pi} \int_{-\xi_c}^{\xi_c} \frac{\sqrt{\xi_c^2 - \xi^{*2}}}{\xi^* - \xi} \int_0^{\xi^*} \frac{\partial^2 \eta_n}{\partial \tau^2} \mathrm{d}\xi_* \mathrm{d}\xi^* + c_0 \right], \end{aligned}$$

therefore the acceleration potential in the wetted part of the lid is given by

$$\frac{\partial \Phi}{\partial \tau} = -\frac{1}{\sqrt{\xi_c^2 - \xi^2}} \left[\frac{1}{\pi} \int_{-\xi_c}^{\xi_c} \frac{\sqrt{\xi_c^2 - \xi^{*2}}}{\xi^* - \xi} \int_0^{\xi^*} \frac{\partial^2 \eta_n}{\partial \tau^2} \mathrm{d}\xi_* \mathrm{d}\xi^* + c_0 \right]. \quad (2.162)$$

The solution to the problem (2.146)–(2.149) is not unique in contrast to the problem (2.86)–(2.93), since $\Phi(\xi, \zeta, \tau)$ is continuous, whereas the acceleration potential $\frac{\partial \Phi}{\partial \tau}(\xi, \zeta, \tau)$ is not continuous and has a square root singularity at the contact points $\xi = \pm\xi_c(\tau)$. That is as $\xi \to \xi_c - 0$ the acceleration potential behaves like

$$\frac{\partial \Phi}{\partial \tau} = O\left(\frac{1}{\sqrt{\xi_c - \xi}} \right).$$

In addition to the solution given by equation (2.109), we have solutions which are eigensolutions, which correspond to the homogeneous problem where $\frac{\partial^2 \Phi}{\partial \zeta \partial \tau} = 0$ in the contact region where $|\xi| < \xi_c$. Therefore the constant c_0 represents an eigenvalue for an eigensolution in equation (2.162). The pressure on the wetted interval can be calculated with the help of eigenvalues in equation (2.162). Since the wetted interval is moving and expanding on both sides, we should calculate the pressure and plot it at different instants.

To calculate the constant c_0 in equation (2.162), we start from the velocity potential given in equation (2.109) which is the solution of the problem (2.86)–(2.93). We denote the integral part of equation (2.109) by

$$I(\xi, \xi_c) = \int_{-1}^{1} \frac{\sin(k_n \xi_c \xi_*)}{(\xi_c \xi_* - \xi)\sqrt{1 - \xi_*^2}} \mathrm{d}\xi_*, \quad (2.163)$$

at the boundaries where $\zeta = 0$ as $\xi \to \xi_c$, by using some analysis the integral (2.163) can be converted to

$$I(\xi, \xi_c)|_{\xi \to \xi_c} = \frac{2}{\xi_c} \int_0^{\pi/2} \frac{\sin\left(k_n \xi_c \sin^2(\xi^*)\right) \cos\left(k_n \xi_c \cos^2(\xi^*)\right)}{\sin^2(\xi^*)} \mathrm{d}\xi^*, \quad (2.164)$$

and now, as $\xi \to \xi_c$ on $\zeta = 0$, the velocity potential given in equation (2.109) can be rewritten as

$$\Phi(\xi, 0, \tau)|_{\xi \to \xi_c} = \frac{2\sqrt{2}\sqrt{\xi_c - \xi}}{\sqrt{\xi_c}} \sum_{n=1}^{\infty} \frac{\bar{f}_n \omega_n}{k_n} \sin(\omega_n \tau) I(\xi, \xi_c)|_{\xi \to \xi_c}. \quad (2.165)$$

Equation (2.162) can be rewritten as

$$\frac{\partial \Phi}{\partial \tau} = \frac{-1}{\sqrt{\xi_c^2 - \xi^2}} \left[\frac{-1}{\pi} \sum_{n=1}^{\infty} \frac{\bar{f}_n \omega_n^2}{k_n} \cos(\omega_n \tau) I_1(\xi, \xi_c) + c_0 \right], \quad (2.166)$$

having done with the inner integral in the right-hand side of equation (2.162), $I_1(\xi, \xi_c)$ refers to

$$I_1(\xi,\xi_c)=\fint_{-\xi_c}^{\xi_c}\frac{\sqrt{\xi_c^2-\xi^{*2}}}{\xi^*-\xi}\sin(k_n\xi^*)\mathrm{d}\xi^*.$$

The above integral is too complicated to give an analytic solution for $|\xi|<\xi_c$, but as $\xi\to\xi_c$ on $\zeta=0$ we obtain

$$I_1(\xi,\xi_c)|_{\xi\to\xi_c}=-\int_{-\xi_c}^{\xi_c}\frac{\xi^*\sin(k_n\xi^*)}{\sqrt{\xi_c^2-\xi^{*2}}}\mathrm{d}\xi^*,$$

the substitution $\xi^*=\xi_c\cos(\beta)$ leads us to the integral

$$I_1(\xi,\xi_c)|_{\xi\to\xi_c}=-\xi_c\int_0^{\pi}\cos(\beta)\sin(k_n\xi_c\cos(\beta))\mathrm{d}\beta.$$

From (Gradshteyn & Ryzhik 2014), page 421, equation 13, the above can be evaluated in closed form

$$I_1(\xi,\xi_c)|_{\xi\to\xi_c}=-\pi\xi_c J_1(k_n\xi_c), \tag{2.167}$$

where J_1 is the Bessel function of the first kind. Therefore as $\xi\to\xi_c$ on $\zeta=0$ equation (2.166) takes the form

$$\frac{\partial\Phi}{\partial\tau}=\frac{-1}{\sqrt{2\xi_c}\sqrt{\xi_c-\xi}}\left[\xi_c\sum_{n=1}^{\infty}\frac{\bar{f}_n\omega_n^2}{k_n}\cos(\omega_n\tau)J_1(k_n\xi_c)+c_0\right]. \tag{2.168}$$

Equation (2.168) is the time-derivative of the velocity potential. Differentiating the velocity potential in equation (2.165) with respect to time, we can equate it with equation (2.168) which enables us to calculate c_0. Neglecting the non-dominant terms and keeping the dominant term as $\xi\to\xi_c$ of the time derivative of equation (2.165) leads to

$$\frac{\partial\Phi}{\partial\tau}=\frac{\sqrt{2}\ \dot{\xi}_c}{\sqrt{\xi_c}\sqrt{\xi_c-\xi}}\sum_{n=1}^{\infty}\frac{\bar{f}_n\omega_n}{k_n}\sin(\omega_n\tau)I(\xi,\xi_c)|_{\xi\to\xi_c}, \tag{2.169}$$

where $\dot{\xi}_c$ is given in equation (2.135). Equating equations (2.168) and (2.169) gives the constant c_0

$$c_0=-\sum_{n=1}^{\infty}\frac{\bar{f}_n\omega_n}{k_n}\left[\sqrt{2}\dot{\xi}_c\sin(\omega_n\tau)I(\xi,\xi_c)|_{\xi\to\xi_c}+\xi_c\ \omega_n\cos(\omega_n\tau)J_1(k_n\xi_c)\right] \tag{2.170}$$

Our aim is to calculate the pressure distribution on the outer region. Therefore we cannot use the results given by equation (2.167) as we used in equation (2.168) to find the constant c_0. because those results are only relevant to the case when $\xi\to\xi_c$ on the contact region.

Once the constant c_0 has been found numerically from equation (2.170), we return to the acceleration potential in equation (2.166). With change of variables

and after some algebra, the following results for $I_1(\xi, \xi_c)$ have been found in the contact region for $|\xi| < \xi_c$

$$I_1(\xi, \xi_c) = -\pi \xi_c J_1(k_n \xi_c) + (\xi_c^2 - \xi^2) \int_0^{\pi} \frac{\sin\left[k_n\left(\frac{\xi_c \cos(\xi^*) - \xi}{2}\right)\right] \cos\left[k_n\left(\frac{\xi_c \cos(\xi^*) + \xi}{2}\right)\right]}{\frac{\xi_c \cos(\xi^*) - \xi}{2}} \mathrm{d}\xi^*. \quad (2.171)$$

2.3.4 leading-order hydrodynamic pressure

At this stage everything has become ready to calculate numerically the distribution of pressure in the main part of the wetted region during the impact stage on different lengths of contact region, which correspond to the different times as the wetted region expands, starting from the beginning of impact at $t = t_*$. This is now practical by using equation (2.166) where c_0 and $I_1(\xi, \xi_c)$ are defined by equations (2.170) and (2.171), respectively.

The values for $\xi_c(\tau)$ and $\dot{\xi}_c(\tau)$ are obtained by solving the initial-value problem (2.135) and (2.119), the constant c_0 is calculated as $\xi \to \xi_c$ from equation (2.170) by numerically calculating the integral in equation (2.164). Also the integral I_1 in equation (2.171) is evaluated numerically, by using Matlab programming. The impact stage starts at non-dimensional time $t = t_* = 1.0561$ and ends at $t = t^* = 1.6362$. We compute with a time increment Δt=0.01.

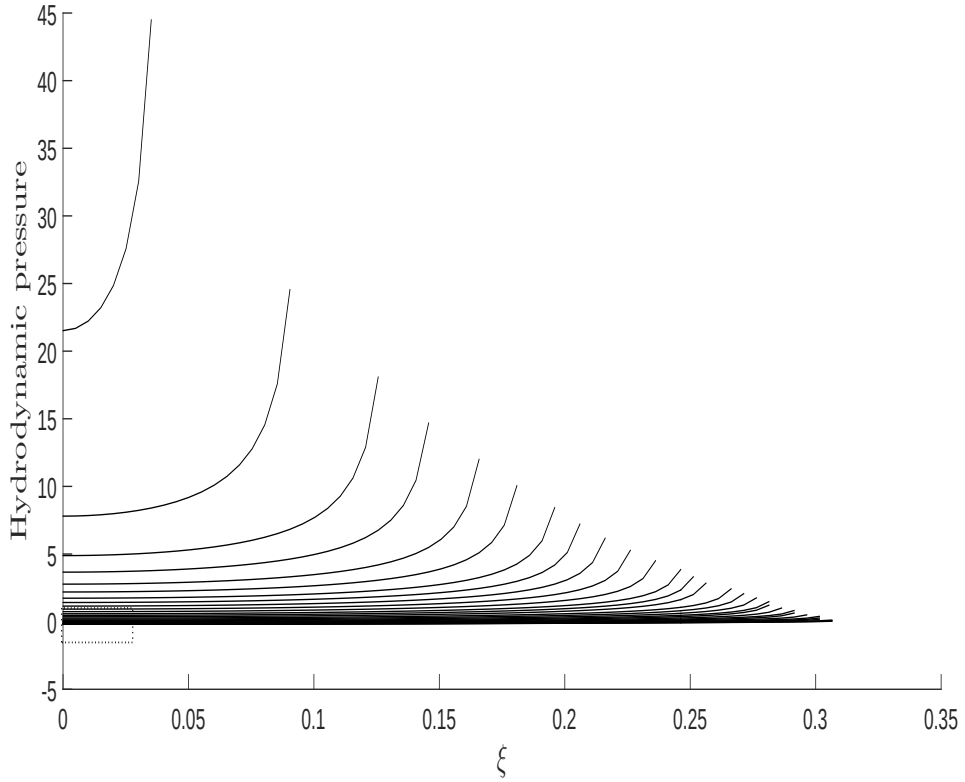

Figure 2.16: The leading-order hydrodynamic pressure distribution on the lid during the impact stage. The left-most curve is for the earliest time depicted; later times are in order, to the right. Note the spread of the wetted zone to the right. The dotted rectangular is zoomed in the next figure.

Figure 2.16 shows the hydrodynamic pressure distribution, at different time instants of sloshing impact. The area of detail enclosed by the dotted rectangle is shown expanded in Figure 2.17. In this figure it is shown that although the wetted region is expanding, negative pressure can be seen for about 36% of the impact stage time. This behaviour of the pressure distribution, even though it is in a small region, motivate us to investigate the influence of gravity when it comes to this stage.

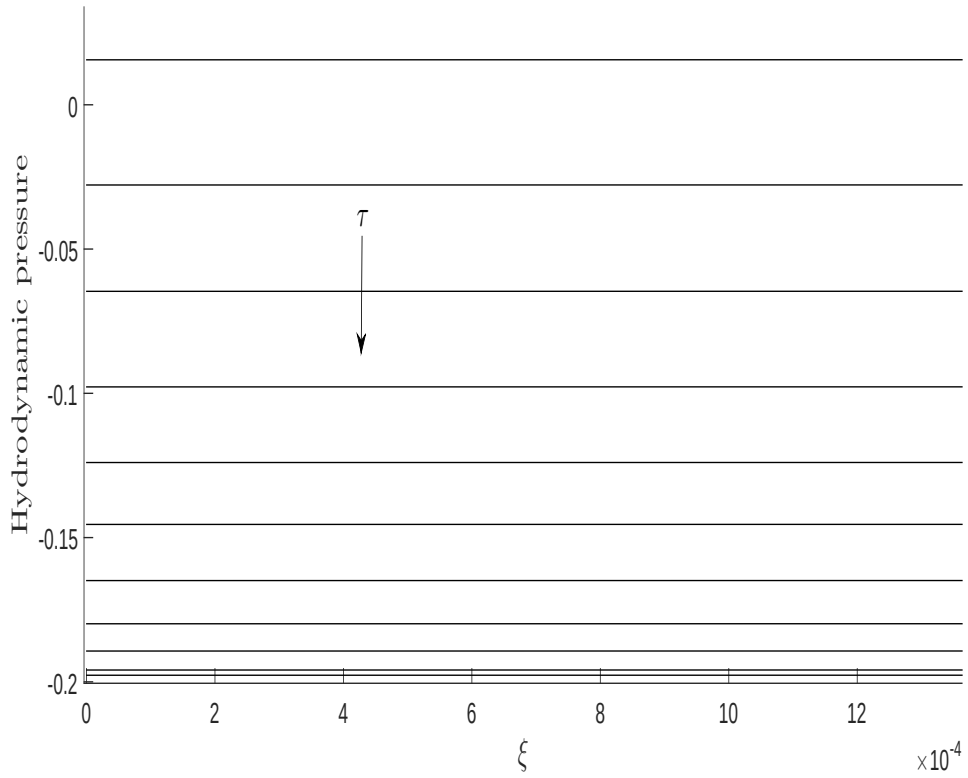

Figure 2.17: The negative hydrodynamic pressure distribution on the lid during the impact stage. For about 36% of the impact stage time negative pressure appears.

2.4 The energy balance in the tank

In this section we are concerned about the energy distribution in the tank. The tank is rigid so no work is done on the walls, bottom and lid of the tank. For the neglected elastic potential energy and acoustic effects contributions, see (Korobkin 1995), (Cooker 2002), (Korobkin & Khabakhpasheva 2006) and (Reinhard et al. 2013) . Also the viscosity and surface tension effects on the total energy are neglected. (Faltinsen & Timokha 2009) discussed these effects, and they related the time rate of dissipation of energy along with the potential and kinetic energies in the tank. (Keulegan 1959) discussed the viscosity and surface tension contributions to the dissipation of energy in standing waves in a rectangular basin. As the tank is assumed to be fixed, there is no external energy flux into or out of the tank. Therefore, in this closed system the only contribution to the energy distributions comes from the kinetic and potential energy of the fluid. In 2-dimensions the total energy $\mathrm{E_T}(t)$ of the fluid in the main part of the tank,

in dimensional variables, is given by

$$\mathrm{E_T}(t) = \iint\limits_{\Omega(t)} \left(\frac{1}{2} \rho \, \vec{U} \cdot \vec{U} + \rho g y \right) \mathrm{d}A, \tag{2.172}$$

where $\Omega(t)$ is the main fluid domain as shown in Figure 2.18-a (dotted line region) where the jets are excluded, $\mathrm{d}A$ is the infinitesimal area of the fluid domain of integration, $\vec{U} = \vec{U}(x, y, t)$ the fluid velocity, ρ the density and g is the gravitational acceleration. The first term of the integrand represents the kinetic energy and the second gives the potential energy in the fluid domain. It is shown in Figure 2.5 that the equilibrium state of the free-surface in the tank is at $y = H - h$, where H is the position of the lid and h is the distance from the equilibrium free-surface, $\eta(x, t) = 0$ for all $-L \leq x \leq L$, up to the lid. The non-dimensional free-surface elevation is given by equation (2.40). Having these, from equation (2.172) and by using the initial condition (2.53) the total energy of the liquid in the tank at $t = 0$ reads

$$E_T(0) = \rho g \int_{-L}^{L} \int_{0}^{\mathrm{f}(x)} y \; \mathrm{d}y\mathrm{d}x, \tag{2.173}$$

where $x = \pm L$ are the positions of the tank's two walls, and we recall the initial free-surface at rest, $t = 0$

$$\mathrm{f}(x) = H - h + h \sum_{n=1}^{\infty} \bar{f}_n \cos\left(\frac{k_n}{H} x \right), \tag{2.174}$$

where $\bar{f}_n$ and k_n are defined in equations (2.41) and (2.43), respectively. The total initial energy in the tank then reads

$$E_T(0) = \rho g L H (H - 2h) + O(h^2). \tag{2.175}$$

The potential energy is defined up to an additive constant. We can take the first term in (2.175) as a reference and disregard it in the following calculations. Next we will find the rate of energy transfer out of the fluid main domain $\Omega(t)$, the *energy flux*. Applying the Reylond's transport theorem to equation (2.172), the energy flux through the fluid in the tank can be written as

$$\frac{\mathrm{d}}{\mathrm{d}t} \left(\mathrm{E_T}(t) \right) = \rho \int\limits_{\Omega(t)} \frac{\partial}{\partial t} \left(\frac{1}{2} \, \vec{U} \cdot \vec{U} \right) \mathrm{dV} + \rho \int\limits_{\partial\Omega(t)} \left(\frac{1}{2} \, \vec{U} \cdot \vec{U} + g y \right) (\vec{v} - \vec{v}_b) \, . \vec{n} \; \mathrm{dS}, \tag{2.176}$$

where $\partial\Omega(t)$ is the boundary of the fluid domain $\Omega(t)$, dS is the element of arc-length along the boundary, $\vec{v}$ fluid velocity vector, $\vec{v}_b$ boundary surface velocity

vector and $\vec{n}$ is the normal vector pointed outward from the surface of the fluid. The normal velocity of the fluid is zero on the rigid boundaries, see conditions (2.60)–(2.62). The normal component of velocity of the fluid particles on the free-surface equals the normal velocity of the free-surface itself, i.e.

$$\vec{v}.\vec{n} = \vec{v}_b.\vec{n} \qquad x > |x_{c0}|. \tag{2.177}$$

However in the root of the jet (2.177) does not hold. Therefore the limits of the second integral in equation (2.176) are reduced to only the intervals $\eta_j \leq y \leq H$ at $x = \pm x_{c0}(t)$, where $\eta_j = H - h + \eta(x_{c0}(t), t)$ is the free-surface elevation of the jet at the moving contact point which is defined implicitly in equation (2.134). Here $H - \eta_j$ is of $\mathrm{O}(\epsilon)$ which can be regarded as the thickness of the jet. Finding the thickness of the jet requires the inner solution be matched with the outer solution which is not considered in this study. The reader can find the details of the inner and outer region solution in (Cointe & Armand 1987), (Wilson 1989), (Korobkin 1997), (Oliver 2002) and references therein. That is

$$\rho \int\limits_{\partial\Omega(t)} \left(\frac{1}{2}\, \vec{U} \cdot \vec{U} + gy \right) (\vec{v} - \vec{v}_b) \,.\vec{n}\, \mathrm{d}S = 2\rho \int\limits_{\eta_j}^{H} \left(\frac{1}{2} \left(\vec{U} \cdot \vec{U} \right) \big|_{x=x_{c0}} + gy \right) (V_J - V_S)\, \mathrm{d}y. \tag{2.178}$$

For the sake of brevity the integral is only taken at the right contact point as the impact is symmetric and hence the factor 2. Here V_J and V_S are, respectively, the normal component of fluid velocity in the jet and the spray root area velocity, see Figure 2.18. It should be noted that the line integration in equation (2.178) is not accounted for in the Wagner theory. This indicates the fact that the conservation of total energy is not preserved in Wagner theory and there is a loss of energy, from the main fluid domain to the jets.

A moving reference frame OXY is chosen to move with the turnover position which has velocity $\dot{x}_{c0}(t)$. The velocity of the fluid in the jet is $\dot{x}_{c0}(t)$ in the relative reference frame. Therefore, the velocity of the fluid across the spray root and in the jet is $2\dot{x}_{c0}(t)$ in the Earth-fixed coordinate system Oxy, where $\dot{x}_{c0}(t)$ is given in non-dimensional terms in equation (2.135). For the derivation of the velocity of the fluid in the jet see (Faltinsen & Timokha 2009).

Depending on the above description, we conclude that despite the exclusion of the jets from $\Omega(t)$, they are still represented by the vertical cut lines at $x = \pm x_{c0}(t)$ in terms of energy flux. Therefore, $\rho g \dot{x}_{c0}(H^2 - h_j^2)$ is the potential energy flux and $4\rho\dot{x}_{c0}^3(H - h_j)$ is the kinetic energy flux across $x = \pm x_{c0}(t)$ in which both are derived from equation (2.178). As to the first integral in equation

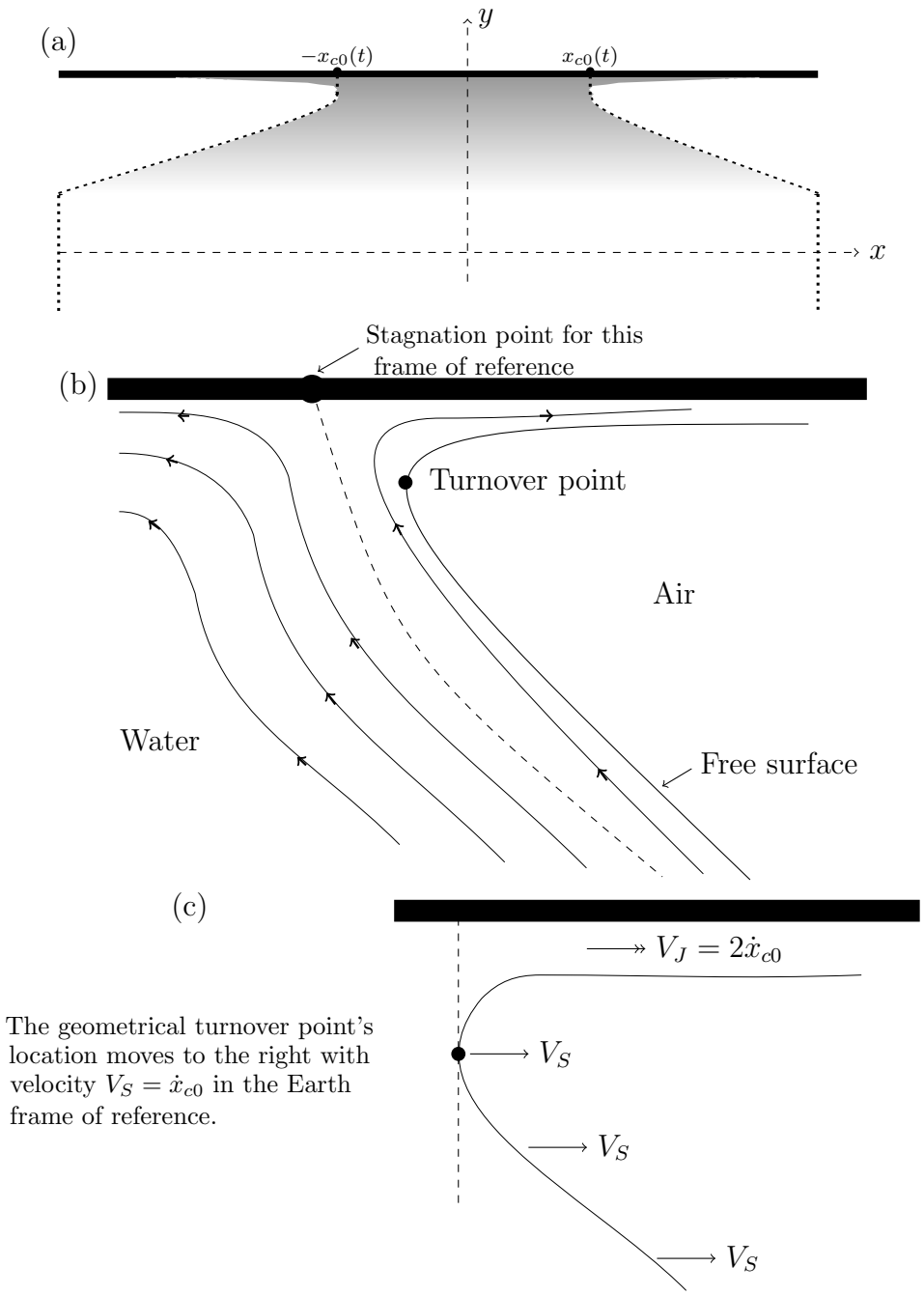

Figure 2.18: a- Sloshing at some instant $t > t^*$, the interval $(-x_{c0},x_{c0})$ is the leading-order wetted part and the dotted region refers to $\Omega(t)$. b- Spray root region, the spray root length is of O(ϵ). c- Jet region, the jet length is of O(1).

(2.176), we convert the double integral to a line integral as follows. (Faltinsen & Timokha 2009) show that the term $\frac{\partial}{\partial t}\left(\frac{1}{2}\,\vec{U}\cdot\vec{U}\right)$ for incompressible and inviscid liquid can be expressed as .

$$\rho\frac{\partial}{\partial t}\left(\frac{1}{2}\,\vec{U}\cdot\vec{U}\right)=-\nabla.\left(\rho\,\vec{U}\left(\frac{1}{2}\,\vec{U}\cdot\vec{U}+\rho^{-1}p+gy\right)\right). \tag{2.179}$$

Therefore using identity (2.179) and generalised Gauss theorem (divergence theorem) the first integral in equation (2.176) presents

$$\rho\int\limits_{\Omega(t)}\frac{\partial}{\partial t}\left(\frac{1}{2}\,\vec{U}\cdot\vec{U}\right)\mathrm{dV}=-\rho\int\limits_{\eta_j}^{H}\left(\frac{1}{2}\,\left(\vec{U}\cdot\vec{U}\right)\big|_{x=x_{c0}}+\rho^{-1}p+gy\right)V_J\mathrm{d}y. \tag{2.180}$$

where the normal conditions (2.60)–(2.62) have applied. The kinetic energy flux and potential energy flux produce by equation (2.180) are, respectively, $-8\rho\dot{x}_{c0}^3(t)(H-h_j)$ and $-2\rho g\dot{x}_{c0}(t)(H^2-h_j^2)$. Summing up the previous kinetic and potential energy fluxes, the total energy flux from the domain $\Omega(t)$ into the jets is identified by equation (2.176) is

$$\frac{\mathrm{d}}{\mathrm{d}t}\left(\mathrm{E_T}(t)\right)=-\rho\dot{x}_{c0}(t)(H-h_j)\left(4\dot{x}_{c0}^2(t)+g(H+h_j)\right). \tag{2.181}$$

Equation (2.181) confirms that the total energy in the part $\Omega(t)$ of the fluid domain, decreases due to its loss from the main part of the fluid domain to the jets.

Chapter 3

Influence of gravity on the moving contact point

It has always been a difficult task for scientists to determine the interaction region in moving boundary problems even in 2D. So far no one has published a method for finding the moving boundary, in 2D and 3D, analytically for non-symmetric impact. For 2D in previous Chapter this challenge addressed and solved for our particular sloshing impact in the tank. In the current Chapter we are interested in going one step further, by updating the wetted region boundary with gravity's influence. This Chapter analyses evolution of the moving point $x = x_c(t)$ in the presence of gravity. We assume that the influence of gravity on the moving point will be proportional to the effect on other quantities. In other words, in this Chapter we will gain a better understanding about the correction due to gravity on force, pressure and surface elevation through the correction we will find for the moving contact point. (Vanden-Broeck & Keller 1982), (Wilson 1989) and (Howison et al. 1991) did some work with inclusion of gravity and its effect on the jets. Also this Chapter shows the correction due to gravity to the pressure distribution applied on the lid during the impact.

3.1 Problem formulation with gravity

In this section we introduce gravity into the problem solved in the previous Chapter. In particular, in section 2.2.5, the problem was formulated in terms of stretched variables by using the small parameter $\delta \ll 1$, close to the contact point and the fluid domain treated as an infinite flow region. Also we formulate the problem in terms of a complex velocity potential, a complex displacement potential and a complex acceleration potential to analyse and then solve our problem described in section 2.1. In section 2.2.5, gravity was disregarded by

dropping out the term $\frac{\partial \Phi}{\partial \zeta}$ in equation (2.91), which was of order $O(\delta^{3/2})$, see (2.91). We used the stretched variables to deal with the flow as in an infinite region. This makes the problem of the flow in the tank and its impact on the lid, to be similar to the case of a flat plate above the fluid in infinite flow region. That is,

- The fluid flow in both problems are governed by Laplace's equation (2.71).
- The boundary conditions, kinematic and dynamic boundary conditions (2.74)–(2.75) on the lid and on the flat plate (on the impact region) are the same.
- The combined kinematic and dynamic boundary conditions (2.76) on the free-surfaces in the tank and on the free-surfaces around or below the flat plate are also the same.

However they are different in the boundary conditions on the bottom and on the walls of the tank in the case of flow in a tank while in infinite fluid domain we use the far-field condition (2.93) in the infinite flow region case. Also they are different in the pressure on the free-surface, for free-surface in tank we have ullage pressure while in infinite fluid region, the pressure on free-surface is atmospheric pressure.

3.1.1 Problem description

In this section we intend to bring into account gravity in the problem. We recall the mixed boundary-value problem (with replacing ξ, ζ, τ and ξ_c by x, y, t and x_c) found in terms of stretched variables in section 2.2.5 at the leading order to be

$$\frac{\partial^2 \Phi}{\partial x^2} + \frac{\partial^2 \Phi}{\partial y^2} = 0 \qquad -\infty < x < \infty, y < 0, \tag{3.1}$$

$$\frac{\partial \Phi}{\partial y} + \frac{\partial \eta_n}{\partial t} = 0 \qquad |x| < x_c,\ y = 0, \tag{3.2}$$

$$\frac{\partial \Phi}{\partial t} + \delta^{3/2}\eta_c = 0 \quad |x| > x_c,\ y = 0, \tag{3.3}$$

$$\frac{\partial \Phi}{\partial y} - \frac{\partial \eta_c}{\partial t} = 0 \qquad |x| > x_c,\ y = 0, \tag{3.4}$$

where $\Phi = \Phi(\xi, \zeta, \tau)$, $\eta_n = \eta_n(\xi, \tau)$ and $\eta_c = \eta_c(\xi, \tau)$ are defined in (2.85). Note that at leading order gravity in non-dimensional variables is represented in the dynamic boundary condition on the free-surface (3.3) and in the dynamic

boundary condition on the impact region (3.5) for the pressure:

$$\frac{\partial \Phi}{\partial t} + \delta^{3/2}\eta_c = -p \qquad\qquad |x| < x_c,\ y = 0, \tag{3.5}$$

Otherwise the problem is unchanged at the leading order in δ. The boundary problem is supplemented by the leading order initial conditions

$$\Phi(x, y, 0) = 0, \tag{3.6}$$

$$\eta_c(x, 0) = 0, \tag{3.7}$$

$$x_c(0) = 0, \tag{3.8}$$

and the far field condition

$$\Phi(x, y, t) \longrightarrow 0 \qquad \text{as} \qquad x^2 + y^2 \longrightarrow \infty. \tag{3.9}$$

We mention for the reader that $y = 0$ represents the position of the free-surface and the wetted region at the leading order. To construct the problem in terms of a displacement potential, first we must introduce the Wagner condition (see (Wagner 1932)).

3.1.2 The Wagner condition

The condition of (Wagner 1932) is imposed on the surface elevation at the moving contact points $x = \pm x_c$ where the vertical distance between the tank lid and the point of the free-surface, where the tangent to the free surface is vertical (turnover point), is tiny due to narrow width of any jets. Therefore at the leading order this distance can be ignored to give

$$\eta_n(x_c(t), t) + \eta_c(x_c(t), t) = 0. \tag{3.10}$$

where only the right hand moving point is considered, as the impact is symmetric. As was done earlier, in section 2.2.4, the surface-elevation is decomposed into two parts.

3.1.3 Mixed boundary-value problem in terms of displacement potential

Next we formulate the problem (3.1)–(3.9) in terms of a displacement potential, as introduced by (Korobkin 1982),

$$\hat{\phi}(x,y,t) = \int_0^t \Phi(x,y,\tau)\mathrm{d}\tau. \tag{3.11}$$

The Laplace equation (3.1), in the flow region takes the form

$$\frac{\partial^2\hat{\phi}}{\partial x^2} + \frac{\partial^2\hat{\phi}}{\partial y^2} = 0. \tag{3.12}$$

The kinematic boundary condition in the impact region, $|x| < x_c(t),\ y = 0$, gives

$$\frac{\partial\hat{\phi}}{\partial y} = \int_0^{t_c(x)} \frac{\partial\Phi}{\partial y}\mathrm{d}\tau + \int_{t_c(x)}^t \frac{\partial\Phi}{\partial y}\mathrm{d}\tau, \tag{3.13}$$

where $t_c(x)$ is the inverse function of $x_c(t)$, i.e. $x_c(t_c(x)) = x$. Using the boundary conditions (3.2) and (3.4), equation (3.13) reads

$$\begin{aligned}\frac{\partial\hat{\phi}}{\partial y} &= \int_0^{t_c(x)} \frac{\partial\eta_c}{\partial t}\mathrm{d}\tau - \int_{t_c(x)}^t \frac{\partial\eta_n}{\partial t}\mathrm{d}\tau, \\ &= \eta_c(x,t_c(x)) - \eta_c(x,0) - \eta_n(x,t) + \eta_n(x,t_c(x)),\end{aligned} \tag{3.14}$$

with the Wagner condition (3.10) and initial condition (3.7), equation (3.13) reads

$$\frac{\partial\hat{\phi}}{\partial y} = -\eta_n(x,t), \tag{3.15}$$

The time-integral of the dynamic boundary condition (3.3) on the free-surface, $|x| > x_c,\ y = 0$, with respect to time from 0 to t, allows us to rewrite in terms of the displacement potential (3.11):

$$\begin{aligned}\hat{\phi}(x,0,t) &= -\int_0^t \Phi(x,0,\tau)\mathrm{d}\tau, \\ &= -\delta^{3/2}\int_0^t\int_0^\tau \eta_c(x,\tilde{\tau})\mathrm{d}\tilde{\tau}\mathrm{d}\tau,\end{aligned} \tag{3.16}$$

where (3.16) can be written as

$$\hat{\phi}(x,0,t) = -\delta^{3/2}\int_0^t (t-\tau)\eta_c(x,\tau)\mathrm{d}\tau. \tag{3.17}$$

Also the kinematic boundary condition (3.4), on the free-surface, $|x| > x_c,\ y = 0$, provides

$$\begin{aligned}\frac{\partial\hat{\phi}}{\partial y} &= \int_0^t \frac{\partial\Phi}{\partial y}d\tau,\\ &= \eta_c(x,t).\end{aligned} \tag{3.18}$$

The initial condition (3.6) and the far field condition (3.9) in terms of displacement potential take the form, respectively

$$\hat{\phi}(x,y,0) = 0, \tag{3.19}$$

$$\hat{\phi}(x,y,t) \longrightarrow 0 \qquad \text{as} \qquad x^2+y^2 \longrightarrow \infty. \tag{3.20}$$

3.1.4 Mixed boundary-value problem in terms of complex displacement

In this section we define the complex displacement $\hat{\mathrm{w}}(z,t)$ by the relation

$$\frac{\mathrm{d}\hat{\mathrm{w}}}{\mathrm{d}z}(z,t) = \frac{\partial\hat{\phi}}{\partial x}(x,y,t) - i\frac{\partial\hat{\phi}}{\partial y}(x,y,t) \qquad z = x+iy,$$

where $\frac{\partial\hat{\phi}}{\partial x}(x,y,t)$ and $\frac{\partial\hat{\phi}}{\partial y}(x,y,t)$ are horizontal and vertical displacements of the liquid particles respectively. To reformulate the problem (3.12)–(3.20) in terms of complex displacement, we calculate

$$\mathrm{Re}\left[\frac{\mathrm{d}\hat{\mathrm{w}}}{\mathrm{d}z}(x-i0,t)\right] = g_1(x,t) \qquad |x| > x_c, \tag{3.21}$$

$$\mathrm{Im}\left[\frac{\mathrm{d}\hat{\mathrm{w}}}{\mathrm{d}z}(x-i0,t)\right] = g_2(x,t) \qquad |x| < x_c, \tag{3.22}$$

where from equation (3.17)

$$g_1(x,t) = -\delta^{3/2}\int_0^t (t-\tau)\frac{\partial\eta_c}{\partial x}(x,\tau)\mathrm{d}\tau, \tag{3.23}$$

and

$$g_2(x,t) = \eta_n(x,t). \tag{3.24}$$

From equation (3.20) we find that

$$\frac{\mathrm{d}\hat{\mathrm{w}}}{\mathrm{d}z}(z,t) \longrightarrow 0 \qquad \text{as} \qquad |z| \longrightarrow \infty. \tag{3.25}$$

We introduce a new unknown function $\hat{\mathrm{W}}(z,t)$ using the characteristic function, $\sqrt{z^2-x_c^2}$, and the complex displacement potential $\hat{\mathrm{w}}(z,t)$ as

$$\hat{\mathrm{W}}(z,t) = \sqrt{z^2-x_c^2}\,\frac{\mathrm{d}\hat{\mathrm{w}}}{\mathrm{d}z}(z). \tag{3.26}$$

The function $\hat{\mathrm{W}}(z,t)$ is the product of two functions that are analytic in the lower half-plane, so it is also analytic, and

$$\hat{\mathrm{W}}(z,t) \longrightarrow 0 \qquad \text{as} \qquad |z| \longrightarrow \infty, \tag{3.27}$$

as $O(z^{-1})$. The real part of $\hat{\mathrm{W}}(x-i0,t)$ takes the form

$$\mathrm{Re}\left[\hat{\mathrm{W}}(x-i0,t)\right] = \begin{cases} \mathrm{Re}\left[\sqrt{x^2-x_c^2}(\frac{\partial\hat{\phi}}{\partial x} - i\frac{\partial\hat{\phi}}{\partial y})\right] = g_1\sqrt{x^2-x_c^2} & x > x_c, \\ \mathrm{Re}\left[-\sqrt{x^2-x_c^2}(\frac{\partial\hat{\phi}}{\partial x} - i\frac{\partial\hat{\phi}}{\partial y})\right] = -g_1\sqrt{x^2-x_c^2} & x < -x_c, \\ \mathrm{Re}\left[-i\sqrt{x_c^2-x^2}(\frac{\partial\hat{\phi}}{\partial x} - i\frac{\partial\hat{\phi}}{\partial y})\right] = -g_2\sqrt{x_c^2-x^2} & |x| < x_c. \end{cases} \tag{3.28}$$

(Gakhov & Sneddon 1966) solve the problem (3.27)–(3.28):

$$\hat{\mathrm{W}}(z,t) = \frac{i}{\pi}\int_{-\infty}^{\infty} \frac{Re\left[\hat{\mathrm{W}}(\sigma-i0)\right]}{\sigma-z}\mathrm{d}\sigma.$$

Decomposing the interval of integration with respect to the impact region and free-surfaces, we find

$$\begin{aligned}\hat{\mathrm{W}}(z,t) = \frac{i}{\pi}\Bigg[&-\int_{-\infty}^{-x_c} \frac{g_1\sqrt{\sigma^2-x_c^2}}{\sigma-z}\mathrm{d}\sigma + \int_{x_c}^{\infty} \frac{g_1\sqrt{\sigma^2-x_c^2}}{\sigma-z}\mathrm{d}\sigma \\ &-\fint_{-x_c}^{x_c} \frac{g_2\sqrt{x_c^2-\sigma^2}}{\sigma-z}\mathrm{d}\sigma\Bigg].\end{aligned} \tag{3.29}$$

Therefore, the solution to the problem (3.21)–(3.23) can be written

$$\begin{aligned}\frac{\mathrm{d}\hat{\mathrm{w}}}{\mathrm{d}z}(z,t) = \frac{i}{\pi\sqrt{z^2-x_c^2}}\Bigg[&-\int_{-\infty}^{-x_c} \frac{g_1\sqrt{\sigma^2-x_c^2}}{\sigma-z}\mathrm{d}\sigma + \int_{x_c}^{\infty} \frac{g_1\sqrt{\sigma^2-x_c^2}}{\sigma-z}\mathrm{d}\sigma \\ &-\fint_{-x_c}^{x_c} \frac{g_2\sqrt{x_c^2-\sigma^2}}{\sigma-z}\mathrm{d}\sigma\Bigg].\end{aligned} \tag{3.30}$$

Note that the last integral on the right-hand side of equation (3.29) is the Cauchy-type integral. Using the Plemelj formula, (Gakhov & Sneddon 1966), as $y \longrightarrow 0^-$ in the impact region, $|x| < x_c$, we find

$$\frac{\mathrm{d}\hat{\mathrm{w}}}{\mathrm{d}z}(x - i0, t) = \frac{-1}{\pi\sqrt{x_c^2 - x^2}}\left[-\int_{-\infty}^{-x_c} \frac{g_1\sqrt{\sigma^2 - x_c^2}}{\sigma - x}\mathrm{d}\sigma + \int_{x_c}^{\infty} \frac{g_1\sqrt{\sigma^2 - x_c^2}\mathrm{d}\sigma}{\sigma - x} + i\pi g_2\sqrt{x_c^2 - x^2} - \fint_{-x_c}^{x_c} \frac{g_2\sqrt{x_c^2 - \sigma^2}}{\sigma - x}\mathrm{d}\sigma\right]. \tag{3.31}$$

The real and imaginary parts of (3.31) give the vertical displacement potential

$$\frac{\partial\hat{\phi}}{\partial y}(x, 0, t) = g_2(x, t), \tag{3.32}$$

and the horizontal displacement

$$\frac{\partial\hat{\phi}}{\partial x}(x, 0, t) = \frac{-1}{\pi\sqrt{x_c^2 - x^2}}\left[-\int_{-\infty}^{-x_c} \frac{g_1\sqrt{\sigma^2 - x_c^2}}{\sigma - x}\mathrm{d}\sigma + \int_{x_c}^{\infty} \frac{g_1\sqrt{\sigma^2 - x_c^2}}{\sigma - x}\mathrm{d}\sigma - \fint_{-x_c}^{x_c} \frac{g_2\sqrt{x_c^2 - \sigma^2}}{\sigma - x}\mathrm{d}\sigma\right]. \tag{3.33}$$

As $x \longrightarrow x_c(t) - 0$, horizontal displacement (3.33) is finite if the expression in the brackets is zero

$$\int_{-\infty}^{-x_c} \frac{-(\sigma + x_c)g_1}{\sqrt{\sigma^2 - x_c^2}}\mathrm{d}\sigma + \int_{x_c}^{\infty} \frac{(\sigma + x_c)g_1}{\sqrt{\sigma^2 - x_c^2}}\mathrm{d}\sigma + \fint_{-x_c}^{x_c} \frac{(x_c + \sigma)g_2}{\sqrt{x_c^2 - \sigma^2}}\mathrm{d}\sigma = 0. \tag{3.34}$$

The functions $g_1(x, t)$ and $g_2(x, t)$ are odd and even respectively, therefore equation (3.34) reads

$$2\int_{x_c}^{\infty} \frac{g_1(\sigma, t)}{\sqrt{\sigma^2 - x_c^2}}\mathrm{d}\sigma + \fint_{-x_c}^{x_c} \frac{g_2(\sigma, t)}{\sqrt{x_c^2 - \sigma^2}}\mathrm{d}\sigma = 0. \tag{3.35}$$

The integral in (3.35) were calculated in section 2.3.1, where gravity was neglected. This means that the first integral on the left hand side of (3.35) was zero and the wetted part calculated without the influence of gravity. However, the calculations in equation (3.35) to be done are more complicated, and the existence of the unknown function, the free-surface elevation, $\eta_c(x, t)$, in the function $g_1(x, t)$ is the matter of concern.

The influence of gravity in our problem is negligible in the short period at the very beginning of impact. This can be concluded from the fact that at the very beginning of impact due to high velocity of the fluid, we have a high Froude number $\frac{U}{\sqrt{Hg}} \gg 1$, which shows that the inertia is dominant compared

with gravitational forces. We are interested to quantify this behaviour in this study. This means that in this short period, the vertical velocity is uninfluenced by gravity without any significant reduction in its velocity. Also in this study we are interested to investigate sloshing with low Froude number $\frac{U}{\sqrt{Hg}} \ll 1$, in which the gravitational forces start to become dominant compared with inertial forces.

The gravitational acceleration term g which is hidden in non-dimensional variables should be brought back again into the model. The presence of gravity in our problem will take us one step closer to a more realistic description of impact. We try to determine the contribution of gravity in the problem by representing it in terms of γ, such that, $\gamma = \delta^{3/2}$. At the beginning of impact, $\gamma \ll 1$, but as time grows, γ becomes more and more important, and eventually it ends the impact. Hence equation (3.3) can be modified to

$$\frac{\partial \Phi}{\partial t} + \gamma\, \eta_c = 0 \qquad\qquad |x| > x_c,\ y = 0. \tag{3.36}$$

3.1.5 Expansion of the moving point in terms of γ

Equation (3.35) provides the position of the moving point $x = x_c(t)$, the half size of the wetted region. The equation to be calculated needs an expansion in terms of the new small parameter, γ. It should be noted that the previous expansions of unknown functions were made in terms of the small parameter $\epsilon = \frac{h}{H}$, where H is the height of the tank and h is the distance between the static free-surface and the lid, see Figure 2.5. However, as to the leading order terms, there will be no difference for both expansions. We start by introducing new variables

$$\tilde{x} = qx, \qquad \tilde{y} = qy, \tag{3.37}$$

where

$$q(t, \gamma) = \frac{x_{c0}(t)}{x_c(t, \gamma)}. \tag{3.38}$$

Such that

$$q(t, \gamma) = 1 + o(1) \quad as \quad \gamma \longrightarrow 0.$$

Here at leading order, the moving point $x = x_{c0}$, represents the half-length of the contact region in the absence of gravity, while the function $x_c(t, \gamma)$, represents the half length of the contact region in the presence of gravity. Here $\gamma = 0$ means gravity is neglected and $x_c(t, \gamma = 0) = x_{c0}(t)$ at the leading order.

The purpose of the following analysis is to define a consistent expansion for the moving contact point $x_c(t, \gamma)$ in terms of γ. We introduce new variables, $\tilde{x}$

and $\tilde{y}$, into the kinematic boundary conditions (3.2)

$$q\frac{\partial\tilde{\phi}}{\partial\tilde{y}} = -\frac{\partial\tilde{\eta}_n}{\partial t} - \tilde{x}\frac{q_t}{q}\frac{\partial\tilde{\eta}_n}{\partial\tilde{x}} \qquad |\tilde{x}| < x_{c0},\ \tilde{y} = 0, \tag{3.39}$$

where $\tilde{\phi} = \tilde{\phi}(\tilde{x}, \tilde{y}, t)$ and $\tilde{\eta_n} = \tilde{\eta_n}(\tilde{x}, t)$, into the dynamic boundary condition (3.3)

$$\tilde{x}\frac{q_t}{q}\frac{\partial\tilde{\phi}}{\partial\tilde{x}} + \frac{\partial\tilde{\phi}}{\partial t} + \gamma\tilde{\eta}_c = 0 \qquad |\tilde{x}| > x_{c0},\ \tilde{y} = 0, \tag{3.40}$$

where $\tilde{\eta_c} = \tilde{\eta_c}(\tilde{x}, t)$, and into the kinematic boundary condition (3.4)

$$q\frac{\partial\tilde{\phi}}{\partial\tilde{y}} = \frac{\partial\tilde{\eta}_c}{\partial t} + \tilde{x}\frac{q_t}{q}\frac{\partial\tilde{\eta}_c}{\partial\tilde{x}} \qquad |\tilde{x}| > x_{c0},\ \tilde{y} = 0. \tag{3.41}$$

To find the expansions of the unknown functions with respect to parameter γ, at this stage, we expand our functions as follows: the velocity potential

$$\tilde{\phi}(\tilde{x}, \tilde{y}, t, \gamma) = \tilde{\phi}_0(\tilde{x}, \tilde{y}, t) + \tilde{\Phi}(\tilde{x}, \tilde{y}, t, \gamma), \qquad \tilde{\Phi} \longrightarrow 0 \quad as\ \gamma \longrightarrow 0, \tag{3.42}$$

the correction to the surface elevation after introducing the lid to the problem

$$\tilde{\eta_c}(\tilde{x}, t, \gamma) = \tilde{\eta}_{c0}(\tilde{x}, t) + \Pi(\tilde{x}, t, \gamma), \qquad \Pi \longrightarrow 0 \quad as\ \gamma \longrightarrow 0, \tag{3.43}$$

the coordinate of the contact point accounting for gravity

$$x_c(t, \gamma) = x_{c0}(t) + X(t, \gamma), \qquad X \longrightarrow 0 \quad as\ \gamma \longrightarrow 0, \tag{3.44}$$

and the stretched coefficient

$$q(t, \gamma) = 1 + \tilde{q}(t, \gamma), \qquad \tilde{q} \longrightarrow 0 \quad as\ \gamma \longrightarrow 0, \tag{3.45}$$

where

$$\tilde{q}(t, \gamma) = \frac{-X}{x_{c0} + X}. \tag{3.46}$$

Hence

$$\frac{d\tilde{q}}{dt}(t, \gamma) = \frac{\dot{x}_{c0}X - x_{c0}\dot{X}}{x_{c0}^2}, \tag{3.47}$$

where $\tilde{q} \sim \frac{d\tilde{q}}{dt} \sim O(X)$ as $\gamma \longrightarrow 0$. Substituting the expansions (3.42)–(3.45) into

(3.39)–(3.41), at the first order, the terms of $o(1)$, on $\tilde{y}=0$, respectively, we find

$$\tilde{q}\frac{\partial\tilde{\phi}_0}{\partial\tilde{y}}+\frac{\partial\tilde{\Phi}}{\partial\tilde{y}}(1+\tilde{q})=-\tilde{x}\frac{d\tilde{q}}{dt}\frac{\partial\tilde{\eta}_n}{\partial\tilde{x}} \qquad |\tilde{x}|<x_{c0},\tilde{y}=0, \tag{3.48}$$

$$\tilde{x}\frac{d\tilde{q}}{dt}\left(\frac{\partial\tilde{\phi}_0}{\partial\tilde{x}}+\frac{\partial\tilde{\Phi}}{\partial\tilde{x}}\right)+\frac{\partial\tilde{\Phi}}{\partial t}+\gamma\tilde{\eta}_{c0}+\gamma\Pi=0 \qquad |\tilde{x}|>x_{c0},\tilde{y}=0, \tag{3.49}$$

$$\tilde{q}\frac{\partial\tilde{\phi}_0}{\partial\tilde{y}}+\frac{\partial\tilde{\Phi}}{\partial\tilde{y}}(1+\tilde{q})=\frac{\partial\Pi}{\partial t}+\tilde{x}\frac{d\tilde{q}}{dt}\left(\frac{\partial\tilde{\eta}_{c0}}{\partial t}+\frac{\partial\Pi}{\partial\tilde{x}}\right) \qquad |\tilde{x}|>x_{c0},\tilde{y}=0. \tag{3.50}$$

Expanding the terms $\tilde{\Phi}$ and Π one step further

$$\tilde{\Phi}(\tilde{x},\tilde{y},t,\gamma)=\gamma\tilde{\phi}_1(\tilde{x},\tilde{y},t)+\tilde{\Phi}_1(\tilde{x},\tilde{y},t,\gamma), \qquad \frac{\tilde{\Phi}_1}{\gamma}\longrightarrow 0 \quad as\ \gamma\longrightarrow 0, \tag{3.51}$$

$$\Pi(\tilde{x},t,\gamma)=\gamma\tilde{\eta}_{c1}(\tilde{x},t)+\Pi_1(\tilde{x},t,\gamma), \qquad \frac{\Pi_1}{\gamma}\longrightarrow 0 \quad as\ \gamma\longrightarrow 0. \tag{3.52}$$

Substitution of (3.51)–(3.52) into (3.48)–(3.50), on $\tilde{y}=0$, and equating the terms of order $O(\gamma)$ imply

$$\frac{1}{\gamma}\tilde{q}\frac{\partial\tilde{\phi}_0}{\partial\tilde{y}}+\frac{\partial\tilde{\phi}_1}{\partial\tilde{y}}=-\frac{1}{\gamma}\tilde{x}\frac{d\tilde{q}}{dt}\frac{\partial\tilde{\eta}_n}{\partial\tilde{x}} \qquad |\tilde{x}|<x_{c0}, \tag{3.53}$$

$$\frac{\tilde{x}}{\gamma}\frac{d\tilde{q}}{dt}\frac{\partial\tilde{\phi}_0}{\partial\tilde{x}}+\frac{\partial\tilde{\phi}_1}{\partial t}+\tilde{\eta}_{c0}=0 \qquad |\tilde{x}|>x_{c0}, \tag{3.54}$$

$$\frac{1}{\gamma}\tilde{q}\frac{\partial\tilde{\phi}_0}{\partial\tilde{y}}+\frac{\partial\tilde{\phi}_1}{\partial\tilde{y}}=\frac{1}{\gamma}\tilde{x}\frac{d\tilde{q}}{dt}\frac{\partial\tilde{\eta}_{c0}}{\partial\tilde{x}}+\frac{\partial\tilde{\eta}_{c1}}{\partial t} \qquad |\tilde{x}|>x_{c0}. \tag{3.55}$$

Now equations (3.53)–(3.55) all force $x_c(t,\gamma)$ to be expanded as

$$x_c(t,\gamma)=x_{c0}(t)+\gamma x_{c1}(t)+o(\gamma), \tag{3.56}$$

and consequently

$$\tilde{q}(t,\gamma)=1+\gamma\chi(t)+o(\gamma), \tag{3.57}$$

where $\chi(t)=-\frac{x_{c1}(t)}{x_{c0}(t)}$. The asymptotic expansion is now clear and we can use it to continue with equation (3.34).

3.1.6 Equation for the moving point

We found the form of the expansion of the functions in power of γ. In this section we start from equation (3.34). Using a change of integration variable, $\sigma=x_c(t)\beta$, we find

$$2\int_1^\infty \frac{g_1(x_c(t)\beta,t)}{\sqrt{\beta^2-1}}\mathrm{d}\beta + \fint_{-1}^1 \frac{g_2(x_c(t)\beta,t)}{\sqrt{1-\beta^2}}\mathrm{d}\beta = 0. \tag{3.58}$$

At this stage the function $x_c(t)$ in $g_1(x_c(t)\beta,t)$ and $g_2(x_c(t)\beta,t)$ are to be expanded, using (3.56). The Taylor expansion for $g_2(x_c(t)\beta,t)$ at $x = x_{c0}(t)$ imply

$$\begin{aligned} g_2(x_c(t)\beta,t) &= \sum_{n=1}^{\infty} \bar{f}_n \cos(k_n\beta[x_{c0}(t)+\gamma x_{c1}(t)+o(\gamma)])\cos(w_n t) \\ &= \sum_{n=1}^{\infty} \bar{f}_n \cos(k_n x_{c0}(t)\beta)\cos(w_n t) \\ &\quad - \gamma\left[\sum_{n=1}^{\infty} \bar{f}_n x_{c1}(t) k_n \beta \sin(k_n x_{c0}(t)\beta)\cos(w_n t)\right] + o(\gamma). \end{aligned} \tag{3.59}$$

Note that the summation is taken to be finite in our problem. Similarly for $g_1(x_c(t)\beta,t)$ we find

$$\begin{aligned} g_1(x_c(t)\beta,t) &= -\gamma\int_0^t (t-\tau)\frac{\partial \eta_c}{\partial\sigma}(x_{c0}(t)\beta+\gamma x_{c1}(t)\beta+o(\gamma),\tau)\mathrm{d}\tau \\ &= -\gamma\int_0^t (t-\tau)\left[\frac{\partial\eta_{c0}}{\partial\sigma}(x_{c0}(t)\beta,\tau)+\gamma\frac{\partial\eta_{c1}}{\partial\sigma}(x_{c0}(t)\beta,\tau)+\right. \\ &\qquad \left.\gamma x_{c1}(t)\beta\frac{\partial^2\eta_{c0}}{\partial\sigma^2}(x_{c0}(t)\beta,\tau)+o(\gamma^2)\right]\mathrm{d}\tau. \end{aligned}$$

Hence

$$g_1(x_c(t)\beta,t) = -\gamma\int_0^t (t-\tau)\frac{\partial\eta_{c0}}{\partial\sigma}(x_{c0}(t)\beta,\tau)\mathrm{d}\tau + o(\gamma). \tag{3.60}$$

Now we substitute the expansion of $g_1(x_c(t)\beta,t)$ and $g_2(x_c(t)\beta,t)$ into equation (3.58) and at the leading order, we find

$$\sum_{n=1}^{\infty} \bar{f}_n \cos(w_n t)\fint_{-1}^1 \frac{\cos(k_n x_{c0}(t)\beta)\mathrm{d}\beta}{\sqrt{1-\beta^2}} = 0, \tag{3.61}$$

which was solved for $x_{c0}(t)$ as shown in Chapter 2, and at the first order we have

$$\begin{aligned} 2\int_1^\infty\int_0^t (t-\tau)\frac{\frac{\partial\eta_{c0}}{\partial\sigma}(x_{c0}(t)\beta,\tau)}{\sqrt{\beta^2-1}}\mathrm{d}\tau\mathrm{d}\beta &= -\sum_{n=1}^{\infty}\bar{f}_n x_{c1}(t)k_n\cos(w_n t) \\ &\quad \fint_{-1}^1 \frac{\beta\sin(k_n x_{c0}(t)\beta)}{\sqrt{1-\beta^2}}\mathrm{d}\beta. \end{aligned} \tag{3.62}$$

Writing equation (3.62) for $x_{c1}(t)$ in the form

$$x_{c1}(t)G_1(t) = G_2(t), \tag{3.63}$$

where

$$G_1(t) = -\sum_{n=1}^{\infty} \bar{f}_n k_n \cos(w_n t) \int_{-1}^{1} \frac{\beta \sin(k_n x_{c0}(t)\beta)}{\sqrt{1-\beta^2}} \mathrm{d}\beta, \tag{3.64}$$

and

$$G_2(t) = 2\int_1^{\infty} \int_0^t (t-\tau) \frac{\frac{\partial \eta_{c0}}{\partial \sigma}(x_{c0}(t)\beta, \tau)}{\sqrt{\beta^2-1}} \mathrm{d}\tau \mathrm{d}\beta. \tag{3.65}$$

show both functions of time. Using the change of variable, $\beta = \cos(\bar{\beta})$, and the special integral given in (Gradshteyn & Ryzhik 2014) p. 421, the function $G_1(t)$ can be rewritten as

$$G_1(t) = -\pi \sum_{n=1}^{\infty} \bar{f}_n k_n \cos(w_n t) J_1(k_n x_{c0}(t)), \tag{3.66}$$

where J_1 is the Bessel function of the first kind. Substituting (3.67)

$$\frac{\partial \eta_{c0}}{\partial t}(x_{c0}(t)\beta, \tau) = \beta \dot{x}_{c0}(t) \frac{\partial \eta_{c0}}{\partial \sigma}(x_{c0}(t)\beta, \tau), \tag{3.67}$$

into equation (3.65), where $\dot{x}_{c0}(t) = \frac{\mathrm{d}x_{c0}}{\mathrm{d}t}(t)$, gives

$$G_2(t) = \frac{1}{\dot{x}_{c0}(t)} \int_1^{\infty} \frac{1}{\beta\sqrt{\beta^2-1}} \int_0^t (t-\tau) \frac{\partial \eta_{c0}}{\partial t}(x_{c0}(t)\beta, \tau) \mathrm{d}\tau \mathrm{d}\beta. \tag{3.68}$$

The evolution of the contact region is plotted at the leading order, i.e. without gravity, in Figure 2.13. Equation (3.63) includes information about the influence of gravity on the moving contact point $x = x_c(t, \gamma)$ in the first order approximation. Calculations for $G_1(t)$ are straightforward. However, for $G_2(t)$ from equation (3.68), the surface elevation velocity $\frac{\partial \eta_{c0}}{\partial t}$ is unknown and must be determined, as considered in the next subsection.

3.1.7 The leading-order correction of the surface elevation

In this section we will determine the leading-order surface elevation $\eta_{c0}(x,t)$ without gravity. This problem in the leading order was formulated in Section 2.2.5, by neglecting the term which contains gravity which has order $O(\gamma) = O(\delta^{\frac{3}{2}})$, $\delta \ll 1$. In section 2.2.7 the problem was formulated in terms of the displacement potential (2.110), and we again use $\hat{\phi}$ in this section. We formulate the problem

(2.111)–(2.119) in terms of complex displacement as follows. We define the complex displacement $\Phi_{cd}(z,t), z = x + iy$, through the displacement potential, see (Carrier et al. 2005)

$$\frac{\mathrm{d}\Phi_{cd}}{\mathrm{d}z}(z,t) = \frac{\partial\hat{\phi}}{\partial x}(x,y,t) - i\frac{\partial\hat{\phi}}{\partial y}(x,y,t). \tag{3.69}$$

From the conditions (2.112)–(2.116), the real and imaginary part of (3.69) read

$$\mathrm{Re}\left[\frac{\mathrm{d}\Phi_{cd}}{\mathrm{d}z}(x-i0,t)\right] = \frac{\partial\hat{\phi}}{\partial x}(x,0,t) = 0, \qquad |x| > x_{c0}, \tag{3.70}$$

$$\mathrm{Im}\left[\frac{\mathrm{d}\Phi_{cd}}{\mathrm{d}z}(x-i0,t)\right] = -\frac{\partial\hat{\phi}}{\partial y}(x,0,t) = \eta_{n0}, \qquad |x| < x_{c0}, \tag{3.71}$$

and the far field condition

$$\frac{\mathrm{d}\Phi_{cd}}{\mathrm{d}z} \longrightarrow 0 \qquad \text{as} \qquad |z| \longrightarrow \infty, \tag{3.72}$$

which converges to zero like $O(z^{-2})$. Introducing a new unknown function $\Phi_{ch}(z,t)$

$$\frac{\mathrm{d}\Phi_{ch}}{\mathrm{d}z} = \frac{\mathrm{d}\Phi_{cd}}{\mathrm{d}z}\sqrt{z^2 - x_{c0}^2} \tag{3.73}$$

$$= \left(\frac{\partial\hat{\phi}}{\partial x} - i\frac{\partial\hat{\phi}}{\partial y}\right)\sqrt{z^2 - x_{c0}^2}, \tag{3.74}$$

we calculate its real part as $y \longrightarrow 0^-$, using conditions (3.70) and (3.71)

$$\mathrm{Re}\left[\frac{\mathrm{d}\Phi_{ch}}{\mathrm{d}z}(x-i0,t)\right] = \begin{cases} Re\left[\sqrt{x^2 - x_{c0}^2}\left(\frac{\partial\hat{\phi}}{\partial x} - i\frac{\partial\hat{\phi}}{\partial y}\right)\right] = 0 & x > x_{c0}, \\ Re\left[-\sqrt{x^2 - x_{c0}^2(t)}\left(\frac{\partial\hat{\phi}}{\partial x} - i\frac{\partial\hat{\phi}}{\partial y}\right)\right] = 0 & x < -x_{c0}, \\ Re\left[-i\sqrt{x_{c0}^2 - x^2}\left(\frac{\partial\hat{\phi}}{\partial x} - i\frac{\partial\hat{\phi}}{\partial y}\right)\right] & \\ \qquad = \eta_{n0}(x,t)\sqrt{x_{c0}^2 - x^2} & |x| < x_{c0}, \end{cases} \tag{3.75}$$

and from the far-field condition (3.72), the far-field behaviour of the characteristic function is

$$\frac{\mathrm{d}\Phi_{ch}}{\mathrm{d}z}(z,t) \longrightarrow 0 \qquad \text{as} \qquad |z| \longrightarrow \infty. \tag{3.76}$$

The analytic solution to the problem (3.75) and (3.76) can be written as

$$\frac{\mathrm{d}\Phi_{ch}}{\mathrm{d}z}(z,t) = \frac{i}{\pi}\int_{-\infty}^{\infty} \frac{Re\left[\frac{\mathrm{d}\Phi_{cd}}{\mathrm{d}z}(\sigma - i0,t)\right]}{\sigma - z}\mathrm{d}\sigma + ic_0 + ic_1 z + \dots\,, \tag{3.77}$$

where the constants c_j for $j = 0, 1, \ldots$, have been forced to be zero by the far field condition (3.76). From boundary conditions (3.75), and equations (3.77) and (3.74) we find

$$\frac{\partial \hat{\phi}}{\partial x} - i\frac{\partial \hat{\phi}}{\partial y} = \frac{i}{\pi\sqrt{z^2 - x_{c0}^2}} \int_{-x_{c0}}^{x_{c0}} \frac{\eta_{n0}\sqrt{x_{c0}^2 - \sigma^2}}{\sigma - z} \mathrm{d}\sigma.$$

On the free-surface, $x > x_{c0}$, as $y \longrightarrow 0^-$, by (Carrier et al. 2005) we find

$$\frac{\partial \hat{\phi}}{\partial x} - i\frac{\partial \hat{\phi}}{\partial y} = \frac{i}{\pi\sqrt{x^2 - x_{c0}^2}} \int_{-x_{c0}}^{x_{c0}} \frac{\eta_{n0}\sqrt{x_{c0}^2 - \sigma^2}}{\sigma - x} \mathrm{d}\sigma.$$

From the imaginary part and equation (2.114), the surface elevation $\eta_{c0}(x, t)$ for $x > x_{c0}$, reads

$$\eta_{c0}(x, t) = \frac{-1}{\pi\sqrt{x^2 - x_{c0}^2(t)}} \int_{-x_{c0}(t)}^{x_{c0}(t)} \frac{\eta_{n0}(\sigma, t)\sqrt{x_{c0}^2(t) - \sigma^2}}{\sigma - x} \mathrm{d}\sigma. \tag{3.78}$$

The correction to the surface elevation $\eta_{c0}(x, t)$ at $t = 0.1997$ in Figure 3.1 and at $t = 0.3997$ in Figure 3.3, are shown. These two figures show that the correction on the surface elevation is found to be very small in the region far from the wetted region comparing to its correction close to the wetted region. This confirm the fact that due to highly localized pressure in space and time (this behaviour is observed in both experiments and numerical computations as well, see (Malenica, Mravak, Besse, Kaminski & Bogaert 2009), (Ten et al. 2011) and references therein) during the impact stage, the real shape of the free surface at a distance from the wetted region can be disregarded. A comparison between the free surface elevation without the lid versus the surface elevation with the lid (due to Wagner) is shown in Figures 3.2 and 3.4 at the previous times mentioned.

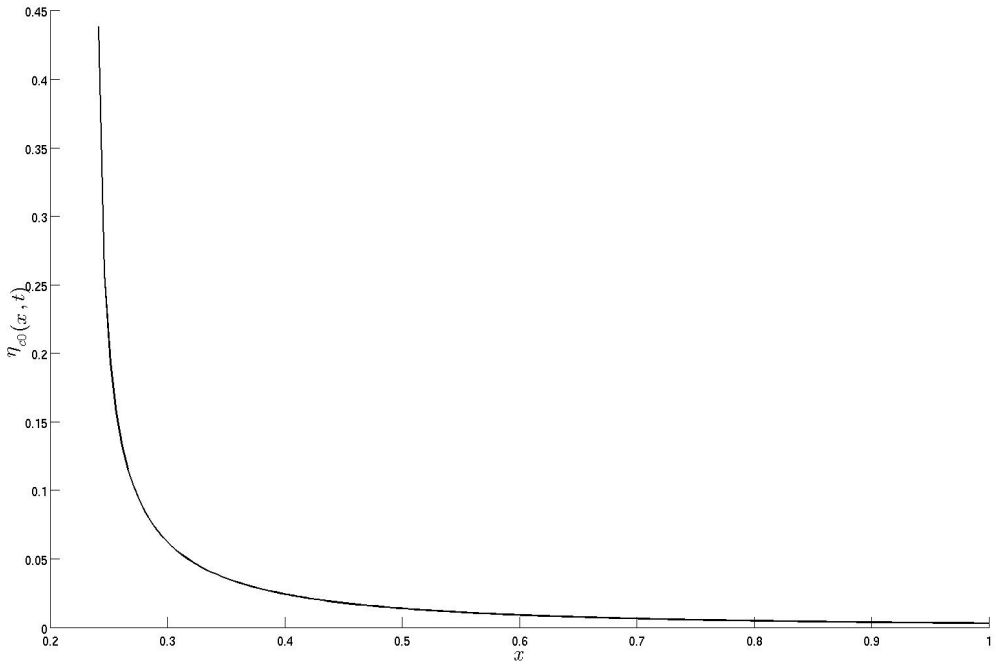

Figure 3.1: The correction to the surface elevation after lid is introduced, $\eta_{c0}(x,t)$, at time $t = 0.1997$.

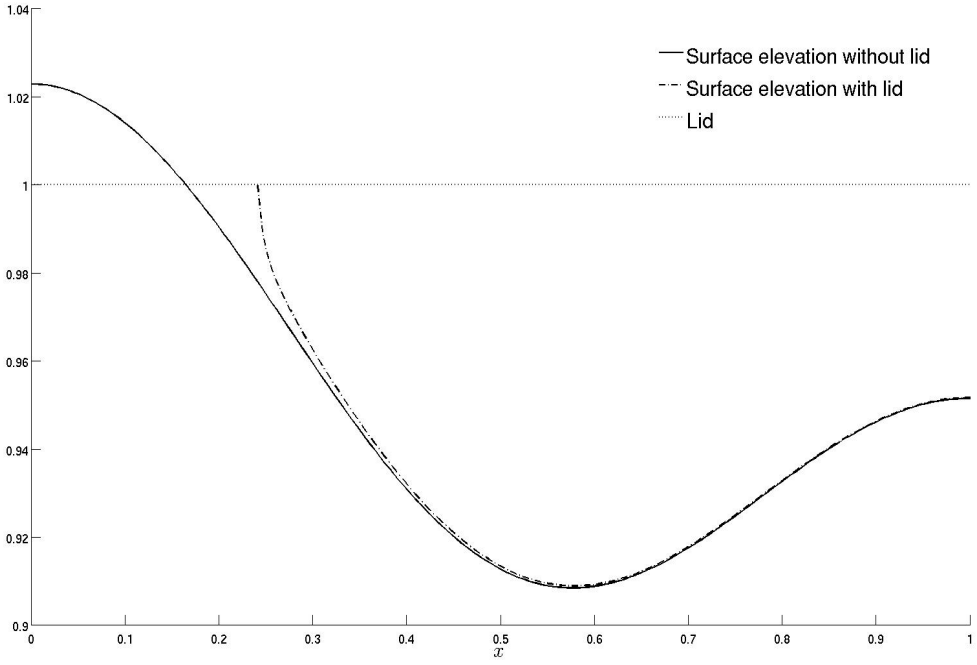

Figure 3.2: The free surface elevation without lid, $1 - \epsilon + \epsilon\eta_{n0}(x,t)$, (solid line), surface elevation with its correction with lid is introduced, $1 - \epsilon + \epsilon(\eta_{n0}(x,t) + \eta_{c0}(x,t))$, (dotted-dashed line), at time $t = 0.1997$.

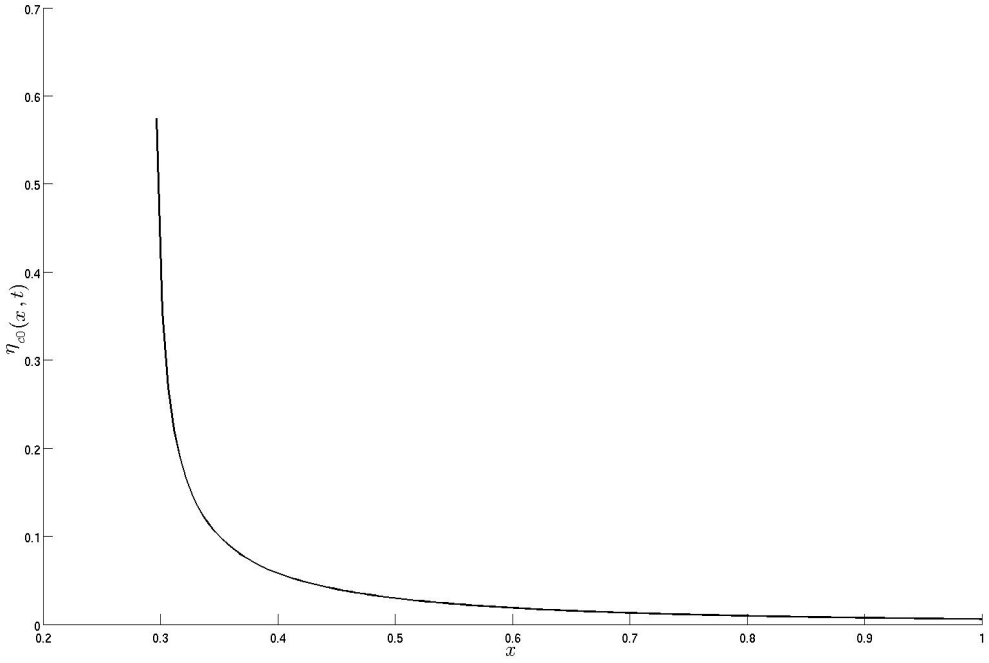

Figure 3.3: The correction to the surface elevation after lid is introduced, $\eta_{c0}(x,t)$, at time $t = 0.3997$.

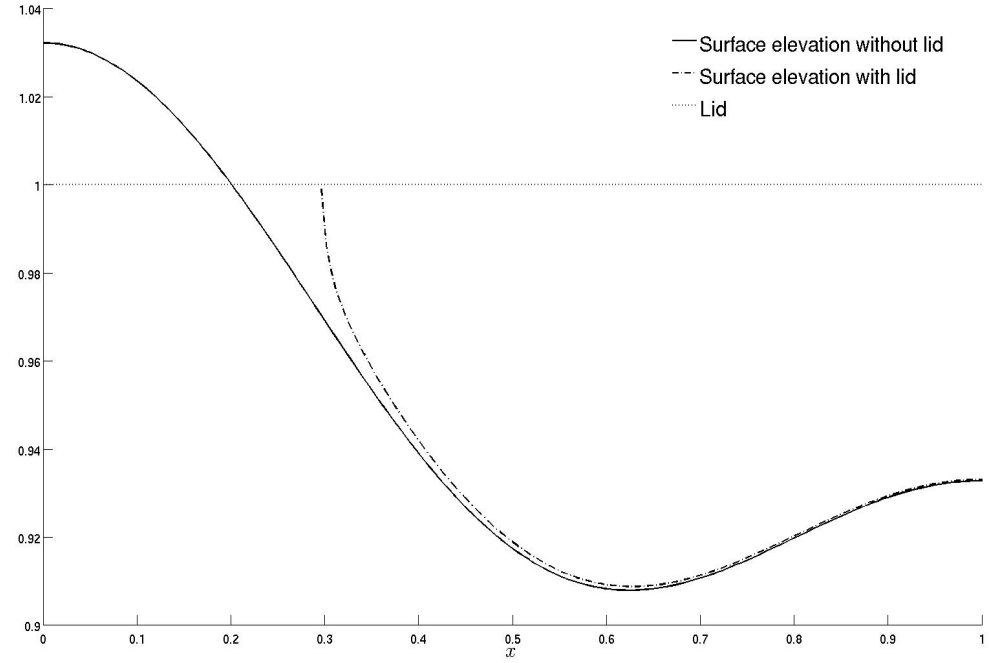

Figure 3.4: The free surface elevation without lid $1 - \epsilon + \epsilon\eta_{n0}(x,t)$, (solid line), surface elevation with its correction with lid is introduced, $1 - \epsilon + \epsilon(\eta_{n0}(x,t) + \eta_{c0}(x,t))$, (dotted-dashed line), at time $t = 0.3997$.

Having the surface elevation with no lid $\eta_{n0}(\sigma,t)$ given by equation (2.40), substituting $x = x_{c0}(t)\beta$ and change of variable $\sigma = x_{c0}(\tau)\cos(\theta)$ we arrive at

$$\eta_{c0}(x_{c0}(t)\beta,\tau) = \frac{-x_{c0}^2(\tau)}{\pi\sqrt{x_{c0}^2(t)\beta^2 - x_{c0}^2(\tau)}}\Bigg[\sum_{n=1}^{\infty}\bar{f}_n\cos(w_n\tau)$$

$$\int_0^{\pi}\frac{\cos(k_n x_{c0}(\tau)\cos(\theta))\sin^2(\theta)}{x_{c0}(\tau)\cos(\theta) - x_{c0}(t)\beta}\mathrm{d}\theta\Bigg]. \tag{3.79}$$

Equation (3.79) contains the correction to the surface elevation at $x = x_{c0}(t)\beta$. Having this we can continue from the previous section 3.1.6 to calculate the correction to the moving contact point due to gravity.

3.1.8 Gravity's effect on the moving contact point

In this section we calculate the correction to the moving contact point semi-analytically. The function $G_2(t)$ in equation (3.68) contains the time derivative of the correction to the surface elevation at the leading order. We use the Leibnitz integral rule as follows

$$\frac{\mathrm{d}}{\mathrm{d}t}\int_0^t(t-\tau)\int_1^{\infty}\frac{\eta_{c0}(x_{c0}(t)\beta,\tau)}{\beta^2\sqrt{\beta^2-1}}\mathrm{d}\beta\mathrm{d}\tau = \int_0^t\int_1^{\infty}\frac{\eta_{c0}(x_{c0}(t)\beta,\tau)}{\beta^2\sqrt{\beta^2-1}}\mathrm{d}\beta\mathrm{d}\tau$$

$$+\int_0^t(t-\tau)\int_1^{\infty}\frac{\dot{x}_{c0}(t)\beta\frac{\partial\eta_{c0}}{\partial t}(x_{c0}(t)\beta,\tau)}{\beta^2\sqrt{\beta^2-1}}\mathrm{d}\beta\mathrm{d}\tau. \tag{3.80}$$

Now by substituting (3.80) into equation (3.68) we arrive at the final analytical form for the function $G_2(t)$

$$G_2(t) = \frac{1}{\dot{x}_{c0}^2(t)}\frac{\mathrm{d}}{\mathrm{d}t}\int_0^t(t-\tau)\int_1^{\infty}\frac{\eta_{c0}(x_{c0}(t)\beta,\tau)}{\beta^2\sqrt{\beta^2-1}}\mathrm{d}\beta\mathrm{d}\tau \tag{3.81}$$

$$-\int_0^t\int_1^{\infty}\frac{\eta_{c0}(x_{c0}(t)\beta,\tau)}{\beta^2\sqrt{\beta^2-1}}\mathrm{d}\beta\mathrm{d}\tau. \tag{3.82}$$

Therefore the functions $G_1(t)$, see Figure 3.5, and $G_2(t)$, see Figure 3.6, are now determined by equations (3.82) and (3.80), respectively. Hence the correction to the moving contact point, $x_{c1}(t)$, due to gravity can be found from equation (3.63). Figures 3.5 and 3.6 make it clear that the ratio of the two functions $G_1(t)$ and $G_2(t)$ is negative. This indicates that the present of gravity decreases the length of the wetted region, see Figure 3.7. It is also shown in Figure 3.8 that the

period of the extension of the wetted region shortens by the influence of gravity. That is, due to gravity the wetted region starts to shrinks earlier than when it is absent.

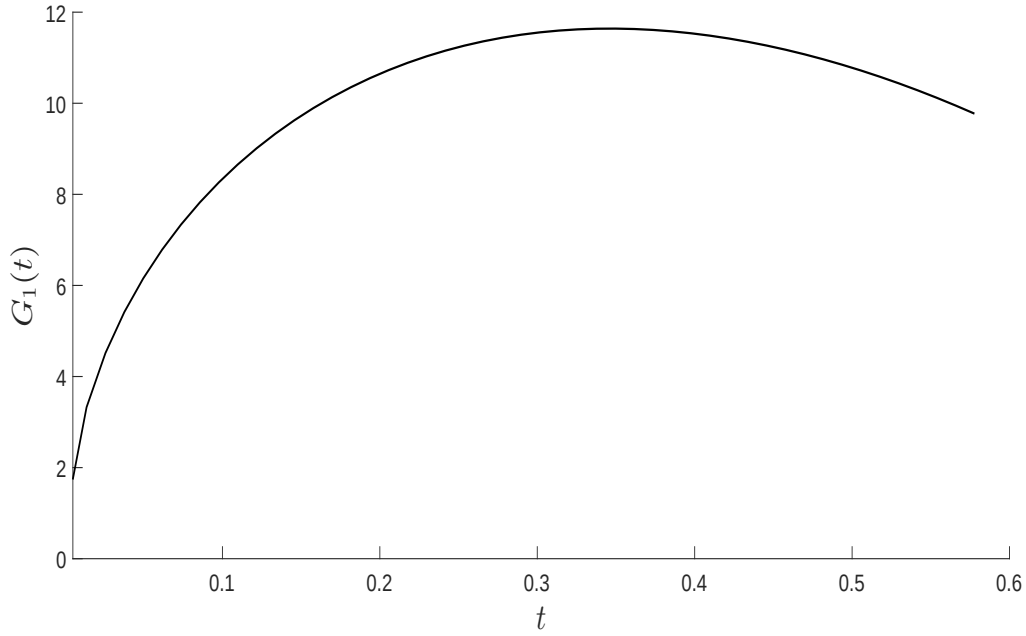

Figure 3.5: The function $G_1(t)$ during the impact stage.

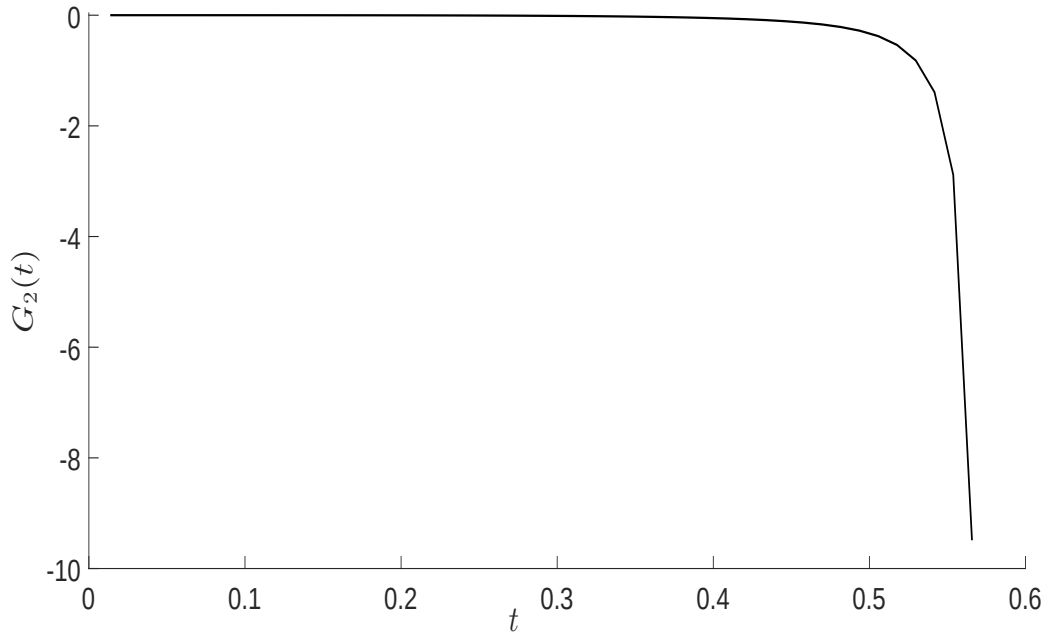

Figure 3.6: The function $G_2(t)$ during the impact stage.

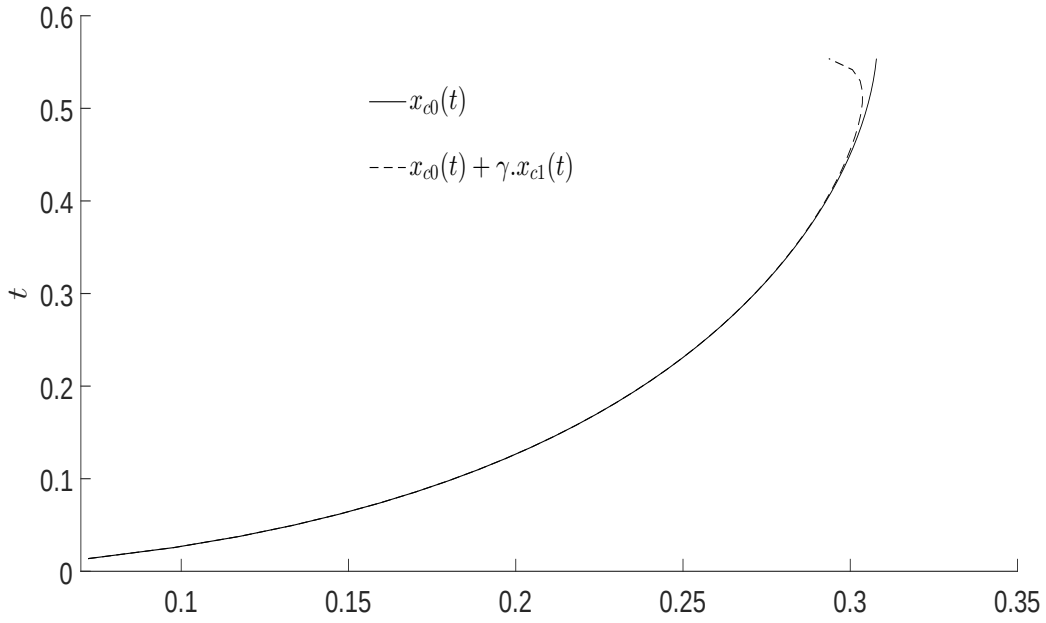

Figure 3.7: The leading-order moving point $x = x_{c0}(t)$, (solid line), and the moving point with correction of gravity $x = x_{c0}(t) + \gamma\, x_{c1}(t)$ (dashed line) during the impact stage with $\delta = 0.05$. At the very beginning of impact gravity has no influence and no difference is seen between the curves.

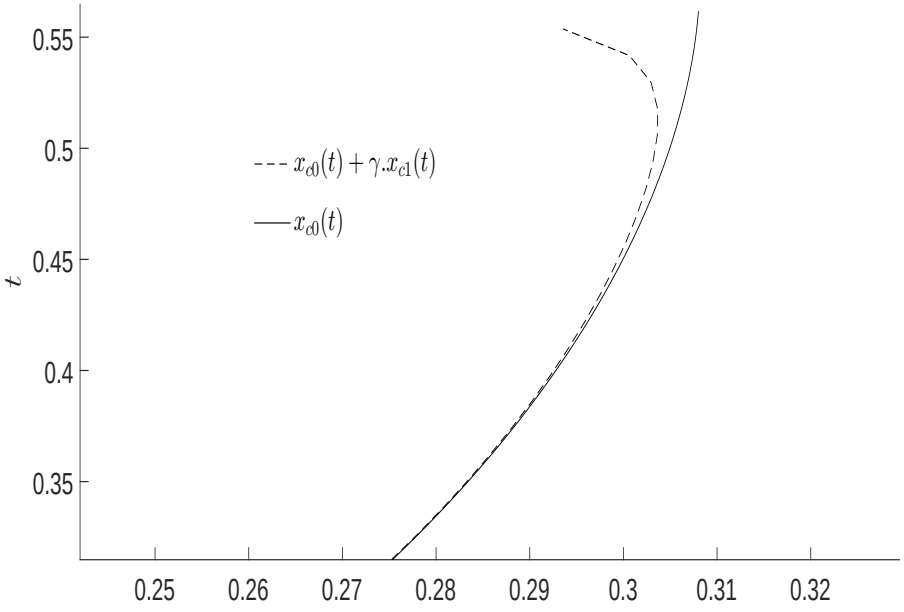

Figure 3.8: Details of the Figure 3.7. The leading-order moving point $x = x_{c0}(t)$, (solid line), and the moving point with correction of gravity $x = x_{c0}(t) + \gamma\, x_{c1}(t)$ (dashed line) show that gravity starts to influence the moving point more and more until the wetted zone starts to contract.

3.2 Moving contact point correction due to gravity

In this section we develop a second method to determine the correction caused by gravity, to the moving point. The importance of the accuracy of the position of the moving point is considered. We carry out this work to validate our previous results.

We recall the leading-order boundary-value problem in terms of displacement potential derived in section 3.1.3 by using the stretched variables (2.84) (variables are replaced to their original).

$$\frac{\partial^2\phi_0}{\partial x^2}+\frac{\partial^2\phi_0}{\partial y^2}=0 \qquad -\infty<x<\infty, y<0 \tag{3.83}$$

$$\frac{\partial\phi_0}{\partial y}=-\eta_n \qquad |x|<x_{c0}, y=0, \tag{3.84}$$

$$\phi_0=0 \qquad |x|>x_{c0}, y=0, \tag{3.85}$$

$$\eta_n+\eta_{c0}=0 \qquad x=x_{c0}, \tag{3.86}$$

$$\phi_0\longrightarrow 0 \qquad \text{as} \qquad x^2+y^2\longrightarrow 0. \tag{3.87}$$

It is worth mentioning here that the leading-order problem, with respect to the parameter $\epsilon=\frac{h}{H}$ was constructed in section 2.2.5, where H was the position of the lid and h was the small distance from the level surface elevation to the lid. Then the above formulation is derived in terms of displacement potential by using the expansion with respect to $\gamma=\delta^{3/2}$ analysed in section 3.1.5. The expansions are rewritten here (hats are dropped) as follows: the velocity potential

$$\phi(x,y,t,\gamma)=\phi_0(x,y,t)+\gamma\phi_1(x,y,t)+O(\gamma^2), \tag{3.88}$$

the correction to the surface elevation when the lid is introduced to the problem

$$\eta_c(x,t,\gamma)=\eta_{c0}(x,t)+\gamma\eta_{c1}(x,t)+O(\gamma^2), \tag{3.89}$$

the moving point

$$x_c(t,\gamma)=x_{c0}(t)+\gamma x_{c1}(t)+O(\gamma^2), \tag{3.90}$$

together with the Taylor expansion of the free-surface elevation about the point $x=\frac{x_c(t,\gamma)}{x_{c0}(t)}\tilde{x}$, (tilde dropped) with no lid:

$$\eta_n(x,t,\gamma)=\eta_n(x,t)+\gamma x\frac{x_{c1}(t)}{x_{c0}(t)}\frac{\partial\eta_n}{\partial x}(x,t)+O(\gamma^2). \tag{3.91}$$

Therefore in this section any order specified is in terms of $\gamma = \delta^{3/2}$. The correction to the impact due to gravity is to be analysed through the next order. Therefore the first-order boundary-value problem in terms of displacement potential is derived as follows. Using the stretched variables (3.37), the governing equation (3.12) at the first order is retained

$$\frac{\partial^2 \phi_1}{\partial x^2} + \frac{\partial^2 \phi_1}{\partial y^2} = 0 \qquad -\infty < x < \infty, y < 0. \tag{3.92}$$

The above expansions and equation (3.15) provide the kinematic condition on the wetted region, at first order,

$$\frac{\partial \phi_1}{\partial y} = -x \frac{x_{c1}}{x_{c0}} \frac{\partial \eta_n}{\partial x} \qquad |x| < x_{c0}, y = 0. \tag{3.93}$$

The second time derivative of the dynamic boundary condition (3.17), combined with the kinematic boundary condition (3.18) all in terms of displacement potential with the above expansion at the first order gives

$$\frac{\partial^2 \phi_1}{\partial t^2} = -\frac{\partial \phi_0}{\partial y} \qquad |x| > x_{c0}, y = 0. \tag{3.94}$$

Also we readily find the initial condition

$$\phi_1 = 0 \qquad \text{at} \quad t = 0, \tag{3.95}$$

and the far field condition

$$\phi_1 \longrightarrow 0 \qquad \text{as} \;\; x^2 + y^2 \longrightarrow 0. \tag{3.96}$$

Suppose that the solution to the problem (3.87)–(3.96) is given by

$$\phi_1(x, y, t) = -\int_0^t (t - \tau) \frac{\partial \phi_0}{\partial y}(x, y, \tau) \mathrm{d}\tau + \phi_{11}(x, y, t), \tag{3.97}$$

where $\phi_{11}(x, y, t)$ is a correction to the solution on the free surface and $\phi_{11}(x, 0, t) = 0$ for $|x| > x_{c0}$. Then we construct the problem in terms of ϕ_{11} as follows

$$\frac{\partial^2 \phi_{11}}{\partial x^2} + \frac{\partial^2 \phi_{11}}{\partial y^2} = 0 \qquad -\infty < x < \infty, \;\; y < 0, \tag{3.98}$$

$$\frac{\partial \phi_{11}}{\partial y} = -x \frac{x_{c1}(t)}{x_{c0}(t)} \frac{\partial \eta_n}{\partial x}(x, t) - \int_{t(x)}^t (t - \tau) \frac{\partial^2 \phi_0}{\partial x^2} \mathrm{d}\tau \;\; |x| < x_{c0}, \;\; y = 0, \tag{3.99}$$

where $\tau = t(x)$ is the inverse function of $x = x_{c0}(\tau)$, and

$$\frac{\partial \phi_{11}}{\partial x} = 0 \qquad\qquad |x| > x_{c0},\ y = 0. \tag{3.100}$$

To solve the above formulation we define an analytic function $W(z,t)$

$$W(z,t) = \big(\frac{\partial \phi_{11}}{\partial x} - i\frac{\partial \phi_{11}}{\partial y}\big)\sqrt{z^2 - x_{c0}^2} \qquad\qquad z = x + iy. \tag{3.101}$$

As $y \longrightarrow 0^-$ the real and imaginary parts of the new unknown function $W(z,t)$ are

$$\mathrm{Re}\big[W(x-i0)\big] = \begin{cases} \frac{\partial \phi_{11}}{\partial x}\sqrt{x^2 - x_{c0}^2(t)} = 0 & x > x_{c0}, \\ -\frac{\partial \phi_{11}}{\partial y}\sqrt{x_{c0}^2(t) - x^2} & |x| < x_{c0}, \\ -\frac{\partial \phi_{11}}{\partial x}\sqrt{x^2 - x_{c0}^2} = 0 & x < -x_{c0}, \end{cases}$$

$$\mathrm{Im}\big[W(x-i0)\big] = \begin{cases} -\frac{\partial \phi_{11}}{\partial y}\sqrt{x^2 - x_{c0}^2} & x > x_{c0}, \\ -\frac{\partial \phi_{11}}{\partial x}\sqrt{x_{c0}^2 - x^2} & |x| < x_{c0}, \\ \frac{\partial \phi_{11}}{\partial y}\sqrt{x^2 - x_{c0}^2} & x < -x_{c0}. \end{cases}$$

In the impact region, $|x| < x_{c0}$, the Hilbert formula gives

$$\frac{\partial \phi_{11}}{\partial x}\sqrt{x_{c0}^2 - x^2} = \frac{1}{\pi}\int_{-x_{c0}}^{x_{c0}} \frac{\sqrt{x_{c0}^2 - \sigma^2}}{\sigma - x}\Bigg[\sigma \frac{x_{c1}}{x_{c0}}\frac{\partial \eta_n}{\partial \sigma}$$

$$+ \int_{t(\sigma)}^{t} (t-\tau)\frac{\partial^2 \phi_0}{\partial \sigma^2}\mathrm{d}\tau\Bigg]\mathrm{d}\sigma. \tag{3.102}$$

The term $\frac{\partial^2 \phi_0}{\partial \sigma^2}$, in the inner integral has a square-root singularity as $\sigma = x_{c0}(t)$, but we assume that the double time integral will overcome this singularity. However, we will try to write it in a more convenient way, to be dealt with inside the integral. The problem (3.83)–(3.87) is reasonably a good place to construct a different form for $\frac{\partial^2 \phi_0}{\partial \sigma^2}$. We construct the following by taking the x-derivative of the whole problem, to arrive at the leading-order problem in terms of horizontal

displacement $\frac{\partial \phi_{0,x}}{\partial x}$

$$\frac{\partial^2 \phi_{0,x}}{\partial x^2} + \frac{\partial^2 \phi_{0,x}}{\partial y^2} = 0 \qquad \infty < x < \infty, y < 0, \tag{3.103}$$

$$\frac{\partial^2 \phi_0}{\partial x \partial y} = -\frac{\partial \eta_n}{\partial x} \qquad |x| < x_{c0}, y = 0, \tag{3.104}$$

$$\frac{\partial^2 \phi_0}{\partial x^2} = 0 \qquad |x| > x_{c0}, y = 0, \tag{3.105}$$

$$\frac{\partial \phi_0}{\partial x} \longrightarrow 0 \qquad \text{as} \qquad x^2 + y^2 \longrightarrow 0. \tag{3.106}$$

We define the characteristic function $\bar{W}(z,t)$ as

$$\frac{\mathrm{d}\bar{W}}{\mathrm{d}z} = \left(\frac{\partial^2 \phi_0}{\partial x^2} - i \frac{\partial^2 \phi_0}{\partial x \partial y} \right) \sqrt{z^2 - x_{c0}^2} \qquad z = x + iy. \tag{3.107}$$

As $y \longrightarrow 0^-$, the real and imaginary parts of the new unknown function $\frac{\mathrm{d}\Phi_{cd}}{\mathrm{d}z}(x,y,t)$ are

$$\mathrm{Re}\left(\frac{\mathrm{d}\bar{W}}{\mathrm{d}z}(x - i0, t) \right) = \begin{cases} \frac{\partial^2 \phi_0}{\partial x^2} \sqrt{x^2 - x_{c0}^2} = 0 & x > x_{c0}, \\ -\frac{\partial^2 \phi_0}{\partial x \partial y} \sqrt{x_{c0}^2 - x^2} & |x| < x_{c0}, \\ -\frac{\partial^2 \phi_0}{\partial x^2} \sqrt{x^2 - x_{c0}^2} = 0 & x < -x_{c0}, \end{cases}$$

and

$$\mathrm{Im}\left(\frac{\mathrm{d}\bar{W}}{\mathrm{d}z}(x - i0, t) \right) = \begin{cases} -\frac{\partial^2 \phi_0}{\partial x \partial y} \sqrt{x^2 - x_{c0}^2} & x > x_{c0}, \\ -\frac{\partial^2 \phi_0}{\partial x^2} \sqrt{x_{c0}^2 - x^2} & |x| < x_{c0}, \\ \frac{\partial^2 \phi_0}{\partial x \partial y} \sqrt{x^2 - x_{c0}^2} & x < -x_{c0}. \end{cases}$$

In the wetted region, $|x| < x_{c0},\ y = 0$, the Hilbert formula relates the imaginary and real parts of $\frac{\mathrm{d}\bar{W}}{\mathrm{d}z}(x,0,t)$ as follows

$$\frac{\partial^2 \phi_0}{\partial \sigma^2}(\sigma, 0, \tau) = \frac{1}{\pi \sqrt{x_{c0}^2(\tau) - \sigma^2}} \int_{-x_{c0}(\tau)}^{x_{c0}(\tau)} \frac{\sqrt{x_{c0}(\tau)^2 - \mu^2}}{\mu - \sigma} \frac{\partial \eta_n}{\partial \mu}(\mu, \tau) \mathrm{d}\mu. \tag{3.108}$$

Equation (3.108) seems to be convenient for $\frac{\partial^2 \phi_0}{\partial x^2}$ to be substituted in equation

(3.102). Doing this, at $x = x_{c0}(t)$ we find

$$-\pi\frac{x_{c1}(t)}{x_{c0}(t)}\int_{-x_{c0}(t)}^{x_{c0}(t)}\frac{x_{c0}(t)+\sigma}{\sqrt{x_{c0}^2(t)-\sigma^2}}\sigma\frac{\partial\eta_n}{\partial\sigma}(\sigma,t)\mathrm{d}\sigma = \int_{-x_{c0}(t)}^{x_{c0}(t)}\frac{x_{c0}(t)+\sigma}{\sqrt{x_{c0}^2(t)-\sigma^2}}\int_0^t\frac{(t-\tau)}{\sqrt{x_{c0}(\tau)^2-\sigma^2}} \int_{-x_{c0}(\tau)}^{x_{c0}(\tau)}\frac{\sqrt{x_{c0}(\tau)^2-\mu^2}}{\mu-\sigma}\frac{\partial\eta_n}{\partial\mu}(\mu,\tau)\mathrm{d}\mu\mathrm{d}\tau\mathrm{d}\sigma. \tag{3.109}$$

Taking the equation for the surface elevation with no lid (2.40), the left hand side of equation (3.109), excluding the moving point correction $x_{c1}(t)$, can be written as

$$\mathbf{G}_1(t) = -\pi^2 x_{c0}(t)\sum_{n=1,2} f_n k_n \cos(w_n t)\mathrm{J}_1\left(k_n x_{c0}(t)\right). \tag{3.110}$$

The function $\mathbf{G}_1(t)$ is plotted in Figure 3.9.

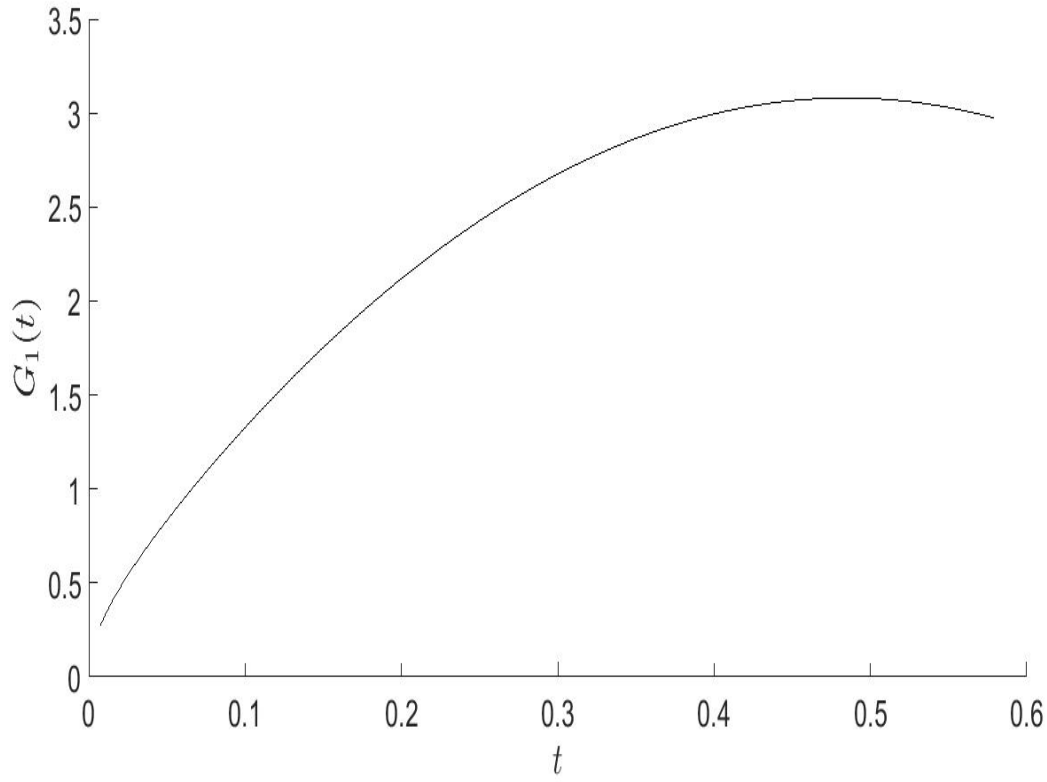

Figure 3.9: The function $\mathbf{G}_1(t)$ during the impact stage. Variables are non-dimensional.

As to the right-hand side of equation (3.109) it follows that

$$\mathbf{G}_2(t) = x_{c0}(t)\int_0^t (t-\tau)\int_{-x_{c0}(\tau)}^{x_{c0}(\tau)} \sqrt{x_{c0}(\tau)^2-\mu^2}\frac{\partial \eta_n}{\partial \mu} \int_{-x_{c0}(\tau)}^{x_{c0}(\tau)} \frac{\mathrm{d}\sigma}{\sqrt{x_{c0}^2(t)-\sigma^2}\sqrt{x_{c0}(\tau)^2-\sigma^2}(\mu-\sigma)}\mathrm{d}\mu\mathrm{d}\tau. \tag{3.111}$$

Here we use bold $\mathbf{G}_1(t)$ and $\mathbf{G}_2(t)$ to avoid confusing with $G_1(t)$ and $G_2(t)$ in previous section. Having the following identity

$$\int_{-x_{c0}(\tau)}^{x_{c0}(\tau)} \frac{\mathrm{d}\sigma}{\sqrt{x_{c0}(\tau)^2-\sigma^2}(\mu-\sigma)} = 0, \tag{3.112}$$

and using some manipulations we can rewrite equation (3.111) in a way convenient to estimate it by a numerical method

$$\mathbf{G}_2(t) = 4x_{c0}(t)\int_0^t (t-\tau)x_{c0}^3(\tau) \int_0^{\pi/2}\int_0^{\pi/2} \frac{\sin(\theta_1)\cos^2(\theta_1)\sin(k_n x_{c0}(\tau)\sin(\theta_1))}{\sqrt{x_{c0}^2(t)-(x_{c0}(\tau)\sin(\theta))^2}\ \sqrt{x_{c0}^2(t)-(x_{c0}(\tau)\sin(\theta_1))^2}} \frac{1}{\left(\sqrt{x_{c0}^2(t)-(x_{c0}(\tau)\sin(\theta))^2}+\sqrt{x_{c0}^2(t)-(x_{c0}(\tau)\sin(\theta_1))^2}\right)}\mathrm{d}\theta\mathrm{d}\theta_1\mathrm{d}\tau, \tag{3.113}$$

where $\mathbf{G}_2(t)$ is negative and decreasing as time goes in, see Figure 3.10.

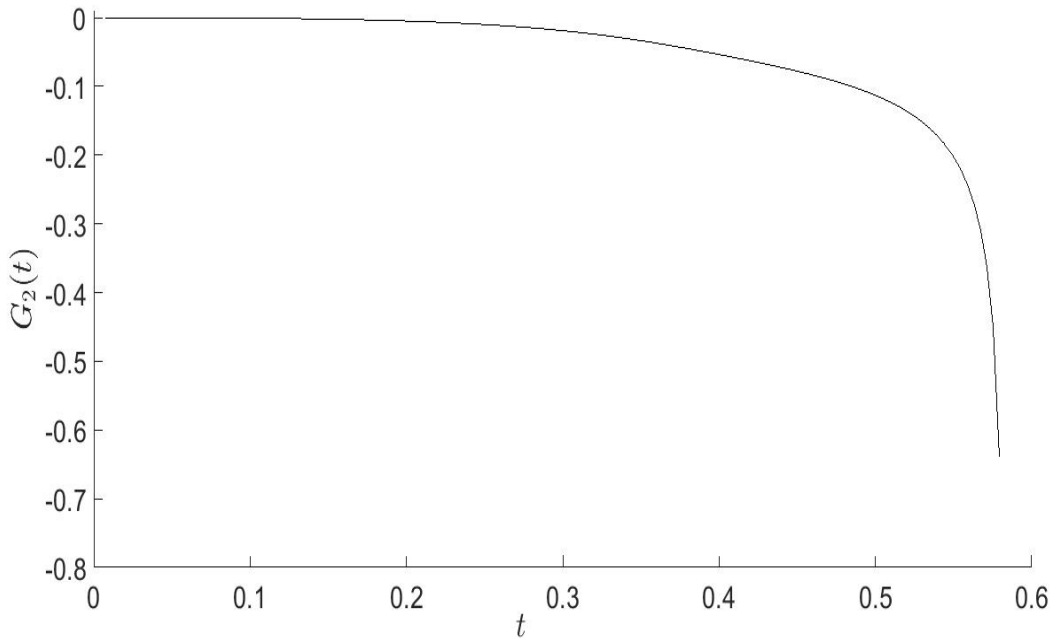

Figure 3.10: The function $\mathbf{G}_2(t)$ during the impact stage. Variables are non-dimensional.

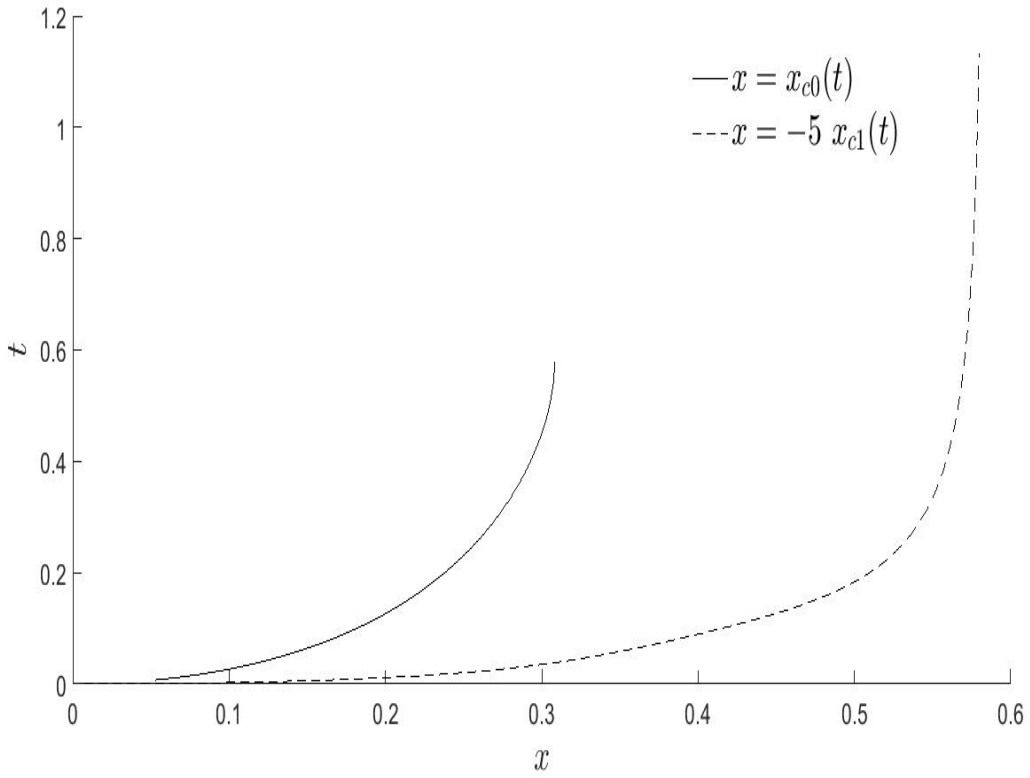

Figure 3.11: The moving contact point $x_{c0}(t)$ and the correction due to gravity $x_{c1}(t) = \gamma \frac{\mathbf{G}_2}{\mathbf{G}_1}$ during the impact stage. The correction is exaggerated by a factor of -5 and variables are non-dimensional.

The correction to the moving contact point, $x_{c1}(t)$, is found to be

$$x_{c1}(t) = \frac{\mathbf{G}_2(t)}{\mathbf{G}_1(t)}, \tag{3.114}$$

where $\mathbf{G}_1(t)$, given by (3.110) and $\mathbf{G}_2(t)$, given by (3.113), have opposite signs. Therefore the correction due to gravity on the moving point $x = x_{c0}(t)$ reduces it. In Figure 3.11 this effect is magnified by a factor of -5 to show the behaviour of the correction. It shows that gravity has clearly negligible effect at the beginning. However this neglecting has to be restricted to a very short period as at later times gravity has a noticeable effect and slows the spread of the impact.

In Figure 3.12 the two lines coincide initially during the impact, and start to separate as time increase. The inner line includes the influence of gravity, and shows that, compared with the outer line, the wetted zone is shortened especially during late period of impact stage.

To validate our results, regarding the influence of gravity on the moving contact point, we make a comparison between this result and the results showed in the previous section. At the beginning, in both solutions, gravity seems to

be negligible, as seen in Figures (3.7) and (3.12). However, these figures also show a remarkable point that gravity pulls on the moving contact point causing a shorter wetted region during the later period of impact stage, Figure 3.13 shows a comparison between two solutions for a notable period. The effects of $\frac{G_2}{G_1}$ on the leading-order moving contact point, $x = x_{c0}(t)$, starts at the very late period of the impact stage but it rapidly grows, however, as to $\frac{\mathbf{G_2}}{\mathbf{G_1}}$, its effects starts earlier with with gradually decreasing the size of $x = x_{c0}(t)$.

In the next section we show the influence of gravity on the pressure distribution of the fluid along the wetted lid.

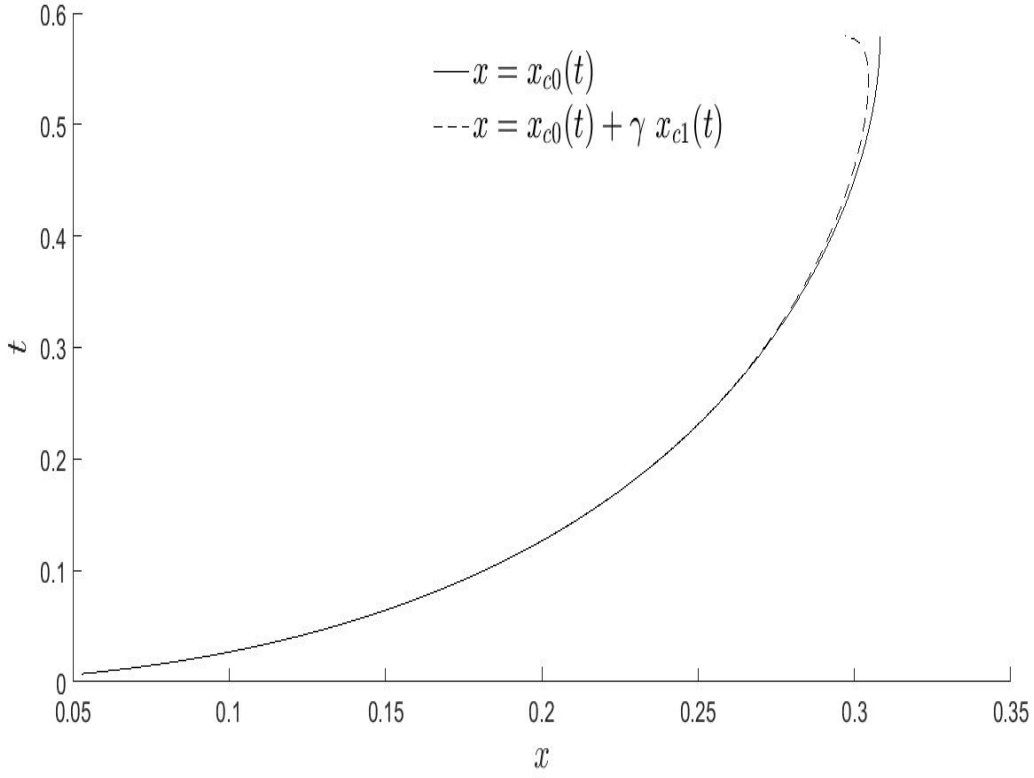

Figure 3.12: The leading-order moving point $x = x_{c0}(t)$, (solid line), and the moving point with correction of gravity $x = x_{c0}(t) + \gamma\, x_{c1}(t)$ where $x_{c1}(t) = \frac{\mathbf{G_2}}{\mathbf{G_1}}$, (dashed-line), during the impact stage. At the very beginning of impact gravity has no significance. Variables are non-dimensional and $\gamma = 0.05$.

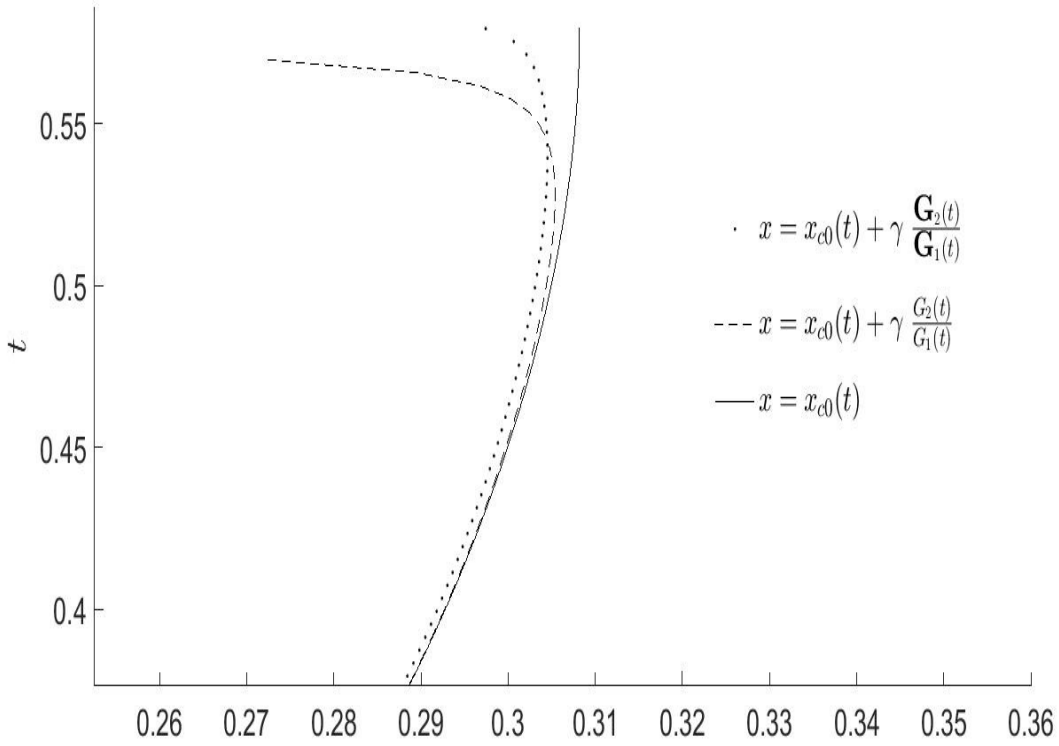

Figure 3.13: The leading-order moving point $x = x_{c0}(t)$, (dashed line), and the moving point with correction due to gravity, $x = x_{c0}(t) + \gamma \frac{\mathbf{G_2}}{\mathbf{G_1}}$, (dotted-line), and $x = x_{c0}(t) + \gamma \frac{G_2}{G_1}$, (solid-line) when gravity starts to affect the moving contact point significantly. Variables are non-dimensional and $\gamma = 0.05$.

3.3 Correction due to gravity to the pressure

In this section we find how pressure distribution of the fluid on the wetted region is affected by gravity. Pressure expansion with respect to the δ is

$$p(x, y, t, \gamma) = p_0(x, y, t) + \gamma p_1(x, y, t) + O(\gamma^2), \tag{3.115}$$

where p_0 is the leading order pressure distribution when gravity is neglected and p_1 is correction due to gravity on the pressure distribution which is to be determined. Substitute the above expansion (3.115) and expansions (3.88) and (3.89) into equation (3.5), at the leading order we arrive at

$$p_1 = \frac{\partial^2 \phi_1}{\partial t^2} + \eta_{c0} \qquad\qquad |x| < x_c,\ y = 0. \tag{3.116}$$

The correction due to lid to the surface elevation η_{c0} is given by equation (3.78). Therefore, we need only to find the double time-derivative of (3.97), since it is in terms of displacement potential, which follows

$$\frac{\partial^2\phi_1}{\partial t^2} = -\frac{\partial\phi_0}{\partial y} + \frac{\partial^2\phi_{11}}{\partial t^2}, \qquad \text{in fluid.} \tag{3.117}$$

The first term in (3.117) is the free-surface elevation of the fluid without the lid, (3.84). However, for calculating the second term the following steps are needed. The integral of both sides of equation (3.102) with respect to x from $-x_{c0}(t)$ to x, as $y \longrightarrow^{-} 0$, leads to

$$\phi_{11}(x,0,t) = \frac{1}{\pi}\int_{-x_{c0}}^{x_{c0}} \sqrt{x_{c0}^2-\sigma^2}\left[x_{c1}\sigma\frac{\partial\eta_n}{\partial\sigma} + \int_{t(\sigma)}^{t}(t-\tau)\frac{\partial^2\phi_0}{\partial\sigma^2}\mathrm{d}\tau\right]$$

$$\int_{-x_{c0}}^{x}\frac{1}{(\sigma-\bar{x})\sqrt{x_{c0}^2-\bar{x}^2}}\mathrm{d}\bar{x}\mathrm{d}\sigma, \tag{3.118}$$

where $\phi_{11}|_{x=-x_{c0}(t)} = 0$ which comes from the continuity of the displacement potential. Substitution of $\sigma = x_{c0}(t)\cos(\theta)$ in equation (3.118) and $\mu = x_{c0}(\tau)\cos(\theta_1)$ in equation (3.108), imply

$$\phi_{11}(x,0,t) = \frac{-x_{c1}(t)}{\pi}\sum_{n=1}^{\infty} f_n k_n \int_0^{\pi}\sin^2(\theta)\left[x_{c0}(t)\cos(\theta)\sin(k_n x_{c0}(t)\cos(\theta)) + \right.$$
$$\left.\int_{t(\sigma)}^{t}\frac{(t-\tau)x_{c0}^2(\tau)}{\sqrt{x_{c0}(\tau)^2 - x_{c0}(t)^2\cos^2(\theta)}}\int_0^{\pi}\frac{\sin^2(\theta_1)\sin(k_n x_{c0}(\tau)\cos(\theta_1))}{x_{c0}(\tau)\cos(\theta_1) - x_{c0}(t)\cos(\theta)}\mathrm{d}\theta_1\right]$$
$$B(x,\theta,t)\mathrm{d}\theta, \tag{3.119}$$

where

$$B(x,\theta,t) = \frac{1}{\sin(\theta)}$$
$$\ln\left|\frac{\frac{\cos(\theta)\left(\sqrt{x_{c0}(t)^2-x^2}-x_{c0}(t)\right)}{x} + \sin(\theta) + 1}{\frac{\cos(\theta)\left(\sqrt{x_{c0}(t)^2-x^2}-x_{c0}(t)\right)}{x} - \sin(\theta) + 1} \times \frac{\cos(\theta)-\sin(\theta)+1}{\cos(\theta)+\sin(\theta)+1}\right|. \tag{3.120}$$

Figure 3.14 shows the correction due to gravity on the pressure distribution $p_1(x,t)$ on the wetted region, equation (3.116). This correction is applied on the leading-order pressure distribution, see Figure 3.15, at the instant $t = 1.102$. It is found that the correction due to gravity is decreasing the pressure distribution on the wetted region.

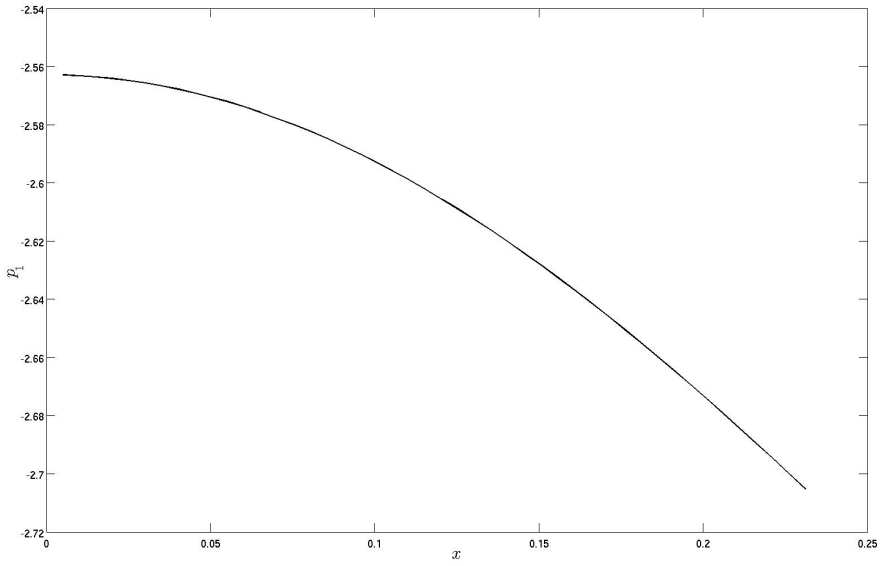

Figure 3.14: Correction due to gravity on the pressure distribution at the instant $t = 1.102$ with $\gamma = 0.05$.

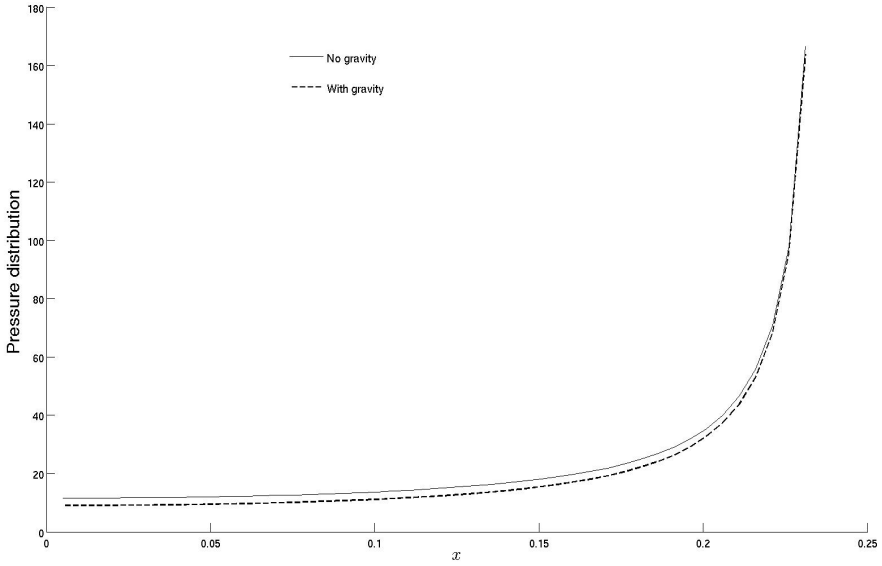

Figure 3.15: Pressure distribution without gravity (solid line) and with gravity (dashed line) at the instant $t = 1.102$ with $\gamma = 0.05$.

Chapter 4

Numerically analysis of impact with gravity included

In this chapter we numerically study the problem with the inclusion of gravity. Recently some remarkable numerical and semi-numerical work has been done for sloshing inside a tank (Rognebakke & Faltinsen 2005) and (Ten et al. 2011). We start from the leading-order problem with gravity formulated in section 2.1. First, in section 4.1, we give a description to the problem. In section 4.2, we relate the surface elevation and pressure distribution by representing both in terms of Fourier series. In section 4.3, we discretise the problem and derive a system to be solved numerically. In section 4.4 , we specify how to approximate some coefficients, and discuss absolute and relative errors. Then we regularise the ill-conditioned problem in section 4.5 and some results are shown in the final section, 4.6.

4.1 Problem description

In this section we refer to the boundary-value problem (2.59)–(2.68) derived in Chapter 2. This problem is the linearised form of the full equations (2.45)–(2.54) based on the relatively small available space for the free surface to elevate. The formally linearised problem is obtained by setting the aspect ratio ϵ given in (2.24) to zero. Therefore all quantities dealt with in this chapter are at the leading order, but for simplicity we do not write the leading-order index. To remind the reader we give a brief description of the problem below. As shown in Figure 4.1, $H-h$ is the still water depth, h is the small (relative to the height of the tank H) distance between the equilibrium water surface and the lid at $y=H$, and $2L$ is the width of the tank, with its walls positioned at $x=\pm L$. In our model, zero viscosity and zero surface tension are assumed, ρ is the water density and g is the

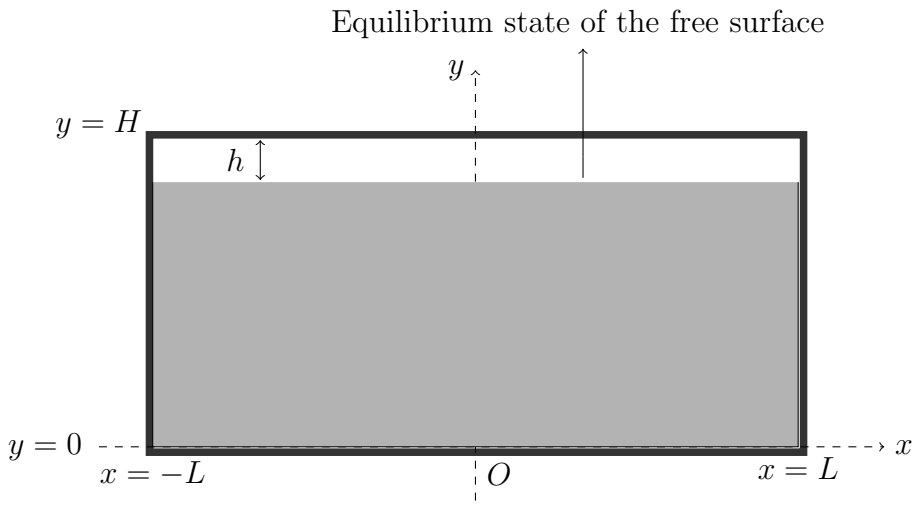

Figure 4.1: Tank's configuration and coordinates in dimensional variables.

gravity acceleration. The flow is two dimensional and irrotational and the liquid is assumed to be incompressible.

The equation $y = H - h + \eta(x,t)$ describes the upper boundary of the flow region. When $y = H - h$, the liquid is at its equilibrium state ($\eta \equiv 0$) as shown in Figure 4.1. If $\eta(x,t) < h$, then free surface of the liquid is the only upper boundary. If $\eta(x,t) = h$, this part of the upper boundary corresponds to the region of contact between the liquid and the solid lid. Note that $\eta(x,t) \leq h$, for all x and t is a constraint on the problem under consideration.

From now on, we work with non-dimensional variables (with tilde dropped), as discussed in section 2.2.2. The boundary conditions on the lid, now at $y = 1$, are given by equations (2.62) and (2.64). The constancy of volume of incompressible liquid ensure that we can safely assume that the constant ullage pressure is zero, $p(x,t) = 0$, the pressure of the gas between the liquid surface and the lid of the tank. Hence $p(x,t) = 0$ for all x such that $\eta(x,t) < 1$ and $p(x,t)$ is to be determined for all x such that $\eta(x,t) = 1$. As we investigated in section 2.2, there is no air trapped during the impact. For details of this effect see (Malenica et al. 2006).

As shown in Figure 2.2, the flow is symmetric, and hence, $\mathrm{f}(x) = \mathrm{f}(-x)$, (see equation 2.1), $\eta(x,t) = \eta(-x,t)$, $\phi(x,y,t) = \phi(-x,y,t)$ and the wetted part of the lid corresponds to an interval of the x-axis $(-x_c(t), x_c(t))$, where the function $x_c(t)$, the half length of the wetted region, is unknown in advance and is to be determined.

To solve the problem, we suppose that $p(x,t)$, where $|x| \leq x_c(t)$, is known and we can compute the corresponding elevation of the free surface $\eta(x,t)$, where

$x_c(t) \leq |x| \leq \lambda$. Note that

$$\eta(x,t) < 1 \qquad |x| < \lambda,\ 0 < t < t_1, \tag{4.1}$$

before the impact. During this stage there is no contact between the fluid and the lid and the calculations are performed with

$$p(x,t) = 0 \qquad |x| < \lambda,\ 0 < t < t_1. \tag{4.2}$$

At the instant $t = t_1$, the first contact of the surface with the lid occurs at $x = 0$. So $\eta(0,t_1) = 1$ and the fluid is ascending just before impact: $\frac{\partial \eta}{\partial t}(0,t_1) > 0$.

4.2 Numerical approach

Combining the surface elevation and the boundary pressure in a single formulation is considered in this section. To do this, the symmetric function $\eta(x,t)$ on the finite interval, $-1 < x < 1$, is represented by the Fourier cosine series of the form

$$\eta(x,t) = \sum_{n=1}^{\infty} \bar{\eta}_n(t) \cos(n\pi x), \tag{4.3}$$

in which the Fourier coefficients $\bar{\eta}_n(t)$ are time-dependent. For simplicity we use the non-dimensional parameter $\lambda = \frac{L}{H}$ to be one in our numerical analysis, hence the interval $[-1,1]$. Note that $\bar{\eta}_0(t)$ is missing from the series, because of the conservation of fluid volume,

$$\int_{-1}^{1} \eta(x,t)dx = 0, \tag{4.4}$$

which arises from the incompressiblity of the liquid and $\eta = 0$ being the equilibrium position of the free surface. The initial shape of the free surface, f(x), given in equation (2.1) also satisfies condition (4.4). The function $\eta(x,t)$ satisfies the conditions $\frac{\partial \eta}{\partial x}(\pm 1,t) = 0$ at the walls of the tank. These conditions follow from matching the dynamic condition on the free surface,

$$\frac{\partial \phi}{\partial t} + \eta = 0, \qquad \text{where} \qquad \eta(x,t) < 1, \tag{4.5}$$

and the boundary condition at the walls of the tank, $\frac{\partial \phi}{\partial x} = 0$. Differentiating the dynamic condition (4.5) in x,

$$\frac{\partial^2 \phi}{\partial x \partial t} + \frac{\partial \eta}{\partial x} = 0, \qquad \text{where} \qquad \eta(x,t) < 1, \tag{4.6}$$

and applying (4.6) at $x = \pm 1$, where $\frac{\partial \phi}{\partial x} = 0$, we find,

$$\frac{\partial \eta}{\partial x}(\pm 1, t) = 0. \tag{4.7}$$

The velocity potential $\phi(x, y, t)$ and the pressure $p(x, t)$ along the upper boundary of the flow region can also be represented by Fourier series, in the forms:

$$\phi(x, y, t) = \sum_{n=1}^{\infty} \phi_n(y, t) \cos(n\pi x), \tag{4.8}$$

$$p(x, t) = \sum_{n=1}^{\infty} p_n(t) \cos(n\pi x). \tag{4.9}$$

Applying the Fourier representations (4.3) and (4.8)–(4.9) to the boundary conditions (2.63)–(2.64) on $y = 1$ give the following pair of equations:

$$\frac{\partial \phi_n}{\partial t}(1, t) + \bar{\eta}_n(t) = -p_n(t), \tag{4.10}$$

$$\frac{\partial \bar{\eta}_n}{\partial t}(t) = \frac{\partial \phi_n}{\partial y}(1, t). \tag{4.11}$$

Combining these two conditions on $y = 1$ we can eliminate $\bar{\eta}_n$ and write equations (2.59)–(2.68) in terms of $\phi_n(y, t)$ as follows

$$\frac{\partial^2 \phi_n}{\partial y^2} - (n\pi)^2 \phi_n = 0 \qquad 0 < y < 1, \tag{4.12}$$

$$\frac{\partial \phi_n}{\partial y} = 0 \qquad y = 0, \tag{4.13}$$

$$\frac{\partial^2 \phi_n}{\partial t^2} + \frac{\partial \phi_n}{\partial y} = -\frac{\mathrm{d}p_n}{\mathrm{d}t} \qquad y = 1. \tag{4.14}$$

If $p_n(t)$ are known, then $\frac{\mathrm{d}p_n}{\mathrm{d}t}$ on the right-hand side is a forcing term for the problem. We also have initial data at $t = 0$:

$$\phi_n = 0, \tag{4.15}$$

$$\frac{\partial \phi_n}{\partial t} = -\bar{f}_n, \tag{4.16}$$

where $\bar{f}_n$ are the Fourier coefficients of $\mathrm{f}(x)$,

$$\mathrm{f}(x) = 1 - \epsilon + \epsilon \sum_{n=1}^{\infty} \bar{f}_n \cos(n\pi x), \tag{4.17}$$

as defined in (2.41). The problem (4.12)–(4.17) is solved below. A function, which satisfies equations (4.12) and (4.13), has the form

$$\phi_n(y,t) = \phi_n(1,t)\frac{\cosh(n\pi y)}{\cosh(n\pi)}. \tag{4.18}$$

Substituting (4.18) in the boundary condition (4.14) gives a forced ordinary differential equation for $\phi_n(1,t)$:

$$\frac{\partial^2\phi_n}{\partial t^2}(1,t) + \phi_n(1,t)n\pi\tanh(n\pi) = -\frac{\mathrm{d}p_n}{\mathrm{d}t}(t). \tag{4.19}$$

We introduce $\omega_n^2 = n\pi\tanh(n\pi)$ and write down the solution of (4.19) with the initial conditions (4.15)–(4.16):

$$\phi_n(1,t) = -\frac{\bar{f}_n}{\omega_n}\sin(\omega_n t) - \frac{1}{\omega_n}\int_0^t \frac{\mathrm{d}p_n}{\mathrm{d}\tau}(\tau)\sin(\omega_n(t-\tau))d\tau. \tag{4.20}$$

Then from the dynamic boundary condition (4.10) and the solution (4.20) we arrive at an expression for the coefficients for the free-surface shape:

$$\eta_n(t) = \bar{f}_n\cos(\omega_n t) - \omega_n\int_0^t p_n(\tau)\sin(\omega_n(t-\tau))d\tau. \tag{4.21}$$

Before the free surface touches the lid, $0 < t < t_1$, we have $p_n(\tau) = 0$, (see condition (4.2)). Substituting (4.21) in (4.3) we obtain

$$\eta(x,t) = \eta_0(x,t) - \sum_{n=1}^{\infty}\omega_n\left(\int_0^t p_n(\tau)\sin(\omega_n(t-\tau))d\tau\right)\cos(n\pi x), \tag{4.22}$$

where $\eta_0(x,t)$ is the free-surface elevation in the absence of lid:

$$\eta_0(x,t) = \sum_{n=1}^{\infty}\bar{f}_n\cos(\omega_n t)\cos(n\pi x). \tag{4.23}$$

The integrand in equation (4.22) is zero for all t in the time interval $(0,t_1)$, because $p(x,t) = 0$ when $0 < t < t_1$. The equation (4.22) is useful if the pressure $p(x,t)$ is given, but in the problem we want to solve, $p(x,t)$ is one of the unknowns. The above formulation is supplemented by the Wagner condition, (Wagner 1932)

$$\eta(x,t) = 1 \qquad \text{at} \quad x = x_c(t). \tag{4.24}$$

We will use this condition later in section 4.6 to find the moving contact point position, $x = x_c(t)$.

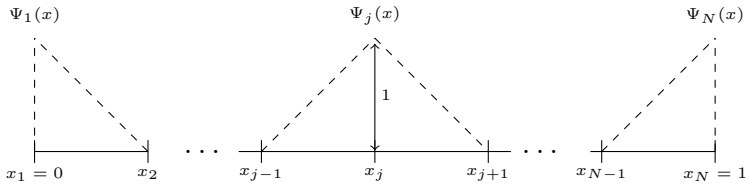

Figure 4.2: Discretization on the lid of the tank from the centre $x = 0$ to the wall $x = 1$.

4.3 Discretization

We use the collocation method by discretisizing the interval $x \in [0, 1]$ into $N - 1$ regular intervals. Since the flow is symmetric, the solution has a mirror image on the other half, $-1 \leq x \leq 0$, of the fluid domain, here we chose the right half. For negative x we have $\eta(-x, t) = \eta(x, t)$, $\eta_0(-x, t) = \eta_0(x, t)$ and $p(-x, t) = p(x, t)$. The functions $\left\{\Psi_j(x)\right\}_{j=1}^{N}$ are a set of basis functions (each one is a, so called, hat function, see Figure 4.2, defined by

$$\Psi_j(x) = \frac{1}{\triangle} \begin{cases} x - x_{j-1} & x_{j-1} \leq x \leq x_j, \\ x_{j+1} - x & x_j \leq x \leq x_{j+1}, \\ 0 & \textit{otherwise}, \end{cases} \tag{4.25}$$

where $\triangle = \frac{1}{N-1}$ and the nodes have positions $x = x_j = (j-1)\triangle$ for $2 \leq j \leq N-1$. For $j = 1$ and $j = N$ we have

$$\Psi_1(x) = \frac{1}{\triangle} \begin{cases} x_2 - x & x_1 \leq x \leq x_2, \\ 0 & \textit{otherwise}, \end{cases} \tag{4.26}$$

$$\Psi_N(x) = \frac{1}{\triangle} \begin{cases} x - 1 + \triangle & x_{N-1} \leq x \leq x_N, \\ 0 & \textit{otherwise}. \end{cases} \tag{4.27}$$

The discretization and basis functions on the x-axis are shown in Figure 4.2. As shown, the discretisation starts from the centre, $x = 0$, where the index $j = 1$ and increases towards the wall, $x = 1, (j = N)$. Note that $\Psi_j(x_j) = 1$, where $1 \leq j \leq N$.

We shall approximate the functions $\eta(x, t)$, $\eta_0(x, t)$ and $p(x, t)$ piece-wise linear functions in both x and t by using the basis functions $\Psi_j(x)$ and $\Psi^m(t)$. In

particular,

$$\eta(x,t) = \sum_{j=1}^{N} \eta_j(t)\Psi_j(x), \tag{4.28}$$

$$\eta_0(x,t) = \sum_{j=1}^{N} \eta_{0j}(t)\Psi_j(x), \tag{4.29}$$

where $\Psi_j(x)$ are defined by (4.25), the unknown elevation with lid $\eta_j(t) = \eta(x_j,t)$ and the known elevation without lid $\eta_{0j}(t) = \eta_0(x_j,t)$. Substituting discretized elevations (4.28)–(4.29) in equation (4.22), multiplied by $\Psi_q(x)$, $1 \le q \le N$ and integrated in x from $x = -1$ to $x = 1$, we obtain

$$\sum_{j=1}^{N} \eta_j(t)e_{j,q} = \sum_{j=1}^{N} \eta_{0j}(t)e_{j,q} - \sum_{n=1}^{\infty} \omega_n C_{n,q} \int_0^t p_n(\tau)\sin(\omega_n(t-\tau))d\tau, \tag{4.30}$$

where the product coefficients $e_{j,q}, 1 \le j,q \le N$ are defined by

$$e_{j,q} = \int_{-1}^{1} \Psi_j(x)\Psi_q(x)dx. \tag{4.31}$$

Using definitions (4.25)–(4.27), we find for $1 \le j,q \le N-1$

$$e_{j,q} = \begin{cases} \frac{2\triangle}{3} & ; j = q, \\ \frac{\triangle}{6} & ; |j-q| = 1, \\ 0 & ; otherwise. \end{cases} \tag{4.32}$$

For the last node, $x_N = 1$, we have $e_{N,N} = \frac{\triangle}{3}$. The coefficients, $C_{n,q}$, are defined for $2 \le q \le N-1$, and $n = 1,2,\ldots$ by

$$\begin{aligned} C_{n,q} &= \int_{-1}^{1} \cos(n\pi x)\Psi_q(x)dx \\ &= \frac{1}{(n\pi)^2\triangle}\left[2\cos(n\pi x_q) - \cos(n\pi x_{q-1}) - \cos(n\pi x_{q+1})\right] \\ C_{n,q} &= \frac{4}{\triangle(n\pi)^2}\sin^2(n\pi\frac{\triangle}{2})\cos(n\pi x_q). \end{aligned} \tag{4.33}$$

For the special cases $j = 1$ and $j = N$, for all $n = 1,2,\ldots,$ we have

$$C_{n,1} = \frac{1}{(n\pi)^2\triangle}\left[1 - \cos(n\pi\triangle)\right], \tag{4.34}$$

and

$$C_{n,N} = (-1)^n C_{n,1}. \tag{4.35}$$

Multiplying both sides of (4.9) by $\cos(\pi l x)$, $l \in \{1, 2, \dots\}$ and integrating with respect to x over the lid, we find that the Fourier coefficients of the lid pressure distribution can be written as

$$\begin{aligned} p_l(\tau) &= \int_{-1}^{1} p(x,t)\cos(l\pi x)dx \\ &= 2\int_{0}^{1} p(x,t)\cos(l\pi x)dx, \end{aligned} \tag{4.36}$$

The square-root singularity of the pressure distribution at the moving contact points, $x = \pm x_c(t)$ is a well-known behaviour of the impact pressure, see (Wagner 1932). Therefore we try to approximate the pressure in terms of a smooth function $Q(x,t)$ multiplied by a square-root singular function $1/\sqrt{x_c^2(\tau) - x^2}$ for $|x| \leq x_c(\tau)$, as shown in equation (4.37). This approach is carried out only along the wetted region, $-x_c(\tau) \leq x \leq x_c(\tau)$. Having in mind that the pressure on the free surface is zero. The pressure distribution overall can be presented as follow

$$p(x,\tau) = \begin{cases} \frac{Q(x,\tau)}{\sqrt{x_c^2(\tau)-x^2}} & |x| \leq x_c(\tau), \\ 0 & x_c(\tau) < |x| < 1, \end{cases} \tag{4.37}$$

where $Q(x,\tau)$ is assumed to have no singularity in space and time. Equation (4.36), using (4.37), now becomes

$$p_l(\tau) = 2\int_0^{x_c} \frac{Q(x,\tau)}{\sqrt{x_c^2(\tau) - x^2}}\cos(l\pi x)dx. \tag{4.38}$$

For the space discretization of the function $Q(x,t)$ we write

$$Q(x,\tau) = \sum_{i=1}^{N_c} Q_i(\tau)\Psi_i(x), \tag{4.39}$$

where the basis function $\Psi_i(x)$ for $i = 1, 2, \dots, N_c$, are defined in (4.25)–(4.26) and N_c is an integer between 1 and N such that $x_{N_c} \leq x_c(\tau) \leq x_{N_c+1}$. Substituting (4.39) in equation (4.38) we arrive at

$$p_l(\tau) = 2\sum_{i=1}^{N_c} Q_i(\tau)\tilde{C}_{l,i}(x_c(\tau)), \tag{4.40}$$

where the coefficients $\tilde{C}_{l,i}(x_c(\tau))$, for $1 \leq i \leq N_c$, and $l = 1, 2, \dots$, are defined by

$$\tilde{C}_{l,i}(x_c(\tau)) = \int_0^{x_c(\tau)} \frac{\Psi_i(x)}{\sqrt{x_c^2(\tau) - x^2}}\cos(l\pi x)dx. \tag{4.41}$$

Note that the coefficients $\tilde{C}_{l,i}(x_c(\tau))$ depend on l, i and $x_c(\tau)$. The integral in (4.41) has square-root singularity at $x = x_c(\tau)$ and there is no closed form avail-

able for this integral. The rest of this section aims at evaluating $\tilde{C}_{l,i}(x_c(\tau))$ in a numerically efficient way so that it can be used in our computation. The integer $N_c = N_c(\tau)$ in equation (4.39) means we do not need Q_i for $i > N_c$ outside the contact region,

$$Q_i(\tau) = \begin{cases} \text{unknown} & ; i \leq N_c, \\ 0 & ; N_c < i, \end{cases} \tag{4.42}$$

for $i = 1, 2, \ldots, N$.

By definition (4.25), equation (4.41) reads

$$\tilde{C}_{l,i}(x_c(\tau)) = \left(\int_{x_{i-1}}^{x_i} + \int_{x_i}^{x_{i+1}} \right) \frac{\Psi_i(x)}{\sqrt{x_c^2(\tau) - x^2}} \cos(l\pi x) dx. \tag{4.43}$$

From the definition of the hat function, $\Psi_i(x), i = 1, 2, \ldots, N$, in (4.25) we write equation (4.43) as

$$\begin{aligned} \triangle\tilde{C}_{l,i}(x_c(\tau)) = & \int_{x_{i-1}}^{x_c(\tau)} \frac{x - x_{i-1}}{\sqrt{x_c^2(\tau) - x^2}} \cos(l\pi x) dx + 2x_i \int_{x_i}^{x_c(\tau)} \frac{\cos(l\pi x)}{\sqrt{x_c^2(\tau) - x^2}} dx \\ & - 2 \int_{x_i}^{x_c(\tau)} \frac{x \cos(l\pi x)}{\sqrt{x_c^2(\tau) - x^2}} dx - \int_{x_{i+1}}^{x_c(\tau)} \frac{x_{i+1} - x}{\sqrt{x_c^2(\tau) - x^2}} \cos(l\pi x) dx, \end{aligned} \tag{4.44}$$

where $x = x_c(\tau)$ is the moving contact point on the right which gives the half length of the wetted region. Using a change of variable $x_c(\tau)u = x$ in equation (4.44) we arrive at

$$\begin{aligned} \triangle\tilde{C}_{l,i}(x_c(\tau)) = & \int_0^1 \frac{x_c(\tau)u - x_{i-1}}{\sqrt{1 - u^2}} \cos(l\pi x_c(\tau)u) du + 2x_i \int_0^1 \frac{\cos(l\pi x_c(\tau)u)}{\sqrt{1 - u^2}} du \\ & - 2x_c(\tau) \int_0^1 \frac{u \cos(l\pi x_c(\tau)u)}{\sqrt{1 - u^2}} du - \int_0^1 \frac{x_{i+1} - x_c(\tau)u}{\sqrt{1 - u^2}} \cos(l\pi x_c(\tau)u) du \\ & + \tilde{C}_{l,i}^c(x_c(\tau)), \end{aligned} \tag{4.45}$$

where

$$\begin{aligned} \tilde{C}_{l,i}^c(x_c(\tau)) = & - \int_0^{\frac{x_{i-1}}{x_c(\tau)}} \frac{x_c(\tau)u - x_{i-1}}{\sqrt{1 - u^2}} \cos(l\pi x_c(\tau)u) du \\ & - 2x_i \int_0^{\frac{x_i}{x_c(\tau)}} \frac{\cos(l\pi x_c(\tau)u)}{\sqrt{1 - u^2}} du + 2x_c(\tau) \int_0^{\frac{x_i}{x_c(\tau)}} \frac{u \cos(l\pi x_c(\tau)u)}{\sqrt{1 - u^2}} du \\ & + \int_0^{\frac{x_{i+1}}{x_c(\tau)}} \frac{x_{i+1} - x_c(\tau)u}{\sqrt{1 - u^2}} \cos(l\pi x_c(\tau)u) du. \end{aligned} \tag{4.46}$$

All integrals in the right-hand side of equation (4.45) with the lower and upper limits 0, 1, respectively, contain the term $u^n, n = 0, 1$. For those with $n = 0$

the results are given in terms of the Bessel function of the first kind and with $n = 1$ the integrals are given in terms of the Struve function, see (Gradshteyn & Ryzhik 2014). To evaluate the latter, for example in Matlab, one needs to produce a code because it is not implemented in Matlab. An accurate approximation for the Struve function, was suggested by (Aarts & Janssen 2003). They used only a limited number of elementary functions and the Bessel function of the first kind to find this approximation which is quite accurate for small and large values of the argument of the cosine function (here this is $l\pi x_c(\tau)$).

However, the right-hand sides of equations (4.45) and (4.46) can be simplified more and we skip over all the integrals in equation (4.45) excluding the term $\tilde{C}^c_{l,i}(\tau)$ as they cancel each other, except for the two special cases $i = N_c$ and $i = N_{c+1}$, which will be discussed later in this section. We simplify further the remaining terms in equations (4.46), to arrive at

$$\begin{aligned}\triangle\tilde{C}_{l,i}(x_c(\tau)) = &\left(-x_{i-1}\int_{\frac{x_{i-1}}{x_c(\tau)}}^{\frac{x_i}{x_c(\tau)}} + x_{i+1}\int_{\frac{x_i}{x_c(\tau)}}^{\frac{x_{i+1}}{x_c(\tau)}}\right)\frac{\cos(l\pi x_c(\tau)u)}{\sqrt{1-u^2}}du \\ &+ x_c(\tau)\left(\int_{\frac{x_{i-1}}{x_c(\tau)}}^{\frac{x_i}{x_c(\tau)}} - \int_{\frac{x_i}{x_c(\tau)}}^{\frac{x_{i+1}}{x_c(\tau)}}\right)\frac{u\cos(l\pi x_c(\tau)u)}{\sqrt{1-u^2}}du, \qquad (4.47)\end{aligned}$$

and again the change of variable $u = \sin\theta$ transforms equation (4.47) to a non-singular integral of the form

$$\begin{aligned}\triangle\tilde{C}_{l,i}(x_c(\tau)) = &\left(-x_{i-1}\int_{\theta_{i-1}(\tau)}^{\theta_i(\tau)} + x_{i+1}\int_{\theta_i(\tau)}^{\theta_{i+1}(\tau)}\right)\cos(l\pi x_c(\tau)\sin\theta)d\theta \\ &+ x_c(\tau)\left(\int_{\theta_{i-1}(\tau)}^{\theta_i(\tau)} - \int_{\theta_i(\tau)}^{\theta_{i+1}(\tau)}\right)\sin\theta\cos(l\pi x_c(\tau)\sin\theta)d\theta, \qquad (4.48)\end{aligned}$$

where for $1 \le i \le N_c$:

$$\theta_i(\tau) = \sin^{-1}\left(\frac{x_i}{x_c(\tau)}\right). \qquad (4.49)$$

Equation (4.48) holds for $i \in \{2, \ldots, N-1\}$. For $i = 1$, using the definition (4.26) and applying it on equation (4.43), then by the substitutions $x = x_c(\tau)u$ and $u = \sin(\theta)$ respectively we arrive at

$$\triangle\tilde{C}_{l,1}(\tau) = \int_0^{\theta_2(\tau)} (\triangle - x_c(\tau)\sin\theta)\cos(l\pi x_c(\tau)\sin\theta)d\theta, \qquad (4.50)$$

where

$$\theta_2(\tau) = \sin^{-1}\left(\frac{\triangle}{x_c(\tau)}\right). \qquad (4.51)$$

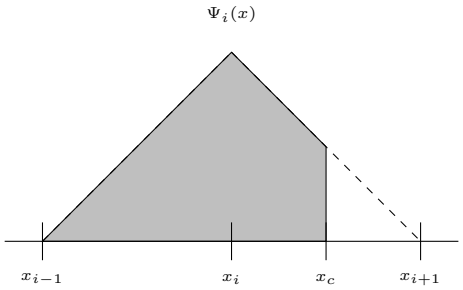

Figure 4.3: $\Psi_i(x)$ when $x_i < x_c(\tau) < x_{i+1}$. Grey area is where $\Psi_i(x)$ is active, and white area is where it is deactivated.

It is unlikely that the last node, x_N, will be covered by the wetted region, therefore $Q_N(\tau) = 0$ by definition (4.42). The integrals in the right-hand side of equation (4.48) can not be expressed in closed form, and must be calculated numerically. It is to be noticed here that the singularity is removed from the integrand. This singularity exists only when $x_{N_c} = x_c(\tau)$ or x_{N_c} is the node such that $x_{N_c} < x_c(\tau) < x_{N_c+1}$ at some time during the impact which is to be considered carefully. For such cases we have to replace the upper limit and shorten it to $x = x_c(\tau)$ in order to avoid complex numbers in (4.49) and to respect the fact that the function $Q(x, \tau)$ is zero outside of the wetted region, $x > x_c(\tau)$. Therefore by definition (4.25), for the particular case, for $i = N_c$, i.e. $x_{N_c} < x_c(\tau) < x_{N_c+1}$, the hat function $\Psi_{N_c}(x)$, takes the form

$$\Psi_{N_c}(x) = \frac{1}{\triangle} \begin{cases} x - x_{N_c-1} & ; x_{N_c-1} \leq x \leq x_{N_c}, \\ x_{N_c+1} - x & ; x_{N_c} \leq x \leq x_c(\tau), \\ 0 & ; \textit{otherwise}, \end{cases} \tag{4.52}$$

as shown in Figure 4.3. In this figure the interval of integration has been cut at the point $x = x_c(\tau)$. Note that the increment $\triangle$ is to remain unchanged. We do not account for the hat function $\Psi_{N_c+1}(x)$, Figure 4.4, as the function $Q_i(\tau)$ is considered zero for all $i > N_c + 1$.

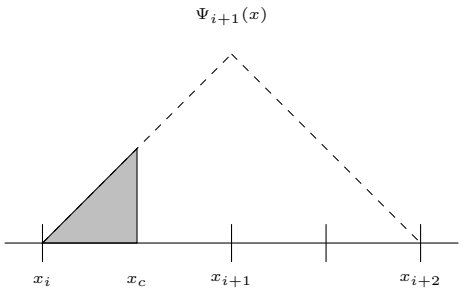

Figure 4.4: $\Psi_{i+1}(x)$ when $x_i < x_c(\tau) < x_{i+1}$. Grey area is where $\Psi_{i+1}(x)$ is active, and white area is where it is deactivated.

Therefore, in a similar way, by definition (4.52) and the approximation for the Struve function given by (Aarts & Janssen 2003), we find

$$\begin{aligned}\triangle\tilde{C}_{l,N_c}(\tau) = 2\int_0^{\theta_{N_c}(\tau)} &(x_c(\tau)\sin\theta - x_{N_c})\cos(l\pi x_c(\tau)\sin\theta)d\theta \\ &- \int_0^{\theta_{N_c-1}(\tau)} (x_c(\tau)\sin\theta - x_{N_c-1})\cos(l\pi x_c(\tau)\sin\theta)d\theta \\ &+ (x_{N_c+1} - \frac{\pi}{2}x_c(\tau))J_0(n\pi x_c(\tau)) + (8 - \frac{5}{2}\pi)\frac{\sin(n\pi x_c(\tau))}{n\pi} \\ &+ (6\pi - 18)\frac{1-\cos(n\pi x_c(\tau))}{x_c(\tau)(n\pi)^2}, \end{aligned} \tag{4.53}$$

where

$$\theta_{N_c-1}(\tau) = \sin^{-1}\left(\frac{x_{N_c-1}}{x_c(\tau)}\right), \quad \theta_{N_c}(\tau) = \sin^{-1}\left(\frac{x_{N_c}}{x_c(\tau)}\right). \tag{4.54}$$

Now equation (4.30) can be rewritten to become

$$\sum_{j=1}^{N}\eta_j(t)e_{j,q} = \sum_{j=1}^{N}\eta_{0j}(t)e_{j,q} - \sum_{i=1}^{N_c}\int_0^t Q_i(\tau)\mathcal{K}_{i,q}(t,\tau)d\tau, \tag{4.55}$$

where we define

$$\mathcal{K}_{i,q}(t,\tau) = \sum_{n=1}^{\infty}\omega_n C_{n,q}\tilde{C}_{n,i}(\tau)\sin(\omega_n(t-\tau)), \tag{4.56}$$

which are the sloshing impact coefficients. Here τ is the variable of integration, $0 \leq \tau \leq t$. Before we proceed to further analysis, because of the importance of the coefficients (4.56) as kernels of the integrals in (4.55), we will discuss the convergence and behaviour of these impact coefficients. The behaviour of the function $\mathcal{K}_{i,q}(t,\tau)$ for some $1 \leq q, i \leq N$ are shown in Figures 4.5–4.9, where the index q refers to coefficient $C_{n,q}$ given in equations (4.34)–(4.35) and the index i is for $\tilde{C}_{n,i}(\tau)$ which is given in equations (4.48) and (4.50). For these plots we fix the time variable t ($t = 1$) and let $0 \leq \tau \leq t$. We worked on the interval for $x \in [0,1]$ with uniform space mesh applied with 200 nodes. Also the moving contact point $x_c(\tau) = \sqrt{\tau}$ is assumed. Also to show the number of terms needed for the summations to bring about adequate convergence for the partial sum $S_{\bar{n}}$, of the first $\bar{n}$ terms of the infinite series in equation (4.56). It is found that the convergence is guaranteed with minimum of 2 significant digits reliable for $\bar{n} > 400$, see Figures 4.5–4.14. While partial sum for $\bar{n} < 400$ fluctuates from $O(10^{-2})$ up to $O(10^{-4})$, as shown for $\bar{n} = 100$ and $\bar{n} = 200$, for example see Figures 4.5 and 4.9.

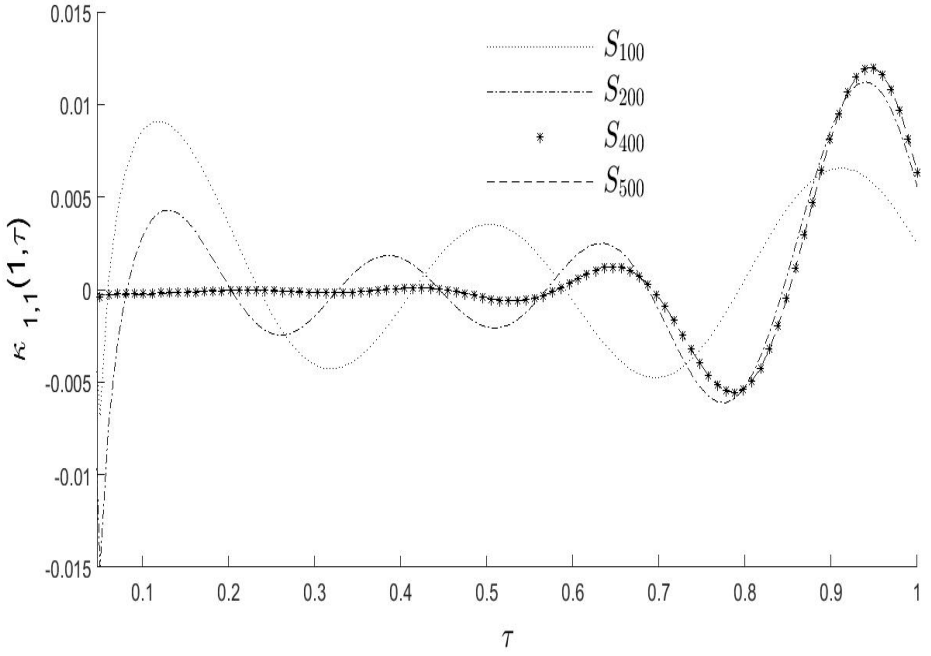

Figure 4.5: Sloshing impact coefficient $\mathcal{K}_{1,1}(1,\tau)$. Dotted line with $\bar{n} = 100$, dashed-dotted line with partial sum of $\bar{n}$ terms $\bar{n} = 200$, stars with $\bar{n} = 400$ and dashed line with $\bar{n} = 500$.

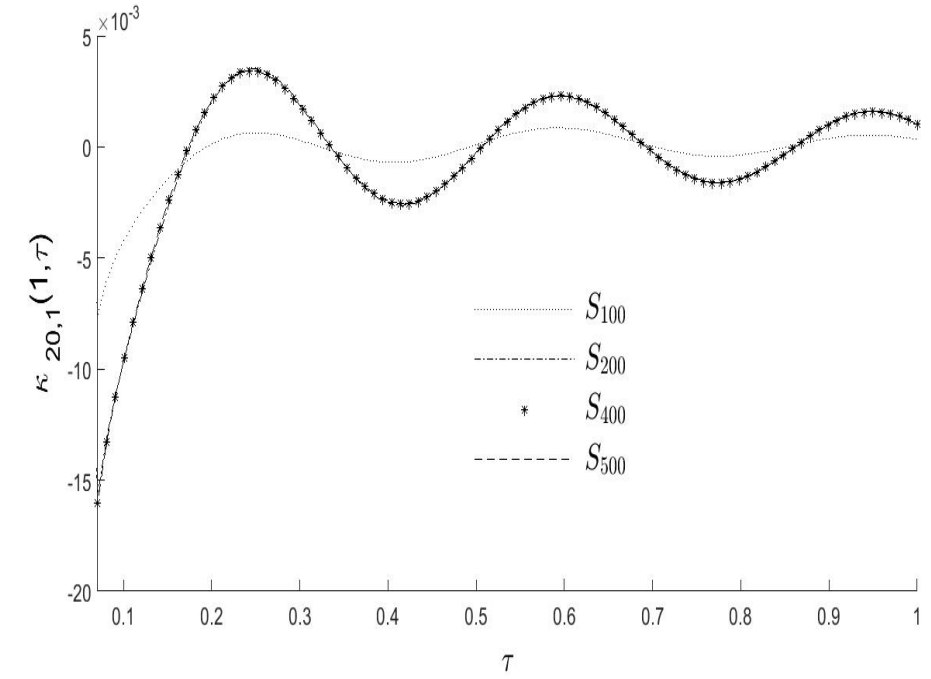

Figure 4.6: Sloshing impact coefficient $\mathcal{K}_{20,1}(1,\tau)$. Dotted line with partial sum of $\bar{n}$ terms $\bar{n} = 100$, dashed-dotted line with $\bar{n} = 200$, stars with $\bar{n} = 400$ and dashed line with $\bar{n} = 500$. The last 3 sets of results are indistinguishable on this plot.

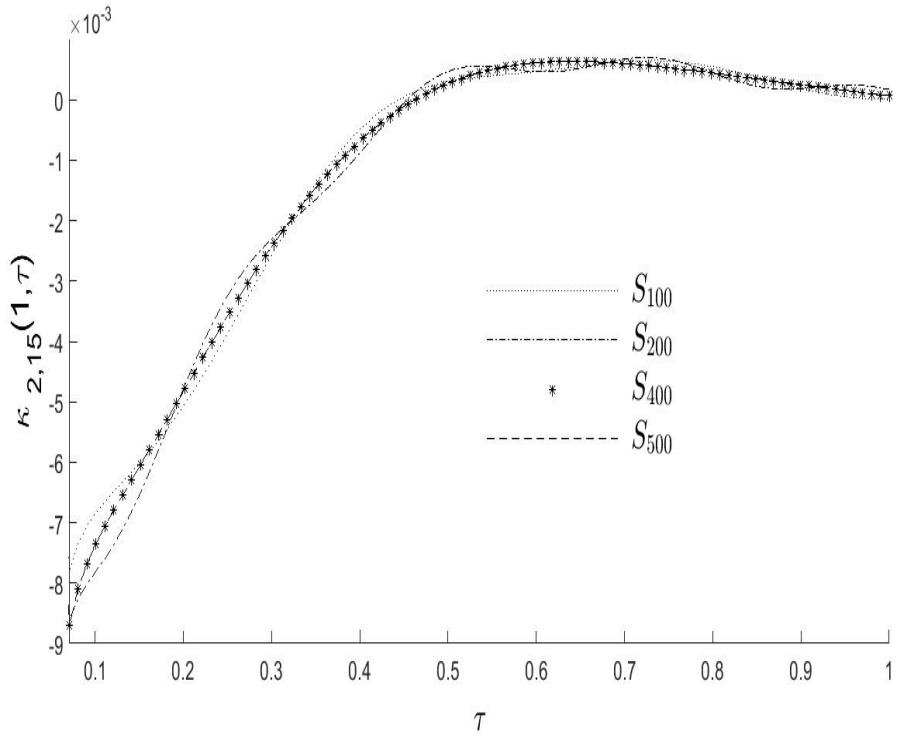

Figure 4.7: Sloshing impact coefficient $\mathcal{K}_{2,15}(1,\tau)$. Dotted line with partial sum of $\bar{n}$ terms $\bar{n} = 100$, dashed-dotted line with $\bar{n} = 200$, stars with $\bar{n} = 400$ and dashed line with $\bar{n} = 500$.

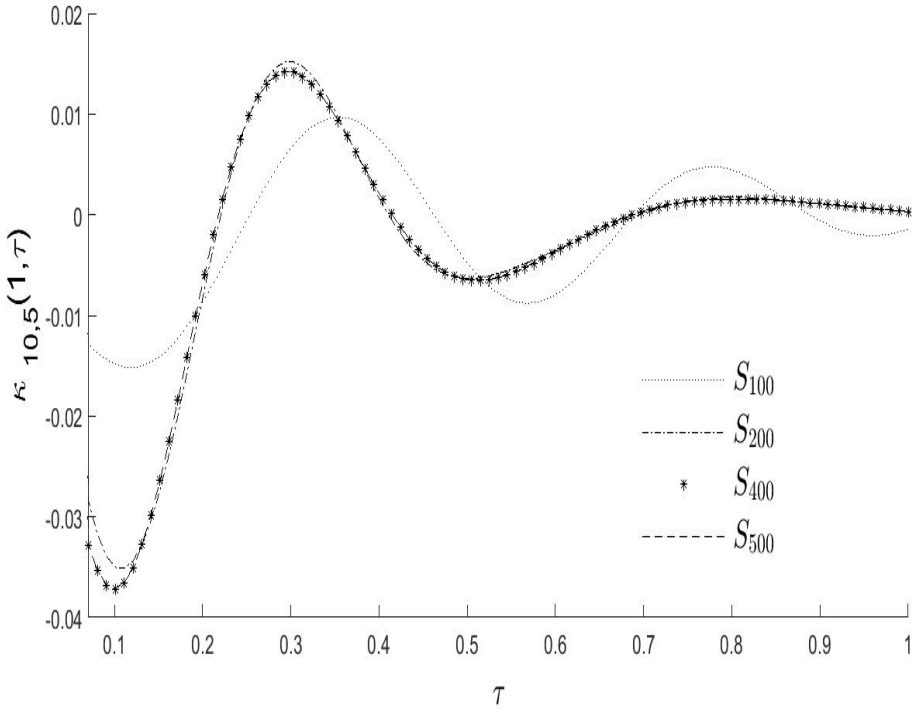

Figure 4.8: Sloshing impact coefficient $\mathcal{K}_{10,5}(1,\tau)$. Dotted line with partial sum of $\bar{n}$ terms $\bar{n} = 100$, dashed-dotted line with $\bar{n} = 200$, stars with $\bar{n} = 400$ and dashed line with $\bar{n} = 500$.

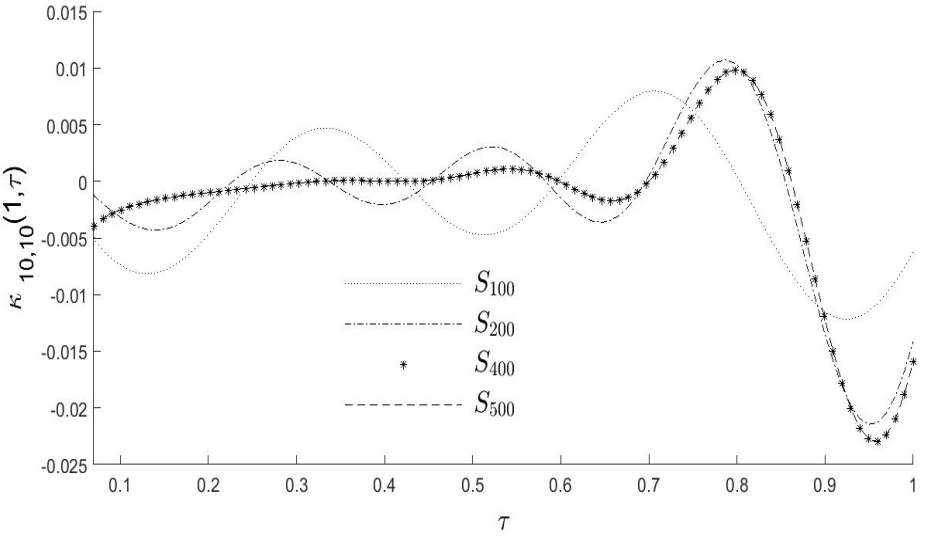

Figure 4.9: Sloshing impact coefficient $\mathcal{K}_{10,10}(1,\tau)$. Dotted line with partial sum of $\bar{n}$ terms $\bar{n} = 100$, dashed-dotted line with $\bar{n} = 200$, stars with $\bar{n} = 400$ and dashed line with $\bar{n} = 500$.

To verify and analyse the rate of convergence for the partial sums we plot their difference. In Figures 4.10–4.14, we show the differences for the partial sums S_{500} and S_{400} for every node. It is shown that the maximum error is of $O(10^{-4})$ or higher negative order. Therefore we can proceed accurately with the numerical computations with summing up the first 400 terms in (4.56).

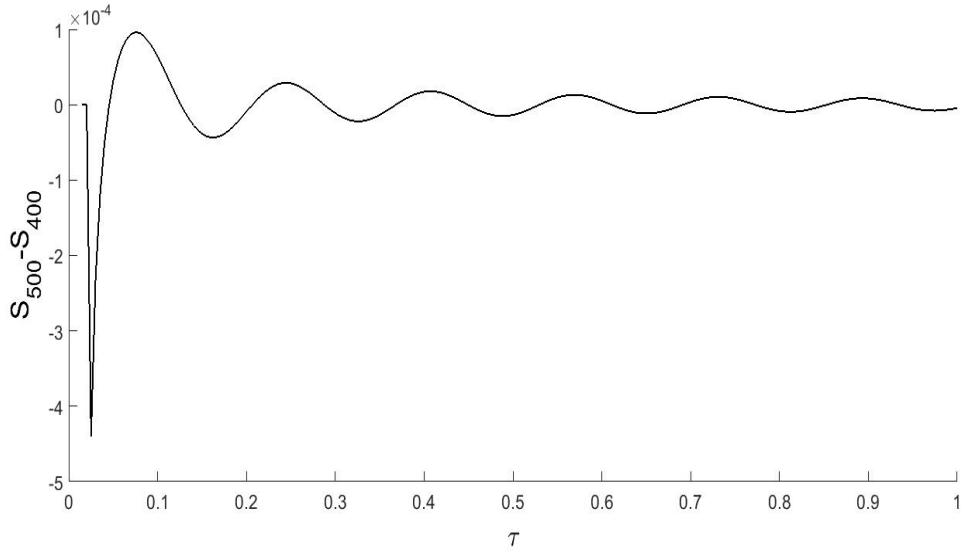

Figure 4.10: The difference in partial sums S_{400} and S_{500} for the sloshing impact coefficient $\mathcal{K}_{1,1}(1,\tau)$.

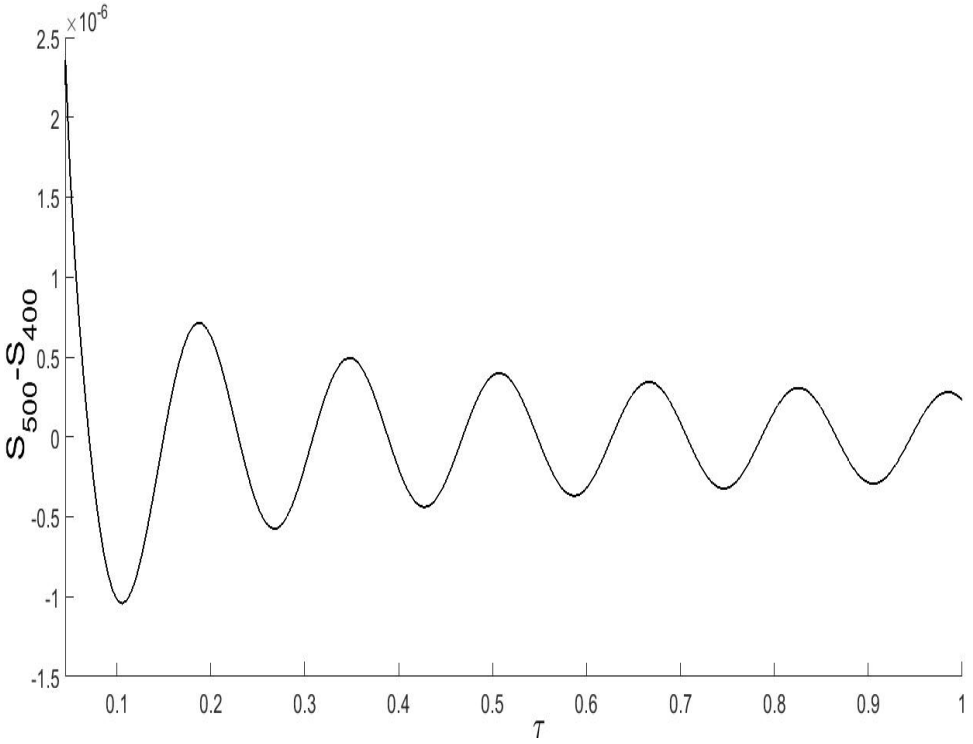

Figure 4.11: The difference in partial sums S_{400} and S_{500} for the sloshing impact coefficient $\mathcal{K}_{20,1}(1,\tau)$.

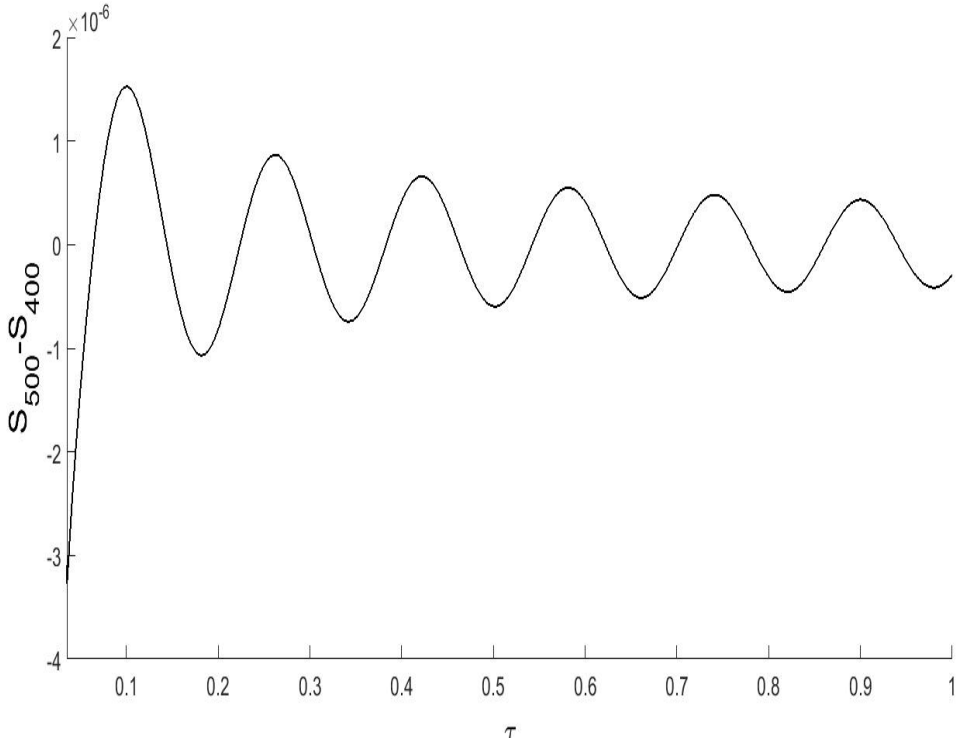

Figure 4.12: The difference in partial sums S_{400} and S_{500} for the sloshing impact coefficient $\mathcal{K}_{2,15}(1,\tau)$.

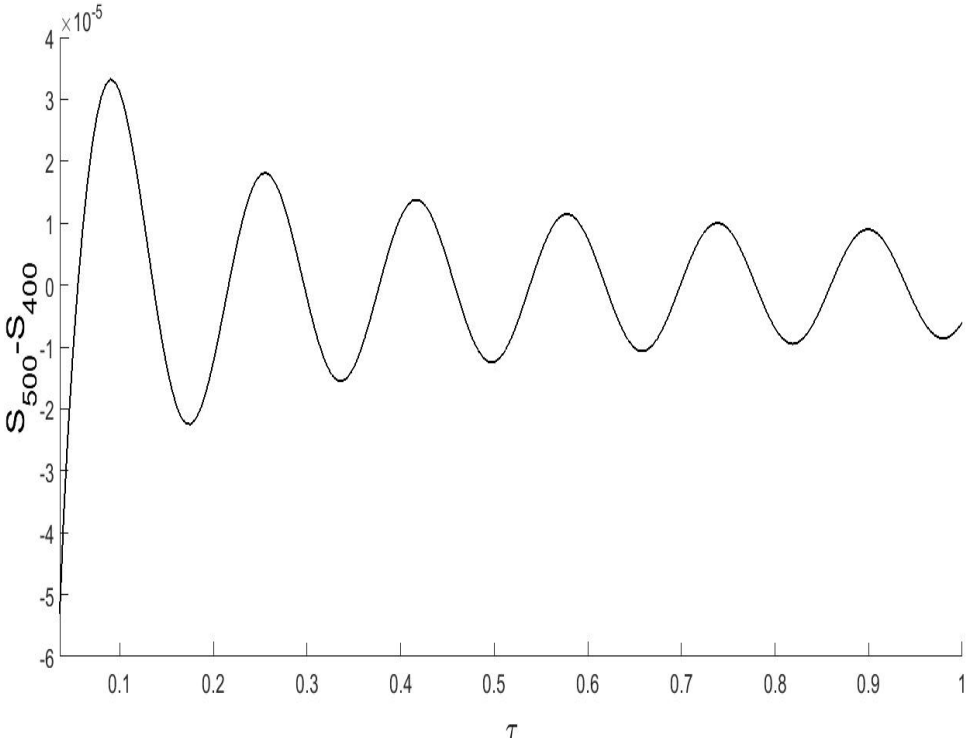

Figure 4.13: The difference in partial sums S_{400} and S_{500} for the sloshing impact coefficient $\mathcal{K}_{5,10}(1,\tau)$.

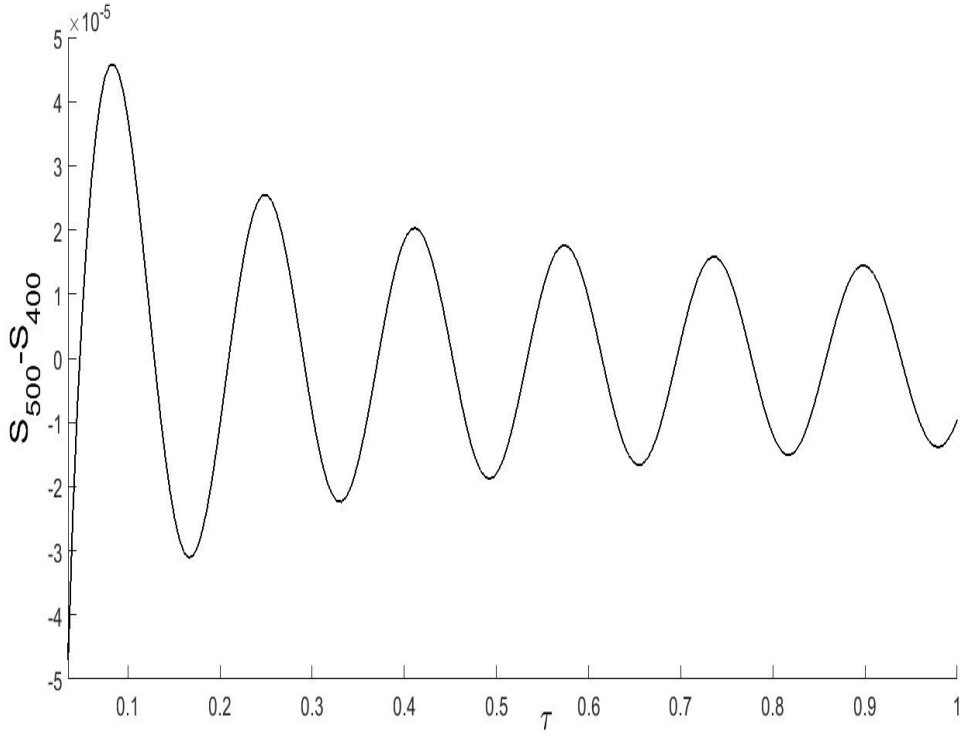

Figure 4.14: The difference in partial sums S_{400} and S_{500} for the sloshing impact coefficient $\mathcal{K}_{10,10}(1,\tau)$.

4.4 Approximating integrals in (4.48), (4.50) and (4.53)

The integrals in (4.48), (4.50) and (4.53) have no closed form and must be calculated with numerical integral computation. This makes the process of numerical computations last for a much longer period, as in Matlab calcualting integrals is very time-consuming. For the sake of reducing the computation time, especially for equations (4.48), (4.50) and (4.53), where integrals are to be calculated numerically, we use an approximation method for the integrands and integrate them analytically. To do this we make a partition on the space interval $0 \leq \theta \leq \frac{\pi}{2}$. Then for each subinterval $[\theta_i, \theta_{i+1}]$, such that $0 = \theta_1 < \theta_2 < \cdots < \theta_{N_c-1} < \theta_{N_c} = \frac{\pi}{2}$ and $1 \leq i \leq N_1$, we use the linear approximation for the function $\sin\theta$. That is

$$\sin\theta \simeq c_i\theta + d_i, \tag{4.57}$$

where c_i and d_i are the coefficients which give the best fit for our linear approximation on the subinterval $[\theta_i, \theta_{i+1}]$, $1 \leq i \leq N_c$. In order to show how accurate this approximation works, we apply it to the well-known Bessel function of the first kind, $J_0(n\pi x_c(\tau))$, with its integral representation (see (Gradshteyn & Ryzhik 2014))

$$J_0(n\pi x_c(\tau)) = \frac{2}{\pi}\int_0^{\pi/2} \cos(n\pi x_c(\tau)\sin\theta)d\theta. \tag{4.58}$$

We choose this Bessel function representation to test the approximation because the integral in $\triangle\tilde{C}_{l,i}(x_c(\tau)), 1 \leq i \leq N_c$ term contains integrals similar to (4.58), except at the limits. In Figures 4.15–4.16 the comparison is shown for $n = 1, 10$ respectively, with its linear approximation

$$J_0(n\pi x_c(\tau)) \simeq \frac{2}{\pi}\sum_{i=1}^{M}\int_{\theta_i}^{\theta_{i+1}} \cos(n\pi x_c(\tau)(c_i\theta + d_i))d\theta, \tag{4.59}$$

each term of which is integrable analytically. We choose the function $x_c(\tau)$ to vary between its minimum and possible maximum values. Both figures show that the approximation is close to the exact function. To see how well the approximations behave we show the relative errors as well (see Figures 4.17–4.18), which are of $O(10^{-3})$ or less. While the absolute error approximation (see Figures 4.19–4.20) are of $O(10^{-7})$. Spikes in relative error occur because the function being approximated vanishes at certain values of $x_c(\tau)$.

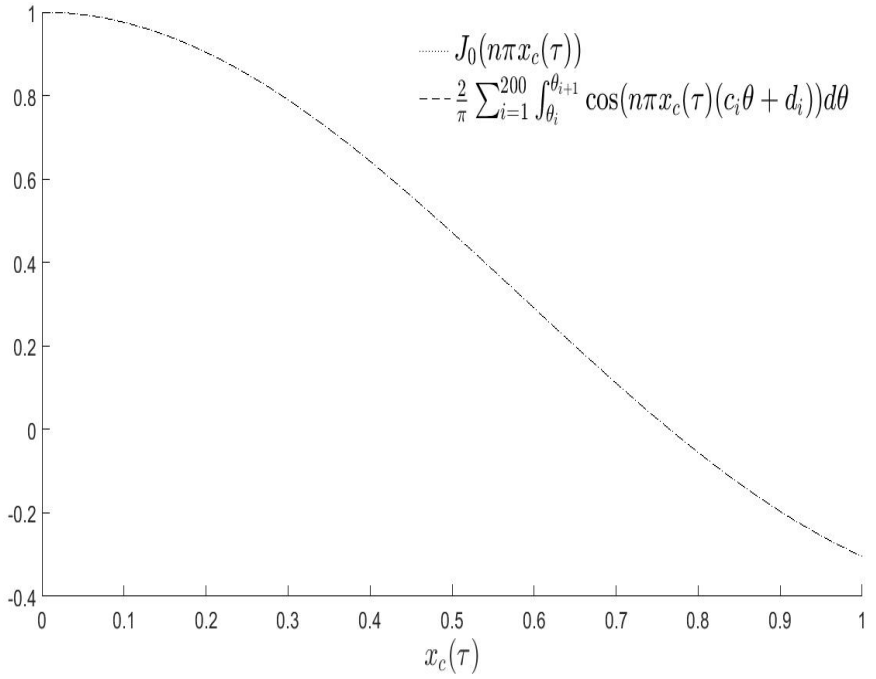

Figure 4.15: The comparison of (4.58), dotted line, with its linear approximation (4.59), dashed line, with $n = 1$. On this plot the two curves are indistinguishable.

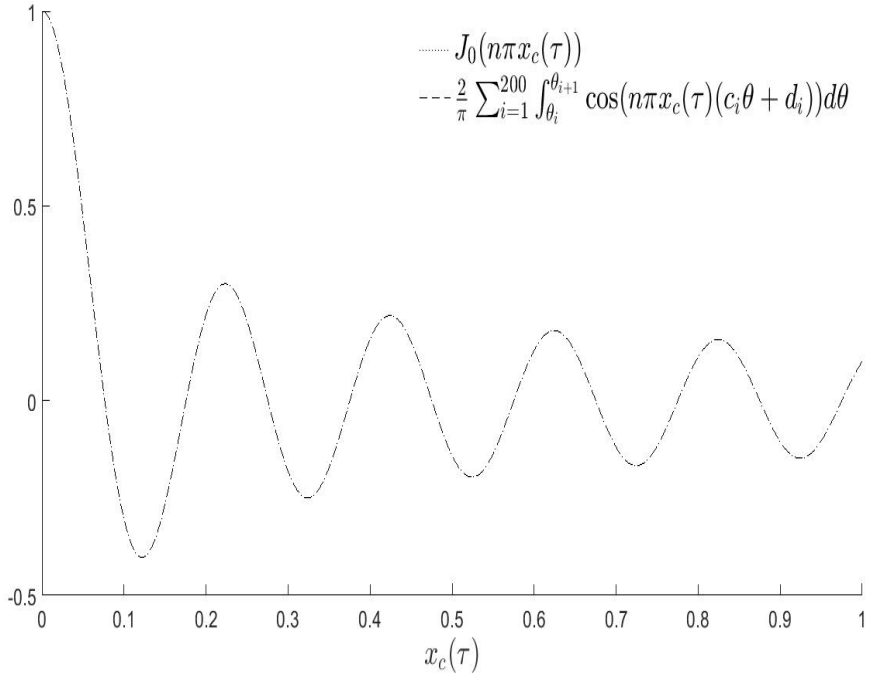

Figure 4.16: The comparison of (4.58), dotted line, with its linear approximation (4.59), dashed line, with $n = 10$. On this plot the two curves are indistinguishable.

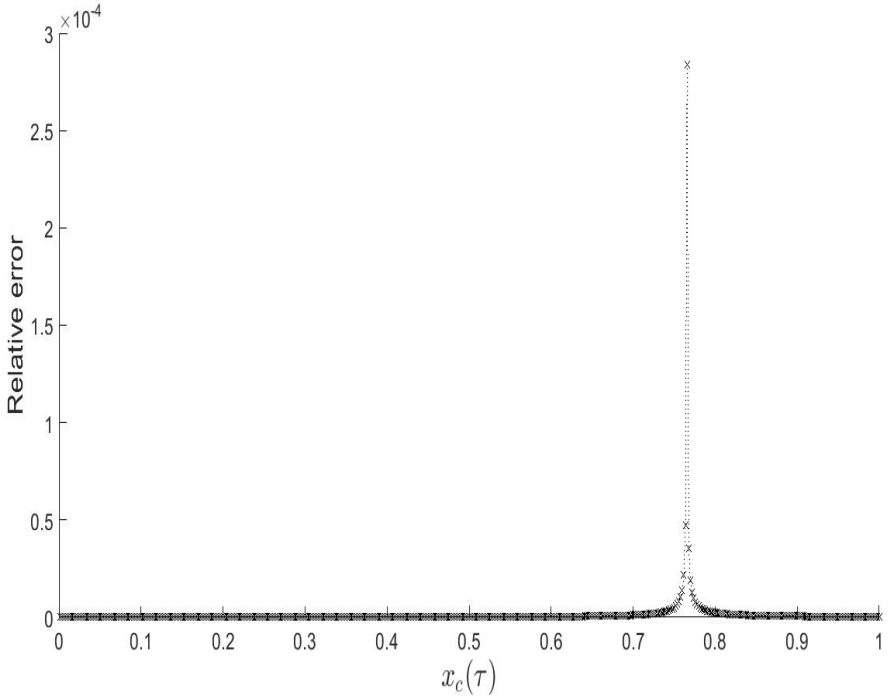

Figure 4.17: Relative error between (4.58) and its linear approximation (4.59) with $n = 1$.

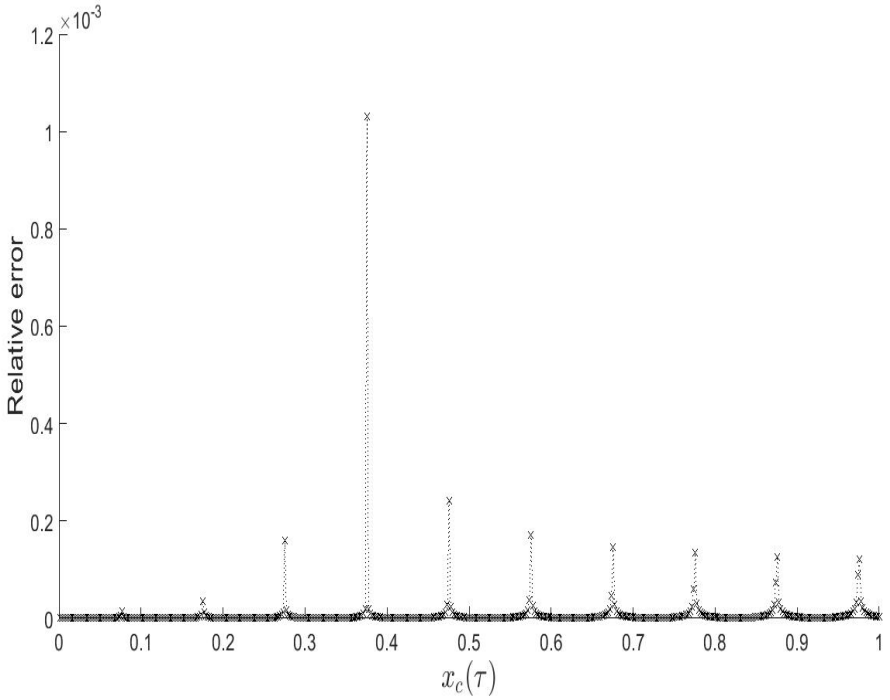

Figure 4.18: Relative error between (4.58) and its linear approximation (4.59) with $n = 10$.

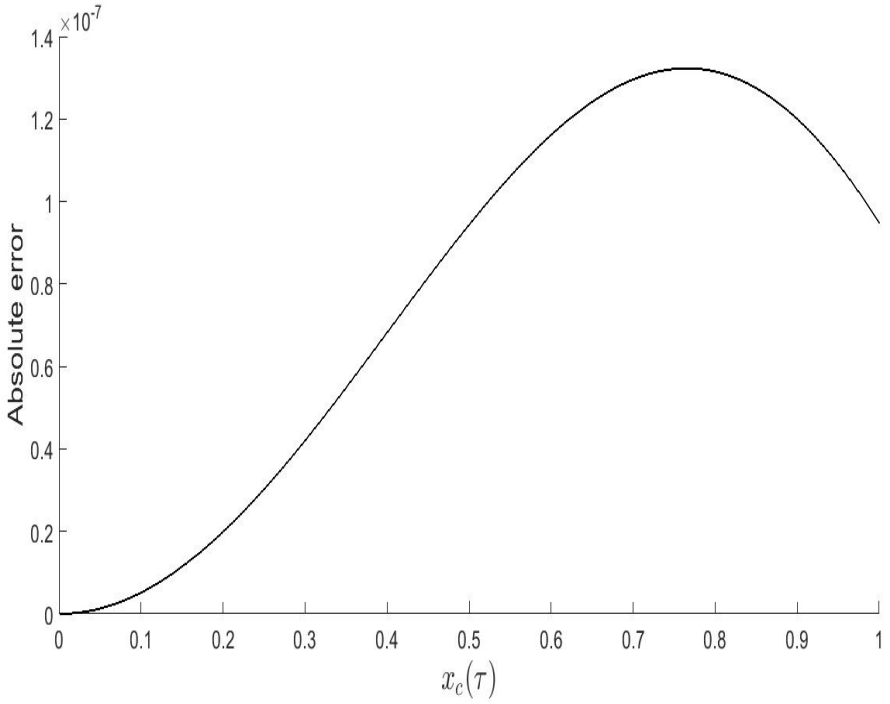

Figure 4.19: Absolute error between (4.58) and its linear approximation (4.59) with $n = 1$.

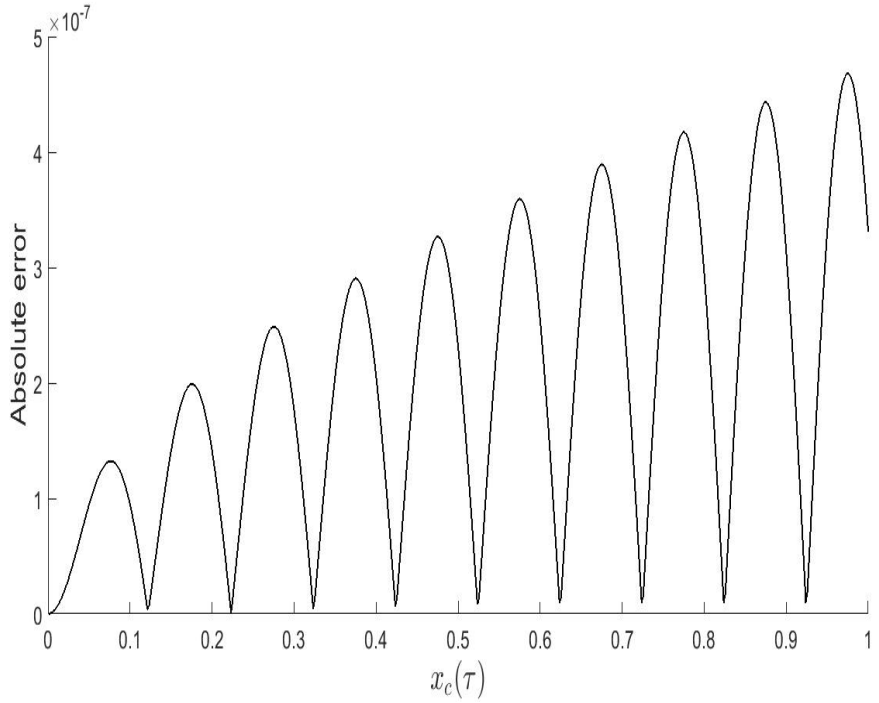

Figure 4.20: Absolute error between (4.58) and its linear approximation (4.59) with $n = 10$.

Also as shown in Figures 4.21–4.22, the integral

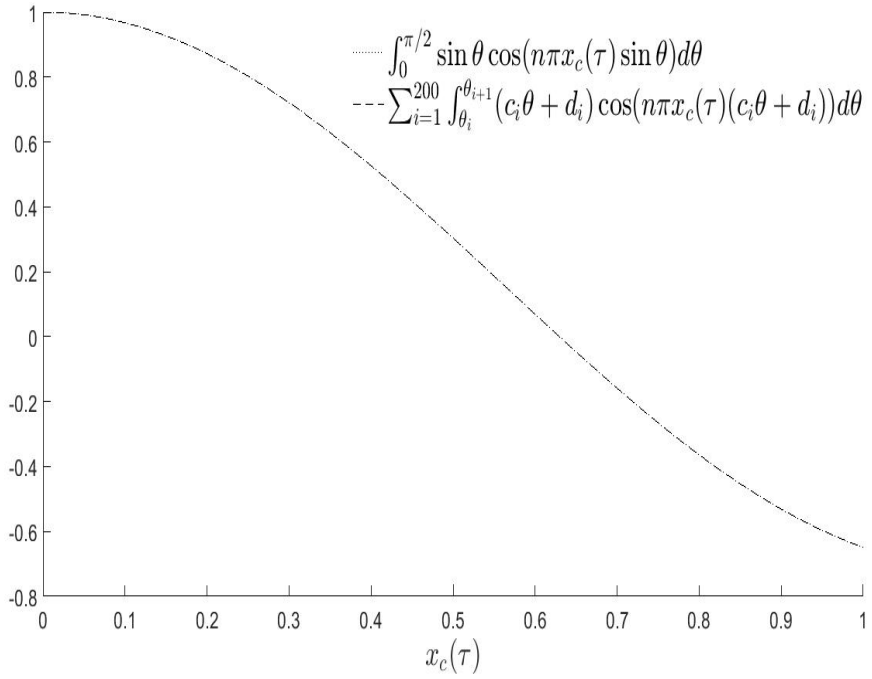

Figure 4.21: The comparison of (4.60), dotted line, with its linear approximation (4.61), dashed line, with $n = 1$. On this plot the two curves are indistinguishable.

$$\int_0^{\pi/2} \sin\theta \cos(n\pi x_c(\tau)\sin\theta)d\theta \tag{4.60}$$

is approximated by using the same previous approximation method to be rewritten as

$$\sum_{i=1}^{M} \int_{\theta_i}^{\theta_{i+1}} (c_i\theta + d_i)\cos(n\pi x_c(\tau)(c_i\theta + d_i))d\theta. \tag{4.61}$$

Again the figures show how close the approximation lies to the exact result, and the relative error plotted in Figures 4.23–4.24 shows the order of difference relative to its actual value is of $O(10^{-3})$. The absolute error, shown in Figures 4.25–4.26 is of $O(10^{-7})$.

Having only these small differences we can safely apply the linear approximation (4.57) for each of the equations (4.49), (4.51) and (4.53). By calculating the integral in these equations, the approximate and final form of the coefficients $\triangle\tilde{C}_{n,i}(\tau), i = 1, 2, \ldots, N_c + 1$ are given as follows. Equation (4.49) is for $i = 2, \ldots, N_c - 1$ and it becomes

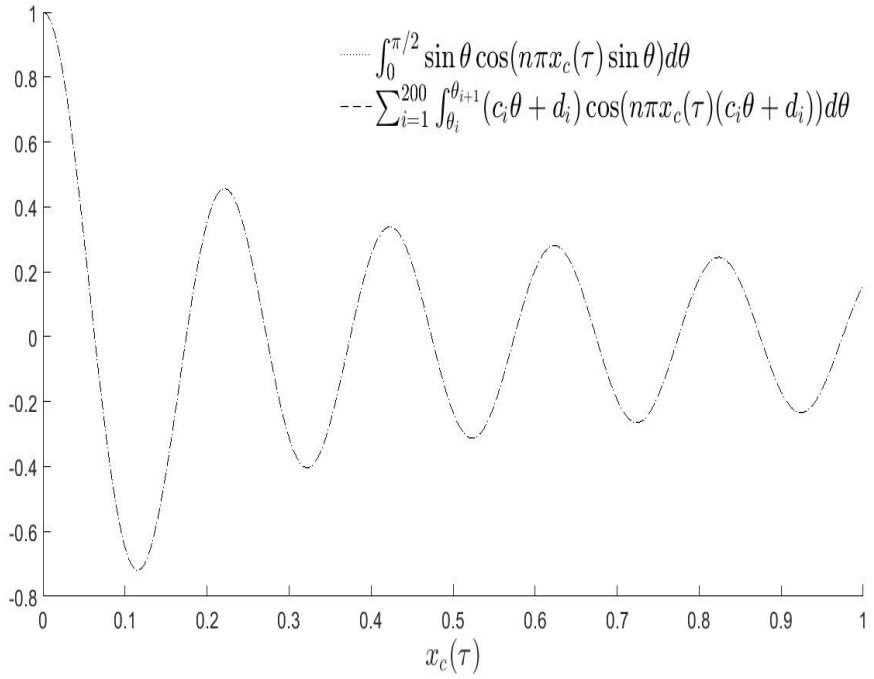

Figure 4.22: The comparison of (4.60), dotted line, with its linear approximation (4.61), dashed line, with $n = 10$. On this plot the two curves are indistinguishable.

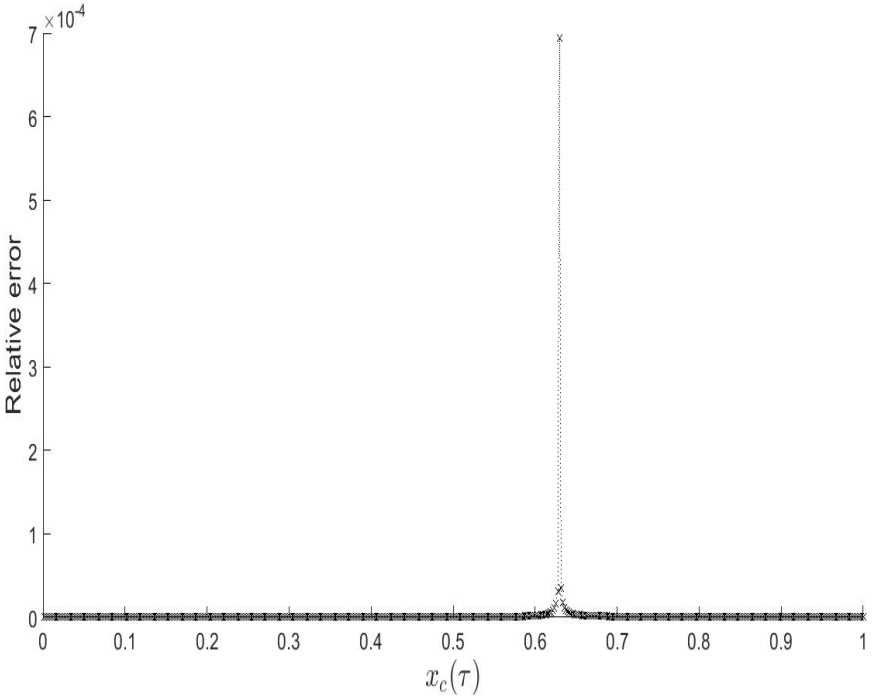

Figure 4.23: Relative error between (4.60) and its linear approximation (4.61) with $n = 1$.

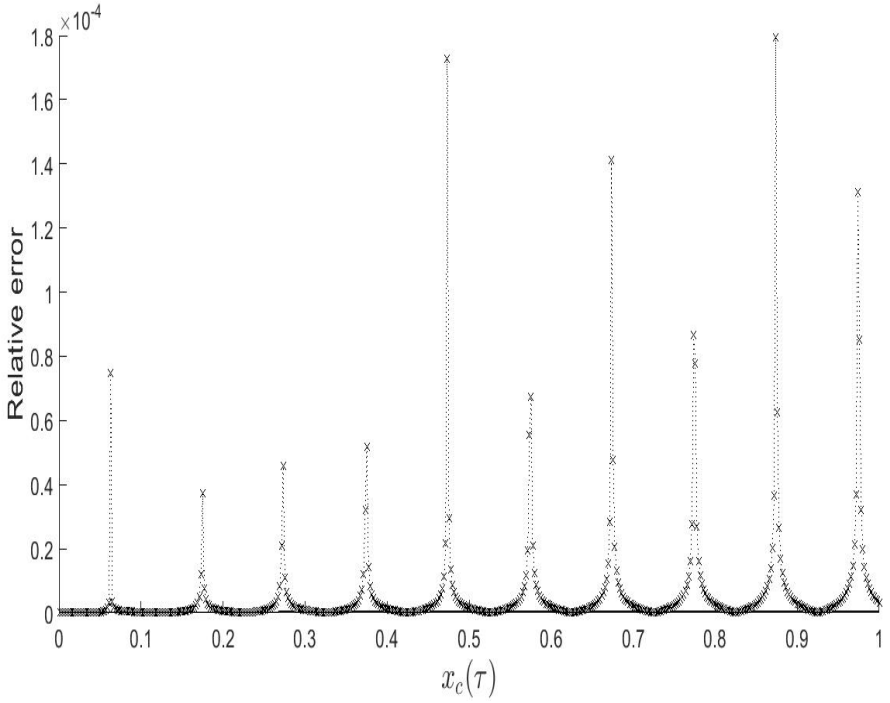

Figure 4.24: Relative error between (4.60) and its linear approximation (4.61) with $n = 10$.

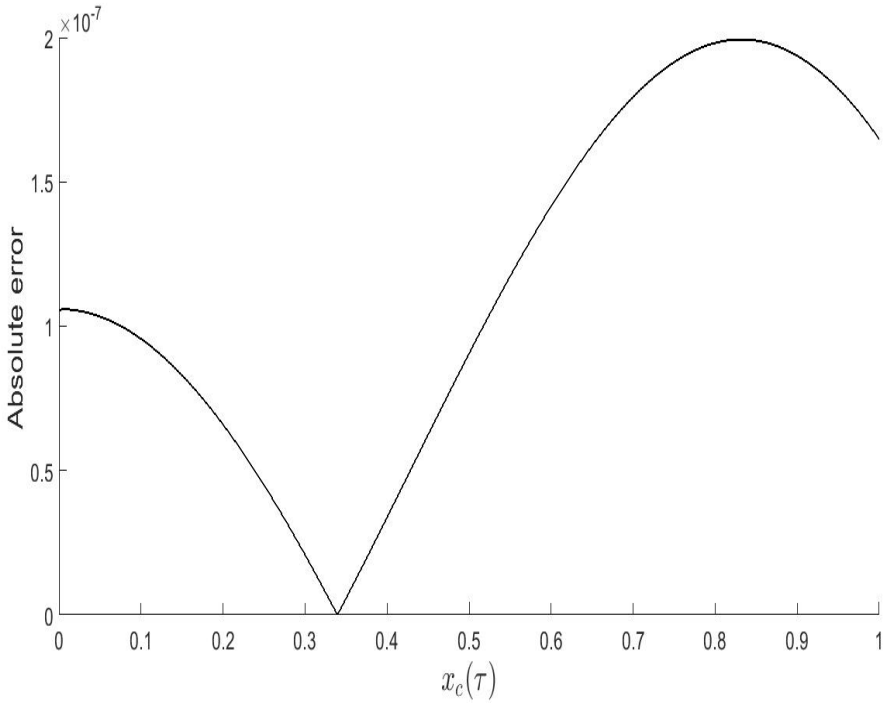

Figure 4.25: Absolute error between (4.60) and its linear approximation (4.61) with $n = 1$.

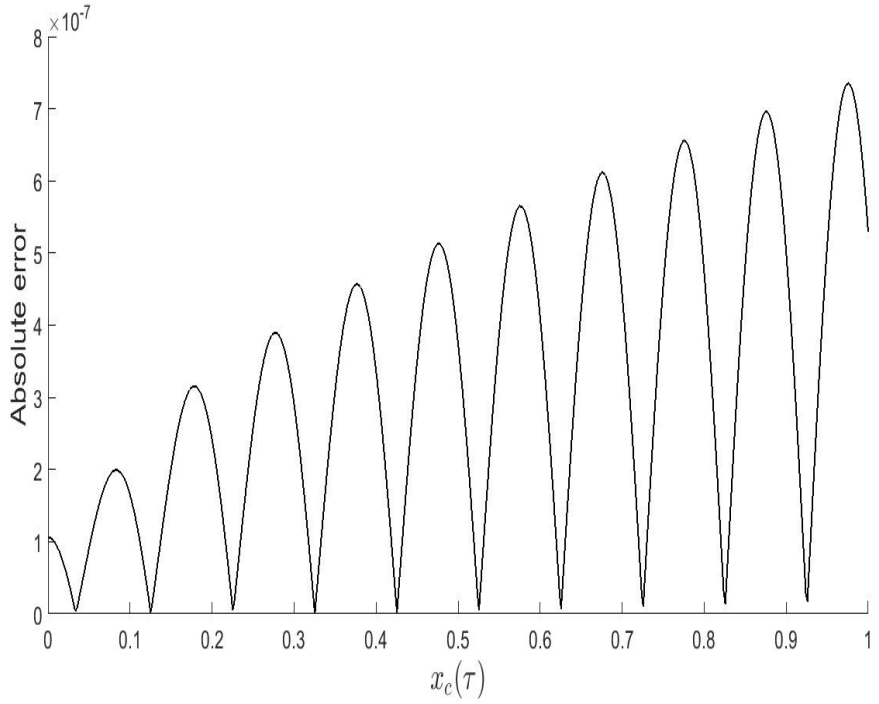

Figure 4.26: Absolute error between (4.60) and its linear approximation (4.61) with $n = 10$.

$$\begin{aligned}\triangle\tilde{C}_{n,i}(\tau) = {} & 2\frac{\frac{x_i}{x_c(\tau)} - c_i\theta_i(\tau) - d_i}{c_i(n\pi)}\sin(n\pi x_c(\tau)(c_i\theta_i(\tau)+d_i)) \\ & + \frac{c_i\theta_{i-1}(\tau) + d_i - \frac{x_{i-1}}{x_c(\tau)}}{c_i(n\pi)}\sin(n\pi x_c(\tau)(c_i\theta_{i-1}(\tau)+d_i)) \\ & + \frac{c_i\theta_{i+1}(\tau) + d_i - \frac{x_{i+1}}{x_c(\tau)}}{c_i(n\pi)}\sin(n\pi x_c(\tau)(c_i\theta_{i+1}(\tau)+d_i)) \\ & - \frac{1}{c_i x_c(\tau)(n\pi)^2}\Big[2\cos(n\pi x_c(\tau)(c_i\theta_i(\tau)+d_i)) \\ & - \cos(n\pi x_c(\tau)(c_i\theta_{i-1}(\tau)+d_i)) - \cos(n\pi x_c(\tau)(c_i\theta_{i+1}(\tau)+d_i))\Big], \quad (4.62)\end{aligned}$$

where $\theta_i(\tau)$ is defined in equation (4.49) and we recall that c_i and d_i are coefficients which give the best fit to the linear approximation on the subinterval $[\theta_i, \theta_{i+1}]$. Equation (4.51) which accounts for the case $i = 1$ takes the form

$$\begin{aligned}\triangle\tilde{C}_{n,1}(\tau) = {} & \frac{\frac{\triangle}{x_c(\tau)} - c_1\theta_2(\tau) - d_1}{c_1(n\pi)}\sin(n\pi x_c(\tau)(c_1\theta_2(\tau)+d_1)) \\ & + \frac{d_1 - \frac{\triangle}{x_c(\tau)}}{c_1(n\pi)}\sin(n\pi x_c(\tau)d_1) \\ & - \frac{1}{c_1 x_c(\tau)(n\pi)^2}\left[\cos(n\pi x_c(\tau)(c_1\theta_2(\tau)+d_1)) - \cos(n\pi x_c(\tau)d_1)\right], \quad (4.63)\end{aligned}$$

where $\theta_2(\tau)$ is defined in equation (4.51) and c_1 and d_1 are coefficients of the linear approximation on the subinterval $[\theta_1, \theta_2]$. Also for $i = N_c$ we have equation

(4.53) and it can be rewritten as

$$\begin{aligned}\triangle\tilde{C}_{n,N_c}(\tau) = &\frac{\frac{x_{N_c-1}}{x_c(\tau)} - c_{N_c}\theta_{N_c-1}(\tau) - d_{N_c}}{c_{N_c}(n\pi)}\sin(n\pi x_c(\tau)(c_{N_c}\theta_{N_c-1}(\tau)+d_{N_c}))\\ &+\frac{(x_c(\tau)-2)d_{N_c}+2\frac{x_{N_c}}{x_c(\tau)}-x_{N_c-1}}{c_{N_c}(n\pi)}\sin(n\pi x_c(\tau)d_{N_c})\\ &+\frac{1}{c_{N_c}x_c(\tau)(n\pi)^2}[2\cos(n\pi x_c(\tau)(c_{N_c}\theta_{N_c}(\tau)+d_{N_c}))\\ &-\cos(n\pi x_c(\tau)(c_{N_c}\theta_{N_c-1}(\tau)+d_{N_c}))-\cos(n\pi x_c(\tau)d_{N_c})]\\ &+\frac{\pi}{2}(x_{N_c+1}-x_c(\tau))J_0(n\pi x_c(\tau))+(8-\frac{5}{2}\pi)\frac{\sin(n\pi x_c(\tau))}{n\pi}\\ &+(6\pi-18)\frac{1-\cos(n\pi x_c(\tau))}{x_c(\tau)(n\pi)^2},\end{aligned} \tag{4.64}$$

where $\theta_{N_c-1}(\tau)$ is defined in equation (4.54) and c_{N_c} and d_{N_c} are coefficients of the linear approximation on the subinterval $[\theta_{N_c}, \theta_{N_c+1}]$.

We are now ready to describe a numerical procedure to solve equation (4.55). The equation (4.55) is solved in a time interval $t_1 < t < t_M$ say, and the current time step in the computation procedure is at instant, $t = t_K$ say, see the time discretization in Figure 4.27. We introduce the $N \times 1$ vectors $\vec{\eta}^K$ and $\vec{\eta}_0^K$, where the upper index K refers to the time instant $t = t_K$. These vectors have entries $\eta_j(t_K)$ and $\eta_{0,j}(t_K), j = 1, 2, \ldots, N$, respectively. The matrix form of equation (4.55) take the form

$$A\vec{\eta}^K = A\vec{\eta}_o^K - \int_0^{t_K} \mathcal{K}(t_K, \tau)\vec{Q}(\tau)d\tau, \tag{4.65}$$

where the matrix A is a tri-diagonal symmetric matrix, with positive definite entries, $e_{i,q}$ are defined in equation (4.32). The vector $\vec{Q}(\tau)$, which will be time-discretized later on, has entries $Q_j(\tau), j = 1, 2, \ldots, N$. The elements of the matrix $\mathcal{K}(t_K, \tau)$ are $\mathcal{K}_{j,q}(t_K, \tau)$ as defined in (4.56). We assume that the inverse matrix A^{-1} exists. By introducing

$$\widehat{\mathcal{K}}(t_K, \tau) = A^{-1}\mathcal{K}(t_K, \tau), \tag{4.66}$$

the system (4.65) multiplied on the left by A^{-1} can be rewritten as

$$\vec{\eta}^K = \vec{\eta}_0^K - \int_0^{t_K} \widehat{\mathcal{K}}(t_K, \tau)\vec{Q}(\tau)d\tau. \tag{4.67}$$

Recall that here $\vec{\eta}^K$ is the vector which represents the surface elevation with a lid and $\vec{\eta}_0^K$ represents the surface elevation without a lid at $t = t_K$ on the discretized domain shown in Figure 4.2.

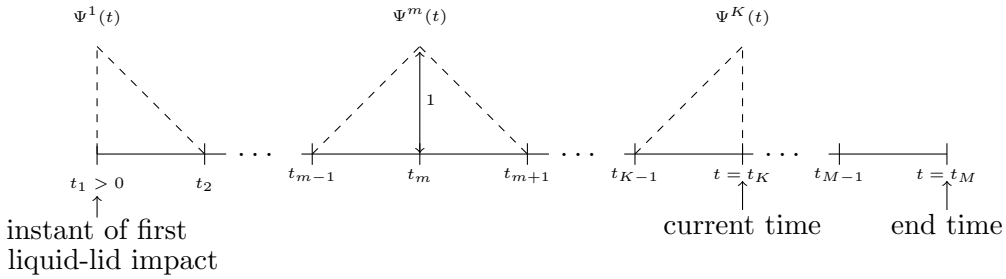

Figure 4.27: Time discretization from $t_1 > 0$ to $t = t_1 + (M-1)\delta = t_M$, where δ is a constant time-increment.

Before the impact, for $t < t_1$, both surface elevations, with and without lid are below $y = 1$, i.e. $\eta_j(t < t_1) < 1$ and $\eta_{0,j}(t < t_1) < 1$, for all $1 \leq j \leq N$, here $y = 1$ refers to the non-dimensional position of the lid. Then after some time steps, it is detected that for all $j \leq N_c$, $\vec{\eta}^1_{0,j} > 1$ and $\vec{\eta}^1_j = 1$, since the lid is rigid. We mention for the reader that N_c is the number of nodes inside the wetted region at some particular time instant. As to the pressure along the wetted region on the lid there will be non-zero fluid pressure and zero pressure on the free surface. Therefore after time-discretization we can identify non-zero and zero elements of the vector $\vec{Q}(\tau)$ using the relation (4.37). Starting from $t = t_1$, the instant of impact, the system (4.67) reads

$$\vec{\eta}^K = \vec{\eta}^K_o - \int_{t_1}^{t_K} \widehat{\mathcal{K}}(t_K, \tau)\vec{Q}(\tau)d\tau, \qquad \text{for} \quad t_K \geq t_1. \tag{4.68}$$

One should notice that $\eta_j(t < t_1) = \eta_{0,j}(t < t_1)$ for all j: $1 \leq j \leq N$. Time discretization will give us the chance to simplify and then calculate analytically the integral in the system (4.68). Figure 4.27 shows the uniform discretization of the interval of time-integration into $M-1$ small time intervals. Each time step is defined as $t_m = t_1 + (m-1)\delta$ for $1 \leq m \leq M$, where $\delta = \frac{t_M - t_1}{M-1}$ is the time-increment. The smaller the value of δ, the more detail is captured of the overall sloshing behaviour. However, the choice of δ depends on the nature of the particular problem. During our investigations with small time increments we found the system unstable. This complication was then treated well by the Tikhonov regularization method, see (Tikhonov & Arsenin 1977), which will be discussed in more detail in next section.

During time discretization one seeks to approximate the vector $\vec{Q}(\tau)$ along

the lid by projection given by

$$Q_i(\tau) = \sum_{m=1}^{K} Q_i^m \Psi^m(\tau), \tag{4.69}$$

where $i \in \{1, \ldots, N\}$ for every node $x = x_i$, and the linear hat function $\Psi^m(\tau)$ is defined by

$$\Psi^m(\tau) = \frac{1}{\delta} \begin{cases} \tau - t_{m-1} & t_{m-1} \leq \tau \leq t_m, \\ t_{m+1} - \tau & t_m \leq \tau \leq t_{m+1}\ , \\ 0 & \textit{otherwise}, \end{cases} \tag{4.70}$$

for $2 \leq m \leq K-1$. Also for the two cases $m = 1$ and $m = K$ separately are, respectively, defined as

$$\Psi^1(\tau) = \frac{1}{\delta} \begin{cases} t_2 - \tau & t_1 \leq \tau \leq t_2, \\ 0 & \textit{otherwise}, \end{cases} \tag{4.71}$$

$$\Psi^K(\tau) = \frac{1}{\delta} \begin{cases} \tau - t_K + \delta & t_{K-1} \leq \tau \leq t_K, \\ 0 & \textit{otherwise}. \end{cases} \tag{4.72}$$

Using equation (4.69) the integral in the right-hand side of the system (4.68) takes the form

$$\int_{t_1}^{t_K} \widehat{\mathcal{K}}(t_K, \tau)\vec{Q}(\tau)d\tau = A^{-1} \sum_{i=1}^{N} \sum_{m=1}^{K} Q_i^m \int_{t_1}^{t_K} \mathcal{K}_{i,q}(t_K, \tau)\Psi^m(\tau)d\tau. \tag{4.73}$$

The pressure and surface elevation are unknown at each instant $t = t_K$ of the time stepping, and must be determined by using the previous time steps information. In other words, for all $t = t_m$ such that $1 \leq m \leq K-1$, the coefficients Q_i^m and $\eta_j(t_m)$ are known for all $1 \leq i, j \leq N$. Therefore right-hand side of (4.73) can be written

$$\begin{aligned} A^{-1} \sum_{i=1}^{N} \sum_{m=1}^{K} Q_i^m \int_{t_1}^{t_K} \mathcal{K}_{i,q}(t_K, \tau)\Psi^m(\tau)d\tau \\ &= A^{-1} \sum_{i=1}^{N} \sum_{m=1}^{K-1} Q_i^m \int_{t_1}^{t_K} \mathcal{K}_{i,q}(t_K, \tau)\Psi^m(\tau)d\tau \\ &+ A^{-1} \sum_{i=1}^{N} Q_i^K \int_{t_{K-1}}^{t_K} \mathcal{K}_{i,q}(t_K, \tau)\Psi^K(\tau)d\tau. \end{aligned} \tag{4.74}$$

We discuss the two integrals on the right-hand side of (4.74) separately. The second integral on the right-hand side of equation (4.74), denoted by $\varkappa_{i,q}^K$, is

related to the time step $t = t_K$. By applying the change of variable $t_K - \tau = \mu$ and using equation (4.72) we find

$$\begin{aligned}\varkappa_{i,q}^K &= \int_0^\delta (1 - \frac{\mu}{\delta})\mathcal{K}_{i,q}(t_K, \mu)d\mu \\ &= 2\sum_{n=1}^{\infty} \omega_n C_{n,q} \int_0^\delta \tilde{C}_{n,i}(t_K, \mu)(1 - \frac{\mu}{\delta}) \sin(\omega_n \mu)d\mu. \end{aligned} \tag{4.75}$$

At this stage it is convenient to approximate the time-dependent coefficient $\tilde{C}_{n,i}(t_K, \mu)$ in (4.75) by

$$\tilde{C}_{n,i}(t_K, \mu) \simeq \tilde{C}_{n,i}(t_K, \hat{\delta}), \tag{4.76}$$

where $\hat{\delta} = \frac{\delta}{2}$ is the midpoint of the interval of integration. We can do this because the integrand is continuous and the interval of integration in (4.75) is very small. From equations (4.75) and using the approximation (4.76), we arrive at

$$\varkappa_{i,q}^K = 2\sum_{n=1}^{\infty} C_{n,q}\ \tilde{C}_{n,i}(t_K, \hat{\delta}) \left(1 - \frac{\sin(\omega_n \delta)}{\omega_n \delta}\right). \tag{4.77}$$

Equation (4.77) is to be evaluated at $t = t_K$ for $1 \leq i, q \leq N$ which $\tilde{C}_{n,i}(t_K, \hat{\delta})$ is the only time-dependent coefficient.

The first integral on the right-hand side of equation (4.74), denoted by $\Lambda_{i,q}^{m,K}$, accounts for the previous time steps. This coefficient depends on both t_m and t_K. Again we apply the approximation (4.76) to the coefficient $\tilde{C}_{n,i}(\tau)$ with the difference that the midpoint of the integral interval is $t = t_m$ due to a change in this integral's lower and upper limits $t = t_{m-1}$ and $t = t_{m+1}$, respectively. That is

$$\tilde{C}_{n,i}(\tau) \simeq \tilde{C}_{n,i}(t_m), \qquad \text{for} \quad t_{m-1} \leq t \leq t_{m+1}. \tag{4.78}$$

Hence with approximation (4.78) the coefficient $\Lambda_{i,q}^{m,K}$ now reads

$$\begin{aligned}\Lambda_{i,q}^{m,K} &= \int_{t_1}^{t_K} \Psi^m(\tau)\mathcal{K}_{i,q}(t_K, \tau)d\tau \\ &= \int_{t_{m-1}}^{t_{m+1}} \Psi^m(\tau)\mathcal{K}_{i,q}(t_K, \tau)d\tau \\ &= 2\sum_{n=1}^{\infty} \omega_n \tilde{C}_{n,i}(t_m) C_{n,q} \int_{t_{m-1}}^{t_{m+1}} \Psi^m(\tau) \sin(\omega_n(t_K - \tau))d\tau, \end{aligned} \tag{4.79}$$

for $2 \leq m \leq K - 1$, where

$$\int_{t_{m-1}}^{t_{m+1}} \Psi^m(\tau)\sin(\omega_n(t_K-\tau))d\tau$$
$$= \frac{1}{\delta\omega_n^2}\left[2\sin(\omega_n(t_K-t_m)) - \sin(\omega_n(t_K-t_{m-1})) - \sin\left(\omega_n(t_K-t_{m+1})\right)\right],$$
$$= \frac{-4}{\delta\omega_n^2}\sin^2\left(\omega_n\frac{\delta}{2}\right)\sin(\omega_n(t_K-t_m)). \tag{4.80}$$

Finally the system (4.68) can be rearranged as follows

$$\vec{\eta}^K = \vec{\eta}_0^K - A^{-1}B^K\vec{Q}^K - A^{-1}\sum_{m=1}^{K-1} G^{m,K}\vec{Q}^m, \tag{4.81}$$

where B_K is an $N \times N$ matrix with entries $\varkappa_{i,q}^K$ defined in equation (4.77), the vector $\vec{Q}^K$ contains unknown coefficients of the function $Q(x,t)$ at the instant $t = t_K$. Also $N \times N$ matrix $G^{m,K}$ contains the coefficients $\Lambda_{j,q}^{m,K}$ given in equation (4.79) and the vector $\vec{Q}^m$ contains the known coefficients of function $Q(x,t)$ found from the previous time steps. To make it straightforward we move all unknowns in the system (4.81) to the left left-hand side, to arrive at

$$\vec{\eta}^K + A^{-1}B^K\vec{Q}^K = \vec{F}^K, \tag{4.82}$$

where

$$\vec{F}^K = \vec{\eta}_0^K - A^{-1}\sum_{m=1}^{K-1} G^{m,K}\vec{Q}^m. \tag{4.83}$$

To give a short description of how the system (4.82) works we assume that the nodes $x = x_1 = 0$ up to $x = x_{N_c}$, for some $1 < N_c < N$, are in the contact region at some instant $t = t_K$. This leaves us with the remaining nodes, $x = x_{N_c+1}$ up to $x = x_N = 1$ which represent the free surface, where

$$Q_i^K = 0 \qquad \text{for all} \quad i = N_c+1, N_c+2\ldots, N. \tag{4.84}$$

This means only the first N_cth elements of the vector $\vec{Q}^K$ are unknown and, the remaining elements are zero. On the other hand, the first N_cth elements of the surface elevation vector $\vec{\eta}^K$ are known by the fact that the lid has known position and that fluid can not pass above it. That is in the wetted zone:

$$\eta_j(t_K) = 1 \qquad \text{for all} \quad j = 1, 2, \ldots, N_c, \tag{4.85}$$

and the other $(N - N_c)$th elements, $\eta_j(t_K)$ for $j = N_c+1, N_c+2\ldots, N$, are to be determined which represent the free-surface elevation at $t = t_K$. The elements of the vector $\vec{\eta}_0^K$ are to be updated at each time step using equation (2.40) which

stands for the solution of the problem without a lid, provided in section 2.2.3. In this way the system (4.82) has N linear equations with N unknowns at every time step of evolution. From the above description, at the nodes where the elements of the elevation are known, the corresponding elements of the pressure are unknown. On the other hand, the elements of the pressure on the free surface are known while the corresponding elements of the elevation are unknown. Hence after some rearrangement system (4.82) can be presented in a matrix form as follows

$$\mathbf{A}\vec{X} = \vec{b}, \tag{4.86}$$

where $\mathbf{A}$ is a combined coefficients matrix of the corresponding unknown pressure and surface elevation elements. In the same manner $\vec{X}$ is the unknown vector at the instant $t = t^K$. The vector $\vec{b}$ is the right-hand side of the system (4.82) along with the coefficients of the known surface elevation moved from the left-hand side.

In the next section we will discuss the behaviour of the system (4.86), whether it is well-conditioned or ill-conditioned. Only after analysing the system (4.86) we can confirm the reliability of its solution. In the next section we investigate why our system is ill-conditioned and what is needed to convert it to a well-conditioned problem.

4.5 Regularization

To understand the properties of the system (4.86), the singular value decomposition (SVD) is needed, see (Press 2007). The singular value decomposition on $\mathbf{A}$ takes the form

$$\mathbf{A} = U\Sigma V^{\mathrm{T}}, \tag{4.87}$$

where the subscript T stands for the matrix transpose, and U and V are $N \times N$ matrices with column entries u_i and v_i for $i = 1, 2, \ldots, N$. Also Σ is an $N \times N$ diagonal matrix with non-negative diagonal entries σ_i placed in order of decreasing size. The elements σ_i are called *singular values* and have the defining properties:

$$\mathbf{A}v_i = \sigma_i u_i, \qquad \mathbf{A}^{\mathrm{T}}u_i = \sigma_i v_i. \tag{4.88}$$

According to (Hansen 1994) and (Aster, Borchers & Thurber 2011), discrete ill-conditioned problems have the following properties:

1. monotone decrease of the singular values towards zero as i increases to N;

2. the *condition number* (the ratio of the largest to the smallest singular value) is very large.

The first property is illustrated in Figure 4.28 where it is shown that the singular values of the matrix **A** of the system (4.86) decay to zero. The rapid decrease in the singular values refer to the fact that the matrix **A** is a combination of the coefficients of the two unknowns, pressure and surface elevation elements. When the two sets of unknowns combine and one has singularity, the problem becomes even more complicated.

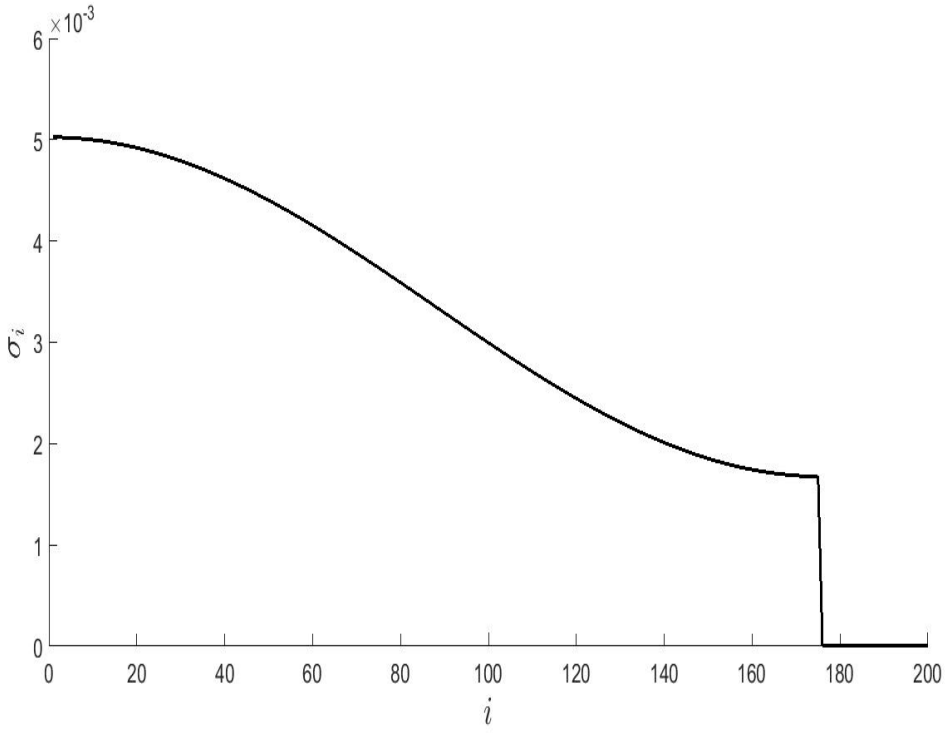

Figure 4.28: Singular values σ_i for $1 \leq i \leq N$ of the matrix **A**. The maximum singular values is 0.00503 and the minimum is 1.0891×10^{-8} with their ratio leads to a large condition number 4.6137×10^5 at $t = 0.0397$ with $N = 200$. The sudden decline of the curve is a result of the structure of the matrix **A**, which is a combined coefficients matrix of the corresponding unknown pressure and surface elevation elements

Also as to the second property, the condition number for the matrix **A**, which is the ratio between the largest and the smallest nonzero singular values of the matrix **A**, is of $O(10^5)$ at $t = 0.0397$. This means that the condition number is so much greater than unity, that the solution will be very sensitive to errors, perturbations and finite rounding arithmetic. To reduce the condition number we will use a regularization method introduced by (Tikhonov & Arsenin 1977). The aim of the Tikhonov regularization is to filter out the noise caused by small singular values as shown in the following solution of (4.86)

$$\vec{X} = \sum_{i=1}^{N} \frac{u_i^T \vec{b}}{\sigma_i} v_i, \tag{4.89}$$

where the SVD of $\mathbf{A}$ (4.87) and the definition of the singular values (4.88) are used to derive this solution. There are some other regularization methods like Truncated Singular Value Decomposition (TSVD), and some iterative methods that are widely in use in inverse problems for dealing with ill-conditioned problems in order to obtain an approximate noise-free solutions, see (Neumaier 1998), (Aster et al. 2011) and the references therein. We apply Tikhonov regularization to our problem (4.86), which requires us to compute the solution $\vec{X}_{\bar{\alpha}}$ such that

$$\vec{X}_{\bar{\alpha}} = \vec{X} : \min_{\vec{X}} \left\{ \left\| \mathbf{A}\vec{X} - \vec{b} \right\|_2^2 + \bar{\alpha}^2 \left\| \mathbf{L} \left(\vec{X} - \vec{X}_0 \right) \right\|_2^2 \right\}, \tag{4.90}$$

(where $\| \cdot \|_2$ is the Euclidean norm) which is equivalent to solving

$$\vec{X}_{\bar{\alpha}} = \left(\mathbf{A}^{\mathrm{T}} \mathbf{A} + \bar{\alpha}^2 \mathbf{L}^{\mathrm{T}} \mathbf{L} \right)^{-1} \left(\mathbf{A}^{\mathrm{T}} \vec{b} + \bar{\alpha}^2 \mathbf{L}^{\mathrm{T}} \mathbf{L} \vec{X}_0 \right), \tag{4.91}$$

where $\bar{\alpha}$ is the regularization parameter, $\vec{X}_{\bar{\alpha}}$ is the solution corresponding to the regularization parameter $\bar{\alpha}$ and $\mathbf{L}$ is a matrix which has to be chosen depending on the particular problem. We choose $\mathbf{L} = \mathbf{I}$, the identity matrix, which is the standard form, or the zeroth-order Tikhonov regularization. For higher order regularization and choosing the matrix $\mathbf{L}$, see (Neumaier 1998) and (Hansen 1994). Also $\vec{X}_0$ is *a priori* estimate of the solution. By $\| \cdot \|_2$ in (4.91) we mean the Euclidean norm (2-norm), which can be evaluated in MATLAB by using the built-in command: norm(A,2) or norm(A).

By choosing $\mathbf{L} = \mathbf{I}$ and $\vec{X}_0 = 0$, the solution (4.91) in its SVD form takes the form:

$$\vec{X} = \sum_{i=1}^{N} \mathcal{F}_i \frac{u_i^T \vec{b}}{\sigma_i} v_i, \tag{4.92}$$

where $\mathcal{F}_1, \ldots, \mathcal{F}_N$ are so-called Tikhonov regularization filters which are defined as

$$\mathcal{F}_i = \frac{\sigma_i^2}{\sigma_i^2 + \bar{\alpha}^2}. \tag{4.93}$$

The Tikhonov filter $\mathcal{F}_i$ is of $O(1)$ for $\sigma_i \gg \bar{\alpha}$ and is of $O(\frac{\sigma_i^2}{\bar{\alpha}^2})$ for $\sigma_i \ll \bar{\alpha}$. The regularization parameter $\bar{\alpha}$ is sensitive and is an important parameter. Determining this parameter is a typical process of the regularization methods. We used the so-called L-curve and the l-corner methods given in the MATLAB package (regularization tools) by (Hansen 1994) to choose the optimal parameter $\bar{\alpha}$. The

L-curve method (see (Hansen & O'Leary 1993)) is a strategy for choosing the regularization parameter. This piecewise linear curve consists of a log-log plot of the residual norm $\left\|\mathbf{A}\vec{X}_{\bar{\alpha}} - \vec{b}\right\|_2$ (vertical axis) and solution norm $\left\|\mathbf{L}\left(\vec{X}_{\bar{\alpha}} - \vec{X}_0\right)\right\|_2$ (horizontal axis). See Figure 4.29.

If the solution norm is very large this means that too much regularization is imposed on the solution and it does not fit the data $\vec{b}$. On the other hand, adding too little regularization to the solution leads to a dominant contribution from the data error and consequently a large growth in the solution norm to unreasonable values. This trade-off is controlled by the so-called optimal regularization parameter $\bar{\alpha}$.

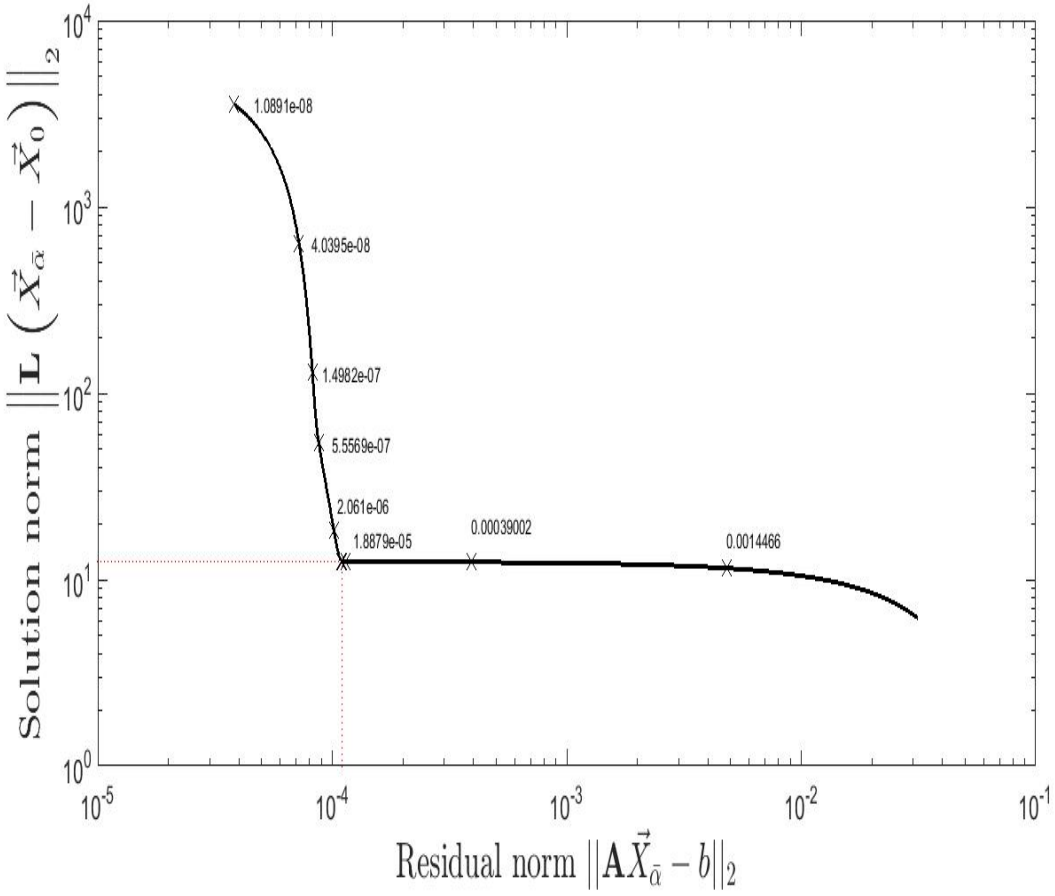

Figure 4.29: The L-curve for the Tikhonov regularization (4.91). Horizontal axes is the residual norm $\left\|\mathbf{A}\vec{X}_{\bar{\alpha}} - \vec{b}\right\|_2$ versus the vertical axes which is the corresponding solution norm $\left\|\mathbf{L}\left(\vec{X}_{\bar{\alpha}} - \vec{X}_0\right)\right\|_2$, with $N = 200$. The stars correspond to the different values of regularization parameters $\bar{\alpha}$, only few of 200 evaluated regularization parameters are shown. At $t = 0.0397$ the optimal value is found on the corner to be $\bar{\alpha} = 1.8879 \times 10^{-5}$.

In Figure 4.29 the L-curve of the problem (4.91) is drawn. From this we see a corner of the curve occurs at time $t = 0.0397$. The l-corner in the regularization

tools of (Hansen 1994) returns the optimal value for the regularization parameter $\bar{\alpha}$ for the problem. The curve is the norm of the regularized solution versus the norm of the corresponding residual as a function of the parameter $\bar{\alpha}$. Since the entries of $\mathbf{A}$ and $\bar{b}$ are time dependent, the procedure of optimizing the regularization parameter is implemented simultaneously for every time step, as shown in Figures 4.29 and 4.30.

Figure 4.30 shows the singular values of the stabilized problem (4.91). Although the maximum singular value is still small, the gradual decay to zero has disappeared. In other words, the condition number drops close to one after regularization. In the next section we will discuss the algorithm of the computation on the regularized problem (4.91). For the sudden decline of the curve read caption in Figure 4.28.

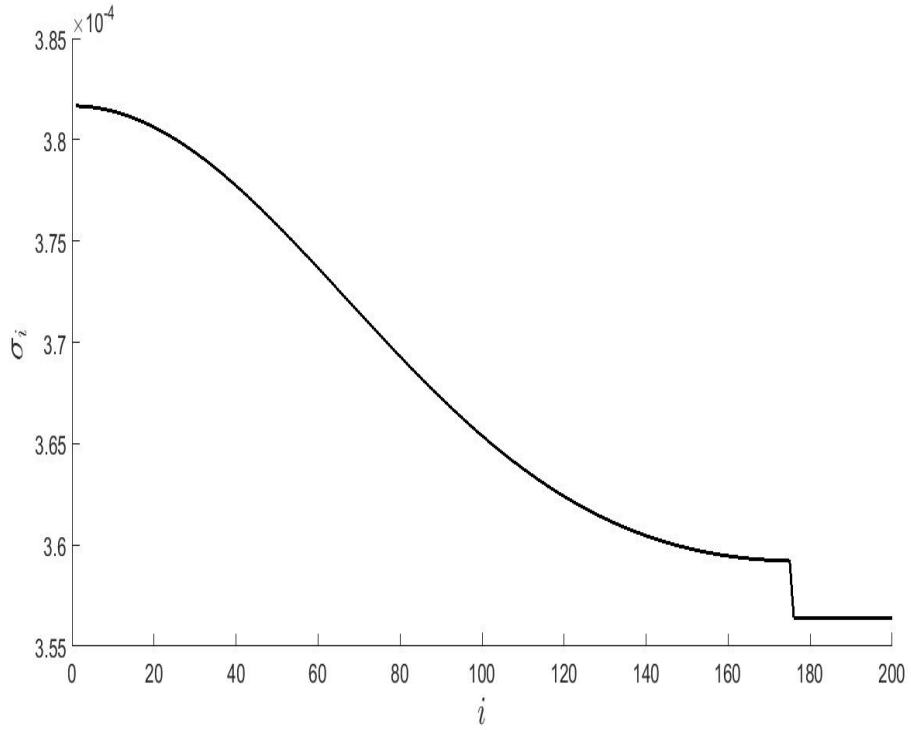

Figure 4.30: Singular values σ_i for $1 \leq i \leq N$ of the matrix $\left(\mathbf{A}^{\mathrm{T}}\mathbf{A} + \bar{\alpha}^2\mathbf{L}^{\mathrm{T}}\mathbf{L}\right)$ after Tikhonov regularization has been applied. The maximum singular values is 0.006425 and the minimum 0.006400 so that their ratio is close to the unity: condition number 1.0708 at $t = 0.0397$ with $N = 200$. Note the small range of values on the vertical axis.

4.6 Numerical algorithm and results

In this section we compute the surface elevation and pressure distribution, along with the moving contact point, $x = x_c(t)$. The computations rely on the semi-analytical results from previous Chapters as an initial estimate. For instance we

use the moving contact point with gravity as the first estimate for x_c, but the adjustment to x_c is carried forward in time as explained below.

The important and challenging part of this procedure is to determine the moving contact point position, $x = x_c(t)$ at every time step. Only after determining its position can we distinguish between the free surface and the wetted region. We know that many things are happening near this point. For example $x = x_c(t)$ separates the free surface from the wetted region, and the pressure is singular at this point. An inaccurate position of the moving contact point would lead us to an irregular free-surface elevation, or an irregular pressure distribution, or both. Therefore this point must be updated correctly very carefully at each time step. The decision for fixing its position must be consistent with the free-surface elevation's profile lying below the lid and the pressure distribution being reasonable on the wetted region.

For determining the moving contact point position, $x = x_c(t)$, it is reasonable to use the semi-analytical solution for this point found in previous chapter, moving contact point with correction due to gravity. After we determined the surface elevation, we use the discretized surface elevation (4.28) at $x = x_c(t)$ for any required adjustment on the position of the moving contact point $x = x_c(t)$. This equation at $x = x_c(t)$ can be rewritten as

$$\eta(x_c(t), t) = \frac{x_{N_{c+1}} - x_c(t)}{\triangle}\eta_{N_c}(t) + \frac{x_c(t) - x_{N_c}}{\triangle}\eta_{N_{c+1}}(t). \tag{4.94}$$

By required adjustment we mean that the surface elevation must be in contact with the lid at $x = x_c(t)$, the Wagner condition. That is

$$\frac{x_{N_{c+1}} - x_c(t)}{\triangle}\eta_{N_c}(t) + \frac{x_c(t) - x_{N_c}}{\triangle}\eta_{N_{c+1}}(t) = 1. \tag{4.95}$$

Otherwise, if it is above the lid at the moving contact point, $x = x_c(t)$ then

$$\frac{x_{N_{c+1}} - x_c(t)}{\triangle}\eta_{N_c}(t) + \frac{x_c(t) - x_{N_c}}{\triangle}\eta_{N_{c+1}}(t) > 1, \tag{4.96}$$

then we replace the moving contact point, $x = x_c(t)$ by $\frac{x_{N_{c+1}} + x_c(t)}{2}$, else if

$$\frac{x_{N_{c+1}} - x_c(t)}{\triangle}\eta_{N_c}(t) + \frac{x_c(t) - x_{N_c}}{\triangle}\eta_{N_{c+1}}(t) < 1, \tag{4.97}$$

then we replace the moving contact point, $x = x_c(t)$ by $x = \frac{x_{N_c} + x_c(t)}{2}$. This process is continue until condition (4.95) is satisfied or the difference $|\eta(x_c(t), t) - 1| < \epsilon_1$, for some small value of ϵ_1.

Thanks to the Tikhonov regularization method of (Tikhonov & Arsenin 1977), we stabilised the ill-conditioned problem (4.86) to become a well-conditioned

problem (4.91). This is accomplished with the selected optimal regularization parameter $\bar{\alpha}$, see (Hansen 1999), Figures 4.29 and 4.34. The computation code is written in Matlab. It is carried out with regular discretisasion on the right half of the lid $[0, 1]$, with $N = 200$ nodes. The truncation to a partial sum $S_{\bar{n}}$ for the infinite series in equations (4.77) and (4.79) is taken with $\bar{n} = 500$, which we showed earlier is sufficiently accurate.

Figures 4.31–4.32 show the smooth function $Q(x, t)$ along the wetted region at two different chosen instants. A very small difference between the behaviour of $Q(x, t)$ with and without gravity is detected in Figure 4.31 when the impact is at its most rapid stage. Hence a negligible influence of gravity in this stage is obvious. However, as time goes on, the difference becomes more visible as depicted in Figure 4.32. Also note the difference in the extension of the wetted region in both of these figures. The pressure distribution corresponding to the smooth function $Q(x, t)$ at time $t = 0.4397$ is shown in Figure 4.33. Again it is found that the extension of the wetted region is shortened by the influence of gravity at this stage of the impact. Also a significant negative pressure is depicted. It is worth taking very carefully this negative pressure into consideration. It could be a sign of a potentially damaging negative force on the tank's lid as the fluid enters the exit stage. It is not yet clear how an elastic lid would response to this negative pressure caused by an impact. For the hydroelastic impacts in an LNG carrier's containment system, see (Ten et al. 2011) and (Malenica et al. 2006).
At the same previously mentioned instant, the shape of the surface elevation is plotted in Figures 4.35–4.36. In these figures a comparison is made between the surface elevation in three different problems, the surface elevation in the problem with no lid and with gravity (analytically evaluated); that with lid and no gravity (semi-analytically evaluated); that with lid and gravity (numerically evaluated). The same effect due to the influence of gravity as discussed for the smooth function $Q(x, t)$ is applied to the surface elevation.

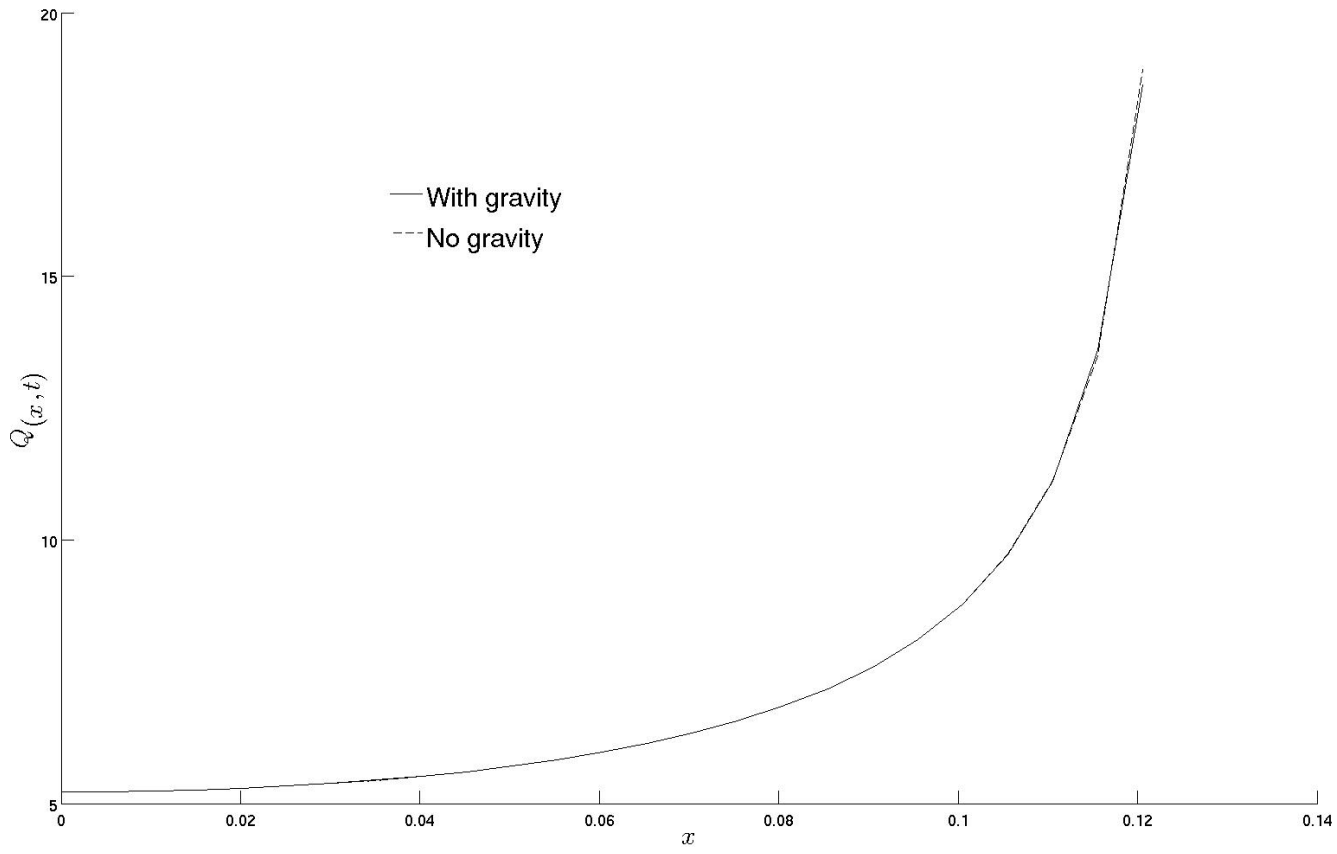

Figure 4.31: The function $Q(x,t)$, solid line with gravity and dashed line with no gravity at $t = 0.0397$ with $N = 200$ and $\bar{\alpha} = 1.8879 \times 10^{-5}$.

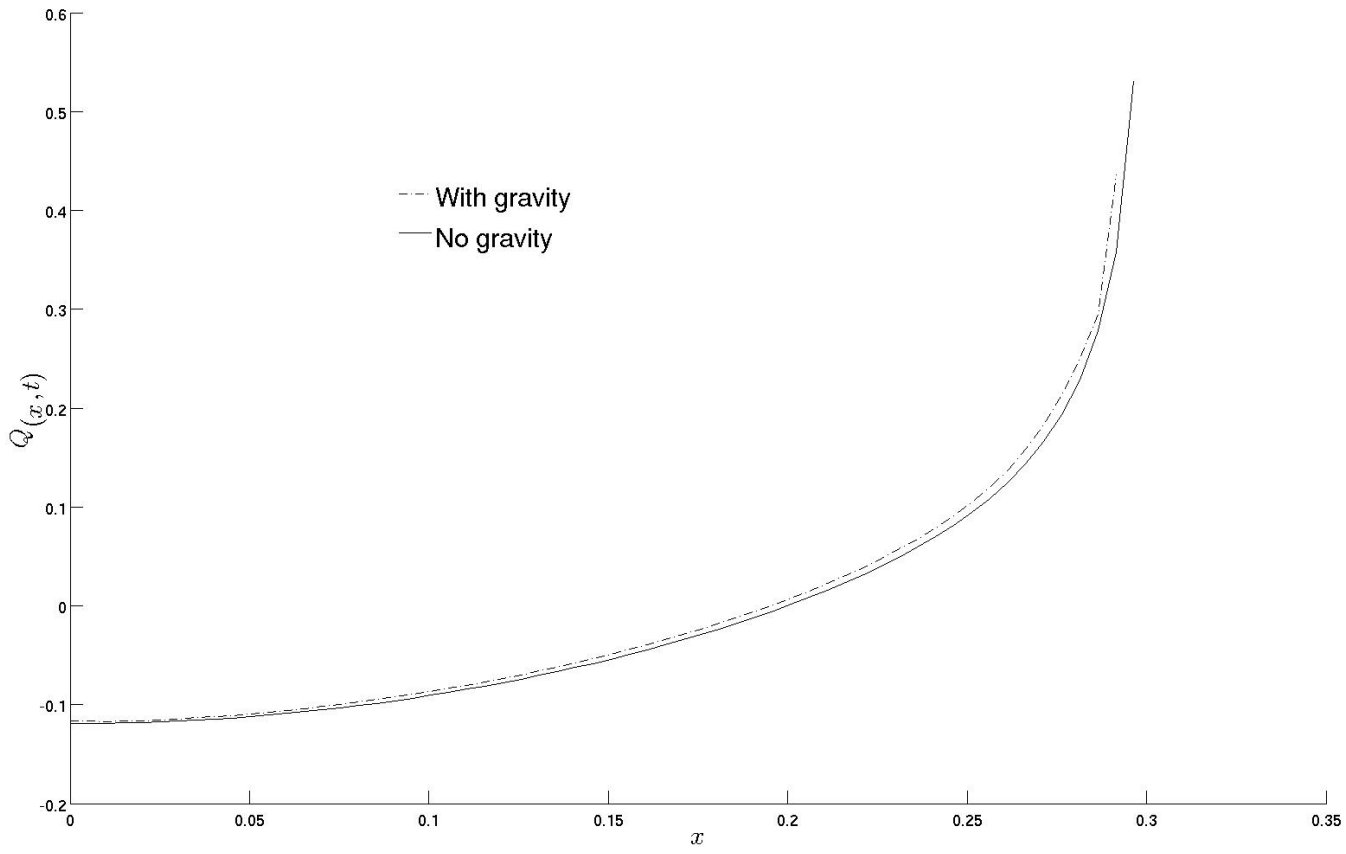

Figure 4.32: The function $Q(x,t)$ magnified over the wetted region, dashed line with gravity and solid line with no gravity at $t = 0.4397$ with $N = 200$ and $\bar{\alpha} = 3.8821 \times 10^{-5}$.

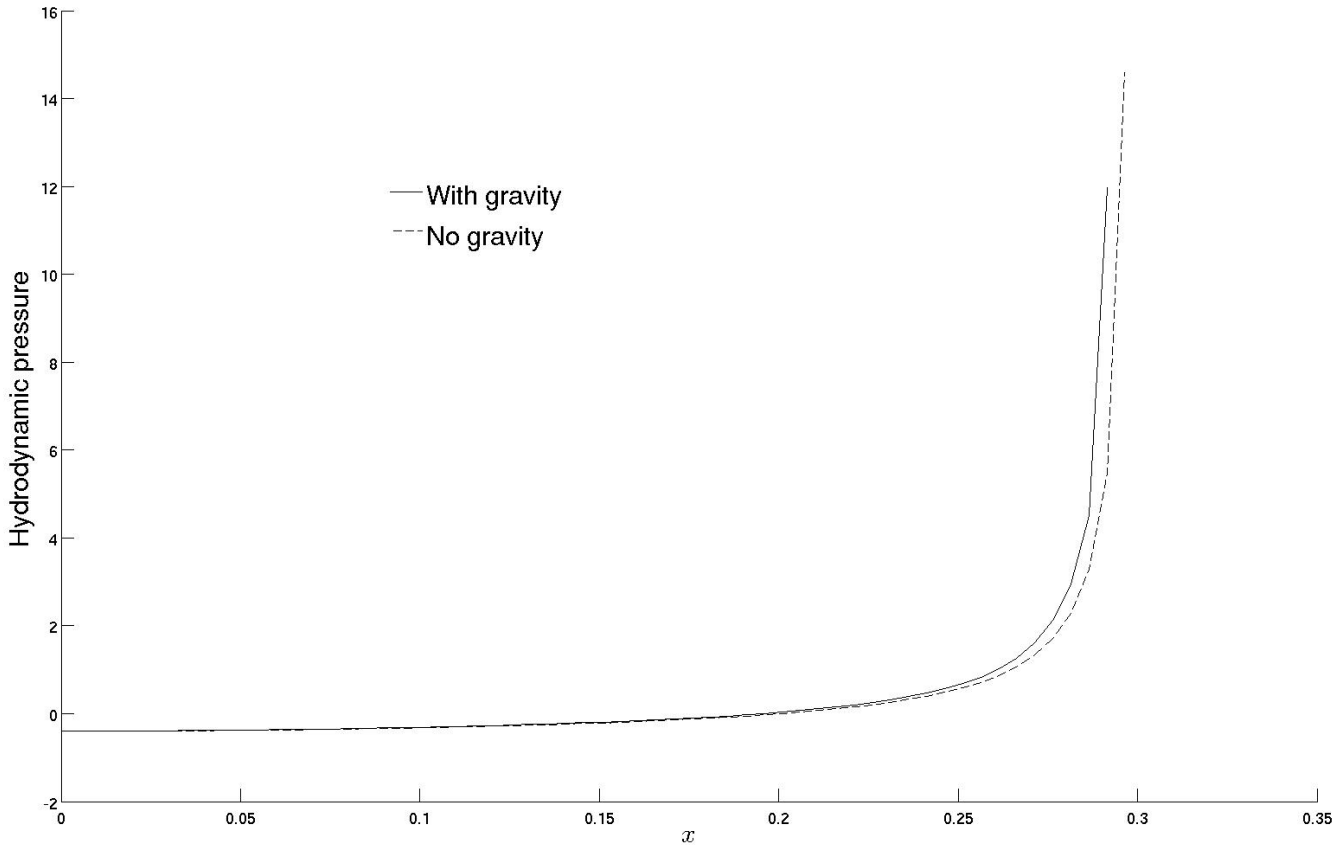

Figure 4.33: The hydrodynamic pressure distribution along the wetted region, solid line with gravity and dashed line with no gravity at $t = 0.4397$ with $N = 200$ and $\bar{\alpha} = 3.8821 \times 10^{-5}$.

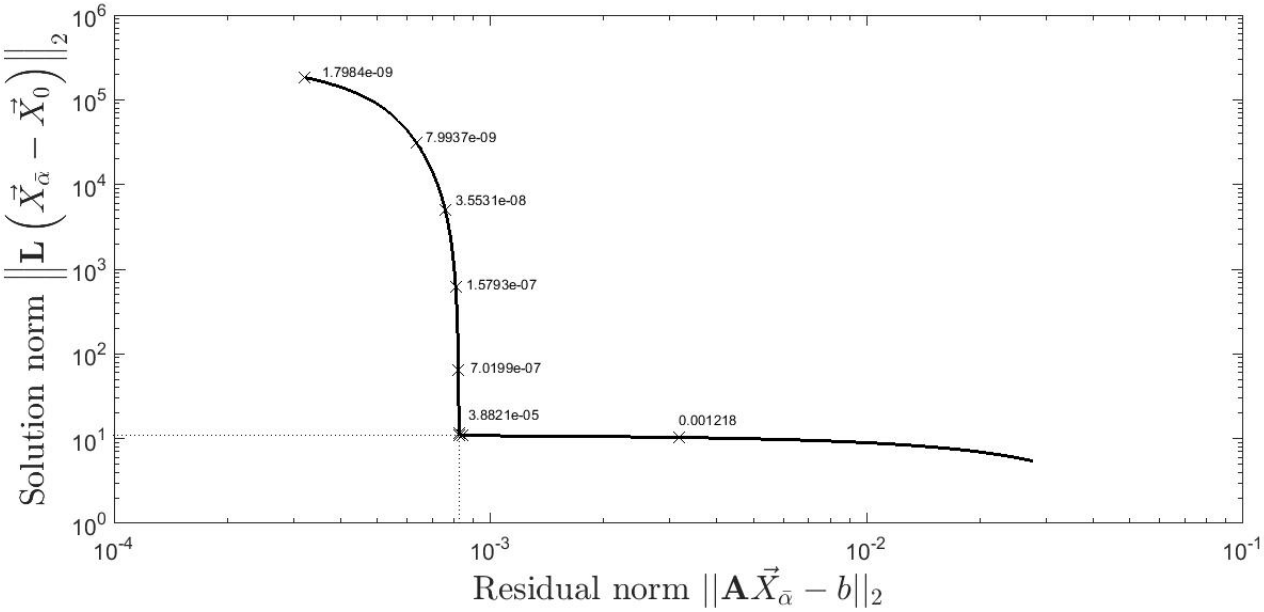

Figure 4.34: The L-curve for the Tikhonov regularization (4.91). Horizontal axis is the residual norm $\left\|\mathbf{A}\vec{X}_{\bar{\alpha}}-\vec{b}\right\|_2$ versus the vertical axis which is the corresponding solution norm $\left\|\mathbf{L}\left(\vec{X}_{\bar{\alpha}}-\vec{X}_0\right)\right\|_2$, with $N = 200$. The stars correspond to the different values of regularization parameters $\bar{\alpha}$, only a few of the 200 evaluated regularization parameter values are shown. At $t = 0.4397$ the optimal value is found at the corner to be $\bar{\alpha} = 3.8821 \times 10^{-5}$.

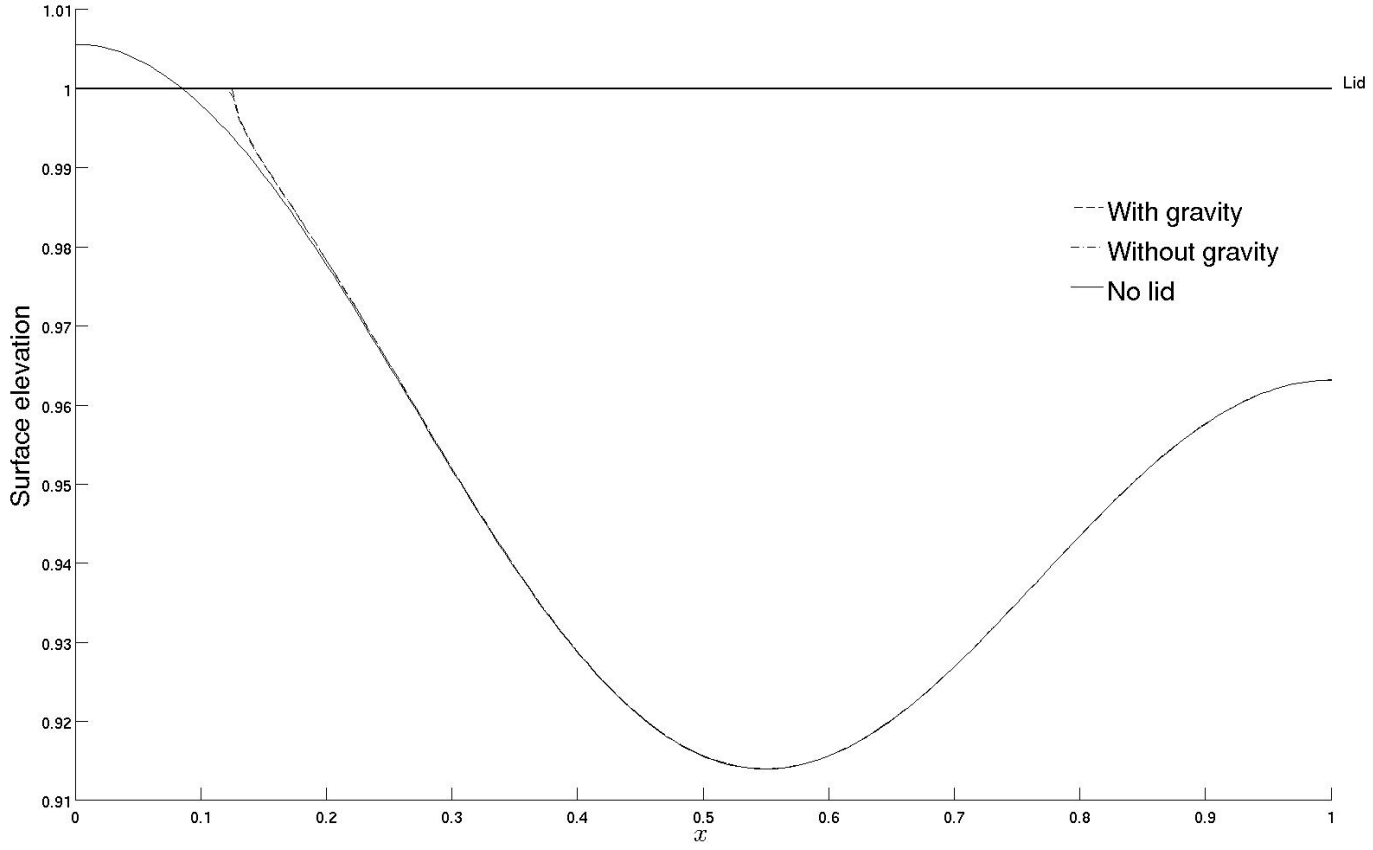

Figure 4.35: The surface elevation, dashed line with gravity (with lid), dotted line with no gravity (with lid) and solid line with gravity (no lid) at $t = 0.0397$ with $N = 200$ and $\bar{\alpha} = 1.8879 \times 10^{-5}$. It is shown that gravity changes nothing during the early stage of impact.

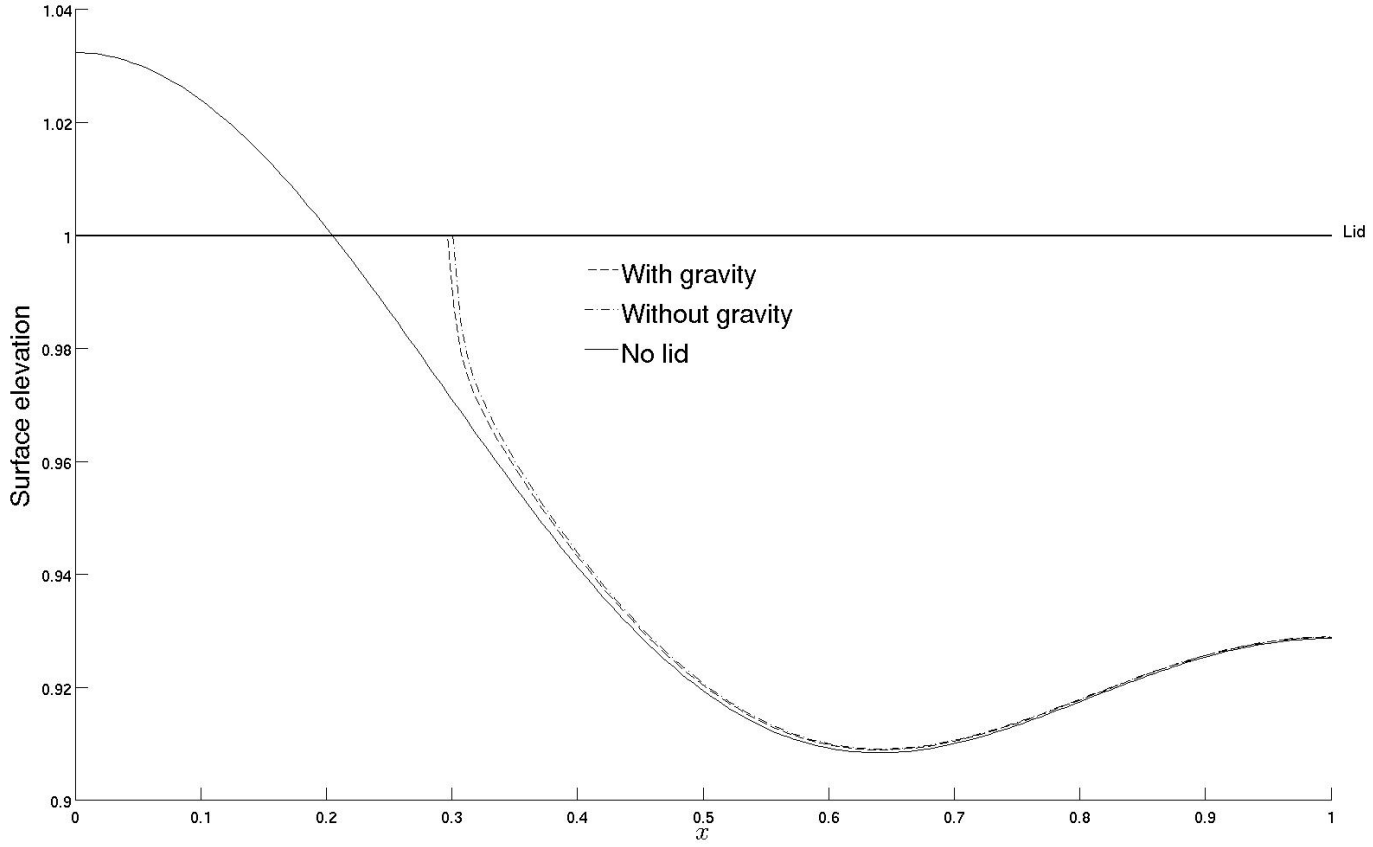

Figure 4.36: The surface elevation, dashed line with gravity (with lid), dotted line with no gravity (with lid) and solid line with gravity (no lid) at $t = 0.4397$ with $N = 200$ and $\bar{\alpha} = 3.8821 \times 10^{-5}$. The contribution of gravity is significant on both the wetted region's width and surface elevation.

Chapter 5

Water-entry problem with gravity included

The two-dimensional water-entry problem considered in this chapter is the normal impact of a smooth body with low constant velocity onto a horizontal free surface of a fluid. The impacting body is nearly flat, see Figure 5.1, and the fluid is inviscid. The water-entry problem has been investigated since the work of (Wagner 1932). The vertical impact by two-dimensional bodies of different shape with constant velocity has been studied by, for example, (Howison et al. 1991), (Zhao & Faltinsen 1993), (Oliver 2002) and (Howison, Ockendon & Oliver 2004). For three-dimensional water-entry problem see (Scolan & Korobkin 2001) and (Korobkin & Khabakhpasheva 2006). Also the problem of water-entry with high horizontal velocity was studied with account for elasticity of the body surface by (Reinhard et al. 2013). In the present study, the body is rigid and the impact is started from a single point, therefore no air entrainment occurs during the body penetration into the fluid.

The aim of this chapter is to investigate the influence of gravity on the vertical water-entry problem. We analyse the gravity effect on some physical properties including: size of the wetted body, force acting on the body, pressure distribution along the wetted body and the energy distribution.

5.1 Problem description and formulation

In this Chapter the initial stage of water impact with constant low speed V is considered. The duration of this stage, T, is formal. The problem is two-dimensional. The flow is potential and symmetric, see Figure 5.1. The position

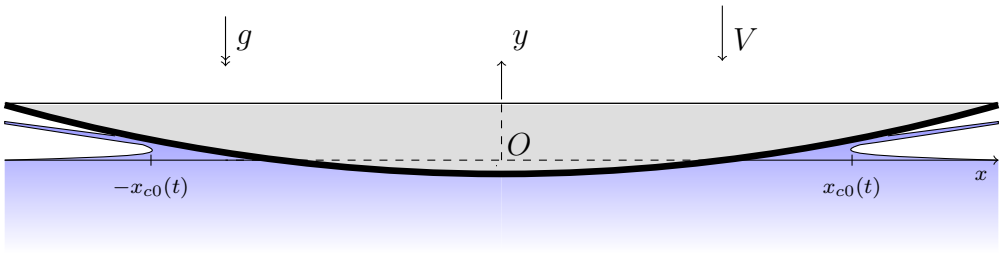

Figure 5.1: Water entry at small time after the body started to penetrate the fluid with constant downward velocity V.

of the body is described by the equation

$$y = \frac{x^2}{2R} - Vt, \tag{5.1}$$

with respect to the coordinates such that $y = 0$ is the undisturbed water surface before impact, and where R is the radius of curvature of the body at its lowest point. Non-dimensional variables denoted by hat are introduced by

$$x = X_{sc}\hat{x}, \quad y = X_{sc}\hat{y}, \quad t = T\hat{t}, \tag{5.2}$$

where X_{sc} is a length scale to be determined. Equation (5.1) in the non-dimensional variables reads

$$X_{sc}\hat{y} = \frac{X_{sc}^2}{2R}\hat{x}^2 - VT\hat{t}. \tag{5.3}$$

Setting $\frac{X_{sc}^2}{R} = VT$, $\frac{VT}{X_{sc}} = \epsilon$, where ϵ is a small parameter of the problem in the following analysis, we obtain

$$X_{sc} = \sqrt{RVT}, \tag{5.4}$$

$$\epsilon = \sqrt{\frac{VT}{R}}. \tag{5.5}$$

Equation (5.4) for the length scale X_{sc} and equation (5.5) for the parameter ϵ imply that the vertical displacement of the body $V.T$ is much smaller than R during the initial stage $0 < t < T$ under consideration, and length scale $X_{sc} = R\epsilon$ is much smaller than R. Then equation (5.1) in the non-dimensional variables provides an equation for the body boundary:

$$\hat{y} = \epsilon\big(\frac{\hat{x}^2}{2} - \hat{t}\big). \tag{5.6}$$

The velocity potential $\hat{\varphi}$ defined by

$$\varphi(x, y, t) = X_{sc} V \hat{\varphi}(\hat{x}, \hat{y}, \hat{t}) \tag{5.7}$$

satisfies the kinematic body boundary condition on $\hat{y} = \epsilon(\frac{\hat{x}^2}{2} - \hat{t})$, says we have zero normal flow through the body,

$$\frac{\partial \hat{\varphi}}{\partial \hat{y}} = -1 + \epsilon \hat{x} \frac{\partial \hat{\varphi}}{\partial \hat{x}}. \tag{5.8}$$

The kinematic boundary condition on the free surface, $\hat{y} = \epsilon \hat{\eta}(\hat{x}, \hat{t})$, which says a fluid particle of the free surface cannot leave the free surface, reads in non-dimensional variables

$$\frac{\partial \hat{\varphi}}{\partial \hat{y}} = \epsilon \frac{\partial \hat{\eta}}{\partial \hat{x}} \frac{\partial \hat{\varphi}}{\partial \hat{x}} + \frac{\partial \hat{\eta}}{\partial \hat{t}}. \tag{5.9}$$

The hydrodynamic pressure is given by the Bernoulli equation

$$p = -\rho V^2 \epsilon^{-1} \left[\frac{\partial \hat{\varphi}}{\partial \hat{t}} + \frac{1}{2} \epsilon |\hat{\nabla} \hat{\varphi}|^2 + \frac{gR}{V^2} \epsilon^2 \hat{y} \right] + p_{atm}. \tag{5.10}$$

The non-dimensional pressure $\hat{p}$ is defined by

$$p = p_{atm} + \frac{\rho V^2}{\epsilon} \hat{p}. \tag{5.11}$$

Then

$$-\hat{p} = \frac{\partial \hat{\varphi}}{\partial \hat{t}} + \frac{1}{2} \epsilon |\hat{\nabla} \hat{\varphi}|^2 + \frac{gR}{V^2} \epsilon^2 \hat{y}. \tag{5.12}$$

The dynamic boundary condition on the free surface $\hat{y} = \epsilon \hat{\eta}(\hat{x}, \hat{t})$ is

$$p = p_{atm} - \sigma \frac{\frac{\partial^2 \eta}{\partial x^2}}{\left(1 + \left(\frac{\partial \eta}{\partial x}\right)^2\right)^{3/2}}, \tag{5.13}$$

where σ is the coefficient of surface tension. Equation (5.13) in non-dimensional variables reads

$$\frac{\partial \hat{\varphi}}{\partial \hat{t}} + \frac{1}{2} \epsilon |\hat{\nabla} \hat{\varphi}|^2 + \frac{gR}{V^2} \epsilon^3 \hat{\eta} = \frac{\sigma \epsilon}{R \rho V^2} \frac{\frac{\partial^2 \hat{\eta}}{\partial \hat{x}^2}}{\left(1 + \epsilon^2 \left(\frac{\partial \hat{\eta}}{\partial \hat{x}}\right)^2\right)^{3/2}}. \tag{5.14}$$

The potential $\hat{\varphi}$ satisfies the Laplace equation,

$$\frac{\partial^2 \hat{\varphi}}{\partial \hat{x}^2} + \frac{\partial^2 \hat{\varphi}}{\partial \hat{y}^2} = 0, \tag{5.15}$$

in the flow region. In the leading order, for small values of ϵ, the non-linear terms in equations (5.8)–(5.14) can be neglected. Three non-dimensional parameters appear in the above formulated problem (5.6) and (5.8)–(5.15). The first parameter ϵ is responsible for non-linear effects, the second parameter, $\delta = \frac{gR}{V^2}\epsilon^3$, is responsible for the gravity effects and the third one, $\mu = \frac{\sigma}{\rho V^2 R}\epsilon$, is responsible for the surface tension effects.

We are concerned with the conditions of the impact when $\mu = O(\epsilon)$ and $\frac{\epsilon}{\delta} = o(1)$. That is, when gravity is more important than the non-linearity, and surface tension effects are of the same or higher order than the non-linear effects. These conditions imply

$$\frac{\sigma}{\rho V^2 R} = O(1), \quad \frac{V^2}{gR} = o(\epsilon^2). \tag{5.16}$$

Let $V = \sqrt{gR}\upsilon$, where υ is a small parameter. Then the asymptotic formulae (5.16) imply

$$\Big(\frac{a/R}{\upsilon}\Big)^2 = O(1), \quad \upsilon = o(\epsilon), \tag{5.17}$$

where $a = \sqrt{\frac{\sigma}{\rho g}}$ is the capillary length. For the air-water interface at 25°C, $a \approx 2.7 \times 10^{-3}$ m. Formulae (5.17) provide

$$C_\sigma \, \frac{a}{R} < \upsilon \ll 1, \quad \epsilon = \upsilon^k, \quad 0 < k < 1, \tag{5.18}$$

where C_σ is a positive constant of order $O(1)$. The parameter δ is computed now as

$$\delta = \frac{\epsilon^3}{\upsilon^2} = \upsilon^{3k-2}. \tag{5.19}$$

The gravity term in equation (5.14) is of order $O(1)$ or smaller, but still of lower order than $O(\epsilon)$, if $\frac{2}{3} \le k < 1$. When $k = \frac{2}{3}$, we have $\delta = 1$, and $\delta \ll 1$ for the earlier stages with $k > \frac{2}{3}$. The first inequality in (5.18) shows that the surface tension term in (5.14) can be neglected when $R \gg a$ and the impact speed is not too small.

In the most interesting case, $k = \frac{2}{3}$, we have $\delta = 1$ and $\upsilon^{2/3} = \epsilon$, which gives

$$\sqrt{\frac{VT}{R}} = \big(\frac{V}{\sqrt{gR}}\big)^{2/3}, \tag{5.20}$$

and consequently

$$T = \left(\frac{RV}{g^2}\right)^{1/3}, \quad \epsilon = \left(\frac{V^2}{gR}\right)^{1/3}. \tag{5.21}$$

Letting $\upsilon \longrightarrow 0$, we obtain the formulation of the problem with low entry velocity in the leading order in δ during the early stage ($\hat{}$is dropped below and all variables are non-dimensional):

$$\frac{\partial^2\varphi}{\partial x^2} + \frac{\partial^2\varphi}{\partial y^2} = 0 \qquad y < 0, \tag{5.22}$$

$$\frac{\partial\varphi}{\partial t} + \delta\eta = 0 \qquad y = 0, |x| > x_c(t), \tag{5.23}$$

$$\frac{\partial\varphi}{\partial y} = \frac{\partial\eta}{\partial t} \qquad y = 0, |x| > x_c(t), \tag{5.24}$$

$$\frac{\partial\varphi}{\partial y} = -1 \qquad y = 0, |x| < x_c(t), \tag{5.25}$$

$$\frac{\partial\varphi}{\partial t} + \delta\left(\frac{x^2}{2} - t\right) = -p \qquad y = 0, |x| < x_c(t), \tag{5.26}$$

$$\varphi \longrightarrow 0 \qquad \text{as} \qquad x^2 + y^2 \longrightarrow \infty. \tag{5.27}$$

The above problem is supplemented by the Wagner condition:

$$\eta(x_c(t), t) = \frac{1}{2}x_c^2(t) - t, \tag{5.28}$$

which is needed to determine the unknown position of the moving points, $x = \pm x_c(t)$, separating the free surface from the contact region between the liquid and the entering body contour. The elevation of the free surface, $y = \eta(x, t)$, in the linearised formulation (5.22)–(5.28) is given by the kinematic condition (5.24) which follows from (5.9).

5.2 Problem in terms of displacement potential and stretched variables

In this section we formulate and solve the problem in terms of displacement potential in new stretched variables. The linearised boundary value problem (5.22)–(5.28) can be written with respect to the displacement potential, defined as follows

$$\phi(x, y, t) = \int_0^t \varphi(x, y, \tau)\mathrm{d}\tau, \tag{5.29}$$

for which the boundary value problem is

$$\frac{\partial^2\phi}{\partial x^2}+\frac{\partial^2\phi}{\partial y^2}=0 \qquad y<0, \tag{5.30}$$

$$\frac{\partial^2\phi}{\partial t^2}+\delta\eta=0 \qquad y=0,|x|>x_c(t), \tag{5.31}$$

$$\frac{\partial\phi}{\partial y}=\eta \qquad y=0,|x|>x_c(t), \tag{5.32}$$

$$\frac{\partial\phi}{\partial y}=\frac{1}{2}x^2-t \qquad y=0,|x|<x_c(t), \tag{5.33}$$

$$\frac{\partial^2\phi}{\partial t^2}+\delta(\frac{x^2}{2}-t)=-p \qquad y=0,|x|<x_c(t), \tag{5.34}$$

$$\phi\longrightarrow 0 \qquad \text{as} \qquad x^2+y^2\longrightarrow\infty, \tag{5.35}$$

$$\phi\in C^2(y<0)\bigcup C^1(y\leq 0). \tag{5.36}$$

The condition (5.36) includes the Wagner condition (5.28). If in equation (5.31), $\delta = 0$, then we arrive at the classical Wagner problem, which is formulated without account for gravity. Note that one can set $\delta = 1$ in equations (5.31) and (5.34) if T and ϵ are given by equation (5.21) and $\epsilon \ll 1$.

We keep δ in formulation (5.30)–(5.36) and assume $\delta \ll 1$, which implies that we are concerned with the early stage of the entry, during which the gravity effects are still small. Note that $x_c = x_c(t,\delta)$ and $x_c(t,0) = x_{c0}(t)$.

We write the asymptotic expansion for the moving contact point in terms of δ as follows

$$x_c(t,\delta)=x_c(t,0)\big[1+\delta x_{c1}(t)+O\left(\delta^2\right)\big], \tag{5.37}$$

where $\delta\longrightarrow 0$. We introduce new stretched variables

$$\tilde{x}=x\frac{x_{c0}(t)}{x_c(t,\delta)}, \quad \tilde{y}=y\frac{x_{c0}(t)}{x_c(t,\delta)}, \tag{5.38}$$

and a new unknown potential $\tilde{\phi}$ by

$$\phi(x,y,t)=\tilde{\phi}(\tilde{x},\tilde{y},t,\delta)=\tilde{\phi}_0(\tilde{x},\tilde{y},t)+\delta\tilde{\phi}_1(\tilde{x},\tilde{y},t)+O\left(\delta^2\right). \tag{5.39}$$

The potential $\tilde{\phi}(\tilde{x},\tilde{y},t,\delta)$ satisfies the Laplace equation in the new stretched variables in the flow region $\tilde{y}<0$. Note that $\tilde{x}=x[1-\delta x_{c1}(t)+O(\delta^2)]$. The boundary condition in the contact region, $|\tilde{x}|<x_{c0}(t)$, reads in the new variables

$$\frac{x_{c0}(t)}{x_c(t,\delta)}\frac{\partial\tilde{\phi}}{\partial\tilde{y}}=\frac{1}{2}\frac{x_c^2(t,\delta)}{x_{c0}^2(t)}\tilde{x}^2-t. \tag{5.40}$$

Multiplying equation (5.40) by $\frac{x_c(t,\delta)}{x_{c0}(t)}$ and using expansion (5.37), we find

$$\frac{\partial\tilde{\phi}}{\partial\tilde{y}} = \frac{1}{2}\tilde{x}^2 - t - \delta x_{c1}(t)\big(\frac{3}{2}\tilde{x}^2 - t\big) + O\left(\delta^2\right). \tag{5.41}$$

Equation (5.41) gives in the leading order and the first order respectively

$$\frac{\partial\tilde{\phi}_0}{\partial\tilde{y}} = \frac{1}{2}\tilde{x}^2 - t \qquad |\tilde{x}| < x_{c0}(t), \tag{5.42}$$

$$\frac{\partial\tilde{\phi}_1}{\partial\tilde{y}} = x_{c1}(t)\big(\frac{3}{2}\tilde{x}^2 - t\big) \qquad |\tilde{x}| < x_{c0}(t). \tag{5.43}$$

On the free surface, $|\tilde{x}| > x_{c0}(t)$, the two boundary conditions (5.31) and (5.32) yield

$$\frac{\partial^2\tilde{\phi}_0}{\partial t^2} + \delta\Big(\frac{\partial\tilde{\phi}_0}{\partial\tilde{y}} + \frac{\partial^2\tilde{\phi}_1}{\partial t^2} - 2x\dot{x}_{c1}(t)\frac{\partial^2\tilde{\phi}_0}{\partial t\partial\tilde{x}} - x\ddot{x}_{c1}(t)\frac{\partial\tilde{\phi}_0}{\partial\tilde{x}}\Big) + O\left(\delta^2\right) = 0, \tag{5.44}$$

which gives

$$\frac{\partial^2\tilde{\phi}_0}{\partial t^2} = 0 \qquad |\tilde{x}| > x_{c0}(t), \tilde{y} = 0, \tag{5.45}$$

$$\frac{\partial^2\tilde{\phi}_1}{\partial t^2} = 2x\dot{x}_{c1}(t)\frac{\partial^2\tilde{\phi}_0}{\partial t\partial\tilde{x}} + x\ddot{x}_{c1}(t)\frac{\partial\tilde{\phi}_0}{\partial\tilde{x}} - \frac{\partial\tilde{\phi}_0}{\partial\tilde{y}} \qquad |\tilde{x}| > x_{c0}(t), \tilde{y} = 0. \tag{5.46}$$

The leading-order free-surface condition (5.45) can be integrated twice with respect to time, subject to the initial conditions (suitable for a fluid starting from rest):

$$\tilde{\phi}(\tilde{x},\tilde{y},0) = 0, \tag{5.47}$$

$$\frac{\partial\tilde{\phi}}{\partial t}(\tilde{x},\tilde{y},0) = 0, \tag{5.48}$$

which gives us a new dynamic boundary condition on the free surface at the leading order,

$$\tilde{\phi}_0(\tilde{x},0,t) = 0 \qquad |\tilde{x}| > x_{c0}(t). \tag{5.49}$$

Equation (5.49) shows that the first and second terms on the right-hand side of equation (5.46) are zero. Then

$$\frac{\partial^2\tilde{\phi}_1}{\partial t^2} = -\frac{\partial\tilde{\phi}_0}{\partial\tilde{y}} \qquad |\tilde{x}| > x_{c0}(t),\ \tilde{y} = 0. \tag{5.50}$$

The unknown potentials $\tilde{\phi}_0(\tilde{x},\tilde{y},t)$ and $\tilde{\phi}_1(\tilde{x},\tilde{y},t)$ satisfy Laplace's equation in

$\tilde{y} < 0$, decay at infinity and belong to the set (5.36). In the leading order, the solution provides ((Wagner 1932))

$$x_{c0}(t) = 2\sqrt{t}, \tag{5.51}$$

$$\frac{\partial\tilde{\phi}_0}{\partial t}(\tilde{x},0,t) = -\sqrt{4t-\tilde{x}^2} \qquad |\tilde{x}| < 2\sqrt{t}, \tag{5.52}$$

$$\frac{\partial\tilde{\phi}_0}{\partial\tilde{y}}(\tilde{x},0,t) = \frac{\tilde{x}^2}{2} - \frac{\tilde{x}}{2}\sqrt{\tilde{x}^2-4t} - t \qquad |\tilde{x}| > 2\sqrt{t}. \tag{5.53}$$

Note that the solution given in equations (5.51)–(5.53) is in terms of displacement potential introduced by (5.29) and stretched variables introduced by (5.38). Substitution of equation (5.53) in equation (5.50) gives

$$\frac{\partial^2\tilde{\phi}_1}{\partial t^2} = t - \frac{\tilde{x}^2}{2} + \frac{\tilde{x}}{2}\sqrt{\tilde{x}^2-4t} \qquad \tilde{x} > 2\sqrt{t},\ \tilde{y} = 0. \tag{5.54}$$

Using the initial conditions (5.47)–(5.48) and integrating (5.54) twice in time, we find

$$\tilde{\phi}_1 = \frac{t^3}{6} - \frac{\tilde{x}^2}{4}t^2 + \frac{\tilde{x}^4}{12}t - \frac{\tilde{x}^6}{120} + \frac{\tilde{x}}{120}\big(\tilde{x}^2-4t\big)^{5/2} \qquad \tilde{x} > 2\sqrt{t},\ \tilde{y} = 0. \tag{5.55}$$

The horizontal displacement on the free surface reads

$$\frac{\partial\tilde{\phi}_1}{\partial\tilde{x}} = -\frac{\tilde{x}}{2}t^2 + \frac{\tilde{x}^3}{3}t - \frac{\tilde{x}^5}{20} + \frac{1}{120}\big(\tilde{x}^2-4t\big)^{3/2}\big(6\tilde{x}^2-4t\big) \quad \tilde{x} > 2\sqrt{t},\ \tilde{y} = 0. \tag{5.56}$$

Equation (5.56) show that the first-order potential $\tilde{\phi}_1(\tilde{x},\tilde{y},t)$ can be presented in the form

$$\tilde{\phi}_1 = 2t^3\Phi(\xi,\zeta), \tag{5.57}$$

where

$$\tilde{x} = 2\sqrt{t}\xi, \qquad \tilde{y} = 2\sqrt{t}\zeta, \tag{5.58}$$

and $\Phi(\xi,\zeta)$ is the new unknown function. Equations (5.43), (5.57) and (5.58) provide that the unknown correction to the position of the contact point, $x_{c1}(t)$, has the form

$$x_{c1}(t) = \mu t^{3/2}, \tag{5.59}$$

where the constant μ is to be determined. Equations (5.56) and (5.43) written in the new variables introduced in (5.57)–(5.59) provide the following boundary

conditions for the potential $\Phi(\xi,\zeta)$:

$$\frac{\partial\Phi}{\partial\xi} = -\xi + \frac{8}{3}\xi^3 - \frac{8}{5}\xi^5 + \frac{4}{15}(\xi^2-1)^{3/2}(6\xi^2-1) \qquad \xi>1,\ \zeta=0, \tag{5.60}$$

$$\frac{\partial\Phi}{\partial\zeta} = \mu(6\xi^2-1) \qquad |\xi|<1,\ \zeta=0. \tag{5.61}$$

In order to find the constant μ and the potential $\Phi(\xi,0)$ in the contact region, $|\xi|<1$, which is needed to determine the correction to the pressure distribution due to the gravity effect, we solve this problem by considering an analytic function $W(\varsigma)$ in $\zeta<0$

$$W(\varsigma) = \big(\frac{\partial\Phi}{\partial\xi} - i\frac{\partial\Phi}{\partial\zeta}\big)\sqrt{\varsigma^2-1}, \tag{5.62}$$

where the complex variable $\varsigma = \xi + i\zeta$ and

$$W(\varsigma) = \longrightarrow 0 \qquad \text{as} \qquad \varsigma \longrightarrow \infty, \tag{5.63}$$

and $W(\pm1)=0$. On the boundary, $\zeta = 0^-$, real and imaginary parts of this function,

$$\mathrm{Real}\big[W(\xi-i0)\big] = \begin{cases} \frac{\partial\Phi}{\partial\xi}(\xi,0)\sqrt{\xi^2-1} & \xi>1, \\ -\frac{\partial\Phi}{\partial\zeta}(\xi,0)\sqrt{1-\xi^2} & |\xi|<1, \\ -\frac{\partial\Phi}{\partial\xi}(\xi,0)\sqrt{\xi^2-1} & \xi<-1, \end{cases} \tag{5.64}$$

$$\mathrm{Im}\big[W(\xi-i0)\big] = \begin{cases} -\frac{\partial\Phi}{\partial\zeta}(\xi,0)\sqrt{\xi^2-1} & \xi>1, \\ -\frac{\partial\Phi}{\partial\xi}(\xi,0)\sqrt{1-\xi^2} & |\xi|<1, \\ \frac{\partial\Phi}{\partial\zeta}(\xi,0)\sqrt{\xi^2-1} & \xi<-1, \end{cases} \tag{5.65}$$

are related by the Hilbert formula

$$\mathrm{Im}\big[W(\xi-i0)\big] = \frac{1}{\pi}\fint_{-\infty}^{\infty}\mathrm{Real}\big[W(\xi-i0)\big]\frac{\mathrm{d}\xi_0}{\xi_0-\xi}, \tag{5.66}$$

where the integral is understood as a Cauchy principal-value integral. In the contact region, $|\xi|<1$, the Hilbert formula provides

$$\begin{aligned} -\frac{\partial\Phi}{\partial\xi}(\xi,0)\sqrt{1-\xi^2} = &-\frac{\mu}{\pi}\fint_{-1}^{1}\frac{(6\xi_0^2-1)(1-\xi_0^2)}{\sqrt{1-\xi_0^2}(\xi_0-\xi)}\mathrm{d}\xi_0 \\ &+\frac{2\xi}{\pi}\int_1^{\infty}\frac{\partial\Phi}{\partial\xi}(\xi_0,0)\frac{\sqrt{\xi_0^2-1}}{\xi_0^2-\xi^2}\mathrm{d}\xi_0, \end{aligned} \tag{5.67}$$

where $\frac{\partial\Phi}{\partial\xi}(\xi_0,0)$ in the second integral is given by equation (5.60). The first integral is evaluated analytically. We obtain

$$\frac{\partial\Phi}{\partial\xi}(\xi,0)\sqrt{1-\xi^2} = 2\mu\xi(2-3\xi^2) - \frac{2\xi}{\pi}\int_1^\infty \frac{\partial\Phi}{\partial\xi}(\xi_0,0)\frac{\sqrt{\xi_0^2-1}}{\xi_0^2-\xi^2}\mathrm{d}\xi_0 \qquad |\xi|<1. \tag{5.68}$$

Note that the left hand side in equation (5.68) is zero at $\xi = \pm 1$. This gives the following equations with respect to μ,

$$-2\mu = \frac{2}{\pi}\int_1^\infty \frac{\partial\Phi}{\partial\xi}(\xi_0,0)\frac{\mathrm{d}\xi_0}{\sqrt{\xi_0^2-1}}. \tag{5.69}$$

The integral in equation (5.69) is equal to $\frac{8}{225}$. Then

$$\mu = -\frac{8}{225\pi} \approx -5.63\times 10^{-3}, \tag{5.70}$$

and therefore the moving contact point with correction due to gravity can be written as

$$x_c(t,\delta) = 2\sqrt{t}\big(1-\delta|\mu|t^{3/2} + O\left(\delta^2\right)\big). \tag{5.71}$$

In this expansion the moving contact point advances a shorter distance with gravity than without gravity. We also see from Figure (5.2) that $x_c(t,\delta) < x_{c0}(t)$ but the correction due to gravity is very small even for moderate values of δ. In Figure (5.2), the moving contact point correction due to gravity is calculated with $\delta = 0.5$. The following work prepares us for the calculation of pressure in the next section.

Now from equation (5.68) we substitute (5.70) and evaluate the integral to get

$$\begin{aligned}\frac{\partial\Phi}{\partial\xi}(\xi,0) =& \frac{24}{225\pi}\xi\sqrt{1-\xi^2}(23-30\xi^2) + \frac{4}{15\pi}(1-\xi^2)^{3/2}(1-6\xi^2)\ln\left|\frac{1+\xi}{1-\xi}\right| \\ &- \frac{1}{15}\xi(24\xi^4-40\xi^2+15) \quad |\xi|<1.\end{aligned} \tag{5.72}$$

We need also $\Phi(\xi,0)$ and $\frac{\partial^2\Phi}{\partial\xi^2}(\xi,0)$ to calculate the pressure correction. The later is calculated in equation (5.73) by differentiating the equation (5.72) with respect to ξ,

$$\begin{aligned}\frac{\partial^2\Phi}{\partial\xi^2}(\xi,0) =& \frac{3600\xi^4-4104\xi^2+672}{225\pi\sqrt{1-\xi^2}} + 8\xi^2(1-\xi^2) - 1 \\ &- \frac{4}{\pi}\xi(1-2\xi^2)\sqrt{1-\xi^2}\ln\left|\frac{1+\xi}{1-\xi}\right| \quad |\xi|<1.\end{aligned} \tag{5.73}$$

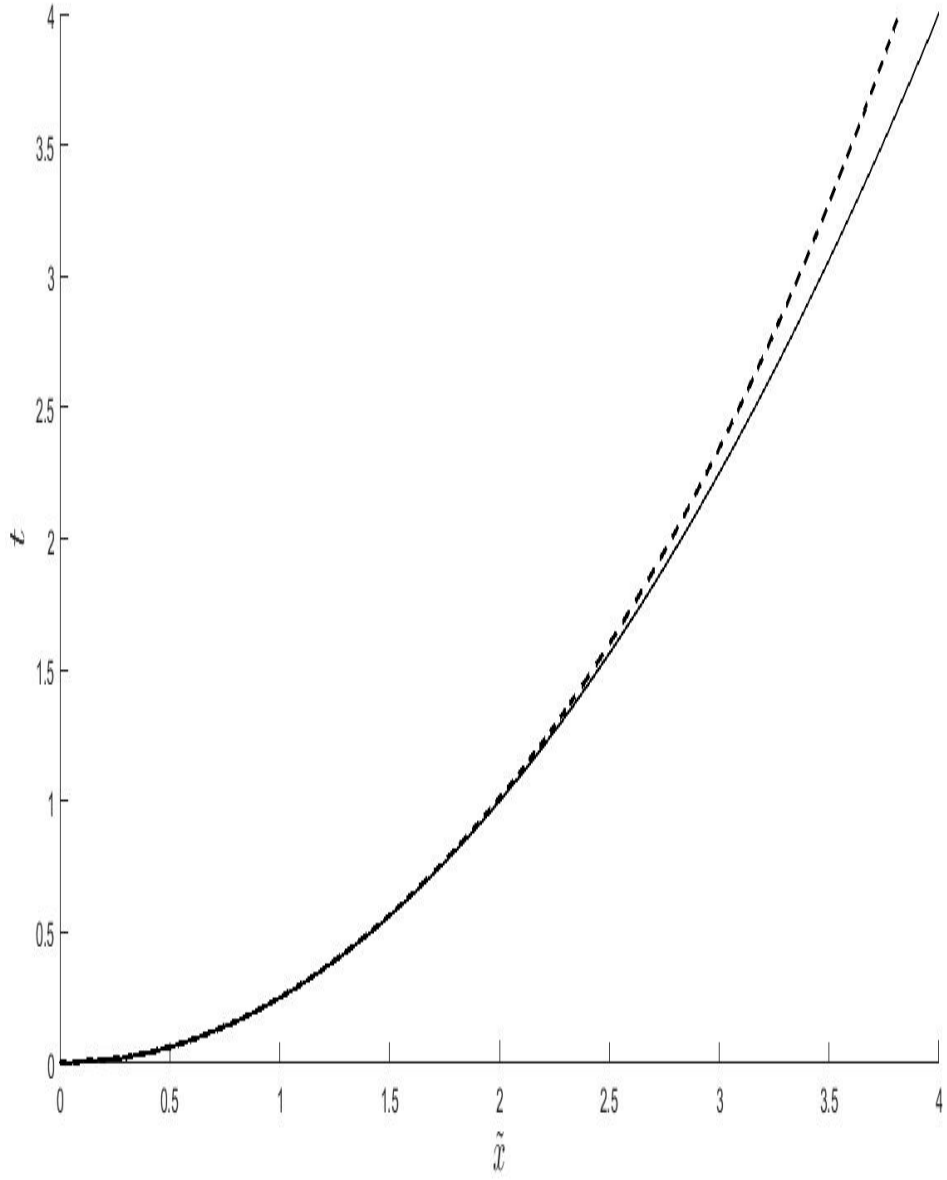

Figure 5.2: In non-dimensional variables, the contact point position without and with correction due to gravity. The leading-order contact point, $\tilde{x} = 2\sqrt{t}$, is the solid line, and the contact point with correction due to gravity, $\tilde{x} = 2\sqrt{t}\big(1 + \delta\mu t^{3/2}\big)$, is the dashed line. Note that $\delta = 0.5$, $\mu = -\frac{8}{225\pi}$ and $t = 0$ is the instant of impact.

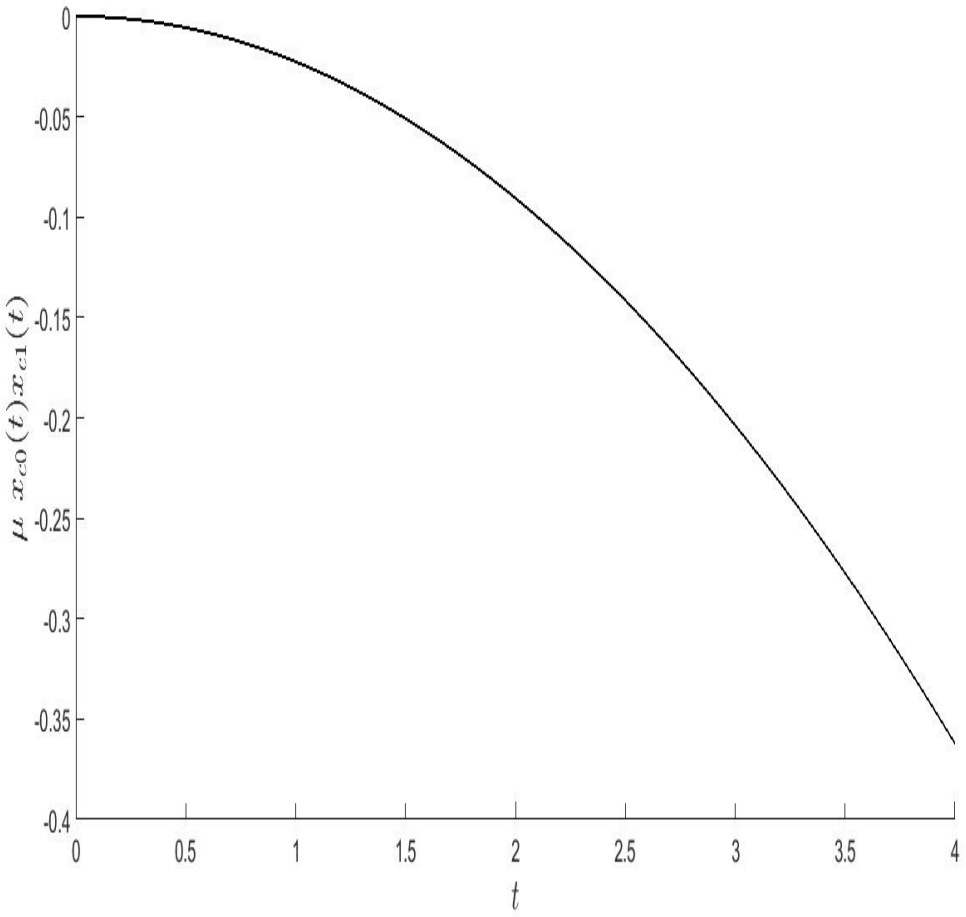

Figure 5.3: Correction to the moving contact point position due to gravity, $\mu x_{c0}(t)x_{c1}(t) = 2\mu t^2$ in non-dimensional variables, here $t = 0$ is the instant of impact, and $\mu = -\frac{8}{225\pi}$.

Also $\Phi(\xi,0)$ is calculated by integrating equation (5.72) with respect to ξ,

$$\Phi(\xi,0) = -\xi^2\Big(\frac{4}{15}\xi^4 - \frac{2}{3}\xi^2 + \frac{1}{2}\Big) - \frac{8}{225\pi}(1-\xi^2)^{3/2}\Big(11-18\xi^2\Big) + \frac{4}{15\pi}\sum_{n=0}^{\infty}\left(\frac{1}{n+1} - \frac{6\xi^2}{n+2}\right)\xi^{2n+2}\sum_{i=0}^{n}\binom{3/2}{i}\frac{(-1)^i}{2n-2i+1} + c, |\xi| < 1, \tag{5.74}$$

where c is the constant of integration to be determined and the bracket in the second summation are the binomial coefficients. We integrate the equation (5.60) for $\xi > 1$ to get

$$\int_1^{\infty}\Phi_{\xi}(\xi,0)\mathrm{d}\xi = \Big[\frac{\xi^2}{15}\big(-\frac{15}{2} + 10\xi^2 - 4\xi^4\big) + \frac{4}{15}\xi\big(\xi^2-1\big)^{5/2}\Big]_{\xi=1}^{\xi=\infty}, \tag{5.75}$$

Using the far-field condition (5.27), equation (5.75) gives

$$\int_1^{\infty}\Phi_{\xi}(\xi,0)\mathrm{d}\xi = \Phi(\infty,0) - \Phi(1,0) = 0.1, \tag{5.76}$$

and from the continuity of the stretched displacement potential $\Phi(\xi,\zeta)$, the constant c can be determined by equating the two expressions (5.76) and (5.74) at the contact point $\xi = 1$ which gives $c = 0.234$. Now we are in the position to rearrange our formulae for calculating the pressure distribution in the next section.

5.3 Pressure distribution

In this section the pressure distribution on the wetted body during the impact is calculated. The pressure distribution in terms of the displacement potential on $|x| < x_c(t), y = 0$ is given by equation (5.34). We introduce the stretched variables (5.38) into equation (5.34),

$$\begin{aligned} -\tilde{p} &= \frac{\partial^2\tilde{\phi}}{\partial t^2} + \delta\left(\frac{\tilde{x}^2}{2}\frac{x_c^2(t,\delta)}{x_{c0}^2(t)} - t\right) \qquad |\tilde{x}| < x_{c0}(t), \tilde{y} = 0, \\ &= \frac{\partial^2\tilde{\phi}}{\partial t^2} + \delta\left(\frac{\tilde{x}^2}{2} - t\right) + O\left(\delta^2\right), \end{aligned} \tag{5.77}$$

where here $\tilde{\phi} = \tilde{\phi}(\tilde{x},0,t,\delta)$ is the unknown potential defined in equation (5.39) and

$$\tilde{p}(\tilde{x},0,t,\delta) = \tilde{p}_0(\tilde{x},0,t) + \delta\tilde{p}_1(\tilde{x},0,t) + O\left(\delta^2\right). \tag{5.78}$$

The first time-derivative of $\tilde{\phi}(\tilde{x}, 0, t, \delta)$ is given by

$$\begin{aligned}\frac{\partial\tilde{\phi}}{\partial t}(\tilde{x}, 0, t, \delta) &= \frac{\partial\tilde{\phi}}{\partial t} + \frac{\partial\tilde{\phi}}{\partial\tilde{x}}\frac{\partial\tilde{x}}{\partial t} \\ &= \frac{\partial\tilde{\phi}_0}{\partial t} + \frac{\partial\tilde{\phi}_0}{\partial\tilde{x}}\frac{\partial\tilde{x}}{\partial t} + \delta\left(\frac{\partial\tilde{\phi}_1}{\partial t} + \frac{\partial\tilde{\phi}_1}{\partial\tilde{x}}\frac{\partial\tilde{x}}{\partial t}\right) + O\left(\delta^2\right). \end{aligned} \tag{5.79}$$

The time-derivative of the variable $\tilde{x}$ is

$$\begin{aligned}\frac{\partial\tilde{x}}{\partial t} &= x\frac{\partial}{\partial t}\left(\frac{x_{c0}(t)}{x_c(t,\delta)}\right) = x\frac{\partial}{\partial t}\left(\frac{1}{1+\delta x_{c1}(t) + O\left(\delta^2\right)}\right) \\ &= -\delta x\dot{x}_{c1}(t) + O\left(\delta^2\right), \end{aligned} \tag{5.80}$$

and in a similar way for $\tilde{y}$ we have

$$\frac{\partial\tilde{y}}{\partial t} = -\delta\tilde{y}\dot{x}_{c1}(t) + O\left(\delta^2\right). \tag{5.81}$$

Hence from the equation (5.59) the time-derivative of the correction to the moving contact point $x_{c1}(t)$ is given by

$$\dot{x}_{c1}(t) = \frac{3\mu}{2}\sqrt{t}. \tag{5.82}$$

Equations (5.80)–(5.82) give, respectively,

$$\frac{\partial\tilde{x}}{\partial t} = O\left(\delta\right), \tag{5.83}$$

$$\frac{\partial\tilde{y}}{\partial t} = O(\epsilon\delta). \tag{5.84}$$

Using equations (5.80) and (5.83), from equation (5.79) we arrive at

$$\frac{\partial\tilde{\phi}}{\partial t} + \frac{\partial\tilde{\phi}}{\partial\tilde{x}}\frac{\partial\tilde{x}}{\partial t} = \frac{\partial\tilde{\phi}_0}{\partial t} + \delta\left(-\tilde{x}\dot{x}_{c1}(t)\frac{\partial\tilde{\phi}_0}{\partial\tilde{x}} + \frac{\partial\tilde{\phi}_1}{\partial t}\right) + O\left(\delta^2\right). \tag{5.85}$$

The time-derivative of equation (5.85) gives us

$$\begin{aligned}\frac{\partial^2\tilde{\phi}}{\partial t^2}(\tilde{x}, 0, t, \delta) &= \frac{\partial}{\partial t}\left(\frac{\partial\tilde{\phi}}{\partial t} + \frac{\partial\tilde{\phi}}{\partial\tilde{x}}\frac{\partial\tilde{x}}{\partial t}\right) \\ &= \frac{\partial^2\tilde{\phi}_0}{\partial t^2} + \frac{\partial^2\tilde{\phi}_0}{\partial t\partial\tilde{x}}\frac{\partial\tilde{x}}{\partial t} + \delta\Bigg(-\frac{\partial\tilde{x}}{\partial t}\dot{x}_{c1}(t)\frac{\partial\tilde{\phi}_0}{\partial\tilde{x}} - \tilde{x}\ddot{x}_{c1}(t)\frac{\partial\tilde{\phi}_0}{\partial\tilde{x}} \\ &\quad - \tilde{x}\dot{x}_{c1}(t)\left(\frac{\partial^2\tilde{\phi}_0}{\partial\tilde{x}\partial t} + \frac{\partial^2\tilde{\phi}_0}{\partial\tilde{x}^2}\frac{\partial\tilde{x}}{\partial t}\right) + \frac{\partial^2\tilde{\phi}_1}{\partial t^2} + \frac{\partial^2\tilde{\phi}_1}{\partial t\partial\tilde{x}}\frac{\partial\tilde{x}}{\partial t}\Bigg) + O\left(\delta^2\right). \end{aligned} \tag{5.86}$$

Using equations (5.80) and (5.83), equation (5.86) can be written

$$\frac{\partial}{\partial t}\Big(\frac{\partial\tilde{\phi}}{\partial t}+\frac{\partial\tilde{\phi}}{\partial\tilde{x}}\frac{\partial\tilde{x}}{\partial t}\Big)= \\ \frac{\partial^2\tilde{\phi}_0}{\partial t^2}+\delta\big[-\tilde{x}\ddot{x}_{c1}(t)\frac{\partial\tilde{\phi}_0}{\partial\tilde{x}}-2\tilde{x}\dot{x}_{c1}(t)\frac{\partial^2\tilde{\phi}_0}{\partial\tilde{x}\partial t}+\frac{\partial^2\tilde{\phi}_1}{\partial t^2}\big]+O\left(\delta^2\right). \tag{5.87}$$

From equation (5.59), the second time-derivative of the correction to the moving contact point $x_{c1}(t)$ is given by

$$\ddot{x}_{c1}(t)=\frac{3\mu}{4\sqrt{t}}. \tag{5.88}$$

Therefore from equations (5.77) and (5.87) the leading-order pressure distribution is given as

$$\tilde{p_0}=-\frac{\partial^2\tilde{\phi}_0}{\partial t^2}\qquad |\tilde{x}|<2\sqrt{t},\ \tilde{y}=0. \tag{5.89}$$

As we mentioned earlier, the non-linearity and surface tension effects are neglected in this study while we keep the gravity influence in the formulation, saying that the latter is more important than both non-linearity and surface tension. However, as shown in equation (5.89), at the leading order, gravity gives no contribution to the pressure distribution.
From the leading-order solution (5.52) in terms of displacement potential we get

$$\tilde{p_0}(\tilde{x},0,t)=\frac{2}{\sqrt{4t-\tilde{x}^2}}\qquad |\tilde{x}|<2\sqrt{t},\ \tilde{y}=0. \tag{5.90}$$

This says that the pressure distribution during the impact is to be positive along the wetted body and it has a singularity at the contact point, $\tilde{x}=2\sqrt{t}$.

In Figure (5.4) the hydrodynamic pressure distribution, at leading order is shown at the given time instants. In the next section we calculate the pressure distribution at the next order.

5.4 Correction to the pressure distribution

In this section the correction to the pressure distribution due to gravity is determined. From equations (5.77) and (5.87) the pressure correction due to gravity on $\tilde{y}=0$ for $|\tilde{x}|<2\sqrt{t}$, is given by

$$\tilde{p_1}=-\frac{\partial^2\tilde{\phi}_1}{\partial t^2}+\tilde{x}\ddot{x}_{c1}(t)\frac{\partial\tilde{\phi}_0}{\partial\tilde{x}}+2\tilde{x}\dot{x}_{c1}(t)\frac{\partial^2\tilde{\phi}_0}{\partial\tilde{x}\partial t}-\frac{\tilde{x}^2}{2}+t. \tag{5.91}$$

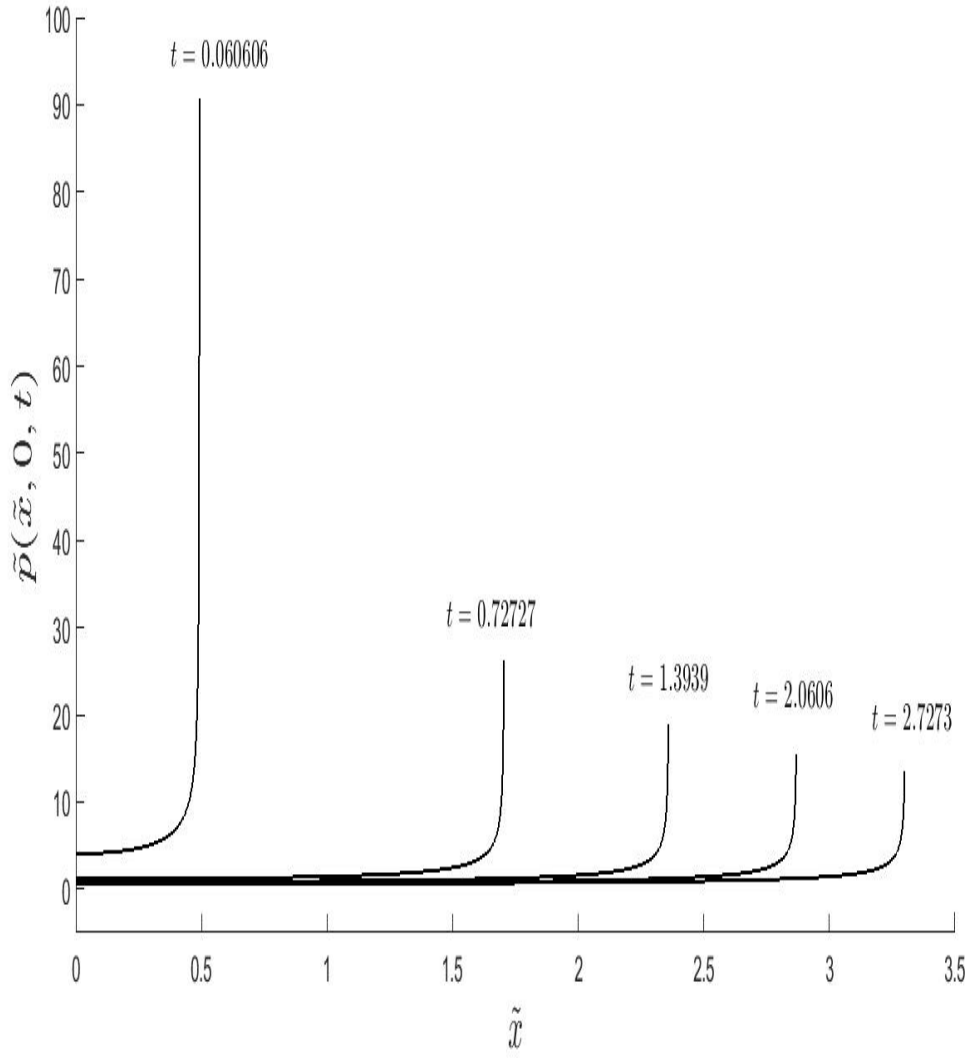

Figure 5.4: Non-dimensional leading-order hydrodynamic pressure distribution along the wetted body at instants shown. Note the extension of the wetted body as time goes on.

In the second term on the right hand side of equation (5.91), the horizontal displacement $\frac{\partial \tilde{\phi}_0}{\partial \tilde{x}}$ can be calculated by integrating both sides of equation (5.52) with respect to time from 0 to t. However, as shown in Figure (5.5), integration from $t = 0$ to $t = \frac{\tilde{x}^2}{4}$ represents the free surface where it gives zero contribution and the only contribution comes from the wetted region for $t > t_*$, where the horizontal line $t = t_*$ corresponds to the liquid boundary at the instant t_*, see Figure (5.5).

$$\tilde{\phi}_0(\tilde{x}, 0, t) \ = -\frac{\left(4t - \tilde{x}^2\right)^{3/2}}{6} \qquad |\tilde{x}| < 2\sqrt{t}, \ \tilde{y} = 0, \tag{5.92}$$

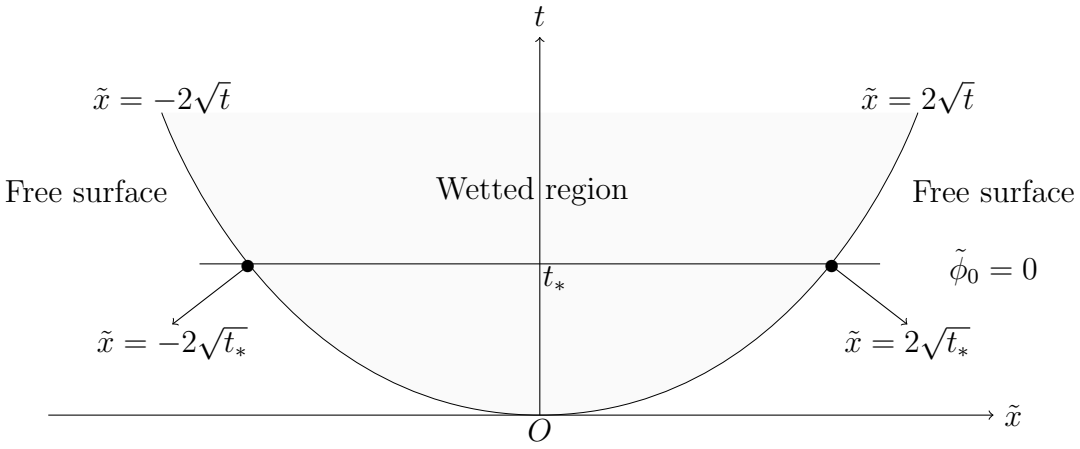

Figure 5.5: The $\tilde{x}, t$ plane of events for the liquid boundary. Horizontal line corresponds to the liquid boundary at the instant $t = t_*$.

and the derivative of the equation (5.92) with respect to $\tilde{x}$ gives

$$\frac{\partial \tilde{\phi}_0}{\partial \tilde{x}} = \frac{\tilde{x}}{2}\sqrt{4t - \tilde{x}^2} \qquad |\tilde{x}| < 2\sqrt{t},\ \tilde{y} = 0. \tag{5.93}$$

The time-derivative of the horizontal displacement potential, $\frac{\partial^2 \tilde{\phi}_0}{\partial \tilde{x} \partial t}$, can be obtained directly from the time derivative of equation (5.52) or from the $\tilde{x}$ derivative of equation (5.93), we get

$$\frac{\partial^2 \tilde{\phi}_0}{\partial \tilde{x} \partial t} = \frac{\tilde{x}}{\sqrt{4t - \tilde{x}^2}} \qquad |\tilde{x}| < 2\sqrt{t},\ \tilde{y} = 0. \tag{5.94}$$

From equation (5.91), to calculate the correction to the pressure, we still have to find the acceleration potential, $\frac{\partial^2 \tilde{\phi}_1}{\partial t^2}$. To do that, we start by taking the time-derivative of equation (5.57) and we arrive at

$$\frac{\partial \tilde{\phi}_1}{\partial t}(\tilde{x}, 0, t) = 6t^2\Phi + 2t^3 \frac{\partial \Phi}{\partial \xi}\frac{\partial \xi}{\partial t}, \tag{5.95}$$

where

$$\frac{\partial \xi}{\partial t} = \frac{-\xi}{2t}. \tag{5.96}$$

Having equation (5.96), the dominant terms of the time-derivative of equation (5.95) follows

$$\frac{\partial^2 \tilde{\phi}_1}{\partial t^2}(\tilde{x}, 0, t) = \frac{t}{2}\Big[24\ \Phi - 9\ \xi \frac{\partial \Phi}{\partial \xi} + \xi^2 \frac{\partial^2 \Phi}{\partial \xi^2}\Big] \qquad |\tilde{x}| < 2\sqrt{t},\ \tilde{y} = 0. \tag{5.97}$$

Where $\frac{\partial^2\Phi}{\partial\xi^2}$, $\frac{\partial\Phi}{\partial\xi}$ and Φ are given, respectively, by equations (5.72)–(5.74). On the boundary $\zeta = 0$, we denote

$$S(\xi) = -12\ \Phi + \frac{9}{2}\ \xi\frac{\partial\Phi}{\partial\xi} - \frac{1}{2}\xi^2\frac{\partial^2\Phi}{\partial\xi^2} \qquad |\xi| < 1. \tag{5.98}$$

The function $S(\xi)$ in (5.98) has a square-root singularity at $\xi = 1$. We need to remove the square-root singularity in the pressure correction $\tilde{p_1}$, in order to understand its behaviour as ξ tends to one. Therefore we remove the singularity by multiplying both sides of equation (5.98) by $\sqrt{1-\xi^2}$ and define

$$\tilde{S}(\xi) = S(\xi)\sqrt{1-\xi^2} \qquad |\xi| < 1. \tag{5.99}$$

Also we introduce $E(\xi)$ to represent the remaining terms of $\tilde{p_1}$ which are uncovered by $S(\xi)$

$$E(\xi) = 3\mu\frac{\xi^2}{\sqrt{1-\xi^2}}\left(3-\xi^2\right) - 2\xi^2 + 1 \qquad |\xi| < 1, \tag{5.100}$$

where $E(\xi)$ is the contribution that ϕ_0 gives to the pressure distribution at the higher order of $O(1)$ while $S(\xi)$ is the contribution of ϕ_1, due to gravity. Again we multiply both sides of equation (5.100) by $\sqrt{1-\xi^2}$ and we denote $\tilde{E}(\xi)$ to be

$$\tilde{E}(\xi) = E(\xi)\sqrt{1-\xi^2} \qquad |\xi| < 1. \tag{5.101}$$

Therefore from equations (5.99)–(5.101), equation (5.91) gives

$$\tilde{p_1}(\xi, 0, t) = \frac{t}{\sqrt{1-\xi^2}}\hat{p_1}(\xi) \quad |\xi| < 1, \tag{5.102}$$

where

$$\hat{p_1}(\xi) = \tilde{E}(\xi) + \tilde{S}(\xi) \qquad |\xi| < 1, \tag{5.103}$$

is the correction to the pressure distribution as a function of ξ only along $|\xi| < 1$ derived from $\tilde{p_1}(\xi, 0, t)$ in (5.102). The behaviour of the functions $\tilde{S}(\xi)$, $\tilde{E}(\xi)$ and $\hat{p_1}(\xi)$ on the boundary $0 \le \xi \le 1$, are shown, respectively, in Figures 5.6–5.8. The two Figures 5.6–5.7 demonstrate the contribution of $\tilde{S}(\xi)$ and $\tilde{E}(\xi)$ to the pressure correction due to gravity. It is shown that the first-order (due to gravity) displacement potential $\tilde{\phi_1}$ is substantial comparing to the leading-order displacement potential $\tilde{\phi_0}$. Therefore from the equation (5.103) gravity will exert a negative influence on the pressure distribution all over wetted body boundary.

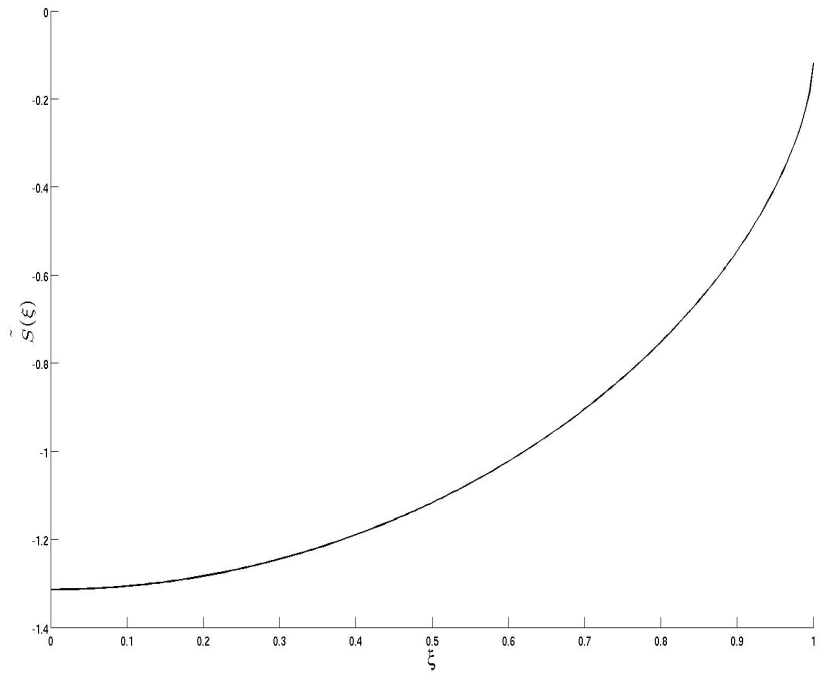

Figure 5.6: The function $\tilde{S}(\xi)$ on $0 \leq \xi \leq 1$, $\tilde{S}(1) = -0.1188$, $\tilde{S}(0) = -1.321$.

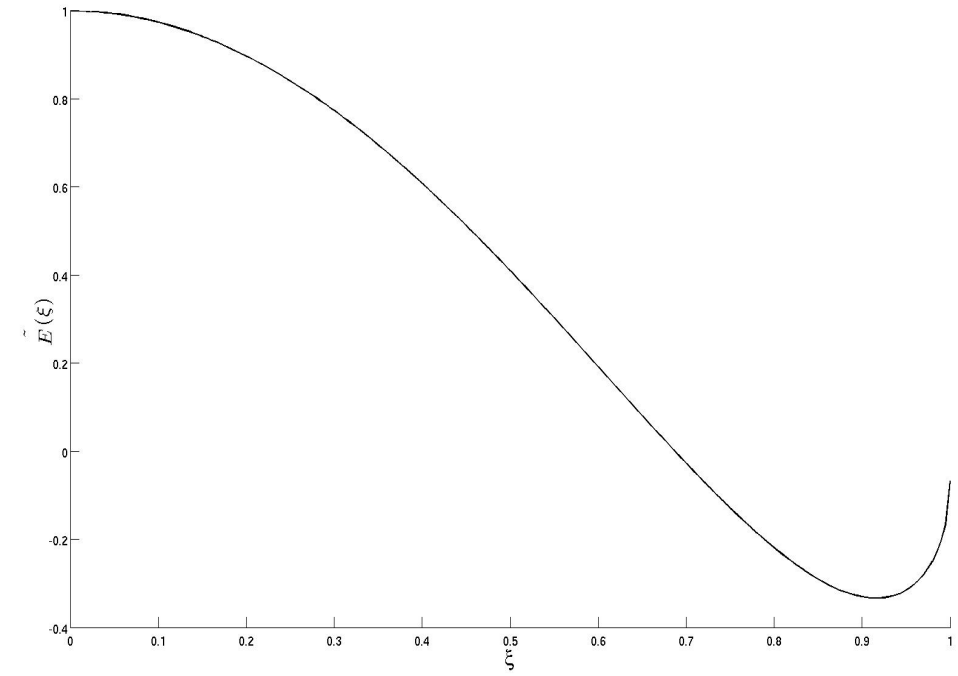

Figure 5.7: The function $\tilde{E}(\xi)$ on $0 \leq \xi \leq 1$, $\tilde{E}(1) = -0.0679$, $\tilde{E}(0) = 1$.

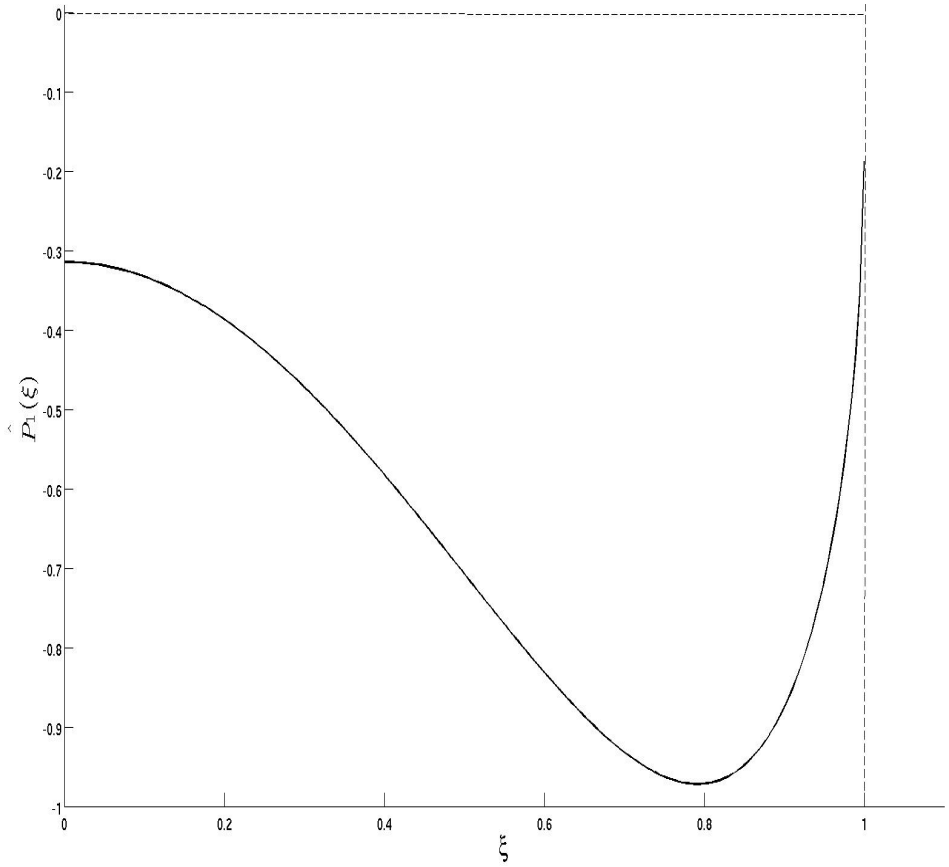

Figure 5.8: The function $\hat{p}_1(\xi)$ on $0 \leq \xi \leq 1$, $\hat{p}_1(1) = -0.1867$ is the absolute maximum. The local maximum, at $\xi = 0$ is where $\hat{p}_1(0) = -0.3141$; the local minimum, at $\xi = 0.7940$ is where $\hat{p}_1(0.7940) = -0.9719$

Combining equations (5.89) and (5.91), the pressure distribution along the wetted body boundary takes the form

$$\tilde{p}(\xi, 0, t) = \frac{t^{-1/2}}{\sqrt{1-\xi^2}}\left(1 + \delta t^{3/2}\hat{p}_1(\xi)\right) + O\left(\delta^2\right) \qquad |\xi| < 1. \tag{5.104}$$

Equation (5.104) makes it clear that the correction due to gravity does not increase the singularity of the pressure compared to that we had in the leading order. Figure (5.8) shows that gravity decreases the pressure along the wetted body boundary, and has its maximum decrease at a short interval just before the contact point. This is clearly shown in Figures 5.9–5.10 where the decline in the pressure distribution due to gravity is always small at the centre and the peak, at $\xi = 1$, while at the region just to the left of the contact point the difference is more compared with the other regions.

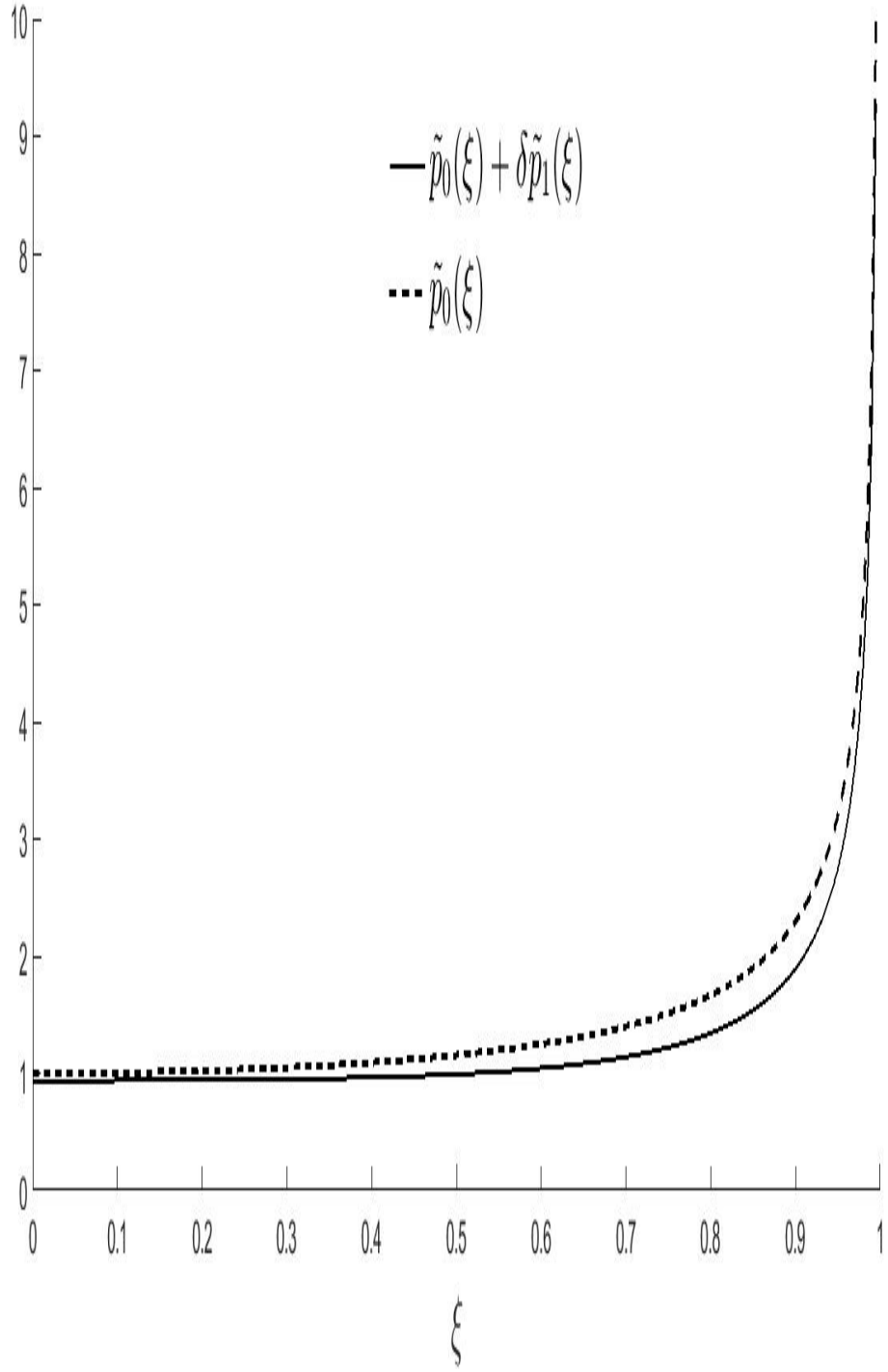

Figure 5.9: In non-dimensional variables, the leading-order pressure distribution p_0, (dashed line), and the pressure distribution with correction due to gravity $\tilde{p}_0 + \delta\tilde{p}_1$, (solid line), with $\delta = 0.2$.

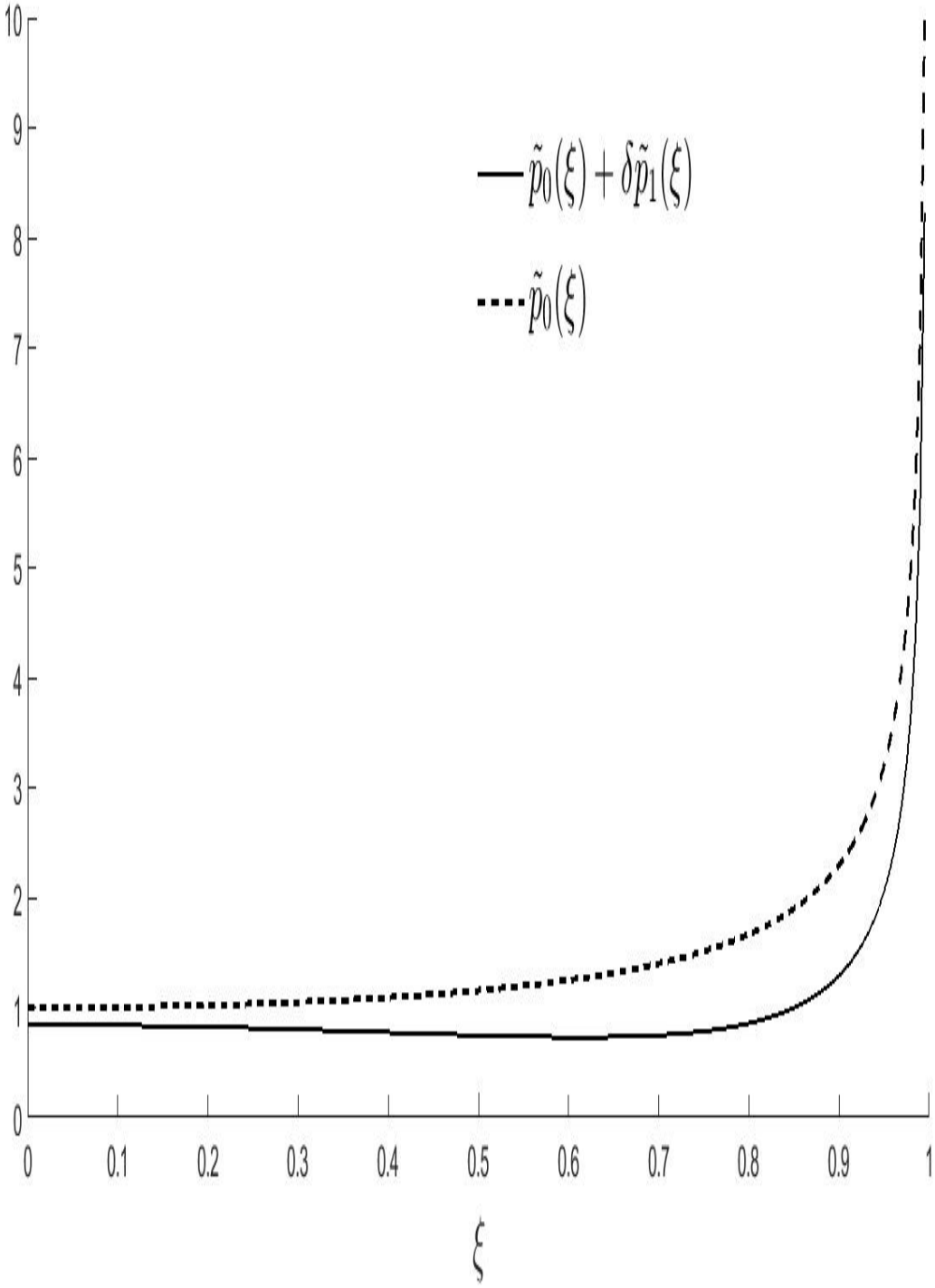

Figure 5.10: In non-dimensional variables, the leading-order pressure distribution p_0, (dashed line), and the pressure distribution with correction due to gravity $\tilde{p}_0 + \delta\tilde{p}_1$, (solid line), with $\delta = 0.5$.

5.5 Hydrodynamic force

In this section we will estimate the hydrodynamic force acting on the body during the impact. For a rigid body entering a liquid, the hydrodynamic force is obtained either by integration of the pressure over the body surface, see (Faltinsen 1993),(Oliver 2002) and (Korobkin 2007) or by using the energy argument, see (Miloh 1981) and (Wu 1998). Identical results, by both approaches were found by (Wu 1998). In this work we use the former method to calculate the hydrodynamic force on the body and the energy distribution will be discussed in the section 5.6. The vector formula of the force exerted by the fluid against the wetted part of the submerged body is given by

$$\vec{F}(t) = \int_{w.b.} p.\vec{n}\ \mathrm{d}S, \tag{5.105}$$

where $w.b.$ refers to the wetted part of the body surface, S is the arc length along the body, $\vec{n}$ is the outer normal unit vector. The horizontal force acting on the symmetric body is zero. The vertical force $F(t)$ is given by

$$F(t) = \int_{-x_c}^{x_c} p\left(x, \frac{x^2}{2R} - Vt, t\right) \mathrm{d}x \qquad\qquad |x| < x_c(t). \tag{5.106}$$

In the non-dimensional variables introduced in section 5.1 and in particular the equation (5.11), the force is non-dimensionalized as

$$F(t) = \rho\ V^2 R\ \hat{F}(\hat{t}), \tag{5.107}$$

where a hat stands for non-dimensional variables. Hence equation (5.106) takes its non-dimensional form as

$$\hat{F}(\hat{t}) = 2\int_0^{x_c} \hat{p}\left(\hat{x}, \epsilon\left(\frac{\hat{x}^2}{2} - \hat{t}\right), \hat{t}\right) \mathrm{d}\hat{x}. \tag{5.108}$$

Dropping the hats and introducing the stretched variables (5.38) into equation (5.108), on $\tilde{y} = 0$, we arrive at

$$\begin{aligned}
\tilde{F}(t) &= 2\int_0^{x_{c0}} \tilde{p}(\tilde{x}, 0, t)\frac{x_c(t,\delta)}{x_{c0}(t)}\mathrm{d}\tilde{x} \\
&= 2\int_0^{2\sqrt{t}} \left(\tilde{p_0} + \delta\tilde{p_1}\right)\left(1 + \delta x_{c1}(t)\right)\mathrm{d}\tilde{x} + O\left(\delta^2\right) \\
&= 2\int_0^{2\sqrt{t}} \left(\tilde{p_0} + \delta(x_{c1}\tilde{p_0} + \tilde{p_1})\right)\mathrm{d}\tilde{x} + O\left(\delta^2\right).
\end{aligned} \tag{5.109}$$

Substituting $\tilde{p_0}$ given by (5.90) and $\tilde{p_1}$ given by (5.102) and introducing new variables of integration $\xi = \frac{\tilde{x}}{2\sqrt{t}}$, we find

$$\begin{aligned}\tilde{F}(t) = 2\int_0^1 \Bigg(&\frac{2}{2\sqrt{t}\sqrt{1-\xi^2}} + \delta\Big(\frac{2\mu t^{3/2}}{2\sqrt{t}\sqrt{1-\xi^2}} \\ &+ t\big(E(\xi)+S(\xi)\big)\Big)\Bigg) 2\sqrt{t}\,\mathrm{d}\xi + O\left(\delta^2\right), \\ \tilde{F}(t) = 4\int_0^1 &\left(\frac{1}{\sqrt{1-\xi^2}} + \delta t^{3/2}\left(\frac{\mu}{\sqrt{1-\xi^2}} + E(\xi) + S(\xi)\right)\right)\mathrm{d}\xi + O\left(\delta^2\right),\end{aligned} \tag{5.110}$$

where $E(\xi)$ is given by (5.100) and where

$$\begin{aligned}S(\xi) = &-12c + 2\xi^2 + \frac{2\xi}{5\pi}\sqrt{1-\xi^2}\ln\left(\frac{1+\xi}{1-\xi}\right)\left(8\xi^4 - 16\xi^2 + 3\right) \\ &- \frac{12}{225\pi}\sqrt{1-\xi^2}\left(126\xi^4 + 25\xi^2 - 88\right) - \frac{\xi^2\big(3600\xi^4 - 4104\xi^2 + 672\big)}{450\pi\sqrt{1-\xi^2}} \\ &- \frac{16}{5\pi}\sum_{n=0}^{\infty}\left(\frac{1}{n+1} - \frac{6\xi^2}{n+2}\right)\xi^{2n+2}\sum_{i=0}^{n}\binom{3/2}{i}\frac{(-1)^i}{2n-2i+1}.\end{aligned} \tag{5.111}$$

The asymptotic expansion of the hydrodynamic force with respect to δ is

$$\tilde{F}(t) = \tilde{F_0}(t) + \delta\tilde{F_1}(t) + O\left(\delta^2\right). \tag{5.112}$$

At the leading order the hydrodynamic force is constant,

$$\tilde{F_0}(t) = 2\pi \qquad |\tilde{x}| < 2\sqrt{t}. \tag{5.113}$$

The correction to the hydrodynamic force due to gravity is of order $O(\delta)$ and is defined by

$$\tilde{F_1}(t) = 4t^{3/2}\int_0^1 \Big[\frac{\mu}{\sqrt{1-\xi^2}} + E(\xi) + S(\xi)\Big]\mathrm{d}\xi. \tag{5.114}$$

This force is time dependent, in contrast to the leading-order hydrodynamic force, equation (5.113), which is constant.

Integration of the first and the second terms of the right hand side of equation (5.114) give $-|\mu|\frac{\pi}{2}$ and $\frac{1}{3} + \frac{27}{16}|\mu|\pi$. Using equation (5.98) and integrating by parts for the last term, we find

$$\int_0^1 S(\xi)\mathrm{d}\xi = -12\Phi(1,0) - \frac{1}{2}\frac{\partial\Phi}{\partial\xi}(1,0) + \frac{35}{2}\int_0^1 \xi\frac{\partial\Phi}{\partial\xi}\mathrm{d}\xi, \tag{5.115}$$

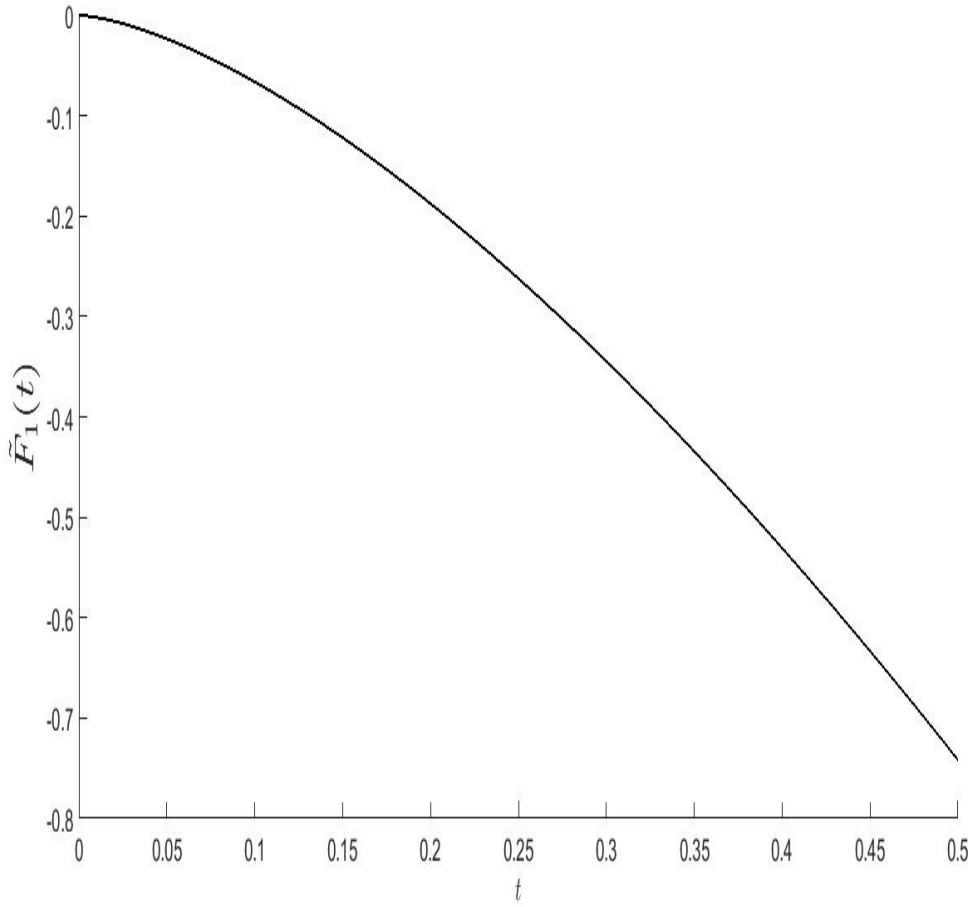

Figure 5.11: The non-dimensional correction to the hydrodynamic force, $\tilde{F}_1(t)$ given by (5.114), due to gravity as a function of non-dimensional time.

where $\Phi(1,0)$ and $\frac{\partial \Phi}{\partial \xi}(1,0)$ can be found from equations (5.74) and (5.72) respectively. The integral on the right hand side of equation (5.115) is straightforward to evaluate, except the term with natural logarithm in equation (5.72), which is numerically integrated. The result is

$$\tilde{F}_1(t) = -2.09\ t^{3/2}. \tag{5.116}$$

The non-dimensional correction to the hydrodynamic force is shown in Figure 5.11 which reveals that gravity decreases the hydrodynamic force even during the early stage. the correction is significant for moderate values of δ, in particular when $\frac{1}{2} < k \leq 1$, see equation (5.19).

5.6 Correction to the free surface

In this section the influence of gravity on the free surface will be discussed. This information is needed for the next section to calculate the effects of gravity on the energy distribution. It is also in our interest to know how significant is the contribution of gravity on the free surface. To find this displacement of the free surface, we write its expansion in powers of δ

$$\eta(x,t) = \eta_0(x,t) + \delta\eta_1(x,t) + O\left(\delta^2\right). \tag{5.117}$$

Where the leading free surface, $\eta_0(x,t)$, is calculated from equation (5.53). For the correction, $\eta_1(x,t)$, the vertical displacement, $\frac{\partial\phi_1}{\partial y}(t,y,t)\big|_{y=0}$ should be determined, see equation (5.39) to find the change of variables provided. The characteristic function, $W(\xi,\zeta)\big|_{\zeta=0}$, in terms of the vertical and horizontal displacement is defined in equation (5.62). In terms of new variables, $\xi = 1$ is the moving contact point on the right. Starting from the Hilbert formula given in (5.66), where the real and imaginary parts of the characteristic function $W(\xi,0)$ are defined in equations (5.64) and (5.65). On the free surface, $\xi > 1$, the Hilbert formula reads

$$\begin{aligned}\frac{\partial\Phi}{\partial\zeta}(\xi,0)\sqrt{\xi^2-1} =& \frac{1}{\pi}\int_{-1}^{1}\frac{\partial\Phi}{\partial\zeta}(\xi_0,0)\frac{\sqrt{1-\xi_0^2}}{\xi_0-\xi}\mathrm{d}\xi_0 \\ &- \frac{2\xi}{\pi}\int_1^{\infty}\frac{\partial\Phi}{\partial\xi}(\xi_0,0)\frac{\sqrt{\xi_0^2-1}}{\xi_0^2-\xi^2}\mathrm{d}\xi_0.\end{aligned} \tag{5.118}$$

Where $\frac{\partial\Phi}{\partial\zeta}$ for $|\xi| < 1$ and $\frac{\partial\Phi}{\partial\xi}$ for $\xi > 1$ are given, respectively, in equations (5.61) and (5.60). The integrals on the right-hand side of equation (5.118) are calculated as we did for equation (5.67). However one should consider $\xi > 1$ for the second integral. Therefore, the equation (5.118) follows

$$\begin{aligned}\frac{\partial\Phi}{\partial\zeta}(\xi,0) =& \frac{24\xi}{225\pi}\sqrt{\xi^2-1}(30\xi^2-23) \\ &+ \frac{4}{15\pi}(\xi^2-1)^{3/2}(1-6\xi^2)\ln\left|\frac{1+\xi}{1-\xi}\right|, \quad \xi > 1, \zeta = 0.\end{aligned} \tag{5.119}$$

Therefore, equations (5.32), (5.117) and (5.119) yield

$$\begin{aligned}\eta_1(x,t) =& \frac{3x\sqrt{t}}{225\pi}\sqrt{x^2-4t}(15x^2-46t) \\ &+ \frac{1}{60\pi}(x^2-4t)^{3/2}(2t-3x^2)\ln\left|\frac{2\sqrt{t}+x}{2\sqrt{t}-x}\right|, \quad x > 2\sqrt{t}, y = 0\end{aligned} \tag{5.120}$$

where change of variables are used by using relations in (5.58). In Figure 5.12 the correction to the free surface due to gravity is shown. The change of sign indicates that the correction will be different in different parts of the domain.

However, from the figure one can note that these changes will be tiny and go to zero as we approach the far-field.

From the equation (5.120) it is clear that the gravity has no influence on the free surface close to the body. This can be seen in Figure 5.13 for the non-dimensional time series $t = 0.5, 0.7, 0.9, 1.1$ and 1.3. In this figure it is shown that the gravity is increasing the height of the free surface as time goes.

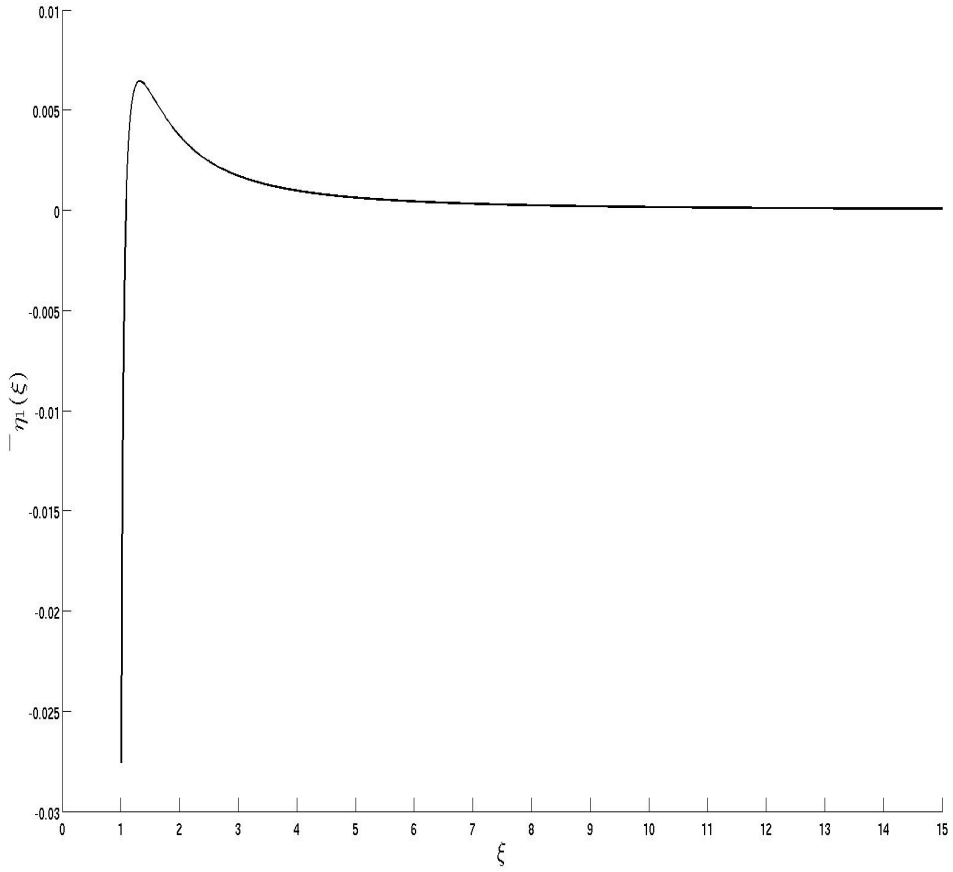

Figure 5.12: The correction due to gravity to the non-dimensional vertical displacement potential $\frac{\partial \Phi}{\partial \zeta}(\xi, 0)$ which is the correction to the free-surface elevation $\eta_1(\xi)$, for $\xi > 1$.

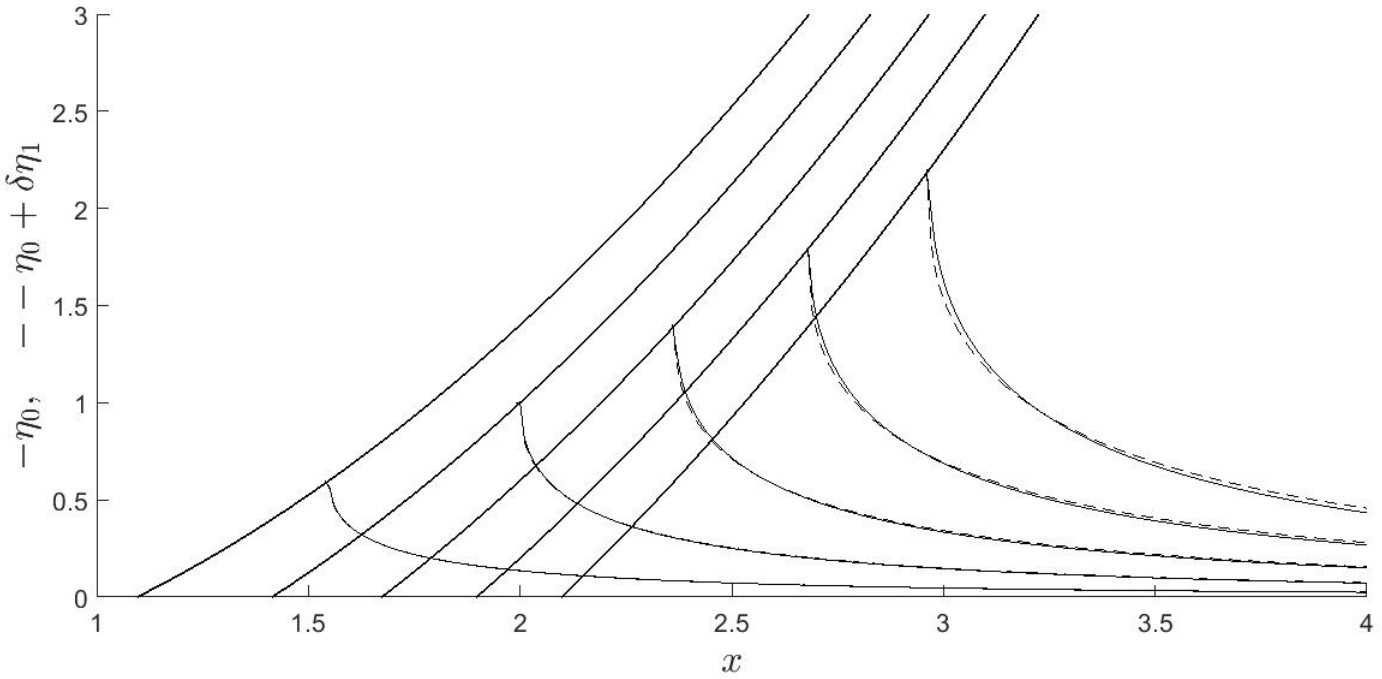

Figure 5.13: The correction to the non-dimensional free surface due to gravity with $\delta = 0.5$. Lines are for η_0, dashed lines for $\eta_0 + \delta\eta_1$ and bold lines for the body.

5.7 The energy distribution

When the body is entering the fluid, the body does work on the fluid, increasing its total energy. In this section we calculate the total energy distribution between the jets and the leading-order flow. So far we have not accounted for the jets during the calculation of the pressure and force. However when we make an account of the energy, these jets contribute significantly to the total energy of the flow. Discussions of energy can be found in (Cooker 2002), (Cointe, Fontaine, Molin & Scolan 2004) and (Reinhard et al. 2013). The entering body is rigid so no body vibration is accounted for in this work. For the elastic potential energy and acoustic effects contribution see (Korobkin 1995) and (Reinhard et al. 2013).

The total energy in this fluid system is expressed as the potential energy (in the presence of gravity) and kinetic energy. In this section we will find the kinetic energy in the system excluding the jets. While the kinetic energy in the jets will be discussed in the next section after the thickness of the jets and velocity of the fluid in the jets have been identified. Also for the potential energy we need information about the jets and this to be considered in later sections.

From (Lamb 1932), for irrotational and incompressible fluid, the total kinetic energy $\mathrm{E_{kin}}$ is defined by

$$\mathrm{E_{kin}} = \frac{1}{2}\rho \iint\limits_{\Omega(t)} |\nabla\varphi|^2 \mathrm{d}x\mathrm{d}y, \tag{5.121}$$

where $\Omega(t)$ is the whole fluid domain excluding the jets. In particular $\Omega(t)$ is a semi-circle in lower-half plane of large radius R. We expect $\mathrm{E_{kin}}$ to be well defined as $\mathrm{R} \longrightarrow \infty$ The energy in the jets will be calculated separately later. The fact that the fluid is incompressible, $\nabla^2\varphi = 0$, gives the identity

$$|\nabla\varphi|^2 = \nabla\varphi.\nabla\varphi = \nabla.(\nabla\varphi), \tag{5.122}$$

Using Green's theorem in (Lamb 1932) and the identity (5.122) for incompressible fluid, the double integral in equation (5.121) reduces to a boundary-integral, hence

$$\mathrm{E_{kin}} = \frac{1}{2}\rho \int_{\partial\Omega(t)} \varphi \, \frac{\partial\varphi}{\partial\hat{n}} \mathrm{d}s, \tag{5.123}$$

where $\hat{n}$ is the outward unit normal vector, $\partial\Omega(t)$ is the boundary of the domain $\Omega(t)$ discribed anticlockwise and s is the arc-length coordinate along the boundary $\partial\Omega(t)$. The kinetic energy is non-dimensionalised by

$$\mathrm{E_{kin}} = \rho X_{sc}^2 V^2 \hat{\mathrm{E}}_{\mathrm{kin}}, \tag{5.124}$$

to arrive at (hats are dropped)

$$\mathrm{E_{kin}} = \frac{1}{2}\int_{\partial\Omega(t)} \varphi\ \frac{\partial\varphi}{\partial n}\ \mathrm{d}s. \tag{5.125}$$

To calculate the kinetic energy over $\Omega(t)$ we separate the boundary $\partial\Omega(t)$ into the interval $[-\mathrm{R}, \mathrm{R}]$ of the x-axis and a semicircle in the lower half plane:

$$\mathrm{E_{kin}} = -\frac{1}{2}\int_{\text{-R}}^{\mathrm{R}} \varphi\ \frac{\partial\varphi}{\partial y}\Big|_{y=0}\ \mathrm{d}x + \frac{1}{2}\int_{-\pi}^{0} \bar{\varphi}\ \frac{\partial\bar{\varphi}}{\partial r}\ \mathrm{R}\ \mathrm{d}\theta. \tag{5.126}$$

Where $\mathrm{R} \longrightarrow \infty$ and $\bar{\Omega}$ is a semi-circle in the region $y < 0$ of radius $\mathrm{R}\longrightarrow \infty$. Here $\bar{\varphi} = \bar{\varphi}(r, \theta), 0 < r < \mathrm{R}, -\pi < \theta < 0$. From the far-field condition (5.27) the far-field boundary is assumed to contribute nothing. As to the first integral in equation (5.126), which is the total kinetic energy, we calculate it separately. The impact is symmetric and the kinetic energy on the left side is the same as that on the right side from the centre of the body, hence

$$\begin{aligned}\frac{1}{2}\int_{\text{-R}}^{\mathrm{R}} \varphi\ \frac{\partial\varphi}{\partial y}\ \mathrm{d}x &= \int_{0}^{\mathrm{R}} \varphi\ \frac{\partial\varphi}{\partial y}\ \mathrm{d}x \\ &= \Big(\int_{0}^{x_c(t)} + \int_{x_c(t)}^{\mathrm{R}}\Big)\varphi\ \frac{\partial\varphi}{\partial y}\ \mathrm{d}x.\end{aligned} \tag{5.127}$$

First to calculate the velocity potential φ and the vertical velocity $\frac{\partial\varphi}{\partial y}$ as the solutions are given in terms of displacement potential $\tilde{\phi}$. Taking the time-derivative of the solution will provide the solution in terms of the velocity potential. The solution in terms of displacement potential on $0 < x < 2\sqrt{t}$ is given in equations (5.42) and (5.52) but in terms of the velocity potential these two functions are

$$\frac{\partial\varphi}{\partial y} = -1 - 6\delta|\mu|t^2(6\xi^2 - 1) + O\left(\delta^2\right) \qquad |\xi| < 1, \tag{5.128}$$

$$\begin{aligned}\varphi = -2\sqrt{t}\sqrt{1-\xi^2} + 6\delta t^2\Bigg(c - \frac{4}{15}\xi^6 + \frac{2}{3}\xi^4 - \frac{1}{2}\xi^2 - \frac{8}{225\pi}(1-\xi^2)^{3/2}\Big(11 - 18\xi^2\Big) \\ + \frac{4}{15\pi}\sum_{n=0}^{\infty}\left(\frac{1}{n+1} - \frac{6\xi^2}{n+2}\right)\xi^{2n+2}\sum_{i=0}^{n}\binom{3/2}{i}\frac{(-1)^i}{2n-2i+1}\Bigg) + O\left(\delta^2\right),\end{aligned}$$

$$|\xi| < 1, \tag{5.129}$$

where for convenience we use the variables introduced in equation (5.58) on the contact region $|\xi| < 1$ and $\varphi = \varphi(\xi, 0, t)$. The bracketed term in the second summation of equation (5.129) is the binomial coefficient. In the same way from equations (5.53) and (5.55) the solution on the free surface in terms of the velocity potential are

$$\frac{\partial \varphi}{\partial y} = \frac{x}{\sqrt{x^2 - 4t}} - 1 + O(\delta) \qquad |x| > 2\sqrt{t}, \quad (5.130)$$

$$\varphi = \delta \left(\frac{t^2}{2} - \frac{x^2}{2} t + \frac{x^4}{12} - \frac{x}{12} \left(x^2 - 4t \right)^{3/2} \right) + O\left(\delta^2\right) \qquad |x| > 2\sqrt{t}. \quad (5.131)$$

Note that the first-order terms in the expression for the vertical velocity in equation (5.130) are not needed to calculate the kinetic energy, because this term will be multiplied by the zero leading-order velocity potential on the free surface given in equation (5.49). The kinetic energy on the contact region $\mathrm{E}_{\mathrm{kin}}^{\mathrm{F_c}}$ is

$$\mathrm{E}_{\mathrm{kin}}^{\mathrm{F_c}} = \pi t + \delta \left(0.1067\sqrt{t} - 1.217 \right) t^{5/2} + O\left(\delta^2\right). \quad (5.132)$$

The second term on the right-hand side of equation (5.132) demonstrates that gravity reduces the kinetic energy in this region. On the free surface the contribution to the kinetic energy $\mathrm{E}_{\mathrm{kin}}^{\mathrm{F_s}}$ is zero at the leading order as the velocity potential is zero. However by including the gravity in calculations a non-zero velocity potential will appear on the free surface. Therefore it will be of $O(\delta)$ and contributes to

$$\mathrm{E}_{\mathrm{kin}}^{\mathrm{F_s}} = -0.1556\ \delta\ t^{5/2} + O\left(\delta^2\right) \qquad |x| > 2\sqrt{t}. \quad (5.133)$$

5.8 The jet root region

The thickness of the jet in the inner region without gravity, $\mathrm{H_J}(t)$, is found , see for example (Wilson 1989), to be

$$\mathrm{H_J}(t) = \frac{\pi x_c(t)}{8\dot{x}_c^2(t)}, \quad (5.134)$$

where overdot denotes the time-derivative. To calculate the thickness of the jet with regard to gravity the moving point is given by equation (5.39) then equation (5.134) be rewritten as

$$\mathrm{H_J^g}(t, \delta) = \frac{\pi x_c(t, \delta)}{8\dot{x}_c^2(t, \delta)}. \quad (5.135)$$

Using the results in Section 5.2, in particular the time-derivative of equation (5.71) which gives the velocity of the non-dimensional moving contact point, we find that

$$\dot{x}_c(t, \delta) = \frac{1}{\sqrt{t}} - 4\delta|\mu|t + O\left(\delta^2\right). \quad (5.136)$$

So from equation (5.135) the thickness of the jet in the inner region, accounting for gravity, $\mathrm{H_J^g}(t, \delta)$, can be shown to be

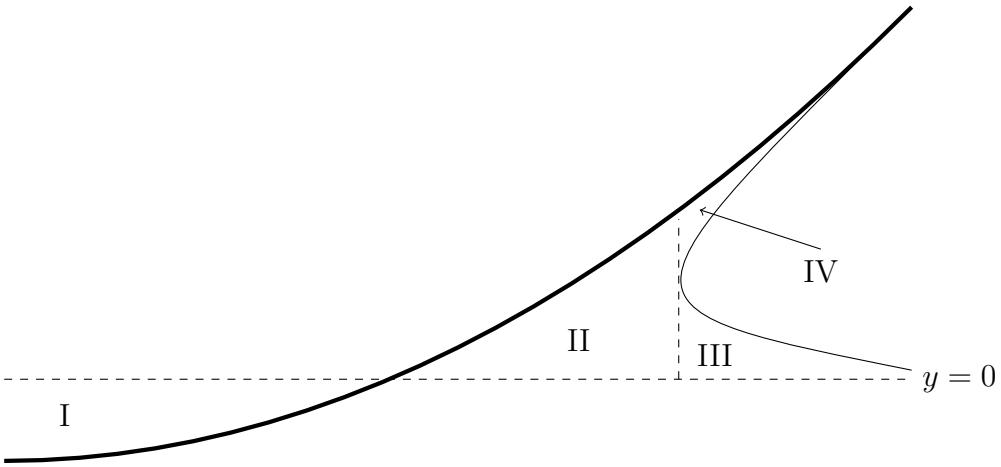

Figure 5.14: A partition where the potential energy to be calculated. The horizantol dashed line is the equiliburium state of the free surface, $y = 0$.

$$\mathrm{H}_{\mathrm{J}}^{\mathrm{g}}(t,\delta) = \frac{\pi}{4} t^{3/2} \left(1 + 7\delta|\mu| t^{3/2}\right) + O\left(\delta^2\right). \tag{5.137}$$

Equation (5.137) says that in the water-entry problem gravity significantly increases the jet's thickness in the jet root region, i.e.

$$\mathrm{H}_{\mathrm{J}}^{\mathrm{g}}(t,\delta) > \mathrm{H}_{\mathrm{J}}(t). \tag{5.138}$$

However, in Figure 5.2 it is shown that gravity decreases the width of the wetted region and the speed of the moving contact point $x = x_c(t)$ is lessened by gravity. This reveals the fact that the effect of gravity on the moving contact point's position is dominant on the same effect on the square of the speed of the moving contact point.

5.9 Potential energy

Before the impact the potential energy of the fluid is some value $\mathrm{E_p}(0)$ relative to the Earth-fixed coordinate system Oxy. However, $\mathrm{E_p}$ changes in time, from the instant of impact and later on. In this section we want to find how gravity changes the potential energy of the system in each individual part of the fluid as shown in Figure 5.14. The impact is symmetric, hence only the right side is shown in the figure.

In non-dimensional variables the change in the potential energy for the system is

$$\mathrm{E_p}(t) - \mathrm{E_p}(0) = 2\left(\iint\limits_{I} + \iint\limits_{II} + \iint\limits_{III} + \iint\limits_{IV} \right) y \mathrm{d}y\mathrm{d}x. \tag{5.139}$$

The potential energy is scaled by $\rho g X_{sc}^3$. The impact is symmetric so the right-hand side of equation (5.139) is multiplied by a factor of 2. We will deal with each region individually. The first integral in equation (5.139) gives the potential energy between the contact points of the body with the equilibrium line of the free surface, $\mathrm{E_p^I}$,

$$\mathrm{E_p^I} = 2\int_0^{\sqrt{2t}} \int_{\frac{x^2}{2}-t}^{0} y\mathrm{d}y\mathrm{d}x = -\frac{8\sqrt{2}}{15}t^{5/2}. \tag{5.140}$$

The second integral in equation (5.139) calculates the potential energy between the body and the moving contact point above the level free surface, $\mathrm{E_p^{II}}$,

$$\begin{aligned}\mathrm{E_p^{II}} &= 2\int_{\sqrt{2t}}^{2\sqrt{t}-2\delta|\mu|t^2} \int_0^{\frac{x^2}{2}-t} y\mathrm{d}y\mathrm{d}x \\ &= \frac{14-8\sqrt{2}}{15}t^{5/2} - 2\ \delta\ |\mu|\ t^4 + O\left(\delta^2\right).\end{aligned} \tag{5.141}$$

The potential energy in region II decreases when the correction due to gravity on the moving contact point is included. From the Figure 5.14 the potential energy in region III, $\mathrm{E_p^{III}}$, in present of gravity, is

$$\mathrm{E_p^{III}} = 2\int_{x_c(t)}^{\infty} \int_0^{\eta(x,t)} y\mathrm{d}y\mathrm{d}x. \tag{5.142}$$

The upper limit of the outer integral refers to the far-field domain. To calculate this potential energy, $\mathrm{E_p^{III}}$, we use the stretched variables in (5.39) and (5.58). Then the integral on the right-hand side of equation (5.142) can be rewritten as

$$\mathrm{E_p^{III}} = 2t^{5/2}\int_1^{\infty} \eta_0^2 \mathrm{d}\xi + 2\delta t^4 \left(\int_1^{\infty} \left(\eta_0\eta_1 - |\mu|\eta_0^2\right)\right) \mathrm{d}\xi. \tag{5.143}$$

Where from equations (5.32) and (5.53), $\eta_0 = \eta_0(\xi)$ is found to be

$$\eta_0(\tilde{x}, t) = t\eta_0(\xi), \tag{5.144}$$

where $\tilde{x}$ is the stretched variable defined in (5.38) and

$$\eta_0(\xi) = -1 + 2\xi^2 - 2\xi\sqrt{\xi^2 - 1} \qquad \xi > 1. \tag{5.145}$$

Also $\eta_1 = \eta_1(\xi)$ is derived from equation (5.32) and the relations given in (5.59)

$$\eta_1(\tilde{x}, t) = t^{5/2}\eta_1(\xi), \tag{5.146}$$

where $\eta_1(\xi)$ is given through equation (5.119). Therefore the potential energy in region III reads

$$\mathrm{E_p^{III}} = \frac{2}{15}t^{5/2} + 2\delta t^4\left(C - \frac{|\mu|}{15}\right), \tag{5.147}$$

where

$$C = \int_1^\infty \eta_0\eta_1 \mathrm{d}\xi. \tag{5.148}$$

Again form Figure 5.14 the potential energy in region IV, the jet region, reads

$$\mathrm{E_p^{IV}} = 2\int_{2\sqrt{t}-2\delta|\mu|t^2}^{\infty}\int_{\frac{x^2}{2}-t-\bar{H}_J}^{\frac{x^2}{2}-t} y\mathrm{d}y\mathrm{d}x, \tag{5.149}$$

where $\bar{H}_J = \bar{H}_J(x,t)$ is the non-dimensional jet's thickness in the jet region. To find $\bar{H}_J$ we need to solve the formulation below of the thin jet, see (Wilson 1989). We introduce bar to denote the variables in the jet region,

$$\frac{\partial \bar{H}_J}{\partial \bar{t}} + \frac{\partial}{\partial \bar{x}}(\bar{H}_J\frac{\partial \bar{\phi}}{\partial \bar{x}}) = 0, \tag{5.150}$$

$$\frac{\partial \bar{\phi}}{\partial \bar{t}} + \frac{1}{2}(\frac{\partial \bar{\phi}}{\partial \bar{x}})^2 = 0. \tag{5.151}$$

Equations (5.150) and (5.151) are known as the shallow water equations with zero gravity, (Howison et al. 1991) and (Oliver 2002). The boundary conditions for the jet problem are constructed from the jet root region. For the jet's thickness from equation (5.134) we have

$$\bar{H}_J(x_{c0}(t),t) = \frac{\pi x_{c0}(t)}{8\dot{x}_{c0}^2(t)} = \frac{\pi}{4}t^{3/2}, \tag{5.152}$$

and for the velocity potential, the boundary condition can be given by the fact that the fluid velocity in the jet root region is $2\dot{x}_{c0}(t)$, see next section. Therefore the boundary condition for the horizontal fluid velocity in the jet region, $\bar{u}(x,t)$ is

$$\bar{u}(x_{c0}(t),t) = 2\dot{x}_{c0}(t) = \frac{2}{\sqrt{t}}. \tag{5.153}$$

By substitution of $\frac{\partial \bar{\phi}}{\partial \bar{x}}$ with the horizontal velocity $\bar{u}(x,t)$ and differentiation of equation (5.151) once with respect to $\bar{x}$ we arrive at

$$\frac{\partial \bar{H}_J}{\partial \bar{t}} + \frac{\partial}{\partial \bar{x}}(\bar{H}_J\bar{u}) = 0, \tag{5.154}$$

$$\frac{\partial \bar{u}}{\partial \bar{t}} + \bar{u}\frac{\partial \bar{u}}{\partial \bar{x}} = 0. \tag{5.155}$$

Using the method of characteristics for the quasi-linear equations (5.154) and (5.155) with having the boundary conditions (5.152) and (5.153), the solution reads

$$\bar{u}(x,t) = \frac{x}{t} \qquad x \geq x_{c0}, \tag{5.156}$$

$$\bar{H}_J(x,t) = 8\pi \frac{t^4}{x^5} \qquad x \geq x_{c0}. \tag{5.157}$$

Having the jet's thickness (5.157), from equation (5.149) we can calculate the potential energy in the jet

$$\mathrm{E}_{\mathrm{p}}^{\mathrm{IV}} = \frac{\pi}{4}\big(3 - \frac{\pi}{18}\sqrt{t}\big)t^3 + \delta|\mu|\pi\big(1 - \frac{\pi}{8}\sqrt{t}\big)t^{9/2} + O\left(\delta^2\right). \tag{5.158}$$

The non-dimensional potential energy and its correction due to gravity in each region are shown in Figures 5.15, 5.16, 5.18 and 5.19. For all figures we used $\delta = 0.2$. At the first glance on these figures, we conclude that gravity affects the potential energy in region II more than any other region. In region I the potential energy is not affected by gravity, see Figure 5.15. Also for the potential energy in region IV, the jet region, the increase is small, see Figure 5.19. This may be due to the fact that although the jets are very fast they are very thin and therefore cannot escape from the influence of gravity. However, In Figure 5.16 it is shown that in region II gravity decreases the potential energy significantly but this correction is less visible in region III as shown in Figure 5.18. This small change is due to the tiny result which comes from the integrand $\eta_0(\xi)\eta_1(\xi)$ as shown in Figure 5.17. Therefore we have a negative effect due to gravity in potential energy in regions II and III, while gravity increased the potential energy in the jets' region IV. The potential energy in regions II and III are similar and together are similar in magnitude but of opposite sign to $\mathrm{E}_{\mathrm{p}}^{\mathrm{I}}$. Hence $\mathrm{E}_{\mathrm{p}}^{\mathrm{I}} + \mathrm{E}_{\mathrm{p}}^{\mathrm{II}} + \mathrm{E}_{\mathrm{p}}^{\mathrm{III}}$ is found to be small compared with the much larger jet energy $\mathrm{E}_{\mathrm{p}}^{\mathrm{IV}}$.

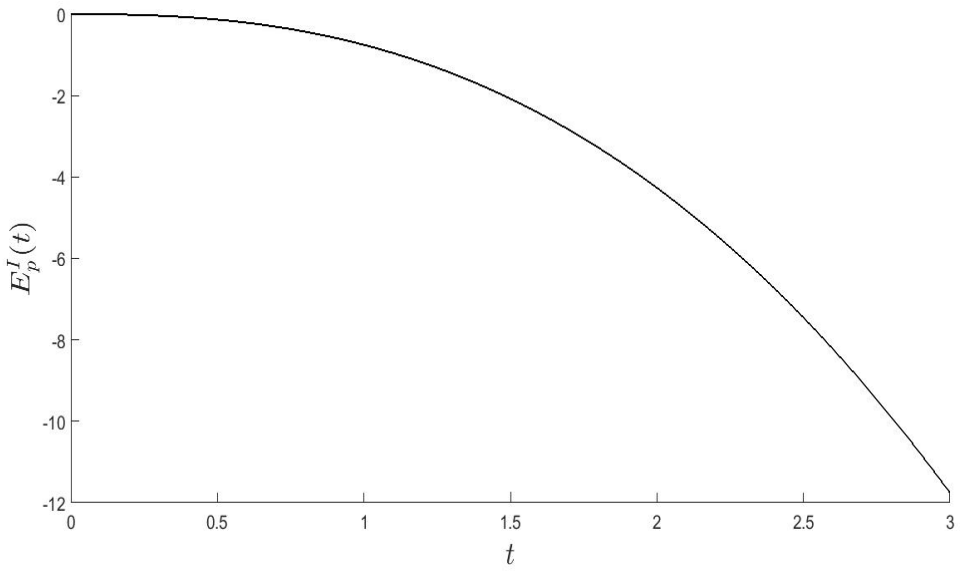

Figure 5.15: The non-dimensional potential energy in region I.

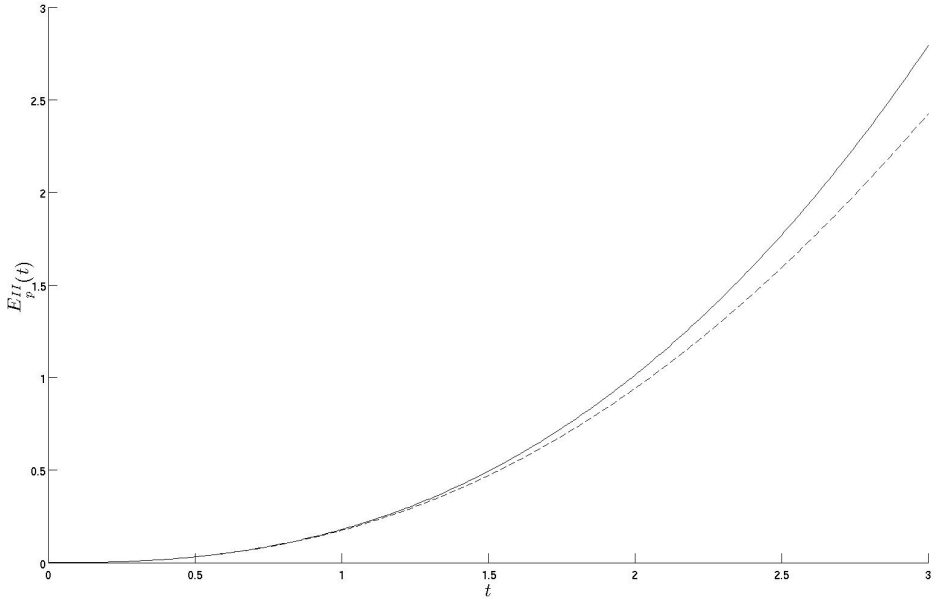

Figure 5.16: The non-dimensional potential energy in region II with (dashed line) and without (solid line) correction due to influence of gravity on the bulk flow.

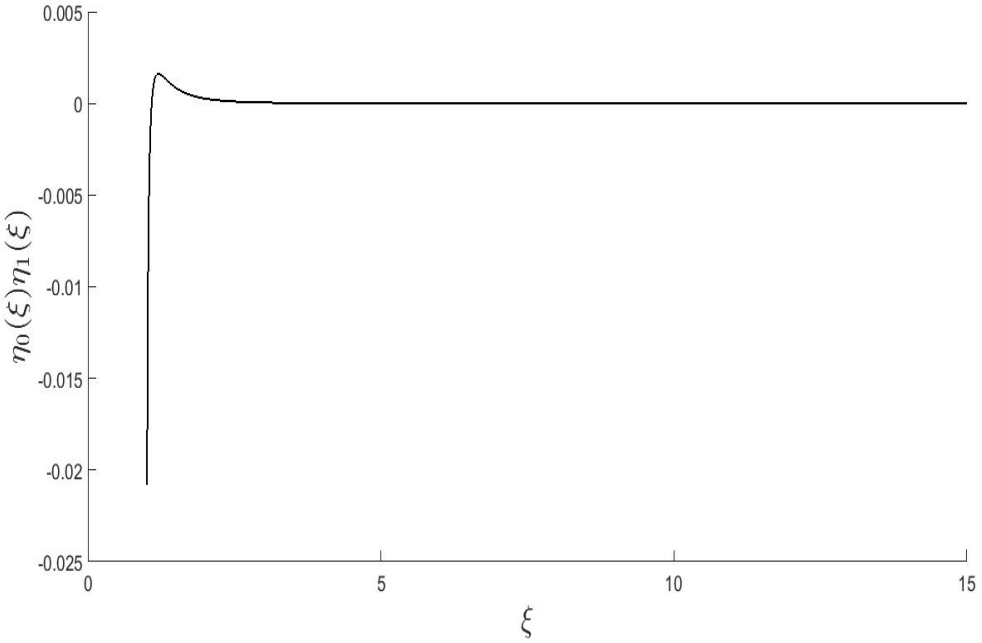

Figure 5.17: The non-dimensional integrand $\eta_0(\xi)\eta_1(\xi)$ in equation (5.143).

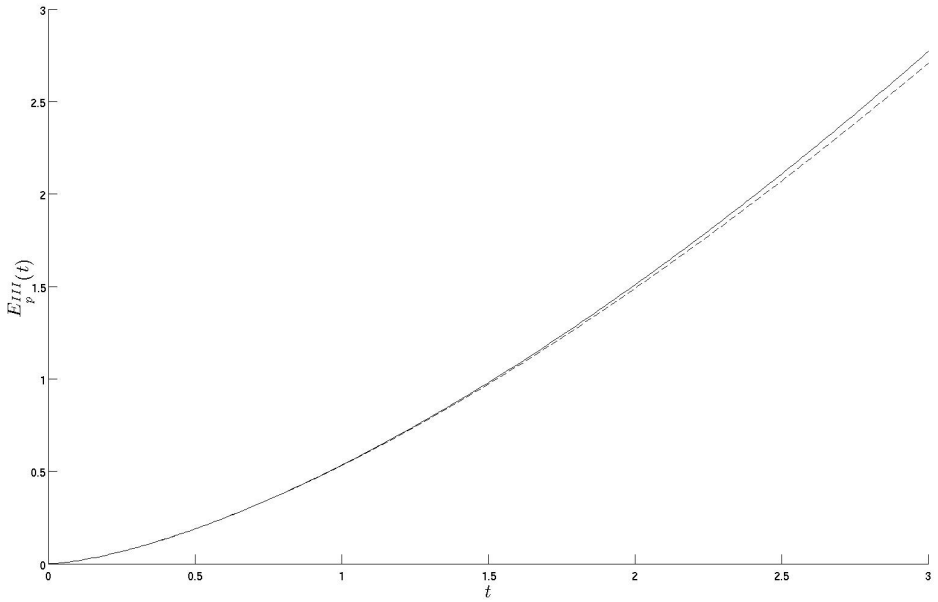

Figure 5.18: The non-dimensional potential energy in region III with (dashed line) and without (solid line) correction due to influence of gravity on the bulk flow.

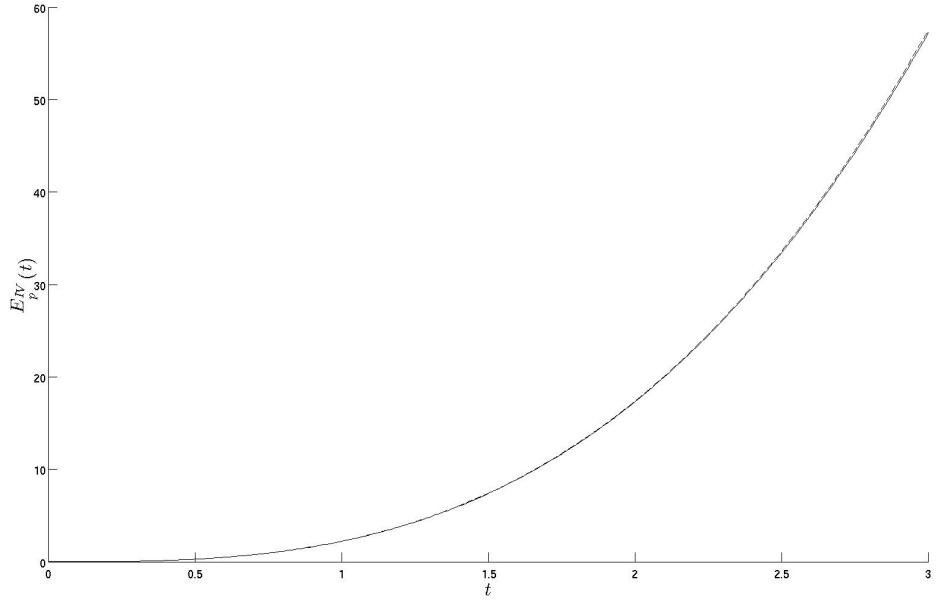

Figure 5.19: The non-dimensional potential energy in region IV and its correction (dashed line) due to influence of gravity on the bulk flow.

5.10 The mass flux into the jet root region

It is in our interest to know the change which is happening due to gravity in the mass flux into the jets during the impact. With no gravity the mass flux for water-entry problem with vertical impact is studied by Howison91 and (Korobkin 1995). The mass flux M_{flux} in the jet is defined by (Faltinsen & Timokha 2009)

$$\mathrm{M_{flux}}(t) = \rho H_J(V_J - V_S). \tag{5.159}$$

Where ρ is the fluid density, $H_J = H_J(t)$ is the jet thickness and V_J is the fluid velocity in the jet and V_S the spray root area velocity. The spray root velocity in the reference frame OXY is the same as the velocity of the moving contact point $\dot{x}_c(t)$. The moving contact point velocity with account for gravity $\dot{x}_c(t,\delta)$ is defined in equation (5.136). However, the velocity of the fluid along the jet is $2\dot{x}_c(t,\delta)$ in the Earth-fixed coordinate system Oxy. For the derivation of the velocity of the fluid in the jet see (Faltinsen & Timokha 2009). Therefore the mass flux through the jet with account for gravity is defined to be

$$\begin{aligned}\mathrm{M^g_{flux}}(t,\delta) &= H_J(t,\delta)\big(2\dot{x}_c(t,\delta) - \dot{x}_c(t,\delta)\big),\\ &= H_J(t,\delta)\dot{x}_c(t,\delta),\end{aligned} \tag{5.160}$$

where $\mathrm{M^g_{flux}}$ is scaled by ρVR. Having the non-dimensional jet thickness given in equation (5.137) and the non-dimensional velocity of the moving contact point in equation (5.136) the non-dimensional flux of fluid volume moving into the jets is

$$\mathrm{M^g_{flux}}(t,\delta) = \frac{\pi}{4}t^{3/2}\Big[\frac{1}{\sqrt{t}} + 3\delta|\mu|t\Big] + O\left(\delta^2\right), \tag{5.161}$$

Equation (5.161) demonstrates that although gravity slows down the moving contact point it increases the fluid volume flux into the jets. It also reveals that the increase (caused by gravity) of the jet root region's thickness overcomes the decrease (caused at the same time by gravity) in the speed of the moving contact point. Together, the effect of including gravity is to increase the fluid volume flux into the jets. This result is also consistent with the increase in potential energy in the jets' regions. We can conclude that the increase in potential energy in jets' region IV is due to the fact that the mass flux into this region is increased by gravity.

5.11 The kinetic energy flux in the jet

According to (Cointe et al. 2004) [during water-entry], the work done by the body on the fluid is expressed as the energy of the fluid. For circular cylinder studied

by (Cointe et al. 2004), half of this energy is in and the other half transported into the jets. However, this energy distribution is a consequence of maintaining the constant entry velocity of the body. For the consequences for the total energy distribution between the jets and the bulk, with non-constant velocity see (Scolan & Korobkin 2003).

Now that we have calculated the jet thickness, the mass flux into the jet, the velocity of the fluid in the jet and the velocity of the spray jet, we are in a position to calculate the kinetic energy flux into the jet. (Faltinsen & Timokha 2009) show that this is, for one jet:

$$\frac{\mathrm{dE}_{\mathrm{kin}}^{J}}{\mathrm{d}t} = \frac{1}{2}\mathrm{M}_{\mathrm{flux}} V_J^2, \tag{5.162}$$

where $\mathrm{M}_{\mathrm{flux}} = \mathrm{M}_{\mathrm{flux}}(t)$ is the mass flux given in equation (5.159) and V_J is the fluid velocity in the jet (in the global frame of reference), $2\dot{x}_c(t,\delta)$. Hence equation (5.162) reads

$$\frac{\mathrm{dE}_{\mathrm{kin}}^{J}}{\mathrm{d}t} = 2\mathrm{M}_{\mathrm{flux}}^{\mathrm{g}} \dot{x}_c^2, \tag{5.163}$$

where $\dot{x}_c = \dot{x}_c(t,\delta)$ is given by equation (5.136) and $\mathrm{M}_{\mathrm{flux}}^{\mathrm{g}} = \mathrm{M}_{\mathrm{flux}}^{\mathrm{g}}(t,\delta)$ is given by equation (5.161). Hence

$$\frac{\mathrm{dE}_{\mathrm{kin}}^{J}}{\mathrm{d}t} = \frac{\pi}{2} - \frac{5}{2}\pi\delta|\mu|t^{3/2} + O\left(\delta^2\right). \tag{5.164}$$

It should be noticed that for this symmetric flow, the total kinetic energy flux through the two jets is $2\frac{\mathrm{dE}_{\mathrm{kin}}^{J}}{\mathrm{d}t}$. In the next section the total energy balance in the system will be investigated.

5.12 The work done by the body on the fluid

Capillary and viscosity forces are not accounted in this study. The total kinetic energy of the fluid in non-dimensional variables is the sum of the equations (5.132), (5.133) with the time integral of the equation (5.164), hence we have

$$\begin{aligned}\mathrm{E}_{\mathrm{kin}}^{T} &= 2\mathrm{E}_{\mathrm{kin}}^{J} + \mathrm{E}_{\mathrm{kin}}^{F_c} + \mathrm{E}_{\mathrm{kin}}^{F_s} \\ &= 2\pi t + \delta\big(0.1067\sqrt{t} - 1.4437\big)\, t^{5/2} + O\left(\delta^2\right).\end{aligned} \tag{5.165}$$

With the note that the time integral of equation (5.164) is multiplied by a factor of 2 to account for both jets' kinetic energy. Equation (5.165) shows that gravity decreases the total kinetic energy of the system. To make a comparison between the kinetic energy and the work, we write the non-dimensional work done by the body force entering the water on the surface, see (Lamb 1932), as follows

$$\mathrm{W} = \int_0^t \tilde{F}(t)\mathrm{d}t. \tag{5.166}$$

This is evaluated by considering the vertical velocity of the body given in equation (5.25) and where $\tilde{F}(t)$ is defined up to first order in equations (5.113)–(5.114). The instant of impact is at $t = 0$ and the work $\mathrm{W} = \mathrm{W}(t)$ (which has the same dimensions as energy) [Joules in S.I units] is scaled by $\rho X_{sc}^2 V^2$. From the non-dimensional hydrodynamic force defined in equation (5.112), the non-dimensional work is

$$\mathrm{W} = 2\pi t + \delta\Big(\frac{1}{3} + \frac{19}{16}|\mu|\pi + \int_0^1 S(\xi)\mathrm{d}\xi\Big)t^{5/2} + O\left(\delta^2\right), \tag{5.167}$$

where $S(\xi)$ is given by equation (5.111). At leading order, from equations (5.165) and (5.167) it is simply observed that the rate of the work done by the body on the water during the period $(0, t)$ is equal to the total kinetic energy flux which is 2π, i.e.

$$\begin{aligned} \frac{\mathrm{dW}}{\mathrm{d}t} &= \frac{\mathrm{dE}_{\mathrm{kin}}^T}{\mathrm{d}t} \\ &= 2\pi + O\left(\delta t^{3/2}\right) \end{aligned} \tag{5.168}$$

It is not clear from equation (5.167) how the work is affected by gravity. Therefore we plot $\mathrm{W}(t)$ in Figure 5.20. In this figure it is found that gravity changes the linearity of the work into a non-linear function. Also gravity decreases the work by $O(\delta t^{5/2})$ which is the same order of decrease due to gravity on the total kinetic energy.

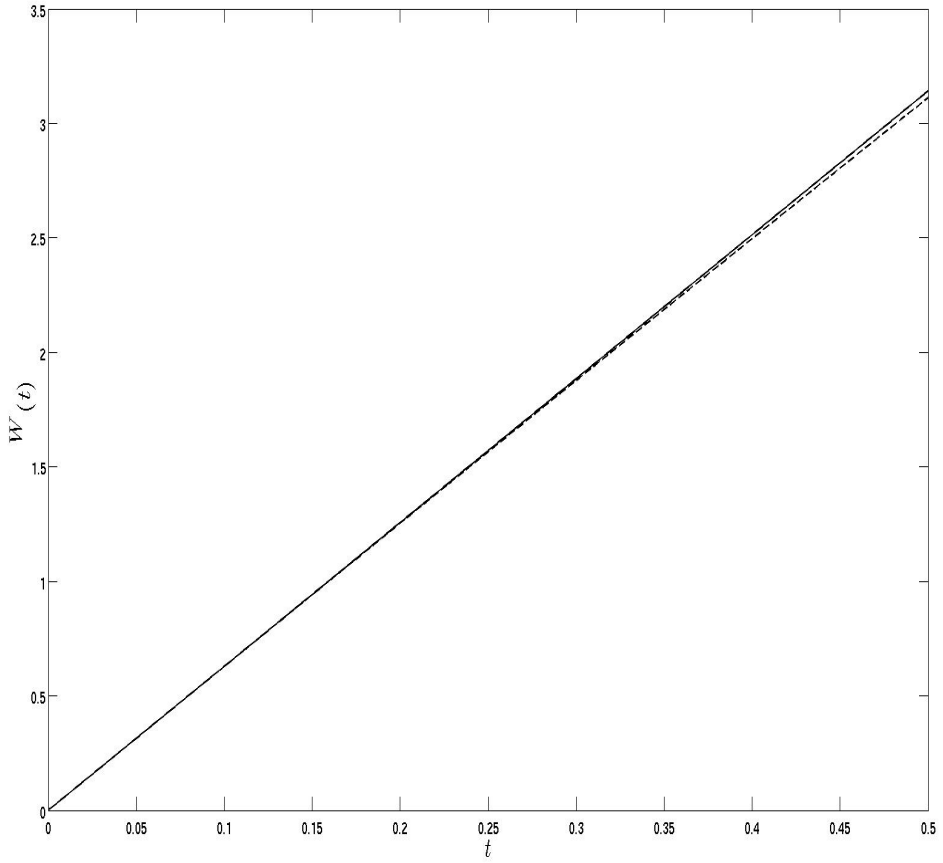

Figure 5.20: The non-dimensional work done on the water by the body with gravity (dashed line) and without gravity (solid line), with $\delta = 0.2$.

In Table 5.1 we present the influence of gravity upon each studied physical property in this thesis. These results are related to the current chapter, the initial impact of a smooth body entering water with low velocity. As to the pressure, force and work, the part of equations of $O(\delta)$, which shows gravity's effect on each of them, the formula is too long to be shown in this table and we only refer to the equations. Also regarding the potential energy in the system, in section 5.9, the results are shown for each partitioned region separately, see Figure 5.14. The potential energy in all regions is affected by gravity except region I where it remains unchanged.

It is found that gravity influences all physical properties. Most are influenced with negative impact, as expected from gravity. The order of decrease due to gravity is as follows. Of $O(\delta t)$ for the moving contact point's velocity and pressure distribution on the impact region as well, of $O(\delta t^{3/2})$ for the force on the impact region and the kinetic energy flux into the jets, of $O(\delta t^2)$ for the moving contact point's position, of $O(\delta t^{5/2})$ for the kinetic energy of the bulk and of $O(\delta t^4)$ for the potential energy in regions II and III.

However, we have different behaviour for the region IV for: the thickness of the jets and the mass flux into the jets. Even though the speed of the moving contact point and its position are decreased, there is an increase in these three properties: the order of increase caused by gravity is of $O(\delta t^{3/2})$ for the thickness of the jets, of $O(\delta t^{5/2})$ for the mass flux into the jets, and of $O(\delta t^{9/2})$ for the potential energy in region IV.

Physical property	Expression	Effect of gravity
Moving contact point's position	$2\sqrt{t}(1-\delta\lvert\mu\rvert t^{3/2})$	Decreasing
Velocity of the contact point	$\frac{1}{\sqrt{t}}(1-4\delta\lvert\mu\rvert t^{3/2})$	Decreasing
Pressure on the impact region	$\frac{2}{\sqrt{4t-x^2}}$+see (5.103)	Decreasing
Force on the impact region	2π+see (5.114)	Decreasing
Kinetic energy of the bulk	$\pi t+\left(0.1067\sqrt{t}-1.4437\right)\delta t^{5/2}$	Decreasing
Potential energy in region I	$-\frac{8\sqrt{2}}{15}t^{5/2}$	Unchanged
Potential energy in region II	$\frac{14-8\sqrt{2}}{15}t^{5/2}-2\delta\lvert\mu\rvert t^4$	Decreasing
Potential energy in region III	$\frac{2}{15}t^{5/2}-2\delta\left(C-\frac{\lvert\mu\rvert}{15}\right)t^4$	Decreasing
Potential energy in region IV	$\frac{\pi}{4}\left(3-\frac{\pi}{18}\sqrt{t}\right)t^3+\delta\lvert\mu\rvert\pi\left(1-\frac{\pi}{8}\sqrt{t}\right)t^{9/2}$	Increasing
Thickness of the jet	$\frac{\pi}{4}t^{3/2}(1+7\delta\lvert\mu\rvert\sqrt{t})$	Increasing
Kinetic energy flux into the jets	$\pi(1-5\delta\lvert\mu\rvert t^{3/2})$	Decreasing
Mass flux into the jet	$\frac{\pi}{2}t(1+3\delta\lvert\mu\rvert t^{3/2})$	Increasing
Work	$2\pi t$+see (5.167)	Decreasing

Table 5.1: Influence of gravity on physical properties in water-entry problem. Where $|\mu|=\frac{8}{225\pi}$.

Chapter 6

Conclusions and future work

The results and conclusions obtained in this thesis are summarized in this chapter. Some ideas and recommendations for future work are also discussed, in section 6.2.

6.1 Conclusions

Due to the complex nature of fluid-structure interaction problems, simplifications are needed to model interaction processes, even in 2D. These simplifications can be mathematical, physical, engineering or chemical. Usually gravity is one of the physical effects that is neglected due to high acceleration of liquid during violent interaction, such as liquid impact. However, this study is focused on the influence of gravity on the liquid impact. In this thesis we have investigated the influence of gravity on fluid-structure interactions. We have studied this influence on sloshing impacts in LNG tanks and also on the impact of a rigid body moving with constant low speed, onto a liquid surface which is initially flat. For sloshing impacts in LNG tanks and water-entry problems, it is known that during the very early stage of impact gravity is negligible. We explained in this thesis why it is so even if the corresponding non-dimensional parameters are not small. After the initial stage of impact we explained how gravity becomes important and how significant it is, by plotting the rise of its influence on some physical characteristics of the impact.

In Chapter 1 we started with the problem motivation and description of the system of tanks on LNG carriers. We discussed the objective of this study, highlighting some of the most relevant results achieved so far in both, sloshing impacts in LNG tanks and the water-entry problem.

Chapter 2 started with a description of the problem in 2D, in which the initial shape of the free-surface elevation is given. Many different impact situations with different filling levels are possible, and we only followed the one that impacts the

centre of the lid with a 95% filling level, and no air entrapped between the liquid surface and the lid. The problem is linearised based on the small distance h between the lid (at $y = H$) and the equilibrium free surface (at $y = H - h$). This distance is small compared with liquid depth, h, in that the ratio $\epsilon = \frac{h}{H} \ll 1$. We introduced an approach for solving this problem. We first solved the simplified problem at the leading order by removing the lid, when there was no impact and the only unknowns were the free-surface elevation and velocity potential. Then we introduced the lid and formulated the problem with respect to the corrections to the solution without the lid, to include the presence of the lid. Due to highly localized impact loads both in space and time we formulated the problem by introducing a small non-dimensional parameter, $\delta \ll 1$, which stretched the time and made it possible to apply asymptotic analysis to the problem. A Wagner problem of impact was then introduced and by setting $\delta = 0$ we excluded gravity from the current formulation. The components of the flow velocity were shown to be singular at the moving contact points $x = \pm x_c(t)$. Therefore we smoothed the velocity potential by integrating it in time and formulating the problem with respect to the displacement potential. By reformulating the Wagner problem at the leading order in terms of a displacement potential, we found the size of the wetted region, hydrodynamic force and the pressure distribution. Negative pressures and forces were found during the impact stage. By keeping $\delta = 0$, the total energy budget of the system was derived by accounting for the spray jets during the impact. It is well-known that the energy is not conserved in the Wagner approximation model when the jets are neglected.

Chapter 3 is a continuation of Chapter 2, but with $\delta > 0$ in the formulation, which means gravity is now included. We established a new formulation of this problem by transforming the dynamic boundary condition on the free surface. The problem was reformulated in terms of the displacement potential by using the Wagner condition. We asymptotically expanded our unknowns with respect to the small parameter δ. Correction to the free-surface elevation, $\eta_{c0}(x, t)$, due to the lid was obtained. Also the correction due to gravity to the size of the wetted region, $\gamma\, x_{c1}(t)$, where $\gamma = \delta^{3/2}$, was obtained. A new approach for finding the correction to the size of the wetted region due to gravity was introduced. In this method we assumed that the displacement potential in the dynamic boundary condition on the free surface is a solution and we introduced an unknown function into that solution as a correction to be determined. The results by these two methods are compared. By both methods we found that the influence of gravity on the size of the wetted region during early stage of impact is very small. However, this influence becomes visible later on, and it becomes significant at later stages of the impact. It was found that gravity decreases the size of the wetted region.

At the end of Chapter 3, we found semi-analytically the influence of gravity on the pressure distribution on the lid of the tank during impact. It was shown that the correction due to gravity on the pressure distribution is negative. It was found that gravity decreases the pressure distribution during impact stage and the results was plotted for some instant to show the difference of the pressure distribution with and without gravity.

In Chapter 4 we solved the sloshing problem numerically by using the Wagner model. We used the same simplifications as in Chapter 2 keeping gravity in the formulation of the impact problem. The problem was formulated in terms of the Fourier coefficients and linear splines for the velocity potential, pressure and surface elevation. We used the kinematic and dynamic boundary conditions to relate the coefficients for the liquid surface elevation and pressure distribution. The unknown pressure in the contact region was sought in terms of a smooth function to be determined, multiplied by a known square-root singularity at the moving contact points $x = \pm x_c(t)$. We faced a new challenge: an ill-conditioned system. The condition number of our system was very large. The solution was not reliable. Tikhonov regularization was applied to the system with the help of the regularization tool provided by (Hansen 1994). We finally managed to stabilize the system and brought down the condition number of equation very close to unity. Numerical results were compared with known semi-analytical results. Again we found only tiny contribution of gravity to the surface elevation and pressure during the early stage of impact. However as times goes on, gravity both decreases the pressure and lowers the surface elevation.

In Chapter 5 we studied the influence of gravity on the water-entry problem with constant velocity. First, we neglected the compressibility of the liquid, and assumed that gravity has a greater contribution to the flow than surface tension and non-linear effects. Then we introduced the displacement potential into our formulation. We sought the asymptotic expansions of the unknown functions in terms of the small parameter δ which is responsible for gravity in this problem. Next we introduced new stretched variables which account for gravity. With asymptotic analysis, at the leading order we arrived at classical Wagner problem. The first-order solution represented the correction due to gravity. By using a characteristic function we found the correction to the size of the wetted region, pressure, force and surface elevation. The kinetic energy of the bulk of the liquid was shown to be decreasing for some time, then it increased due to gravity, and consequently the same was found for the work done by the body force entering the water. The influence of gravity on the total potential energy was calculated by evaluating it in each part of a partition made to the fluid domain. The effect of gravity in each part was studied. On the other hand, despite the decrease due

to gravity in the position and velocity of the moving contact point, we found an increase in the total mass flux passing into the jets. Also it was found that the kinetic energy flux into the jets decreases due to gravity.

6.2 Future work

There are many problems which remain open after this work related to the influence of gravity on fluid-structure interaction. We mention below some of these problems that we are interested in working on in future:

- The results of this thesis on sloshing impact are related to the stage when the wetted region is expanding. Some of the current approaches and methods can be used also for the next stage, the exit stage. Initial positions of the moving contact points $x = \pm x_c(t)$ at the beginning of the exit stage are those at the end of the entry stage.

- In sloshing, analytically we only found the influence of gravity on the moving contact points $x = \pm x_c(t)$. It will be important to work analytically on other characteristics, for example hydrodynamic pressure, under the influence of gravity and then compare the analytical results with available numerical results.

- In both problems, sloshing and water-entry, the influence of gravity was studied for the symmetric case.

  The presence of the surrounding gas which can be entrapped or mixed with the liquid during impact was not studied. The rigid structure was assumed. In asymmetric impact, the speeds of the two moving contact points are different, therefore we expect that gravity waves have significantly different influence on both moving contact points and this consequence will be interesting to know on the other properties during impact.

  Allowing the lid to deflect turns the problem into a coupled fluid-structure interaction problem. The lid deflection may increase or decrease the impact loads relative to the rigid lid, case with gravity further complicating the problem. These two factors can be combined to make a more realistic model.

- Numerically the problem of sloshing impact is ill-conditioned and (as we mentioned in section 6.1), Thikhonov regularization was imposed to stabilize the system. Using other methods of regularization, like truncated singular value method or any iterative method, could improve the stability

of the system. Also we used a regular mesh in this study. Irregular mesh, with finer resolution near the moving contact point, would be interesting to investigate. Do we still arrive at ill-conditioned system for irregular mesh? This could be done by dealing with the pressure directly or, as we did in this thesis, by splitting the pressure into a product of a smooth function and a known square-root singular function, at the moving contact points.

- In the case of sloshing in a tank with moderate filling, breaking waves travelling from one wall to another and impacting the top corners are more likely to happen and could be more violent due to the corners than standing wave impacting the lid. Therefore, it is in our plan to work on how this impact is affected by gravity. Figure 6.1 shows a 3D perspective view of an impact at one edge of a rectangular tank.

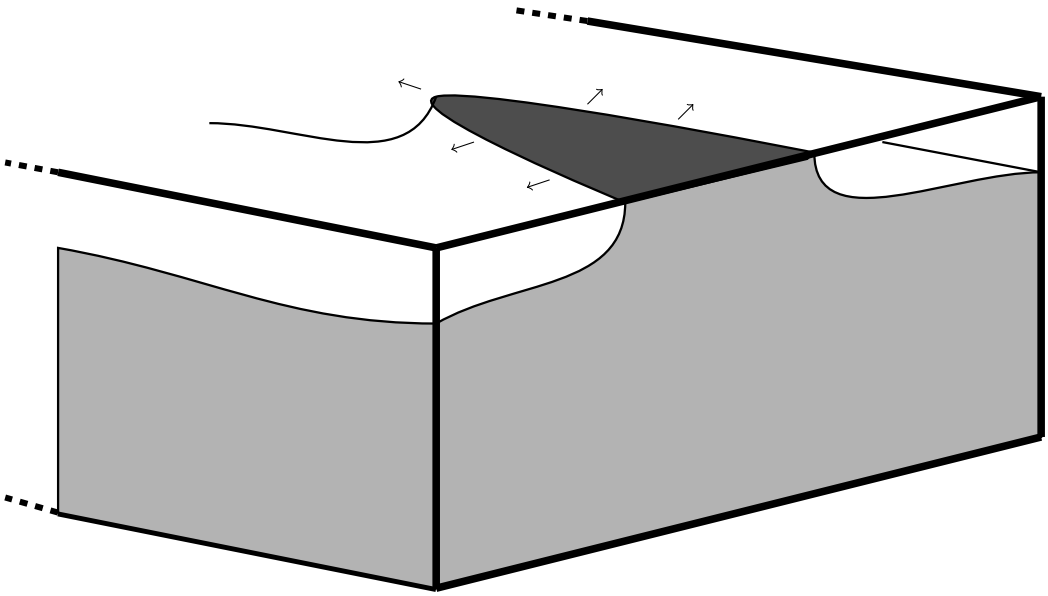

Figure 6.1: A perspective sketch of a highly filled rectangular tank in 3D, in which a standing wave impacts the lid of the tank along the wall. The dark shaded part of the lid is the wetted region of impact (in Wagner model) and the light shaded part of the tank is where the liquid is in contact with the tank's walls. The arrows indicate likely the direction of spreading of the wetted region.

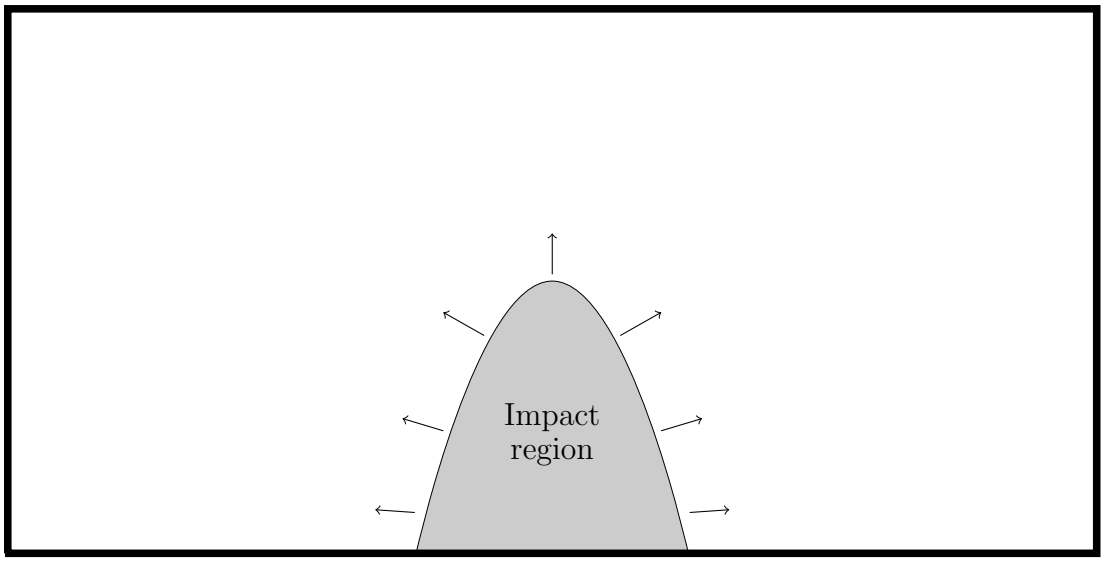

Figure 6.2: Plan view of the impact in Figure 6.1; wetted region shaded. Arrows indicate the direction of the wetted region expansion.

- The wetted region in the 3D configuration shown in Figure 6.1 is similar to what is shown in Figure 6.2 in a 2D configuration. All previously mentioned future work consists of difficult tasks, even in 2D. Extending the work of this thesis with above mentioned future work into 3D will be very interesting. When 3D results become available, they will be compared with 2D results obtained in this thesis such as the plane of right-hand wall shown in Figure 6.1, or the centre-plane of symmetry in 6.1.

Bibliography

Aarts, R. M. & Janssen, A. J. (2003), 'Approximation of the Struve function h1 occurring in impedance calculations', *The Journal of the Acoustical Society of America* **113**(5), 2635–2637.

Abramowitz, M. & Stegun, I. A. (1972), 'Handbook of mathematical functions with formulas, graphs, and mathematical tables. National Bureau of Standards Applied Mathematics Series 55, tenth printing.'.

Abramson, H. N., Bass, R., Faltinsen, O. & Olsen, H. (1976), Liquid slosh in LNG carriers, *in* 'Symposium on Naval Hydrodynamics, 10th, Proceedings, Cambridge, Mass, June 24-28, 1974'.

Aster, R. C., Borchers, B. & Thurber, C. H. (2011), *Parameter estimation and inverse problems*, Academic Press.

Benjamin, T. B. (1968), 'Gravity currents and related phenomena', *Journal of Fluid Mechanics* **31**(02), 209–248.

Bredmose, H., Brocchini, M., Peregrine, D. & Thais, L. (2003), 'Experimental investigation and numerical modelling of steep forced water waves', *Journal of Fluid Mechanics* **490**, 217–249.

Carrier, G. F., Krook, M. & Pearson, C. E. (2005), *Functions of a complex variable: theory and technique*, Vol. 49, SIAM.

Cointe, R. & Armand, J.-L. (1987), 'Hydrodynamic impact analysis of a cylinder', *Journal of Offshore Mechanics and Arctic Engineering* **109**(3), 237–243.

Cointe, R., Fontaine, E., Molin, B. & Scolan, Y. (2004), 'On energy arguments applied to the hydrodynamic impact force', *Journal of Engineering Mathematics* **48**(3-4), 305–319.

Cooker, M. J. (1996), 'Sudden changes in a potential flow with a free surface due to impact', *The Quarterly Journal of Mechanics and Applied Mathematics* **49**(4), 581–591.

Cooker, M. J. (2001), Violently erupting free-surface jets, *in* 'IUTAM Symposium on Free Surface Flows', Springer, pp. 63–70.

Cooker, M. J. (2002), 'Liquid impact, kinetic energy loss and compressibility: Lagrangian, eulerian and acoustic viewpoints', *Journal of engineering mathematics* **44**(3), 259–276.

Cooker, M. J. (2013), 'A theory for the impact of a wave breaking onto a permeable barrier with jet generation', *Journal of Engineering Mathematics* **79**(1), 1–12.

Cooker, M. J. & Peregrine, D. (1995), 'Pressure-impulse theory for liquid impact problems', *Journal of Fluid Mechanics* **297**, 193–214.

Cooker, M. & Peregrine, D. (1990), 'Violent water motion at breaking-wave impact', *Coastal Engineering Proceedings* **1**(22).

Faltinsen, O. (1993), *Sea loads on ships and offshore structures*, Vol. 1, Cambridge University Press.

Faltinsen, O. M. & Timokha, A. N. (2009), 'Sloshing'.

Gakhov, F. D. & Sneddon, I. N. (1966), *Boundary value problems*, Vol. 1966, Pergamon Press Oxford.

George, R. (2015), 'Worse things still happen at sea.'.

Godderidge, B. (2009), A Phenomenological Rapid Sloshing Model for Use as an Operator Guidance System on Liquefied Natural Gas Carriers, PhD thesis.

Graczyk, M. (2008), *Experimental investigation of sloshing loading and load effects in membrane LNG tanks subjected to random excitation*, NTNU.

Gradshteyn, I. S. & Ryzhik, I. M. (2014), *Table of integrals, series, and products*, Academic press.

Greenhow, M. & Moyo, S. (1997), 'Water entry and exit of horizontal circular cylinders', *Philosophical Transactions of the Royal Society of London A: Mathematical, Physical and Engineering Sciences* **355**(1724), 551–563.

Hansen, P. C. (1994), 'Regularization tools: A matlab package for analysis and solution of discrete ill-posed problems', *Numerical algorithms* **6**(1), 1–35.

Hansen, P. C. (1999), *The L-curve and its use in the numerical treatment of inverse problems*, IMM, Department of Mathematical Modelling, Technical University of Denmark.

Hansen, P. C. & O'Leary, D. P. (1993), 'The use of the l-curve in the regularization of discrete ill-posed problems', *SIAM Journal on Scientific Computing* **14**(6), 1487–1503.

Hine, L. (2008), 'GTT tweaks blueprints to combat sloshing damage'.

Howison, S., Ockendon, J. & Oliver, J. (2004), 'Oblique slamming, planing and skimming', *Journal of Engineering Mathematics* **48**(3-4), 321–337.

Howison, S., Ockendon, J., Oliver, J., Purvis, R. & Smith, F. (2005), 'Droplet impact on a thin fluid layer', *Journal of Fluid Mechanics* **542**, 1–23.

Howison, S., Ockendon, J. & Wilson, S. (1991), 'Incompressible water-entry problems at small deadrise angles', *Journal of Fluid Mechanics* **222**(1), 215–230.

Iafrati, A. & Korobkin, A. A. (2004), 'Initial stage of flat plate impact onto liquid free surface', *Physics of Fluids* **16**, 2214.

Keulegan, G. H. (1959), 'Energy dissipation in standing waves in rectangular basins', *Journal of Fluid Mechanics* **6**(01), 33–50.

Kim, J., Shin, Y., Bai, K. et al. (2002), A finite-element computation for the sloshing motion in lng tank, *in* 'The Twelfth International Offshore and Polar Engineering Conference', International Society of Offshore and Polar Engineers.

Korobkin, A. (1982), 'Formulation of penetration problem as a variational inequality', *Din. Sploshnoi Sredy* **58**, 73–79.

Korobkin, A. (1995), Acoustic effects on water impact, *in* 'Proceedings of the 10th Workshop on Water Waves and Floating Bodies, Oxford, UK, Apr', pp. 2–5.

Korobkin, A. (1997), 'Asymptotic theory of liquid–solid impact', *Philosophical Transactions of the Royal Society of London A: Mathematical, Physical and Engineering Sciences* **355**(1724), 507–522.

Korobkin, A. (1998), 'Wave impact on the center of an Euler beam', *Journal of Applied Mechanics and Technical Physics* **39**(5), 770–781.

Korobkin, A. (2007), 'Second-order wagner theory of wave impact', *Journal of Engineering Mathematics* **58**(1-4), 121–139.

Korobkin, A. & Khabakhpasheva, T. (2006), 'Regular wave impact onto an elastic plate', *Journal of Engineering Mathematics* **55**(1-4), 127–150.

Korobkin, A. & Scolan, Y.-M. (2006), 'Three-dimensional theory of water impact. part 2. linearized wagner problem', *Journal of Fluid Mechanics* **549**, 343–373.

Lamb, H. (1932), *Hydrodynamics*, Cambridge University Press.

Lee, D., Kim, M., Kwon, S., Kim, J., Lee, Y. et al. (2005), A parametric and numerical study on LNG-tank sloshing loads, *in* 'The Fifteenth International Offshore and Polar Engineering Conference', International Society of Offshore and Polar Engineers.

LNG-Journal (2016), 'Exxonmobil sees global demand for lng and natural gas rising by 50 percent.'.

Longuet-Higgins, M. S. (2001), Vertical jets from standing waves, *in* 'Proceedings of the Royal Society of London A: Mathematical, Physical and Engineering Sciences', Vol. 457, The Royal Society, pp. 495–510.

Longuet-Higgins, M. S. & Dommermuth, D. G. (2001), Vertical jets from standing waves. ii, *in* 'Proceedings of the Royal Society of London A: Mathematical, Physical and Engineering Sciences', Vol. 457, pp. 2137–2149.

Malenica, Š., Korobkin, A., Scolan, Y.-M., Gueret, R., Delafosse, V., Gazzola, T., Mravak, Z., Chen, X. & Zalar, M. (2006), Hydroelastic impacts in the tanks of LNG carriers, *in* 'Proceedings of the 4th international conference on hydroelasticity in marine technology, Wuxi, China', Vol. 1014.

Malenica, Š., Mravak, Z., Besse, P., Kaminski, M. L. & Bogaert, H. (2009), Full scale experiments and new methodology to assess the structural behaviour of a membrane LNGC containment system under breaking waves project "SLOSHEL", *in* '24th International Conference & Exhibition for the LNG, LPG & Natural Gas Industries, Abu Dabi, UAE'.

Miloh, T. (1981), 'Wave slam on a sphere penetrating a free surface', *Journal of Engineering Mathematics* **15**(3), 221–240.

Neumaier, A. (1998), 'Solving ill-conditioned and singular linear systems: A tutorial on regularization', *SIAM Review* **40**(3), 636–666.

Oliver, J. M. (2002), Water Entry and Related Problems, PhD thesis, University of Oxford.

Press, W. H. (2007), *Numerical recipes 3rd edition: The art of scientific computing*, Cambridge University Press.

Reinhard, M., Korobkin, A. & Cooker, M. (2013), 'Water entry of a flat elastic plate at high horizontal speed', *Journal of Fluid Mechanics* **724**, 123–153.

Reinhard, M. V. (2013), Free Elastic Plate Impact into Water, PhD thesis, University of East Anglia.

Rognebakke, O. F. & Faltinsen, O. M. (2005), Sloshing induced impact with air cavity in rectangular tank with a high filling ratio, *in* '20th International Workshop on Water Waves and Floating Bodies, Spitsbergen, Norway'.

Scolan, Y.-M. & Korobkin, A. (2001), 'Three-dimensional theory of water impact. part 1. Inverse Wagner problem', *Journal of Fluid Mechanics* **440**, 293–326.

Scolan, Y.-M. & Korobkin, A. (2003), 'Energy distribution from vertical impact of a three-dimensional solid body onto the flat free surface of an ideal fluid', *Journal of Fluids and Structures* **17**(2), 275–286.

Scolan, Y.-M., Remy, F. & Thibault, B. (2006), Impact of three-dimensional standing waves on a flat horizontal plate, *in* '21st International Workshop on Water Waves and Floating Bodies', Vol. 21, p. 4pp.

Ten, I., Malenica, Š. & Korobkin, A. (2011), 'Semi-analytical models of hydroelastic sloshing impact in tanks of liquefied natural gas vessels', *Philosophical Transactions of the Royal Society of London A: Mathematical, Physical and Engineering Sciences* **369**(1947), 2920–2941.

Tikhonov, A. N. & Arsenin, V. Y. (1977), 'Solutions of ill-posed problems'.

Vanden-Broeck, J.-M. & Keller, J. B. (1982), 'Jets rising and falling under gravity', *Journal of Fluid Mechanics* **124**, 335–345.

Vanem, E., Antão, P., Østvik, I. & de Comas, F. D. C. (2008), 'Analysing the risk of lng carrier operations', *Reliability Engineering & System Safety* **93**(9), 1328–1344.

von Karman, T. (1929), 'The impact on seaplane floats during landing'.

Wagner, H. (1932), 'Über stoß-und gleitvorgänge an der oberfläche von flüssigkeiten (Phenomena associated with impacts and sliding on liquid surfaces)', *ZAMM-Journal of Applied Mathematics and Mechanics/Zeitschrift für Angewandte Mathematik und Mechanik* **12**(4), 193–215.

Wilson, S. K. (1989), The Mathematics of Ship Slamming., PhD thesis, University of Oxford.

Woodward, J. L. & Pitbaldo, R. (2010), *LNG Risk Based Safety: modeling and consequence analysis*, John Wiley & Sons.

Wu, G. (1998), 'Hydrodynamic force on a rigid body during impact with liquid', *Journal of Fluids and Structures* **12**(5), 549–559.

Zhao, R. & Faltinsen, O. (1993), 'Water entry of two-dimensional bodies', *Journal of Fluid Mechanics* **246**, 593–612.